MASARYK UNIVERSITY

FACULTY OF SCIENCE

DOCTORAL THESIS

Author:
Michal Prišegen

2022
Brno

Masaryk University
Faculty of Science

Doctoral Thesis

Endpoints of stellar evolution in association with star clusters

Author:
Michal Prišegen

Supervisor:
doc. Ernst Paunzen,
Dr.rer.nat

Department of Theoretical Physics and Astrophysics

2022
Brno

Declaration of Authorship

I, Michal Prišegen, declare that this thesis titled, "Endpoints of stellar evolution in association with star clusters" and the work presented in it are my own. I confirm that:

- This work was done wholly or mainly while in candidature for a research degree at Masaryk University.
- Where I have consulted the published work of others, this is always clearly attributed.
- Where I have quoted from the work of others, the source is always given.
- I have acknowledged all main sources of help.

Signed:

Date:

"*The effort to understand the universe is one of the very few things which lifts human life a little above the level of farce and gives it some of the grace of tragedy.*"

Steven Weinberg – The First Three Minutes

A significant portion of the content of this thesis is presented in the form of papers already published in refereed journals. A lot of technical details concerning the studies compiled in the thesis can be found in these articles. Nevertheless, all the results have been summarized and are presented just before the insertion of the original articles. Additionally, the original results are revisited in the light of new data and additional discussion is added as needed. I believe that a complete overview of the science presented in the thesis can therefore be achieved by reading these subsections, including also the first introductory chapter, conclusions, and future research avenues, without having to read the included articles. Of course, to gain a more detailed insight into the science presented in this work, an interested reader will find the attached articles helpful.

Bibliographic Entry

Author:	Michal Prišegen, Přírodovědecká fakulta, Masarykova univerzita, Ústav teoretické fyziky a astrofyziky
Title of the Thesis:	Endpoints of stellar evolution in association with star clusters
Degree Programme:	Physics
Specialization:	Astrophysics
Supervisor:	doc. Ernst Paunzen, Dr.rer.nat
Academic Year:	2021/2022
Number of Pages:	xxvi+142
Keywords:	Star clusters; Neutron stars; White dwarfs; High-mass X-ray binaries; bow shocks; circumstellar matter; X-ray pulsars; astrometry; Gaia; runaway stars

Bibliografický záznam

Autor:	Michal Prišegen, Přírodovědecká fakulta, Masarykova univerzita, Ústav teoretické fyziky a astrofyziky
Název práce:	Konečná stádia hvězdného vývoje asociována s hvězdokupami
Studijní program:	Fyzika
Specializace:	Astrofyzika
Vedoucí práce:	doc. Ernst Paunzen, Dr.rer.nat
Akademický rok:	2021/2022
Počet stran:	xxvi+142
Klíčová slova:	Hvězdokupy; Neutronové hvězdy; Bílý trpaslíci; Rentgenový dvojhvězdy s hmotnou složkou; čelné rázové vlny; okolohvězdná hmota; rentgenové pulzary; astrometrie; Gaia; runaway hvězdy

MASARYK UNIVERSITY

Abstract

Faculty of Science
Department of Theoretical Physics and Astrophysics

Endpoints of stellar evolution in association with star clusters

by Michal Prišegen

There is a myriad of interesting objects across the Universe. However, few push our understanding of the fundamental astrophysics more than the compact stellar remnants – white dwarfs, neutron stars, and black holes – and the last stages of stellar evolution that create them. Much has already been achieved while studying these objects in the Galactic field. Nevertheless, more research avenues open if these objects can be studied in well-defined astrophysical environments, such as star clusters or associations. These are ensembles of stars with common distances, ages, initial chemical compositions, extinction, and overall kinematic properties in the Galactic context. Since the compact object progenitor also shared these common properties, star clusters and associations provide useful means of studying the compact stellar remnants, for which these quantities would be impossible or hard to derive with sufficient accuracy and precision if they were located in the Galactic field.

This thesis attempts to shed some light on some of the most fundamental questions connected with the last stages of stellar evolution. One of them is where lies the stellar mass boundary that separates the regime where stars explode as supernovae from where they do not. How is this boundary affected by metallicity and binarity? How do supernova explosions influence the properties of the nascent compact remnants? How much matter is returned to the local interstellar medium after the end of a star's life?

High-mass X-ray binaries – containing a high-mass main sequence star and a neutron star or a black hole – can be used to study supernova explosions in binaries, as the properties of the primary and the secondary, the orbital parameters, and the peculiar velocities retain a lot of information about the supernovae within these systems. It was discovered that there is a notable paucity of bow shocks and other nebulae around high-mass X-ray binaries as compared to other early-type stars with similarly large velocities (runaways). This is connected to high-mass X-ray binaries being probably kinematically younger than other early-type runaways, as they are generally getting ejected from their parent star clusters after the supernova event. Therefore, they are still moving within the hot and rarefied bubbles around star clusters, with a lower chance of forming observable bow shocks or other nebulae. There is also evidence that a subclass of high-mass X-ray binaries – Be X-ray binaries – consists of two groups with different peculiar velocities. This could be attributed to two different supernova mechanisms producing these two groups.

We also identified new white dwarfs associated with open clusters. We studied their properties and obtained important constraints on how much matter is returned to the local interstellar medium by the end of stellar lives. We also noted an absence of massive cluster white dwarfs that approach the Chandrasekhar limit.

MASARYKOVA UNIVERZITA

Abstrakt

Přírodovědecká fakulta
Ústav teoretické fyziky a astrofyziky

Konečná stádia hvězdného vývoje asociována s hvězdokupami

Michal Prišegen

Ve vesmíru se nachází množství zajímavých objektů. Nicméně, málokteré z nich posouvají hranice našeho chápaní fundamentální astrofyziky tak, jako kompaktní hvězdné objekty – bílí trpaslíci, neutronové hvězdy a černé díry – a poslední stádia hvězdného vývoje s nimi spojená. Mnoho už bylo zjištěno studiem těchto objektů v galaktickém poli. Avšak, nové možnosti výzkumu se nabízejí, když jsou tyto objekty asociovány s hvězdokupami a asociacemi. Ty představují skupiny hvězd se stejnou vzdáleností od pozorovatele, stářím, počátečním chemickým složením, mezihvězdnou extinkcí a kinematickými vlastnostmi v galaktickém kontextu. Jelikož i předchůdci kompaktních objektů sdíleli tyto vlastnosti, hvězdokupy a asociace mohou být užitečnými prostředky pro studium těchto objektů.

Některé ze základních otázek spojených se závěrečnými fázemi hvězdného vývoje, které se tato práce snaží objasnit, jsou, kde leží hmotnostní hranice, která rozděluje hvězdy, které vybuchnou jako supernova od těch, které ne. Jak tato hranice závisí na chemickém složení hvězd a jejich binaritě? Jak ovlivňují exploze supernov vlastnosti vzniklých kompaktních objektů? Jaké množství materiálu se vrátí do okolního mezihvězdného prostoru po ukončení hvězdného vývoje?

Rentgenové dvojhvězdy s hmotnou složkou – obsahující vysoce hmotnou hvězdu a neutronovou hvězdu nebo černou díru – mohou být použity pro studium výbuchů supernov ve dvojhvězdách, neboť jejich orbitální vlastnosti, vlastnosti primární a sekundární složky a pekuliární rychlosti uchovávají informace o výbuchu supernovy. Bylo zjištěno, že je u těchto objektů snížený výskyt čelních rázových vln a mlhovin v porovnání s jinými hvězdami raných spektrálních tříd s vysokou pekuliární rychlostí. Toto je zřejmě zapříčiněno nižším kinematickým stářím rentgenových dvojhvězd s hmotnou složkou v porovnání s hvězdami raných spektrálních tříd s vysokou pekuliární rychlostí. Rentgenové dvojhvězdy s hmotnou složkou jsou převážně vymrštěny z mateřské hvězdokupy až po výbuchu supernovy, tím pádem se většinou ještě stále pohybují v horkých a prázdných bublinách okolo mateřských hvězdokup, s nižší šancí pro vytvoření čelní rázové vlny nebo jiných mlhovin. Je tady také evidence toho, že podskupina rentgenových dvojhvězd s hmotnou složkou – Be rentgenové pulsary – sestávají ze dvou skupin s odlišnými pekuliárními rychlostmi. Toto může být přičteno dvěma rozličným mechanismům výbuchu supernov, který potom vytváří tyto dvě skupiny pulsarů.

Také jsme identifikovali nové bíle trpaslíky v otevřených hvězdokupách a získali nové poznatky o množství hmoty navrácené do okolní mezihvězdné látky po ukončení hvězdného vývoje. Zjistili jsme, že v otevřených hvězdokupách chybí bílí trpaslíci s hmotností blížící se Chandrasekharově mezi.

Acknowledgements

My time as a PhD student over the past couple of years has been a very fulfilling – and, at times, challenging – ride. Despite the various stuff that life can throw at you sometimes, it has been a rewarding journey that allowed me to grow as a scientist and as a person. For this, I would like to express my gratitude to those who made the ride less bumpy and were there by my side when the road was winding a bit too much. Without you, this thesis would have never been complete.

First and foremost, I am extremely grateful to my supervisor, Ernst Paunzen, for his invaluable advice, discussions, and patience, and for steering me in the right direction. Thank you for your friendship, for never losing your faith in me throughout my various projects, and for always managing to find the time to work through whatever problems that came up.

I would like to thank also my co-authors and collaborators, with whom I worked during my graduate student career. Regardless of whether we have met in person or not, I would like to thank you for sharing your expertise, discussing amazing science, and exchanging ideas with me. It helped me to expand my horizons. I am hoping we can continue to work on some exciting projects again soon!

Thanks are also due to my longtime friends – some of them being also the current and former fellow graduate students. You all have managed to help me in one way or another throughout these times.

Last but most importantly, I would like to offer my heartfelt thanks to my family, and especially to my partner. Thank you very much for your love, attention, kindness, and for just being there next to me.

Contents

List of Abbreviations

2MASS	Two Micron All Sky Survey
AF	Astrometric Field
AGB	Asymptotic Giant Branch
BAM	Basic-Angle Monitor
BeXRB	Be X-ray Binary
BH	Black Hole
BHXRB	Black Hole X-ray binary
BP	*Gaia* Blue Photometer
CCD	Charge-coupled Device
CCSN	Iron-core-collapse supernova
CMD	Color-Magnitude Diagram
DPAC	*Gaia* Data Processing and Analysis Consortium
ECSN	Electron-capture supernova
EDR3	*Gaia* Early Data Release 3
GC	Globular Cluster
GDR2	*Gaia* Data Release 2
H-R	Hertzsprung–Russell
HVS	Hyper Velocity Star
HIPPARCOS	HIgh Precision PaRallax COllecting Satellite
HMXB	High-Mass X-ray binary
HST	*Hubble Space Telescope*
ICRS	International Celestial Reference System
IFMR	Initial-to-Final Mass Relation
ISM	Interstellar Medium
LMC	the Large Magellanic Cloud
LSR	Local Standard of Rest
MSP	MilliSecond Pulsar
NS	Neutron Star
OC	Open Cluster
PN	Planetary Nebula
RP	*Gaia* Red Photometer
RVS	*Gaia* Radial Velocity Spectrometer
SAGB	Super Asymptotic Giant Branch star
sgHMXB	supergiant High Mass X-ray Binary
SMC	the Small Magellanic Cloud
SN	Supernova
SNR	Supernova Remnant
TDI	Time-Delayed Integration
VPD	Vector Point Diagram
WFS	WaveFront Sensor
WD	White Dwarf

Dedicated to Ríša

List of relevant publications

The thesis is based on several manuscripts where the author of the thesis (MP) is the lead author.

PAPER 1
Concerning the occurrence of bow shocks around high-mass X-ray binaries
Prišegen, M.
Astronomy & Astrophysics, **621**, id.A37, 12 pp. (2019)

MP conducted all the work for the project.

PAPER 2
Kinematic distinction of the two subpopulations of X-ray pulsars
Prišegen, M.
Astronomy & Astrophysics, **640**, id.A86, 15 pp. (2020)

MP conducted all the work for the project.

PAPER 3
White dwarf-open cluster associations based on Gaia DR2
Prišegen, M.; Piecka, M.; Faltová, N.; Kajan, M.; Paunzen, E
Astronomy & Astrophysics, **621**, id.A37, 12 pp. (2021)

MP came up with the science case, designed the study, analyzed the data, joined his results with the results from co-authors, interpreted and analyzed the results, wrote the majority of the manuscript, and finalized the text after receiving comments from the co-authors.

Other publications not included in this thesis

An analysis of four stellar rings
Paunzen, E.; Florian, J.; Gütl-Wallner, A.; Herdin, A.; Kralofsky, E.; Leschinski, K.; Mach, M.; Maitzen, H. M.; **Prišegen, M.**; Rockenbauer, M.; Rode-Paunzen, M.; Wallner, S.
Astronomische Nachrichten, **339**, Issue 672, pp. 672-679 (2018)

Absolute Magnitudes of Early-type Supergiants from uvbyβ Photometry and Parallax Data
Kaltcheva, N.; Paunzen, E.; **Prišegen, M.**; Golev, V.; Watson, M.
Publications of the Astronomical Society of the Pacific, **132**, Issue 1013, id.074203, 12 pp. (2020)

Rotational modulation and single g-mode pulsation in the B9pSi star HD 174356?
Mikulášek, Z.,Paunzen, E., Hümmerich, S., Niemczura, E., Walczak, P., Fraga, L., Bernhard, K., Janík, J., Hubrig, S., Järvinen, S., Jagelka, M., Pintado, O. I., Krtička, J., **Prišegen, M.**, Skarka, M., Zejda, M., Ilyin, I., Pribulla, T., Kamiński, K., Kamińska, M. K., Tokarek, J., Zieliński, P.
Monthly Notices of the Royal Astronomical Society, **498**, Issue 1, pp.548-564 (2020)

Magnetic chemically peculiar stars investigated by the Solar Mass Ejection Imager
Paunzen, E.; Supíková, J.; Bernhard, K.; Hümmerich, S.; **Prišegen, M.**
Monthly Notices of the Royal Astronomical Society, **504**, Issue 3, pp.3758-3772 (2021)

A case study of ACV variables discovered in the Zwicky Transient Facility survey
Faltová, N.; Kallová, K.; **Prišegen, M.**; Staněk, P.; Supíková, J.; Xia, C.; Bernhard, K.; Hümmerich, S.; Paunzen, E.
Astronomy & Astrophysics, **656**, id.A125, 17 pp. (2021)

Chapter 1

Theoretical background

1.1 Introduction

Black holes (BHs), neutron stars (NSs), and white dwarfs (WDs) are the ultimate fate of almost all stars that have ended their lives since the beginning of the Universe. These so-called compact objects (or remnants) are the inevitable consequence of the physical mechanisms powering stars that have burned hydrogen in their cores at some point in their lives. Eventually, these stars all come to a point in their evolution when the outward radiation pressure from the nuclear fusion in their interior can no longer counter the inward pull of the ever-present gravitational forces. At that point, the star begins to collapse under its own weight, and aside from some massive stars in certain mass and metallicity ranges (see, e.g. Heger et al., 2003, for a general review), creating a compact object in the end. The type of the nascent compact object is dictated primarily by the mass and metallicity of the dying star (provided that the star has been evolving in isolation). Unlike their progenitors, the compact objects can, in general, persist almost forever – long after all main sequence stars have gone out and galaxies have dispersed – into the so-called degenerate era of the Universe (assuming that our current understanding of the cosmology is correct and the Universe will keep on expanding). They will be the last vestiges of the current era until eventually, even these objects will succumb to the effects of proton decay or Hawking radiation.

While the picture painted above seems simple, the exact details behind the processes happening in the last stages of stellar evolution are not well understood. Considering the astrophysical timescales, the end stages of stellar evolution are very rapid, especially in the case of massive stars that end their lives in a supernova (SN) explosion. Because of this, the opportunities to observe SNe in the local Universe have been few. Indeed, the most recent Galactic SN to be seen was SN 1604, before the advent of modern astrophysics, and the next one seems to be long overdue. Therefore, from the observational side, we have relied heavily on the events happening in other galaxies. However, observations of such distant events have had inherent limitations. A breakthrough came in 1987 when SN 1987A exploded in the Large Magellanic Cloud. It was the first time since the invention of the telescope that a core-collapse SN was visible to the naked eye. Its relative proximity and brightness allowed spatially resolved studies in different epochs after the explosion, the detection of its neutrino emission, gamma-ray line radiation from radioactive decay, emergence of the newly-formed NS, and pinpointing its progenitor – just to list a few (e.g., Gilmozzi et al., 1987; Matz et al., 1988; Boggs et al., 2015; McCray and Fransson, 2016; Cigan et al., 2019; Page et al., 2020; Greco et al., 2021, and the references therein). This was not possible for any other SN before and we have not been able to investigate any other SN in this

much detail ever since. This event has provided much insight into core-collapse SNe[1] and served as a calibrator for more distant SN events.

Nevertheless, to gain a more complete understanding of the last stages of stellar evolution and stellar death, rare and transient events such as SNe are not sufficient. Even the supernova remnants (SNRs) and planetary nebulae (PNe; which form as a consequence of the death of a lower-mass star) have lifetimes in the order of several ten thousand years. Due to the scarcity of high-mass stars and the observational limitations, we are aware of about 300 SNRs (Green, 2019) and the known number of planetary nebulae is about an order higher (e.g., Chornay and Walton, 2021; González-Santamaría et al., 2021).

Therefore, studying the compact objects can be of great importance as it can potentially yield a lot of information about the terminal phases of stellar evolution. While these compact objects are completely unlike their stellar progenitors, they can, in certain cases, encode some information about them and the process of stellar death through their nature, kinematics, mass, magnetism, age, and current temperature (where applicable - depending on the nature of the compact object). This can also be said about the more transient phenomena that can be associated with the end of stellar life, such as PNe and SNRs.

One of the most fundamental questions about the evolution of massive stars is, in which mass range do they explode as core-collapse SNe and where they otherwise collapse to BHs without explosions. Where is the stellar mass boundary between the formation of NSs through SNe and WD formation? How is this affected by metallicity, binarity, or rotation? How much matter is lost during the last stages of stellar lives?

While stellar evolution theory gives us some rough predictions on the ultimate fates of stars, observational clues that connect the properties of SNe, SNRs, compact objects, stellar progenitors, and stellar populations associated with them are invaluable and play an important role in constraining the theory.

1.2 *Gaia* mission

In this section, I give a brief introduction to the *Gaia* mission (Gaia Collaboration et al., 2016b), as it forms the backbone of much of the research presented in this thesis. Recent advances in astrometric techniques and instrumentation have brought us to an era where the uncertainties in the astrometric measurements reach the levels of microarcseconds (μas). These capabilities are available across various wavebands: Very-long-baseline interferometry (VLBI) at radio wavelengths, the GRAVITY instrument in the infrared domain, and the *Hubble Space Telescope* (HST) in the optical in its spatial scanning mode. However, it was the launch of the *Gaia* mission that truly revolutionized astrometry in the optical domain, having a significant impact in all fields of astronomy (see, e.g., Brown, 2021, for a recent review of astrometry and its impact).

1.2.1 Need for space-based astrometry

To illustrate the unsatisfactory state of affairs for optical ground-based astrometry, one can inspect the catalogs of parallaxes that were available before the advent of space-based astrometry. Parallaxes are extremely useful for many applications as they provide means of determining model-free distances. This is crucial for measuring the

[1] This SN and its transition into a SNR is still a target of many observations using cutting-edge instruments. Also, still to this day – more than 30 years after its explosion – this SN is a focus of regular dedicated conferences.

fundamental parameters of objects that are distance-dependent, and for calibrating other means of distance estimation (e.g., van Altena, 2012). The highest measurement accuracies were needed for parallax programs. The state-of-the-art catalog of that era was 'The general catalog of trigonometric parallaxes' (van Altena, Lee, and Hoffleit, 1995), with parallaxes for ∼8000 stars. The cataloged parallaxes suffered from large uncertainties, with the mode at ∼10 milliarcseconds (mas). Apart from that, the catalog was inhomogeneous due to the varying nature of the data underlying the parallax results.

To address the problems connected with obtaining more precise astrometry, the first proposals for making astrometric observations from space were put forward back in the 1960s. The main advantages of an astrometric space mission are:

- The absence of an atmosphere results in sharper images, as the systematic and random effects of refraction and turbulence are eliminated.
- Gravity-free environment eliminates the differential mechanical deformation of the instrument as it is pointed in different directions.
- Space is thermally and mechanically very stable.
- A large part of the sky is accessible for a single instrument at any given time, and over a few months, the whole sky is accessible. This ensures the homogeneity of the survey.
- Due to the points above, it is possible to use two telescopes with viewing directions separated by a large angle, and with the images projected onto a common focal plane. This arrangement has many advantages, most notably it allows the measurement of absolute as opposed to relative parallaxes.
- Photometric data of uniform quality can be collected during the mission. They can be used to account for instrument chromatic effects but they also have their own scientific value.

Naturally, space-based missions also bring their own sets of challenges and disadvantages, such as stray light and data transfer issues (e.g., van Altena, 2012; Brown, 2021).

These early proposals eventually brought about the HIPPARCOS (HIgh Precision PaRallax COllecting Satellite) mission. This satellite, launched in August 1989, was the first space mission dedicated to astrometry. HIPPARCOS produced two catalogs. The main one, Hipparcos Catalogue (Perryman et al., 1997), gives astrometric data for about 118000 objects with milliarcsecond accuracy and single-band photometry. A later re-reduction of the mission data by van Leeuwen (2007) further improved the astrometric accuracy. The Tycho Catalogue, derived from the auxiliary star mapper data, provides lower-precision astrometry for more than a million objects and photometry in two bands. A subsequent re-reduction and analysis of the star mapper data, and combination with ground-based catalogs resulted in the more precise Tycho-2 Catalogue with ∼2.5 million objects (Høg et al., 2000). These data proved to be groundbreaking in many areas of astrophysics, and the review by Perryman (2009) based on ∼5000 papers demonstrates the importance of astrometry to many research topics.

1.2.2 Gaia overview

Gaia is the ESA space astrometry mission, launched in December 2013, and can be considered the successor of HIPPARCOS. The currently operating *Gaia* mission has

little in common with its original proposal, submitted to ESA in 1993. At that time, it was believed that interferometry was the most suitable choice to obtain accurate astrometry needed for investigations on the Galactic scales. Therefore GAIA, an acronym for *Global Astrometric Interferometer for Astrophysics*, was planned to be a scanning satellite using three stacked interferometers. The project was afterward modified when the subsequent studies showed that interferometry was not the best solution. The *Gaia* mission that was approved by ESA in 2000 was based on using CCDs (charge-coupled devices) in (non-interferometric) imaging mode, its name no longer being an acronym. The implementation phase started in 2006, with EADS Astrium (later renamed Airbus Defence and Space) as the prime industrial contractor for building the spacecraft and payload. Meanwhile, the large and complex task of processing and analysis of the mission data was entrusted to a consortium of scientists throughout Europe, the Gaia Data Processing and Analysis Consortium (DPAC). A few weeks later after its launch, *Gaia* arrived at its operating point, the second Lagrange point (L_2) of the Sun-Earth-Moon system, which was chosen to facilitate uninterrupted observations. *Gaia* moves around L_2 in a Lissajous-type orbit with a period of ∼180 days. The nominal science operations phase started in the summer of 2014 and was originally planned to last five years, after a half-year period of commissioning and performance verification (Gaia Collaboration et al., 2016b, and the references therein).

Gaia carries two three-mirror anastigmatic telescopes, with apertures of 1.45 m × 0.5 m, which illuminate a shared focal plane. The fields of view of the telescopes are separated by 106.5°. This basic angle is an essential aspect of *Gaia* measurement principle because it allows deriving absolute parallaxes. Every six hours, *Gaia* spins around the axis perpendicular to the lines of sight of the telescopes. This allows *Gaia* to determine the astrometric parameters for a large number of objects by combining a much larger number of essentially one-dimensional (along-scan) angular measurements in the focal plane. The continuous scanning motion of the satellite is designed so that every object is observed many times over the mission lifetime, in directions that are geometrically suitable for the determination of the astrometric parameters. The measurement principle also provides a globally consistent reference system for the positions and proper motions, which is tied to the extragalactic reference system (ICRS) through *Gaia*'s observation of quasars.

The performance improvements compared to the HIPPARCOS mission are the result of several factors. Firstly, *Gaia* carries much larger optics, which gives much-improved resolution and light-collecting area. Secondly, the CCDs aboard *Gaia* have a wider spectral range and much better efficiency than the HIPPARCOS photomultipliers. Most importantly, CCDs can observe tens of thousands of objects in parallel, while the main HIPPARCOS detector could observe only one object at a time. The CCDs of *Gaia* have a pixel size of 10 μm × 30 μm, matched to the optical resolution of the instrument and the effective focal length of 35 m. The focal plane carries 106 CCD detectors, arranged in a mosaic of seven across-scan rows and 17 along-scan strips, totaling almost a billion pixels (see Fig. 1.1). The autonomous onboard processing system detects any source brighter than ∼20 mag as it enters the skymappers at the left side of the focal plane, then tracks the object as it crosses a series of CCDs dedicated to the astrometric, photometric, and radial velocity measurements. Time-delayed integration (TDI) is used to accumulate photo-electrons into a sharp image as the source travels across a CCD. The wide dynamic range of *Gaia* is attained by progressively reducing the integration time for bright sources (below 13 mag) through gates in the CCD detectors. These hold back and discard the photoelectrons accumulated before the gate. To fit the obtained data into the telemetry budget, only the

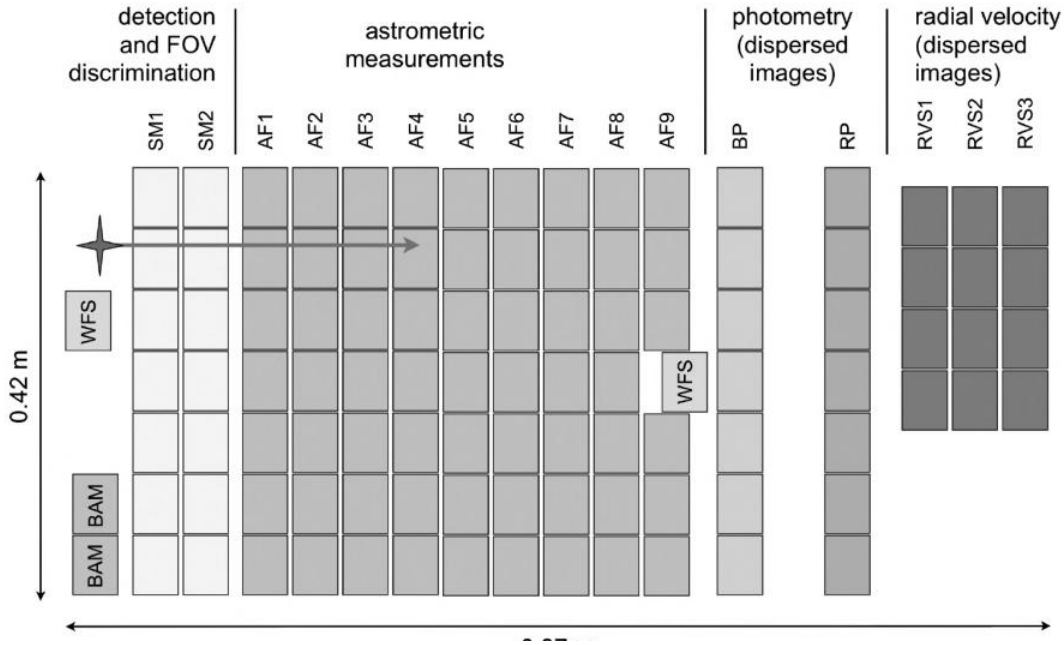

FIGURE 1.1: Schematic image of the focal plane assembly showing the CCD layout. Images travel from left to right, crossing, in turn, the skymappers (SM), astrometric field (AF), blue photometer (BP), and (some of them) the radial velocity spectrometer (RVS). The CCDs for the basic-angle monitor (BAM) and wavefront sensors (WFS) used for in-orbit optical adjustments are also shown. Figure reproduced from van Altena (2012).

pixels around the source are read out and transmitted. For bright sources, the full 2D window around the source is transmitted, while for fainter sources the window pixels are summed in the direction perpendicular to the scanning direction, which yields 1D image profiles which are then transmitted to the Earth (van Altena, 2012; Gaia Collaboration et al., 2016b; Brown, 2021).

Most of the *Gaia* CCDs are dedicated to astrometry, forming the Astrometric Field (AF). However, the source fluxes are also derived from the AF images. These fluxes are collected as the *Gaia* broadband astrometry in the G band (covering the range 330–1050 nm). Aside from that, *Gaia* also collects multicolor photometry for all stars and radial velocities for all stars brighter than ∼17 mag. *Gaia*'s dedicated photometric instrument consists of two low-resolution slitless prisms dispersing the light entering the field of view. The first disperser – called Blue Photometer (BP) – covers the spectral range 330–680 nm; the second one – Red Photometer – operates in the range 640–1050 nm. Two photometric bands, $G_{\rm BP}$ and $G_{\rm RP}$, are defined from the integrated flux in the prism spectra (van Altena, 2012; Gaia Collaboration et al., 2016b; Brown, 2021).

Similarly, radial velocity measurements are made for the brighter objects with a slitless grating Radial Velocity Spectrometer (RVS), which collects spectra over a narrow wavelength range 847–874 nm at a resolution of ∼11000. This spectral region hosts strong lines, most notably the Ca II triplet, which permits robust radial velocity determinations, at the few km/s accuracy levels, for a wide range of late spectral classes (Cropper et al., 2018).

1.2.3 *Gaia* Data Release 2

Unlike the HIPPARCOS mission, the *Gaia* collaboration does not have data rights. After processing, calibration, and validation inside DPAC, data are made available to the world without limitations. For the highest data quality, it is necessary to wait until the end of the mission lifetime and the subsequent data processing. However, to provide some data to address important science cases that do not require the data of the highest attainable quality, several intermediate data releases have been planned throughout the *Gaia* lifetime, with roughly a yearly cadence. The first of these, referred to as the Gaia Data Release 1 (Gaia DR1; Gaia Collaboration et al., 2016a), contained two astrometric data sets. The first one was the Tycho-*Gaia* astrometric solution (TGAS) which provided positions, proper motions, and parallaxes for over two million sources. This was obtained by combining the *Gaia* data with the astrometry of the stars in Hipparcos and Tycho-2 Catalogue. The secondary dataset contained positions for over a billion sources.

The Gaia Data Release 2 (hereafter GDR2; Gaia Collaboration et al., 2018) was released in April 2018. It is based on 22 months of data collected between July 2014 and May 2016. This is a significant improvement over the Gaia DR1 which was based on observations collected in the first 14 months of *Gaia*'s science operational phase. It is also the first data release where the astrometry is completely based on the *Gaia* data – no longer dependent on the Tycho-2 Catalogue. The reference epoch for GDR2 is J2015.5. The contents of GDR2 are as follows:

- Positions on the sky, parallaxes, and proper motions for more than 1.3 billion sources, with a limiting magnitude of G=21 mag and a bright limit of $G \approx$3 mag.
- Median radial velocities for more than 7.2 million stars with a mean G magnitude between about 4 and 13 mag and an effective temperature in the range of about 3550 to 6900 K.
- G magnitudes for more than 1.69 billion sources.
- Positions on the sky combined with mean G magnitude for 361 million sources, where the astrometric data were not of sufficient quality to derive the full astrometric solutions.
- $G_{\rm BP}$ and $G_{\rm RP}$ magnitudes for more than 1.38 billion sources.
- Effective temperatures, extinctions, reddenings, luminosities, and radii for a subset of stars.
- Epoch astrometry for 14000 known solar system objects, variable star classifications for over 550000 sources, and crossmatches of GDR2 with external catalogs (Gaia Collaboration et al., 2018).

Mean uncertainties for some of the parameters that are relevant for the work presented in this thesis are listed in Table 1.1.

While the advent of GDR2 brought precise astrometry for an unprecedented number of sources, it still suffers from various limitations. Some of the relevant ones are:

- All sources are considered as single stars for the astrometric solution.
- Errors of the astrometric parameters cannot be described separately. Strong correlations exist between astrometric parameters and need to be taken into

Parameter	Typical uncertainty
position & parallax (full astrometric solution)	0.02–0.04 mas at $G < 15$
	0.1 mas at $G = 17$
	0.7 mas at $G = 20$
proper motion (full astrometric solution)	0.07 mas yr^{-1} at $G < 15$
	0.2 mas yr^{-1} at $G = 17$
	1.2 mas yr^{-1} at $G = 20$
Mean G band photometry	0.3 mmag at $G < 13$
	2 mmag at $G = 17$
	10 mmag at $G = 20$
Mean $G_{\rm BP}$ and $G_{\rm RP}$ band photometry	2 mmag at $G < 13$
	10 mmag at $G = 17$
	200 mmag at $G = 20$

TABLE 1.1: Mean uncertainties of the GDR2 data relevant for this thesis. Adapted from Table 3. in Gaia Collaboration et al. (2018).

consideration for many science cases. The relevant correlation coefficients are included in the GDR2 archive for all sources with the full astrometric solution.

- Parallax systematics exist depending on celestial position, magnitude, and color, and are estimated to be below 0.1 mas. There is a significant average parallax zero-point of about -30 μas.
- The astrometric uncertainties listed in the GDR2 are derived from the formal errors resulting from the astrometric data treatment and may be underestimated by several percent.
- In crowded regions and near very bright sources, the photometric measurements from BP and RP suffer from an insufficiently accurate background estimation and from the lack of specific treatment of blending and decontamination from nearby sources. This leads to measured fluxes that are inconsistent between the G, and the $G_{\rm BP}$ and $G_{\rm RP}$ bands in the sense that the sum of the flux values in $G_{\rm BP}$ and $G_{\rm RP}$ may be significantly larger than that in G. The quality flag that can be used to indicate the presence of this effect is included in the GDR2 archive (flux-excess factor).

A more complete discussion of the GDR2 limitations can be found in Gaia Collaboration et al. (2018) and Lindegren et al. (2018).

Significant improvements have been made with the release of the astrometric data in the most recent *Gaia* Early Data Release 3 (EDR3). Additional months of observations have brought further refinements – parallax precisions have increased by ∼30 % and proper motion precisions have increased by about a factor of two as compared to the GDR2 (Gaia Collaboration et al., 2021; Lindegren et al., 2021b). Additionally, further suppression of the systematic errors, the inclusion of new quality flags, and diagnostic parameters further facilitate more accurate analyses that rely on the astrometric parameters.

1.3 Star clusters

Star clusters are a broad term for the groupings of stars with a common origin. Most often, they are divided into open clusters (OCs) and globular clusters (GCs). However,

in the broad sense, they also include stellar associations, and sometimes even moving groups and OC remnants. Since there exists a continuous distribution of sizes and densities between these structures, making the distinction arbitrary, I will refer to all these objects as 'clusters' in this work. Nevertheless, the typical properties of the main star cluster subclasses can be summarized as follows:

OB associations: O and B stars are not distributed in the sky randomly and they often form sparse groups of co-moving stars. These groups are known as OB associations. Although these associations are too sparsely populated to be gravitationally bound, their internal velocity dispersion is small enough that they can be identified as overdensities in velocity space. Their sizes range from a few tens to a hundred pc, with typical densities of 0.001–0.1 $M_\odot\,pc^{-3}$. They generally exhibit complicated substructures – often containing OCs or star-forming regions within their boundaries. Despite their name, these groupings are known to include lower-mass stars and pre-main sequence stars, following a continuous mass function. Since they are not gravitationally bound, they quickly disperse into the Galactic field. Therefore, all OB associations are young, with their ages up to a few tens Myr. OB associations are observed throughout the Galactic disk and their distribution has been used to trace the spiral structure of the Milky Way, map young stars, and star formation studies (see, e.g., Wright, 2020; Wright et al., 2022, for a recent review).

Globular clusters: GCs are dense groups of stars, characterized by being compact (with radii up to a few tens of pc), very old (with ages of $\sim$ 10 Gyrs), and, in the context of the Galaxy, representative of the halo, thick disk, and bulge, but absent in the thin disk. GCs contain a high number of stars (up to a few million for the large GCs) packed into a relatively small volume, where the stellar densities can reach up to 1000 stars/pc^3 in GC cores. This extreme number of members means that the total GC masses can reach up to several million $M_\odot$. Around 160 GCs are known in the Galaxy[2], with perhaps a couple more being undiscovered. Due to their old ages, they are often metal-poor and have quite extreme kinematics. There is evidence that the peak of the formation of GCs pre-dates most of the star formation in galaxies (as some GCs have ages comparable to the age of the Universe) and that they may have had an important role in the early galactic evolution. Therefore, except perhaps in certain extragalactic systems and at cosmological distances, direct empirical study of their formation process is not possible (Gratton et al., 2019, and the references therein).

Open clusters: OCs are irregularly-shaped groups of stars, most typically containing a few hundred members. Total OC masses mostly range from 10–10^4 $M_\odot$. They usually consist of a distinct dense core, surrounded by a more diffuse corona of cluster members. Typical stellar densities in OCs can go from 0.1 to about 10 stars/pc^3. On average, they are relatively young objects (the ages of most OCs are below 1 Gyr) and are found in the Galactic disk. The formation of new Galactic OCs is still ongoing. Due to their low ages, OCs generally have metallicities similar to that of the Sun, as they are formed from the interstellar matter that has already been enriched with metals originating from the previous generation of stars (see, e.g., Moraux, 2016, and the references therein).

The properties listed above are relevant for the majority of 'typical' objects of these classes. However, there are some objects that lie on the boundaries of these classifications. For instance, some massive young clusters such as Arches and Westerlund 1 have dimensions and ages consistent with OCs, but the total masses typical for GCs (Portegies Zwart, McMillan, and Gieles, 2010).

[2] https://people.smp.uq.edu.au/HolgerBaumgardt/globular/

Star clusters form within the dense cores of giant molecular clouds. Cluster studies suggest that over 90% of stars form in clusters containing more than 100 members with $M > 50$ $M_\odot$ (Lada and Lada, 2003). These stars remain spatially correlated on physical scales up to ∼100 pc during the first 100 Myr (approximately corresponding to lifetimes of ∼4 $M_\odot$ stars, which are greater than the lifetimes of core-collapse SNe progenitors), even if the cluster is not gravitationally bound (see, Krumholz, McKee, and Bland-Hawthorn, 2019, for a review on star cluster formation and evolution).

Due to a common origin of the cluster stars in a single star formation event within a giant molecular cloud, the following properties should hold for all cluster members:

- All cluster members lie at approximately the same distance from the observer. The cluster dimensions are usually negligible as compared to its distance from the Earth. Therefore, the amount of extinction should be very similar for most cluster members, as they all lie in the same line of sight (provided that the cluster is sufficiently distant and compact). This does not hold for large and close associations and young clusters that still retain some material left over from the star formation episode.

- All cluster stars have approximately the same age (± timescale of star formation for different stellar masses of a few Myr).

- All cluster stars share the same initial metallicity (± some chemical inhomogeneities may be present in the parent molecular cloud).

- All cluster stars share the same kinematic properties in the Galactic context – they all move together through the Galaxy. Some kinematical dispersion of a few $\mathrm{km\,s^{-1}}$ exists among the cluster members (e.g., Moraux, 2016).

Because of these shared properties, star clusters play a fundamental role as tools to investigate the mechanisms of galaxy formation and evolution, test theoretical stellar evolution models, and calibrate the cosmic distance ladder (i.e. by observations of objects that are considered the 'standard candles' such as classical Cepheids), among others (e.g. Moraux, 2016; Wright, 2020; Cantat-Gaudin, 2022, and the references therein).

In this thesis, I am interested in star clusters as birth sites of compact stellar remnants and other objects connected with the terminal phases of stellar evolution. These objects typically do not retain many fundamental properties of their progenitors, such as the initial mass, chemical composition, or kinematics. Therefore, if these objects were to be studied in isolation in the Galactic field, not much could be determined about their stellar progenitors. However, if these objects are members (or former members) of a star cluster, their progenitors must have shared a common age, initial metallicity, and overall kinematics with the rest of the cluster members. This information can potentially shed some light on the physics of compact object formation.

For this reason, obtaining precise cluster parameters – namely distances, ages, kinematics, and metalicities is pivotal. These parameters (except for kinematics) can be obtained by, e.g., isochrone fitting of their color-magnitude diagrams (CMDs), which is the most widely used method of cluster parameter estimation. Cleaner cluster CMDs for isochrone fitting, and more precise distances and kinematics can be obtained by using the astrometry from the *Gaia* mission. A slew of other methods, particularly for the age estimation, exist (see, Barrado, 2016, for a discussion). Cluster metallicities can also be obtained by spectroscopic studies of the cluster members (Netopil et al., 2016; Carrera et al., 2019; Donor et al., 2020; Spina et al., 2021; Netopil et al., 2022).

1.3.1 Open cluster census

To study exotic objects such as the stellar remnants in relation to star clusters it is necessary to have a reliable and extensive cluster census and lists of their members. However, our location within the Galactic disk is not favorable for this. Due to the severe extinction within the disk and projection effects, it has been very hard to gain knowledge on the cluster population further than about 1 kpc. The situation has improved with the advent of *Gaia*, making it possible to detect, characterize, and disentangle many stellar populations. However, the progress is still incremental. Even with *Gaia*, OB associations are hard to detect due to their low densities, and it is even harder to get a full census of their stellar members. Very large areas of the sky need to be covered to identify a few members among many thousands of unrelated field stars based on colors and astrometry. Despite this, the sample of OB associations is expanding (Wright, 2020, and the references therein). The situation is better for GCs. Since many of them are located in fields with low stellar densities, it is reasonable to assume that almost all objects projected onto these compact clusters are associated with them. Therefore, GCs have been extensively studied for quite some time by both ground and space-based missions across all wavelengths. Stellar remnants associated with GCs and their observations will be discussed in more depth in the subsequent sections.

Since OCs are more dense and compact than associations, it is easier to search for them. In the pre-*Gaia* era, the most widely used catalogs of OCs and their fundamental parameters were the New catalogue of optically visible open clusters and candidates by Dias et al. (2002) and the Global survey of star clusters in the Milky Way of Kharchenko et al. (2013). The catalogs included ∼3000 OCs and OC candidates. One of the main issues of that era was the lack of astrometric precision, meaning that the members of an OC and field stars in the proper motion diagram (vector point diagram; VPD) were sometimes very hard to distinguish, and the OC members were often highly contaminated by field stars.

The GDR2 data have significantly furthered the study of OCs with the determination of new memberships for an unprecedented number of stars and clusters. Cantat-Gaudin et al. (2018) systematically searched for members around more than 3000 cataloged OCs, mostly from the large pre-*Gaia* OC catalogs by Dias et al. (2002) and Kharchenko et al. (2013), using positions, proper motions, and parallaxes from GDR2. Mean astrometric parameters, including distances, were derived for 1229 OCs, and membership probabilities were computed for $\sim 4 \times 10^5$ stars. A large number of OCs cataloged in the pre-*Gaia* era (around 50%) could not be confirmed to exist by *Gaia* or were proven to be chance alignments. The number of OCs and OC candidates has also increased either through serendipitous discoveries (e.g., Ferreira et al., 2019; Cantat-Gaudin et al., 2019) or systematic searches. For instance, Castro-Ginard et al. (2018), Castro-Ginard et al. (2019), and Castro-Ginard et al. (2020) discovered more than 600 new OCs by developing a machine learning procedure to detect over-densities in the 5D parameter space of positions, proper motions, and parallaxes. Sim et al. (2019) found 207 OCs by the visual inspection of VPDs. Liu and Pang (2019) identified 76 new OCs by dividing the sky into small 3D regions and employed a friend-of-friends algorithm to search for overdensities in the 5D space of positions, proper motions, and parallaxes. A systematic search carried out in a small field projected towards the Galactic bulge yielded 34 new OCs and OC candidates (Ferreira et al., 2021). Hunt and Reffert (2021) compared the potential of the modern clustering algorithms DBSCAN, HDBSCAN, and Gaussian mixture models for OC discovery using GDR2 data. During these comparisons, they discovered 41 new OC

candidates.

Even this non-exhaustive listing clearly showcases the impact of the GDR2 on OC discoveries and characterization. However, all these OCs were discovered using different methodologies. To compile a large OC catalog, all these OC candidates needed to be verified and characterized in a homogeneous way. Updated catalogs of membership probabilities and OC parameters also including some these new OCs discovered by the aforementioned authors are provided in Cantat-Gaudin and Anders (2020), Cantat-Gaudin et al. (2020), and Dias et al. (2021).

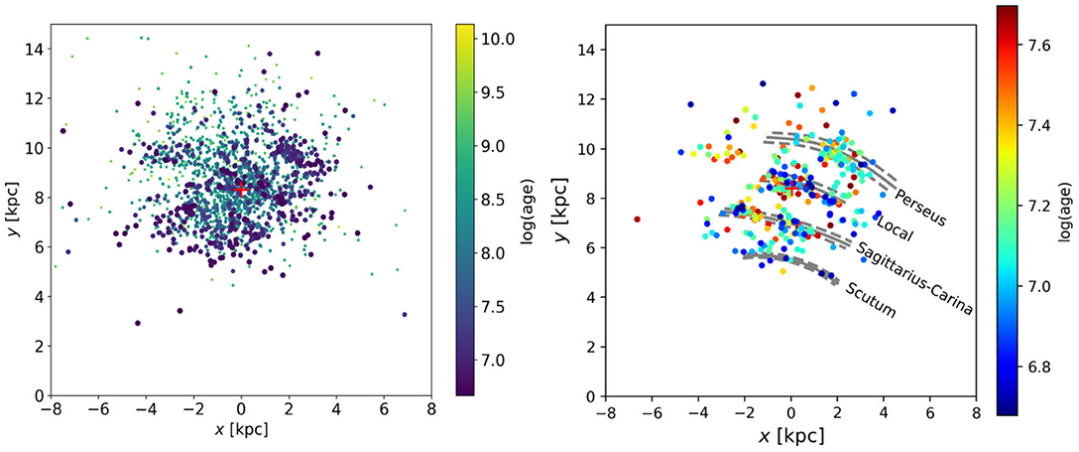

FIGURE 1.2: Left: Distribution of the ∼1750 OCs from the catalog of Dias et al. (2021) in the Galactic plane. Right: OCs with ages lower than 50 Myr. In light-gray are the present zero-age Galactic arms positions. The Sun is marked by the red cross at coordinates (0, 8.3) kpc and the Galactic center is at (0,0). Figure reproduced form Monteiro et al. (2021).

The improvements in astrometry brought in EDR3 (Gaia Collaboration et al., 2021; Lindegren et al., 2021b) further increased the chances of detecting many new and more distant OCs. Castro-Ginard et al. (2021a) reported more than 600 OC candidates using this new dataset, mostly at distances beyond 1 kpc. He et al. (2022) also reported 541 new OC candidates. Around 60 new strong OC candidates were also recently identified by Li et al. (2022). As evidenced by these recent OC discoveries, the list of known OCs within 2 kpc may remain incomplete. Because of that and due to the utility of OCs for many astrophysical applications and the improvements in the astrometry and machine learning methods, it is likely that the current pace of OC discoveries will continue into the foreseeable future.

To mitigate the effects of extinction, it is possible to search for clusters in the infrared (e.g., Camargo, Bica, and Bonatto, 2016; Ivanov et al., 2017). Bica et al. (2019) presented a large catalog of star clusters, associations, and possible candidates, built using the data from the optical band to the far-infrared. The downside of the cluster studies in the infrared is that there is a general lack of precise astrometry – parallaxes and proper motions – that would enable the use of the astrometric criteria for the cluster discovery and construction of lists of the cluster members. Therefore, the physical reality of many of these clusters is not secure and their membership lists are significantly contaminated.

1.3.2 Small Magellanic Cloud star cluster population

The Magellanic Clouds — consisting of the Large Magellanic Cloud (LMC) and the Small Magellanic Cloud (SMC) – are the two most prominent and most well-studied satellite galaxies of the Milky Way. Star clusters are routinely studied also in other galaxies, the LMC and SMC are no exceptions. In this section, I briefly discuss the SMC star clusters, as I will utilize them in this thesis. The study of clusters in the SMC has an extensive history that cannot be properly described here. Due to several advantages of studying stellar populations within the SMC, there has been a significant effort to provide the most complete and clean list of the SMC clusters and their properties.

One of the more recent works that compiled the SMC cluster population is by Chiosi et al. (2006), who determined the ages of almost 500 SMC star clusters younger than 1 Gyr using isochrone fitting. Bica et al. (2008) presented the largest list of the SMC clusters with their central coordinates, values of major and minor diameters, and position angles. However, they did not derive cluster ages, reddenings, and masses. Another large study by Glatt, Grebel, and Koch (2010) lists the ages and reddening of 324 objects in the SMC. They found that the cluster age distribution seems to have peaks at 160 Myr and 630 Myr, which they attributed to the interaction between the LMC and the SMC that resulted in enhanced star formation which gave rise to these peaks. More recent large catalogs of the SMC clusters that also include their ages were compiled by Nayak et al. (2018) and Piatti (2018).

1.4 Core-collapse supernovae

Core-collapse supernovae (CCSNe) are rapid and violent explosions marking the end of the lives of massive stars. At this evolutionary stage, most massive stars have grown an iron core that cannot be supported by hydrostatic pressure and collapses. The resulting explosion releases a large amount of energy in various forms (neutrino radiation, photons, kinetic energy) and completely destroys the progenitor star. CCSNe play a key role in nucleosynthesis, the formation of NSs and BHs, and in the morphological and chemical evolution of galaxies, interstellar medium (ISM), and even intergalactic medium. CCSNe are important sources of cosmic rays, neutrinos, and gravitational waves. CCSNe can also produce dust, and trigger star formation when the shock waves generated in the explosion impact and compress surrounding molecular clouds (e.g., Cerda-Duran and Elias-Rosa, 2018, and the references therein).

In general, SNe are divided into two groups according to the explosion process: CCSNe and thermonuclear SNe. In addition to this, an observational classification scheme is used as well (see Fig. 1.3 Minkowski, 1941), where SNe are divided based on the presence of hydrogen absorption in their spectra, where Type I SNe do not show hydrogen absorption and Type II SNe do. All Type II SNe are CCSNe, but Type I SNe can be either CCSNe or thermonuclear SNe. Type I SNe are usually divided into three further classes:

- Type Ia SNe, which have Si absorption lines in their spectra and are associated with thermonuclear SNe,
- Type Ib SNe (no Si in their spectra), which are CCSNe that have lost their hydrogen envelope due to mass loss (through stellar winds) or binary interaction,
- Type Ic SNe (no Si and no He in their spectra), which are similar to Type Ib SNe, but the mass loss seems to have stripped even the deeper helium-rich layers of the SN progenitor.

Type II SNe are divided into two main classes based on optical spectroscopy and light curve shapes: Type IIL (linear light curve) and Type IIP (light curve with a plateau). The main differentiating factor between them is the thickness of the hydrogen envelope of their progenitors. Type IIP SNe are the most common type of CCSNe, with red supergiant progenitors that still have massive hydrogen envelopes. Type IIL progenitors probably have thinner hydrogen envelopes, that have been partially stripped due to stellar winds or binary interaction (see, e.g., Vink, 2012; Cerda-Duran and Elias-Rosa, 2018, and the references therein).

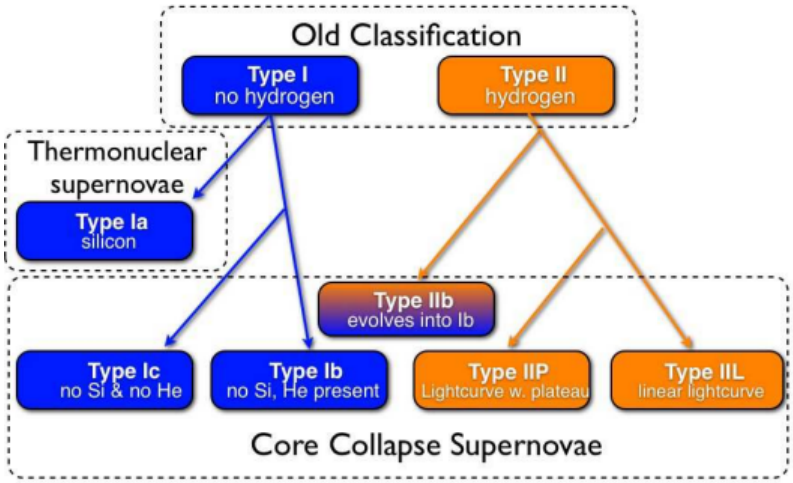

FIGURE 1.3: Observational classification of SNe, based on spectroscopy and shape of light curves. Figure reproduced from Vink (2012).

The CCSNe have been studied, both theoretically and observationally, for more than half a century. Yet, their explosion mechanism is not entirely understood. Just prior to collapse the star consists of different layers with the products of the different consecutive burning stages, starting with the unprocessed hydrogen-rich envelope on the outside. Below it there is helium, then carbon, neon and magnesium, oxygen, then silicon-group elements, and ultimately iron-group elements at the stellar core. The creation of the iron-group core marks the terminal phase of the star's life since no energy can be extracted from the fusion of iron. The iron core is fed by the surrounding silicon-burning shell and grows until it reaches a mass of 1.2–2 $M_\odot$, which is just below its Chandrasekhar mass, which depends on its electron fraction and temperature. At some point, the core starts to collapse due to two processes. First, electron captures by atomic nuclei trap electrons which reduces the electron pressure, while the neutrinos that are produced escape the core, carrying away energy. Second, at the extreme core densities, the photodisintegration of iron nuclei further cools down the core. Both of these processes lower the value of the Chandrasekhar mass until the pressure is not able to counteract the self-gravity of the core and the collapse begins. The dense core of the star implodes within less than a second to extreme densities and a proto-NS is created in the core center. The formation of a proto-NS suddenly terminates the collapse, which drives a rebound shock wave outwards through the infalling outer core. This shock wave should have resulted in an SN, but many theoretical simulations show that the shock wave stalls rather quickly. This has been a major problem in SN simulations for many decades. However, recent studies indicate that the shock wave may be re-energized by absorption of a fraction of neutrinos escaping the core,

neutrino-driven turbulence, and spherical symmetry breaking. Therefore, the shape of the re-energized shock wave and the resulting SN will be highly asymmetric (see, e.g., Janka, 2017; Cerda-Duran and Elias-Rosa, 2018; Burrows and Vartanyan, 2021, and the references therein for a more detailed discussion).

The ejecta of CCSNe consist primarily of stellar material, except for the inner ejecta, which contains explosive nucleosynthesis products, mostly iron and silicon-group elements. Some of these products are radioactive, such as ^{52}Ni and ^{44}Ti. The energy generated by the decay of these products heats the ejecta, which has a major imprint on the evolution of the SN light curve. The yields of these radioactive elements are dependent on the details of the explosion, for instance, the explosion energy, the explosion asymmetry, and the mass cut, which is the boundary between material that gets accreted on the NS and material that is ejected (e.g., Vink, 2012, and the references therein).

An approximate qualitative prediction of the outcomes of stellar evolution is obtained by stellar evolution theory - the mass range of CCSNe is from ∼8 $M_\odot$ to ∼40 $M_\odot$ for low-metallicity stars, or there is no upper stellar mass limit for CCSNe in stars with approximately solar metallicity or higher (see Fig 1.4).

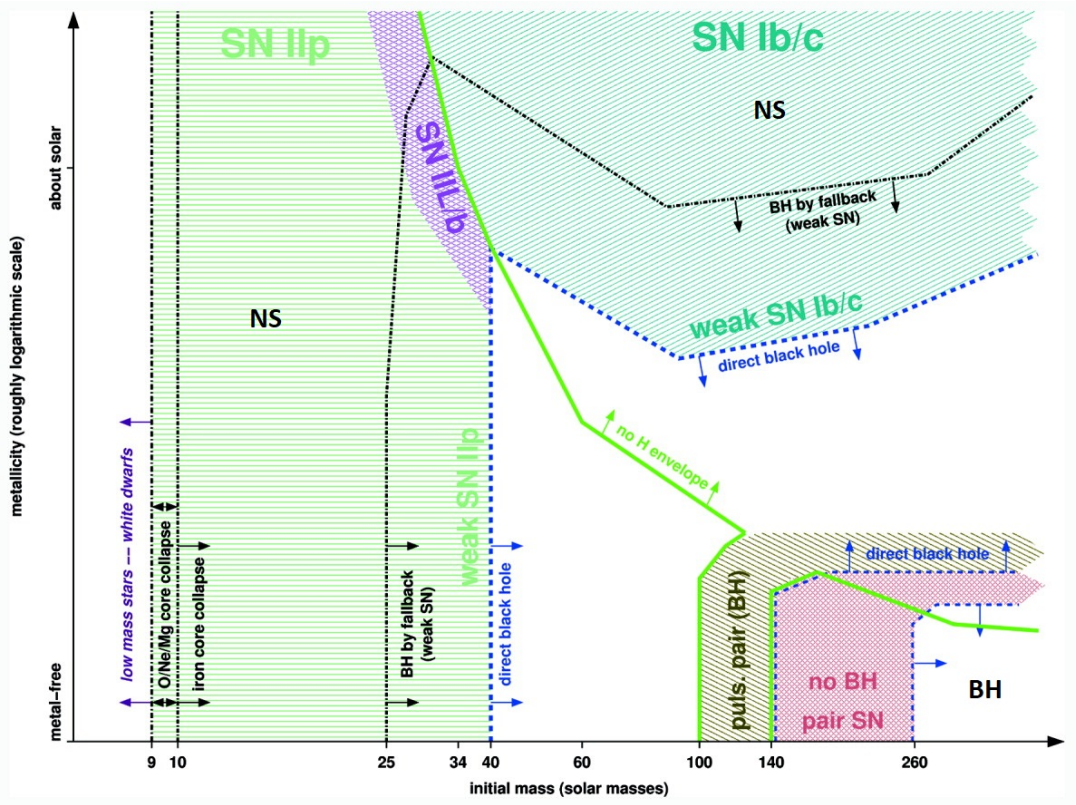

FIGURE 1.4: A qualitative view of SNe types and their outcomes of non-rotating massive single stars as a function of their initial metallicity and initial mass. Figure reproduced from Heger et al. (2003).

Aside from mass and metallicity, binarity also plays a critical role in the evolution of massive stars. Interactions with a companion can change a star's mass, metallicity, and rotation, which influences the ultimate fate of the star and the type of remnant it produces. The binarity fraction of massive young stars is very high (∼100%) and most of them are close enough that they will interact via mass exchange at some point in their lives (e.g. Sana et al., 2012). Rotation of the star also has a profound influence

on, for instance., the mass of the exploding cores, the mass and chemical composition of the envelopes, and mass loss via stellar winds (Meynet and Maeder, 2017).

Simulations of CCSNe have shown that not all massive stars explode (e.g., Sukhbold and Woosley, 2014; Sukhbold et al., 2016). There could be certain ranges in the parameter space of massive star progenitors in which stars are less likely to explode and instead collapse straight into a BH, and that there is no single mass below or above which a progenitor will explode or implode, even if the progenitor is very massive (e.g., Pejcha and Thompson, 2015). One way to determine the limits of these mass ranges is to accumulate a large sample of measured properties of CCSNe progenitors. Dedicated searches for these 'failed' SNe can be conducted as well, where one would search for disappearing stars in a series of images (e.g. Gerke, Kochanek, and Stanek, 2015).

As evidenced by extremely high velocities of isolated Galactic pulsars (e.g., Arzoumanian, Chernoff, and Cordes, 2002; Verbunt, Igoshev, and Cator, 2017), SN explosions impart a large velocity kick to the nascent NSs. The most natural explanation for these large kicks are recoils during the SN explosion directly related to asymmetric matter ejection and/or asymmetric neutrino emission. Therefore, the principle of momentum conservation in the context of asymmetric ejection can result in the observed velocities. It is known that neutrino emissions can have a dipolar component and the associated net momentum can be substantial. As neutrinos travel close to the speed of light and make up as much as 0.15 $M_\odot c^2$ of mass-energy, a small 1% angular asymmetry can yield a kick of 300 $km\,s^{-1}$. However, it is not known how the ejecta and neutrino momentum vectors are orientated to each other, and whether they have a tendency to add up or counteract each other. As the stars towards the low-mass end tend to explode more spherically, eject less core mass, and emit less energy in neutrinos, it can be expected that these stars impart low kicks to their nascent NSs. On the other hand, the more massive stars that tend to explode asymmetrically, eject more core mass, and emit more mass-energy in neutrinos, should impart substantial velocity kicks (e.g., Cerda-Duran and Elias-Rosa, 2018; Burrows and Vartanyan, 2021, and the reference therein).

The formation channel in which a BH is born influences its velocity kick. BHs can form through direct collapse, or via the delayed collapse channel, where an SN can occur, but the stellar envelope is not completely unbound, leading to a large amount of matter falling back onto the nascent NS (the so-called fallback). Since the velocity kick mechanisms occur prior to the fallback of matter on the short-lived NS and subsequent BH formation, it is plausible that BHs formed by the fallback should also receive strong natal kicks. However, the presence of fallback dampens the velocity kick. Also, since BHs are expected to have much more inertia (mass), the resulting BH velocity should be smaller. The BHs born from direct collapse are expected to receive even lower kicks. Therefore, natal kick measurements should, in principle, provide effective means of differentiating between the SN and direct collapse BH formation pathways (e.g., Mirabel, 2017; Renzo et al., 2019; Atri et al., 2019; Burrows and Vartanyan, 2021).

There is also a peculiar class of SNe, just at the mass boundary that separates NS and WD formation regimes (see Fig 1.4). Electron capture SNe (ECSNe) are a separate class of CCSNe. An ECSN progenitor is a super asymptotic giant branch (SAGB) star with a mainly oxygen and neon (ONe) core, surrounded by a thin helium shell and diffuse hydrogen envelope and an initial mass of 8–10 $M_\odot$ (Nomoto, 1984; Nomoto, 1987). For such stars, the core temperatures are not high enough to ignite Ne. Instead, the almost degenerate core grows to a mass of about $\sim 1.34\ M_\odot$, very close to the Chandrasekhar mass. At some point, neon and magnesium nuclei in the

core start absorbing electrons, which removes pressure and triggers the collapse of the core. The ECSNe progenitors have a very steep density gradient outside the core, and due to this structure, only a small fraction of neutrino energy is needed to power the explosion. The resulting explosion is weak and ejects only a small amount of matter (normally $\lesssim 1.0$ $M_\odot$). Since the explosion is very fast, convectively driven instabilities are unable to grow, leading to more symmetric explosions and rather small NS kick velocities. They are also expected to produce somewhat less massive NSs compared to classic CCSNe. ECSNe exploded even in the 1D models, which failed for other SN mechanisms. While the mass range where single stars explode as ECSNe is very narrow, it can be significantly wider for interacting close binaries (Podsiadlowski et al., 2004; Cerda-Duran and Elias-Rosa, 2018). Observationally, they are probably responsible for some sub-luminous Type II SNe, and several SN events with properties consistent with ECSNe are known (Hiramatsu et al., 2021, and the references therein).

1.4.1 Constraining SN progenitors

Due to these complexities, it is difficult for current theories to confidently predict which stars undergo core-collapse and produce an SN of a given type and which produce an NS or a BH. To constrain the SN models, it is needed to better characterize the mapping between the explosion scenario and the progenitor parameter (mass, metallicity, binarity, and rotation) distribution.

The cleanest and ideal way to get information regarding the progenitors of nearby CCSNe is by the identification of massive stars that have disappeared after the explosions in archival images. Their initial zero-age main sequence mass can be determined by using the luminosity and the color of the star and comparing them with theoretical stellar models. These models are chosen to take into account the metallicity of the SN environment, the distance of the host galaxy, and the extinction to the star, which can be derived from light curves and the spectral evolution of the SN. This was first done for SN 1987A (Gilmozzi et al., 1987). The number of cataloged SNe is of the order of several ten thousand (e.g., Guillochon et al., 2017). However, serendipitous pre-explosion images of the SN fields are still rare – only about 30 progenitors are detected at present, with the upper limits for around 40 objects constrained as well (e.g., Smartt, 2015; Van Dyk, 2017; Kilpatrick et al., 2021; Koplitz et al., 2021, and the references therein). This is understandable since the SN rate for a large spiral galaxy is roughly one event per century (e.g., Cappellaro, Evans, and Turatto, 1999; Anderson and Soto, 2013), and the largest distance where the SN progenitor can potentially be reliably resolved for photometry is a few tens of Mpc. In practice, only the HST or some of the largest ground-based telescopes equipped with adaptive optics can usually be used to reliably identify the candidate progenitor. Also, high-resolution archival images of the SN region must exist in the first place and high source densities associated with sites of recent star formation might make it impossible to reliably identify the progenitor. Moreover, this direct identification technique is reliant on the inference of the initial stellar parameters from the last, most uncertain, and unstable stages of stellar evolution. This can lead to significant biases in the derived progenitor masses.

An alternative way to determine the mass of the progenitor is to use the local stellar population around it. As massive stars are born in the same star-formation event, they should remain spatially correlated (within 50 pc) in their lifetime (e.g., Lada and Lada, 2003), which is also experimentally confirmed (e.g., Gogarten et al., 2009; Murphy et al., 2011). In this method, the age distribution of the local stellar

population around an SN is estimated and then used to measure the star formation history of the region. In short, the age of an SN progenitor can be inferred from the CMD diagram of the surrounding stellar population. By modeling a superposition of stellar populations, we can use the observed CMD and find the most likely age from theoretical stellar isochrones. Assuming the SN progenitor comes from the youngest population, it is possible to infer the progenitor mass based on stellar evolution models (e.g., Williams et al., 2018; Díaz-Rodríguez et al., 2021). This technique requires spatially-resolved photometry and can potentially be used up to ∼10 Mpc. The main disadvantage of this method is that we assume that the local stellar population has a single and well-defined starburst and that the SN progenitor was not in a close binary or a high-velocity star that did not originate in this region. Because of these factors, this method is best utilized for statistical population studies, rather than for determining accurate individual progenitor masses.

More stringent results can be obtained if SNe are observed in star clusters. Since star clusters are well-defined populations that originate from a single starburst event, it is possible to study them using integrated photometry and spectroscopy to considerable distances, much further than the previous method. Still, the best results are obtained when some of the individual cluster members can be resolved, making the information that can be obtained in this way much more detailed and reliable. For instance, a detailed study of the immediate neighborhood of SN 1987A revealed a loose young cluster with an age of 12±2 Myr, which is probably the birthplace of SN 1987A's progenitor (Efremov, 1991; Panagia et al., 2000). This was also applied to SNe in other galaxies as well (e.g. Barth et al., 1996; Van Dyk et al., 1999; Maíz-Apellániz et al., 2004; Wang et al., 2005; Crockett et al., 2008; Vinkó et al., 2009; Smartt et al., 2009; Smartt, 2015).

As can be seen here, there are still a lot of unknowns and every single new SN that we study in this way provides new insights into this complicated picture.

1.5 Supernova remnants

Supernova remnants (SNRs) are formed via the interaction of ejecta from violent SN explosions with the surrounding ISM. The SN ejecta blasted into the surrounding region contain heavy elements produced in the stellar progenitors and via explosive nucleosynthesis which chemically enriches the local ISM. Moreover, these ejecta, launched at velocities over 10^4 km s^{-1}, also drive shock waves into the ISM. After the shock wave has swept up as much ISM mass as the ejecta mass, the pressure difference between the shocked ISM and the hot ejecta drives a second shock wave back into the interior of the SNR, heating it and ejecta up to X-ray emitting temperatures. The energy deposited by the explosions drives the mechanical evolution of the ISM and cosmic rays can be accelerated in the fast-moving shocks (see, e.g., Vink, 2012, for a review). SNRs remain visible for several 10^4 yr, in contrast to a few hundred days for their parent SNe.

We know about ∼300 Galactic SNRs, arising from both the CCSNe and thermonuclear SNe (Green, 2019). Aside from many old SNRs, whose emission is mainly coming from the swept-up ISM, it is possible to use X-ray spectroscopy to distinguish between these two formation channels. It is also possible to use secondary indicators, such as the presence of an NS in the SNR, the proximity of the SNR to a star-forming region, or the distance from the Galactic plane if X-ray spectroscopy is not viable. A significant number of SNRs are also known in the neighboring galaxies. For instance, the LMC and SMC host 59 and 21 cataloged SNRs, respectively (Maggi et al., 2016;

Maggi et al., 2019). Several hundred SNRs are also visible in the more distant galaxies (see Sasaki, 2020, and the references therein).

The main limiting factor of our understanding of SNRs is their distances, which are notoriously difficult to determine accurately. The diameter, brightness, age, and all other related properties of SNRs depend sensitively on the distance. This can largely be circumvented if the extragalactic SNRs are observed, where it is often sufficient to adopt the distance to the galaxy hosting the studied SNRs. Various methods of obtaining distances to Galactic SNRs exist (e.g., analyzing the H I absorption spectra, using the empirical power-law relation between the radio brightness and the SNR linear diameter, the X-ray flux, and using the distance of the associated source, Wang et al., 2020, and the references therein). These methods generally yield ambiguous and imprecise results, and more precise techniques can be used only in some specific cases.

Recent photometric and spectroscopic sky-surveys and the release of the GDR2 have made it possible to derive more precise distances to a significant number of Galactic SNRs. For instance, by combining multi-wavelength photometric, spectroscopic, and astrometric information of the stars in SNRs sightlines, it is possible to derive the distances to some Galactic SNRs from the change of extinction with the distance of the stars toward the sightline of the SNRs, or through the detection of SNR absorption features in the stellar spectra (e.g., Zhao et al., 2020). A similar technique using red clump stars (standard candles) was used in Wang et al. (2020).

The progenitor mass of an SNR resulting from a CCSN can be obtained by comparing relative elemental abundances of SN ejecta with those in SN nucleosynthesis models. Particularly useful is the Fe/Si ratio, which is sensitive to the CO core mass and initial mass of the progenitor (see, e.g. Vink, 2012; Katsuda et al., 2018).

Similarly to SNe, the analysis of the stellar population in the vicinity of SNRs can also provide mass distributions of massive stars which can be used to infer the progenitor mass (Badenes et al., 2009; Jennings et al., 2012; Jennings et al., 2014; Díaz-Rodríguez et al., 2018; Auchettl et al., 2019; Koplitz et al., 2021). As SNRs remain observable for $\sim 10^4$ yr, assuming an SN rate of one event per century, one would naively expect to be able to make ∼100 progenitor mass estimates per galaxy, provided they are close enough for the resolved stellar population analysis. Aside from the same downsides this method has when used on SNe, there are additional caveats. Notably, the nature of the SN is not known for SNRs, meaning it is impossible to distinguish between the various classes of CCSNe based on the observations of SNRs (there is also some degree of contamination from SNRs from Type Ia SNe, that cannot be completely filtered out). Therefore, it is not possible to investigate where the boundaries between various types of CCSNe lie in terms of the progenitor mass, metallicity, and so on. Also, while this method is not affected by the particular details of a given progenitor system, it offers no direct way to probe the binarity of the system, which is relevant given the role binarity likely plays in a lot of CCSN scenarios. Another possible caveat is that the lifetime and visibility of SNRs arising from different SNe types may be different, which introduces observational biases. While this method may not yield accurate progenitor masses for individual SNRs, it can be utilized on a larger SNR population in a statistical sense, especially in other galaxies. It has provided important insights into the mass distribution of the SN progenitors, the lower mass limit, and the upper mass limit for SNe. For instance, assuming single-star evolution, Díaz-Rodríguez et al. (2018) established the minimum mass of CCSNe in the galaxies M31 and M33 of $7.33^{-0.16}_{+0.02}$ $M_\odot$ and the upper limit of $M_{\rm max} > 59$ $M_\odot$. Similar results were obtained by the combined analysis of SNRs, historically observed SNe, and the BH formation candidate in NGC 6946 by Koplitz

et al. (2021). Recently, Kochanek (2022) used this method on the Galactic Vela SNR and found out that the stellar progenitor was probably a relatively lower-mass star (8–10 $M_{\odot}$). Studying Galactic SNRs is advantageous since the nature of the created compact object is often known. While the main problem of analyzing Galactic SNRs in this manner is the lack of accurate SNR distances, it can be expected that the future *Gaia* data releases and more observational work will yield improved distances for a larger number of SNRs.

Studying an SNR in the context of its parent star cluster would be very advantageous. Most notably, it would be relatively easy to get a precise progenitor mass and its initial metallicity. One of the first literature studies of SNR-OC associations was conducted by Pauls (1977). He hypothesized that SNR G127.1+00.5 that is projected on NGC 559 might be physically related to the OC. This is merely a chance projection. Even nowadays, the distance to the SNR is highly uncertain – probably around 1.15 kpc with the upper limit of 2.9 kpc (Leahy and Tian, 2006; Zhao et al., 2020). The distance to NGC 559 is 2.8 kpc (Cantat-Gaudin and Anders, 2020) and its age of ∼260 Myr (Cantat-Gaudin et al., 2020) is too high for a likely association with a SNR. Shortly after, Kumar (1978) systematically searched for projected SNR-OC pairs and discovered two new coincidences in projection. One of them was determined to be a chance projection while the second one, SNR G291.0-0.1 and Trumpler 18, could be physical according to then available distance estimates. However, in light of the modern data, SNR G291.0-0.1 seems to lie far in the background of Trumpler 18 (Harrus, Hughes, and Slane, 1998; Cantat-Gaudin and Anders, 2020). Four more OCs (Lynga 1, Pismis 20, Stock 14, and Trumpler 21) were investigated for possible association with the projected SNRs by Peterson and Fitzgerald (1988), but none of these associations could be established.

More recently, Messineo et al. (2020) also searched for SNRs in OCs. They cross-matched the positions of SNRs from Green (2019) with the positions of OCs by Kharchenko et al. (2016). They recovered three matches: BDSB 141 with SNR G049.2–00.7, NGC 559 with SNR G127.1+00.5 (same as in Pauls, 1977), and FSR 0891 with SNR G189.1+03.0 (IC 443). Except for BDSB 141, all other OCs appear to be too old to host SNRs. Additionally, only BDSB 141 and SNR G049.2–00.7 seem to have comparable distances. According to Kharchenko et al. (2016), BDSB 141 lies at 5.8 kpc (no distance error estimate given in the catalog), and SNR G049.2–00.7 seems to lie at 5.7±1.0 kpc according to Wang et al. (2020). This pairing is very promising and merits further investigation. On the other hand, pairing between NGC 559 with SNR G127.1+00.5 is probably not physical (as discussed above). Apart from the old age of the OC (∼ 230 Myr, Kharchenko et al., 2016), FSR 0891 and SNR G189.1+03.0 lie at different distances, ∼2.1 kpc (Kharchenko et al., 2016) and 1.80±0.05 kpc (Zhao et al., 2020), respectively. Messineo et al. (2020) also conducted an equivalent cross-match with the OC catalog from Bica et al. (2019). A possible association of NGC 6834 with SNR G065.7+01.2 was proposed. While NGC 6834 seems to be rather young (∼19 Myr, Cantat-Gaudin et al., 2020), the distance to the SNR is not known and therefore their physical relation cannot be confirmed at this time.

The search for SNRs in star clusters is not limited to the Galactic objects. For instance, Camps-Fariña et al. (2016) found three currently expanding SNRs within a single young star cluster in M33. Also, the projections of star clusters near SNRs in the LMC and SMC were useful in providing tighter progenitor mass constrains (Badenes et al., 2009; Auchettl et al., 2019).

Due to the small sample of direct-imaging SN observations, the mapping between progenitors and various SN types remains unclear. However, by combining various direct and indirect SN and SNR studies, it is possible to construct a broad mapping

between massive progenitors and SN outcomes. It needs to be noted that predicting the exact mapping is not trivial and depends upon a variety of factors such as metallicity, binary interactions, mixing processes, rotation, etc. (e.g., see the discussion in Díaz-Rodríguez et al., 2021).

The minimum mass for SNe, $M_{\rm min}$, seems to be around 7–9 $M_\odot$(Smartt et al., 2009; Jennings et al., 2012; Díaz-Rodríguez et al., 2021). However, it is more difficult to predict the fate of more massive stars and the progenitors of uncommon SN types due to their rarity. Because of this, it is hard to determine the maximum stellar mass for SNe, $M_{\rm max}$, draw any strong conclusion due to the low statistical robustness of such results. Jennings et al. (2014) derived $M_{\rm max}$ ∼35–45 $M_\odot$, Díaz-Rodríguez et al. (2018) derive even a higher estimate $M_{\rm max}$ >59 $M_\odot$. However, a BH progenitor with the initial mass of about 18 $M_\odot$ was identified as well (Murphy et al., 2018). The BH could have been formed by fallback, or, alternatively, there is no clear single upper mass limit for SN explosions. This is supported by Sukhbold et al. (2016), who concluded that the region above 15 $M_\odot$ shows both successful explosions and failed SNe. While the more massive stars are more likely to fail, there is no monotonic trend. Instead, there appear to be islands of SN production.

1.6 Planetary nebulae

Planetary nebulae (PNe) are one of the terminal phases of about 90% of stars more massive than the Sun (low and intermediate stars with $M \lesssim 8$ $M_\odot$). Near the end of their lives, most of these stars pass through the Asymptotic Giant Branch (AGB) phase where the majority of mass loss occurs. At this point, if their exposed remnant stellar cores have temperatures high enough to ionize the ejected material, a PN is formed around them. These central stars of PNe quickly evolve at constant luminosities towards higher effective temperatures. Ultimately, after the exhaustion of their fuel, they will cool along the WD cooling track. The properties of PNe and their central stars strongly depend on their preceding evolutionary stages and the physical processes associated with them (for a contemporary review see, e.g., Kwitter and Henry, 2022, and the references therein). The lifetime of PNe is very short – 10^3–10^5 yr – almost instantaneous with respect to stellar evolution, and varies strongly with the mass of the PN progenitor and subsequent mass loss (Schönberner and Blöcker, 1996; Köppen and Acker, 2000; Majaess et al., 2014). PNe are excellent laboratories with many astrophysical applications, such as studying the enrichment of the ISM, tracing stellar populations, and studying the kinematics and dynamics of galaxies, galaxy clusters, and mergers (e.g., Kwitter and Henry, 2022).

The knowledge of the intrinsic properties of the Galactic population of individual PNe has been restricted by large uncertainties in their derived distances. For instance, Zhang (1995) estimated that the average relative error in the distances listed for Galactic PNe was around 35%–50%. Model-independent trigonometric parallaxes for the central stars of PNe were rare before the advent of *Gaia*. However, after the release of GDR2, a lot of work has been done to cross-identify the central stars of PNe to *Gaia* sources, derive their precise distances and parameters (for PNe within ∼2.5 kpc), and calibrate other means of determining the PN distances using these new distance measurements (Kimeswenger and Barría, 2018; González-Santamaría et al., 2019; Stanghellini et al., 2020; Chornay and Walton, 2020). The work on these topics has also continued after the release of EDR3 (Chornay and Walton, 2021; González-Santamaría et al., 2021).

While a distance measurement resulting from an individual *Gaia* parallax can be significantly more precise than the previous distance measurements for many PNe, it is possible to obtain even tighter constraints on the PN distance – if the PN can be associated with a star cluster. Such associations are expected to be rare since the majority of star clusters disperse before this stellar evolutionary stage can be reached (e.g., Lada and Lada, 2003). Nevertheless, such associations have been found. Relying on robust statistics made possible by (usually) a large number of cluster members, it was possible to obtain very precise distances to star clusters, even in the pre-*Gaia* era. Another key problem that is resolved by associating a PN with a cluster is that the mass and abundance of its main sequence progenitor can be established, which is crucial for understanding the PN evolution and chemistry. The main issue for this kind of study was to verify the cluster membership of the studied PNe. In the past, the primary criteria to establish the cluster membership were the differences in radial velocity, the reddening (color excess) difference between the PN and the cluster, and the ratio of the estimated distances. However, this approach was hampered by many issues. Apart from the difficulties in deriving precise distances to PNe that would be informative enough, the PN reddening may be substantially higher than the reddening for the OC stars if there is an inherent self-absorption by dust within the PN itself. There are also spatial variations in reddening across the fields of many OCs (differential reddening; Majaess, Turner, and Lane, 2007). This meant that it was extremely difficult to obtain solid evidence for the PN/OC associations, and there were many examples of such associations being claimed, then deprecated, then possibly reclaimed, when new data or analysis techniques were used. A lot of work has been done to find PNe physically related to OCs (e.g. Koester and Reimers, 1989; Majaess, Turner, and Lane, 2007; Bonatto, Bica, and Santos, 2008; Turner et al., 2011; Moni Bidin et al., 2014; González-Díaz et al., 2019, and the references therein).

The census of PNe within OCs has recently stabilized on only two physically related PN/OC pairs. Fragkou et al. (2019a) report an association between a high-mass PN, BMP J1613-5406, and a young OC NGC 6067. Due to the young age of the parent cluster and the short time-scale of the PN phase, the PN progenitor must have been very massive, around ~ 5 $M_{\odot}$, which was derived from the OC main sequence turn-off mass. This association provides a rare additional datum for the fundamental initial-to-final mass relation (IFMR) currently best determined from cluster WDs. Such massive PNe are very rare and are interesting to study. The other pairing is between PN PHR 1315-6555 and its host OC, Andrews-Lindsay 1 (Majaess et al., 2014; Fragkou et al., 2019b). The progenitor of this PN is less massive since the turn-off mass of this OC is $\sim$2.2 $M_{\odot}$. Some PNe are also known in the OCs of other galaxies (e.g., Larsen and Richtler, 2006; Davis et al., 2019).

There is also a strong motivation to identify PNe physically associated with GCs. Currently, there are four PNe associated with GCs: Ps 1 = K648 in M15 (Pease, 1928), GJJC 1 = IRAS 18333-2357 in M22 (Gillett et al., 1989), JaFu 1 in Palomar 6, and JaFu 2 in NGC 6441 (Jacoby et al., 1997). An extensive search by Jacoby et al. (1997) and the recent survey by Göttgens et al. (2019) did not reveal any other PN/GC associations. Bond, Bellini, and Sahu (2020) verified the physical association of these PN/GC pairs using radial velocity measurements and proper motions of PN central stars obtained from the GDR2 and HST archival frames. They confirmed the physical association for all the pairs, except JaFu 1/Pal 6, where the proper motion evidence is marginal. Recently, Minniti et al. (2019) took advantage of the recent GC discoveries in the obscured central regions of the Galaxy using the photometric near-infrared surveys and searched for possible PNs associated with them. They searched for PNe projected on these new GCs and uncovered three new possible

PN/GC associations: SB 2 in Minni 06, G354.9-02.8 in Minni 11, G356.8-03.6 in Minni 28, and Pe 2-11 in Minni 31. However, they emphasize that these pairs are only preliminary candidates and more data – especially radial velocities, proper motions, and parallaxes are required to ascertain whether they are physically related. There is also a handful of PNe in extragalactic GCs (Minniti and Rejkuba, 2002; Larsen, 2008; Jacoby et al., 2013; Walsh, Rejkuba, and Walton, 2015; Sun et al., 2019).

The mere presence of PNe in GCs poses a challenge to the models of stellar evolution. In such old stellar populations as GCs, stars leave the AGB with masses of about $\sim$0.5 $M_\odot$ (Kalirai et al., 2009). This is less than the minimum mass needed to form a PN, since the theoretical post-AGB evolutionary timescales of these low-mass remnants are too long (e.g., Schoenberner, 1983). This means that any nebular material ejected at the end of the AGB phase has enough time to disperse before the central star becomes hot enough to ionize it. However, some theoretical models suggest that even post-AGB evolution of these low-mass objects may be fast enough to give rise to PNe (Miller Bertolami, 2016). Another possibility is that they may arise from binary stars – either blue stragglers resulting from mergers, producing more massive stars with faster evolutionary timescales, or systems that underwent a common envelope stage that rapidly removed the AGB envelope, exposing a hot core that could photoionize the ejecta (see e.g., Jacoby et al., 2013; Jacoby et al., 2017).

The post-AGB phase is arguably one of the least understood phases of the evolution of low and intermediate-mass stars. These couple of known GC PNe are of great value, can serve as distance calibrators, and are relevant for the study of more distant populations.

1.7 White dwarfs

White dwarfs (WDs) are the evolutionary endpoint of stars with initial masses $\leq 8\,M_\odot$ (e.g., Smartt et al., 2009). For this reason, WDs are very common objects. As there is a strong correlation between the stellar mass and the luminosity, implying rapidly decreasing main sequence lifetimes for stars more massive than the Sun, the vast majority of stars with M>1.5 $M_\odot$ that have ever formed in the Galaxy have already become WDs. A comprehensive review paper focused on the origin and evolution of WDs is presented in Althaus et al. (2010).

WDs are characterized by the planetary-like sizes, with stellar radii $R_{\rm WD} \sim 0.01\ R_\odot$. This implies that the matter inside them is highly compressed, with the average densities being of the order $\rho \sim 10^6\ {\rm g\,cm^{-3}}$. The equation of state in the WD interior is that of a highly-degenerate Fermi gas, where the hydrostatic equilibrium in the interior is being provided by the pressure of degenerate electrons opposing gravity (Chandrasekhar, 1939), making stable objects of this kind possible. The electron degeneracy is also responsible for the fact that, unlike in most other stars, there is an anti-correlation between the WD mass and its radius – meaning that the more massive the WD, the smaller its size. Chandrasekhar (1931) showed that, since the WD properties are described by a Fermi gas of degenerate electrons, there is an upper mass limit for WDs, which is roughly 1.4 $M_\odot$. It is also expected from the evolution of ECSN progenitors, that when the mass of the ONe core reaches about 1.37 $M_\odot$, the core collapses due to electron capture on magnesium and neon nuclei, leading to the formation of an NS (Nomoto, 1987; Takahashi, Yoshida, and Umeda, 2013). Hence, single star evolution cannot produce WDs more massive than about 1.37 $M_\odot$. However, even the WDs with masses approaching this limit are very rare. Generally, WDs are found in a range of masses, with the most massive WDs close to this mass

limit and the lightest objects of ∼0.15 $M_\odot$ on the other side of the mass spectrum. However, the mean mass of WDs in the solar neighborhood is about 0.6 $M_\odot$ (Tremblay et al., 2020). The WDs with masses $0.45 \lesssim M_\odot$ are generally thought to be the result of close binary evolution because single progenitors of such low-mass WDs have main sequence lifetimes exceeding the age of the Universe (e.g., Kilic, Stanek, and Pinsonneault, 2007).

Their structure is relatively simple – WDs contain a core of degenerate matter and its composition depends on the WD mass:

- Massive WDs – those with $M \gtrsim 1.04\,M_\odot$ have an oxygen and neon (ONe) core.
- Low-mass WDs – those with $M \lesssim 0.45\,M_\odot$ have cores made up of helium (He),
- And those with masses between these two classes have carbon and oxygen (CO) cores.

This core is surrounded by a thin layer of lighter elements, most typically a thin pure-helium envelope, itself surrounded by an even thinner pure-hydrogen atmosphere (e.g., Fontaine, Brassard, and Bergeron, 2001). Such WDs with the atmospheres consisting almost entirely of hydrogen with at most traces of other elements are called DA WDs. Hydrogen deficient WDs, known as non-DA WDs, comprise ∼15% of the remaining WD population. These WDs are split into several other classes:

- DO spectral type which are hot objects ($45000 < T_{\rm eff} < 200000$ K) that show strong lines of He II,
- DB spectral type which are cooler objects ($11000 < T_{\rm eff} < 35000$ K, the second most common class of WDs) and show lines of He I,
- and even cooler objects of types DC, DQ, and DZ that show traces of carbon and other metals in their spectra, or their spectra are featureless.

There are also a lot of transitional classes, and the WD atmospheric composition may also evolve with time due to various competing processes such as gravitational settling, radiative levitation, convection, mass loss episodes, and accretion (e.g., Althaus et al., 2010).

While some WDs were known for quite some time, it was the advent of modern wide-field surveys that enabled the discovery of the most currently known WDs. For instance, the Sloan Digital Sky Survey (SDSS, York et al., 2000) has been instrumental in collecting a large number of spectroscopically confirmed WDs, the number of which has accumulated to over 36000 by the SDSS Data Release 16 (Kepler et al., 2021). Another big jump in the number of WD detections has been made after the release of GDR2, which led to the discovery of ∼260000 high-confidence WD candidates (Gentile Fusillo et al., 2019). Recently, Gentile Fusillo et al. (2021) has expanded this sample to a catalog of almost 360000 high-confidence WD candidates selected from the EDR3.

With such a large number of known WDs, it is reasonable to expect that a lot of them are also star cluster members. Such WDs are interesting for many applications, but perhaps the most important one is the derivation of the initial-final mass relation (IFMR, e.g., Cummings et al., 2018), which is a mapping between the WD mass and the initial mass of its progenitor for a single star evolution. Thus, it also gives the total mass lost by a star during its entire evolution from the zero-age main sequence to the WD stage. The mass loss for the main sequence stars is relatively well-understood, as they are relatively stable, long-lasting, and plentiful for observations in different environments. However, the final and also the shortest stages of stellar life are the

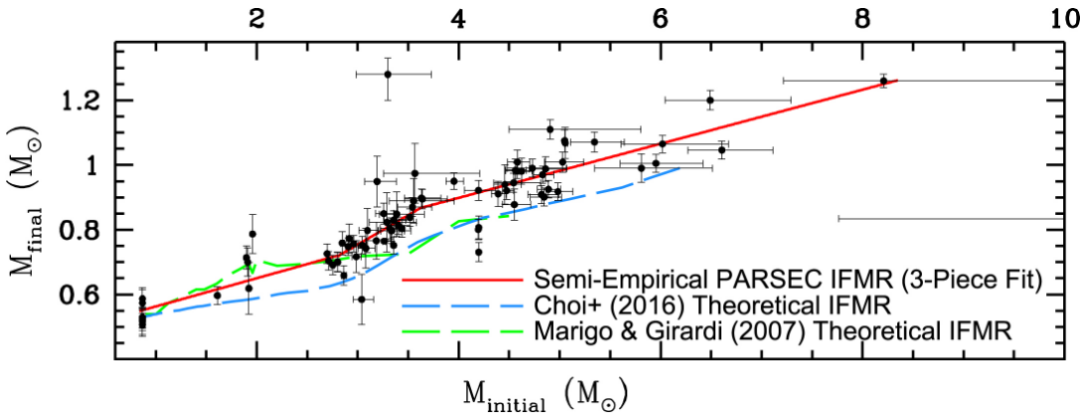

FIGURE 1.5: IFMR data derived using PARSEC (Bressan et al., 2012) isochrones. The three-piece semi-empirical fit is shown by a red line. Also overplotted are theoretical IFMRs from Marigo and Girardi (2007) and Choi et al. (2016), shown by green and blue lines, respectively. Figure reproduced from Cummings et al. (2018).

most enigmatic, since stellar evolution here becomes very sensitive to nuclear reaction rates, dredge-up, convection, overshooting, and mass loss (e.g., Marigo and Girardi, 2007; Choi et al., 2016). The analysis of WDs can be very helpful in constraining these processes. The high-mass end of the IFMR is also informative of the boundary in the parameter space of stellar properties, which divides the stars that eventually explode in SNe and form NSs, and those that form WDs instead (e.g., Cummings et al., 2016a; Cummings et al., 2016b; Richer et al., 2019; Miller et al., 2022).

While it is possible to study the IFMR using wide binaries where one of the components is a WD (e.g., Barrientos and Chanamé, 2021), the IFMR calibration using star clusters has proven to be the most successful. With the WDs that are cluster members, a simple comparison of their cooling age to the total cluster age gives the evolutionary time to the tip of the AGB for their progenitor. From this, it is possible to get the WD's progenitor initial mass using stellar evolutionary models (see, e.g., Fig 1.5). For the IFMR analysis, the determination of the precise ages of the clusters is as important as determining the precise WD masses and cooling ages. This is most critical for the highest-mass WDs, where the derived masses of their progenitors change rapidly with evolutionary time.

Because WDs have ceased energy production by the core fusion, their temperature and luminosity decline with time in a predictable way, at least in the absence of interactions with a companion. Because of this, they have been utilized as astrophysical chronometers (e.g., Moss et al., 2022), as it is possible to derive their cooling ages with the knowledge of WDs masses, surface temperatures, and atmospheric compositions. The WD mass is informative of core composition and the original thermal energy of the WD, the WD surface temperature reflects its current thermal state, and the atmosphere composition governs the opacity for photons that carry away the thermal energy of the WD core (e.g., Fontaine, Brassard, and Bergeron, 2001). Most often, spectroscopy has been instrumental in the determination of these parameters (e.g., Cummings et al., 2016a; Cummings et al., 2016b). However, with the advent of the *Gaia* mission and the availability of precise trigonometric parallaxes, the astrometric–photometric approach has become more viable. If the distance to the WD is determined using trigonometric parallax, and its apparent luminosity and temperature are known as well, it is possible to calculate its radius. The WD mass can then be derived

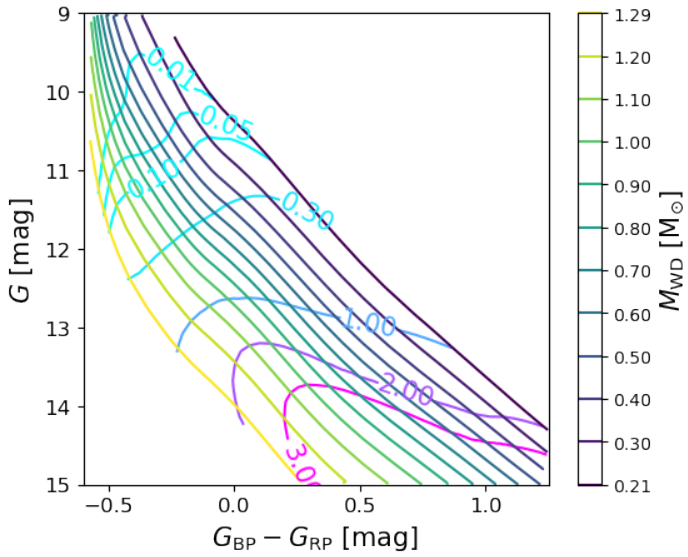

FIGURE 1.6: Cooling curves based on models of Bédard et al. (2020) of DA (hydrogen atmosphere) WDs in the G vs $G_{BP} - G_{RP}$ CMD for various WD masses, ranging from 0.21 to 1.29 $M_\odot$, from top to bottom. As a WD ages and cools down, it moves from the upper left part of the diagram towards the lower right. The cooling age contours for cooling ages 0.01, 0.05, 0.1, 0.3, 1,0, 2.0, and 3.0 Gyr are also overplotted.

using the mass-radius relation for degenerate matter (e.g., Bédard, Bergeron, and Fontaine, 2017; Joyce et al., 2018). The advantage of the astrometric–photometric approach over spectroscopy is its universality and the potential for obtaining more precise WD masses if parallaxes are sufficiently precise. Even more precise distances can be obtained if the studied WD is found to be a member of a star cluster.

Therefore, using the WD cooling models, it is possible to derive WD cooling ages and masses from *Gaia* parallaxes and photometry (see Fig. 1.6) for nearby WDs with negligible extinction to a high precision of ∼2% (Bergeron et al., 2019; Tremblay et al., 2019). However, in order for this technique to be usable, WD atmospheric composition must be known to correctly transform colors into atmospheric temperatures. Incorrectly assuming pure-hydrogen or pure-helium atmospheres can lead to 5–20% systematic errors in WD masses and other biases. However, the vast majority ($\gtrsim$ 80%) of all WDs (Kepler et al., 2016; Kepler et al., 2021) have hydrogen atmospheres. Furthermore, the fraction of DA WDs in OCs seems to be even higher than in the field (e.g., Kalirai et al., 2005; Salaris and Bedin, 2019).

1.8 Runaway stars

High-velocity stars are important for numerous astrophysical applications. Their kinematics, trajectories, and stellar properties often retain imprints of the processes that imparted the high velocities to these systems. Of particular interest are possible constraints on the physics of SNe. High-velocity stars are also important sources of stellar feedback (especially the massive stars), as they can travel long distances during their lifetimes, straying far away from their formation sites. Therefore, they can emit ionizing photons far away from the dense ISM associated with the sites of stellar

formation, where the photons are less likely to get absorbed by the molecular clouds. Such photons are available for ionization of hydrogen in the ISM and intergalactic medium. Also, at the end of their lives, their SN explosions are an important source of turbulence and chemical enrichment for the local ISM and intergalactic medium as well (e.g., Kimm and Cen, 2014; Gatto et al., 2015; Ma et al., 2016).

The most extreme stars with the fastest velocities that are sufficient for the stars to be considered unbound from the Galaxy are often termed Hyper Velocity stars (HVS, e.g., Brown et al., 2005; Hirsch et al., 2005; Brown, 2015). The measurements from *Gaia* show that HVSs comprise unbound disc stars (Irrgang et al., 2021), WDs ejected from a double-degenerate and peculiar type Ia SNe (e.g., Shen et al., 2018; Vennes et al., 2017; Raddi et al., 2018; Raddi et al., 2019), LMC runaways (e.g., Boubert et al., 2017; Erkal et al., 2019), and stars having trajectories that are consistent with the origin near the Galactic Center (e.g., Koposov et al., 2020). The last group of stars also possess the highest velocities, which are most commonly explained by a three-body interaction and ejection in the vicinity of the super-massive BH at the Galactic Center (Hills, 1988).

However, most stars with the above-average velocities are not unbound objects. While the most early-type stars are found in clusters, there is also a significant number (10—30%, see, e.g. Stone, 1979; Renzo et al., 2019) of young massive stars which are frequently observed in the Galactic field away from the sites of recent star formation. The presence of these stars at such locations seems to be at odds with their limited lifetimes of only a few tens Myr. These stars possess unusually large peculiar velocities $v \gtrsim 30$ km s^{-1} and called are often called 'Runaway stars' (a term first introduced by Blaauw, 1961).

The identification of the parent cluster of a runaway is important because it provides unique constraints on its evolution. When the system's proper motion and parent cluster are known, the kinematic age of the runaway can be derived. The kinematic age (especially when compared to the age of the cluster) can provide information on the ejection mechanism. This has an added benefit that by determining the parent cluster, it is possible to calculate more precise peculiar velocities by using the cluster to define the local standard of rest (LSR). In other words, the peculiar velocity defined as the relative velocity of a runaway with respect to its parent cluster should be more precise than the peculiar velocity derived from the stellar astrometry, which includes removing the velocity components arising from the Galactic rotation and peculiar motion of the Sun. While our knowledge of the Galactic constants and the solar peculiar motion has recently improved (e.g., Bland-Hawthorn and Gerhard, 2016), there are still significant uncertainties, particularly in the Galactic rotational curve shape. Moreover, the parent cluster itself can have a significant peculiar velocity with respect to the surrounding stellar population. Therefore, the peculiar velocities calculated with respect to the parent cluster are more informative, and can potentially provide tighter constraints on the SN explosion details (SN mass loss and natal kicks, Ankay et al., 2001; Hambaryan et al., 2022).

The age of the runaway system should also be the same as the age of the cluster. If the runaway is hosting a compact object, subtracting the kinematic age of the runaway from the age of the cluster yields the lifetime of the compact object progenitor. From this, it is possible to derive the initial mass of its progenitor using stellar evolutionary models. Studying other cluster member stars can also yield the cluster metallicity, which also applies to the compact object progenitor. This is important for many early-type runaways since a lot of them originate in binaries, where the star can be rejuvenated (i.e. its evolutionary clock partly reset) or its metallicity can be changed (e.g., Pfahl et al., 2002; Renzo et al., 2019; Gvaramadze et al., 2019). Therefore, this

relatively straightforward observation can be used to determine the system parameters that would be unavailable if the object was studied in isolation (e.g., Ankay et al., 2001; Hambaryan et al., 2022).

1.8.1 Kick mechanisms

Assuming a purely symmetric SN explosion, the post-SN binary only remains bound if the system loses less than half of its mass. In other words, when the SN ejecta $M_{\rm ej}$ comprises less than a half of the system's pre-SN mass, $M_{ej} < (1/2)(M_1+M_2)$, where M_1 and M_2 are the masses of the primary and secondary components, respectively (Blaauw, 1961). If we assume that the center of mass of the pre-SN binary is at rest in the frame of the rotating Galactic disk and that the SN ejecta is assumed to leave the system 'instantaneously', the remnant binary system gains a velocity with a magnitude (in the frame of the rotating Galactic disk) given by:

$$v_{\rm sym} = \left(\frac{GM_2}{a_{\rm pre-SN}}\right)^{1/2}\left(\frac{M_2}{M_1+M_2}\right)^{1/2}\left(\frac{M_1-M_{\rm co}}{M_2+M_{\rm co}}\right), \tag{1.1}$$

where $M_{\rm co} = M_1 - M_{\rm ej}$ is the mass of the compact object, G is the gravitational constant and $a_{\rm pre-SN}$ is the pre-SN semimajor axis of the binary. The last term on the right-hand side of this equation,

$$\frac{M_1-M_{\rm co}}{M_2+M_{\rm co}} = e, \tag{1.2}$$

is the eccentricity of the remnant binary. This corresponds to a maximum imparted velocity kick of a few tens of $\rm km\,s^{-1}$, depending on the binary mass, progenitor velocity, orbital period, and ejected mass of the system (e.g., Iben and Tutukov, 1997, for more details).

As discussed in the previous sections, SNe are often significantly asymmetric. In that case, the newly-formed compact object receives a kick at birth and the acquired peculiar velocity (and eccentricity) of the remnant binary can be higher. However, these kicks also lead to binary disruption (e.g., Renzo et al., 2019). Depending on the orientation and magnitude of the kick, the acquired peculiar velocity is:

$$v_{\rm asym} = \left(v_{\rm sym}^2 - 2v_{\rm sym}v_{\rm k}\cos\psi + v_{\rm k}^2\right)^{1/2}, \tag{1.3}$$

with

$$v_{\rm k} = \frac{M_{\rm co}w}{M_{\rm co}+M_2}, \tag{1.4}$$

where $v_{\rm sym}$ is given by Eq. 1.1, w is the kick velocity of the newly-formed NS, and ψ is the angle between the kick velocity and the pre-SN relative orbital velocity. According to Eq. 1.3, the highest peculiar velocity is attained if $\cos\psi$ = -1, that is if the direction of the kick at the SN explosion was opposite to the direction of the relative orbital velocity (e.g., Gvaramadze et al., 2011). In that case, Eq. 1.3 can be rewritten simply as

$$v_{\rm max} = v_{\rm sym} + v_{\rm k} = v_{\rm sym} + \frac{M_{\rm co}w}{M_{\rm co}+M_2} \tag{1.5}$$

An alternative scenario for the formation of early-type runaways is dynamical ejection from dense, compact clusters (e.g., Poveda, Ruiz, and Allen, 1967). Due to the dynamical interaction between single stars and binaries, there is a chance that a

massive star is ejected from a cluster. The probability for ejection is higher in the early phases of the cluster lifetime, where the stellar density is high and close encounters between cluster members are frequent. Observational evidence shows that both the binary SN mechanism and the dynamical ejection mechanism are responsible for the population of the Galactic runaways (Hoogerwerf, de Bruijne, and de Zeeuw, 2001).

These scenarios are not mutually exclusive and some runaway systems may form through a combination of these two mechanisms. For instance, a binary system may be ejected by a close stellar encounter from its parent cluster, and at a later time, the system will get an additional velocity kick in a random direction when one of the binary components explodes in an SN. In such cases, it may not be possible to reliably identify the parent star cluster (Pflamm-Altenburg and Kroupa, 2010).

1.8.2 Estimating peculiar velocities

In principle, estimating stellar distances and space velocities from astrometry (parallaxes and proper motions) is simple. However, this simple picture breaks down in practice with the presence of measurement uncertainties. Most problems arise due to the nonlinearity of the transformation and the positivity constraint of the distance. The sources studied in this thesis often have parallax measurements with high relative uncertainties, and some of them even have negative parallax values. The simple methods fail in these cases and give non-physical results when utilizing such measurements. However, even these noisy measurements are perfectly valid and still hold informational value so it would be a mistake to discard them. The only viable way to handle such measurements is to use probabilistic analysis (see, e.g., Luri et al., 2018, and technical note GAIA-C8-TN-MPIA-CBJ-081, for a more detailed discussion)[3].

Given the data vector containing the parallax (ϖ, in mas), proper motion in right ascension (μ_{α^*}, multiplied by $\cos\delta$), and proper motion in declination (μ_δ, both in mas yr^{-1}), written as the column vector

$$\mathbf{x} = (\varpi, \mu_{\alpha^*}, \mu_\delta)^T, \tag{1.6}$$

we would like to infer the distance (r, in pc), tangential speed ($v_{\rm tan}$, in km s^{-1}), and direction of travel (ϕ, increasing anticlockwise from North, in radians), written as

$$\boldsymbol{\theta} = (r, v_{\rm tan}, \phi)^T. \tag{1.7}$$

Given the true parameters $\boldsymbol{\theta}$, the noise-free prediction of the data vector $\mathbf{x}$ is relatively easy to compute via the simple geometrical transformation:

$$\mathbf{m} = \left(\frac{10^3}{r}, \frac{10^3}{c_2}\frac{v_{\rm tan}\sin\phi}{r}, \frac{10^3}{c_2}\frac{v_{\rm tan}\cos\phi}{r}\right)^T, \tag{1.8}$$

where $c_2 = 4.74047$. The inverse transformation, to give the nominal parameters in terms of $\mathbf{x}$, is similarly easy to derive analytically:

$$\theta_{\rm nom} = \left(\frac{10^3}{\varpi}, c_2\frac{\sqrt{\mu_{\alpha^*}^2, \mu_\delta^2}}{\varpi}, \arctan\frac{\mu_{\alpha^*}}{\mu_\delta}\right)^T. \tag{1.9}$$

[3] https://github.com/agabrown/astrometry-inference-tutorials/blob/master/3d-distance/resources/3D_astrometry_inference.pdf

However, because the data are noisy, this inverse transformation does not generally behave well. Therefore, a more suitable approach is Bayesian inference where all observational uncertainties and correlations are taken into account at the same time. Since the *Gaia* archive supplies all necessary quantities, uncertainties, and correlations, we can consider as the likelihood for $\mathbf{x}$ a multidimensional Gaussian:

$$P(\mathbf{x} \mid \boldsymbol{\theta}) = \frac{1}{(2\pi)^{3/2}|\Sigma|^{1/2}} \exp\left(-\frac{1}{2}(\mathbf{x}-\mathbf{m})^T\Sigma^{-1}(\mathbf{x}-\mathbf{m})\right), \tag{1.10}$$

where Σ is the full (non-diagonal) covariance matrix.

The 3D posterior distribution over θ

$$P(\boldsymbol{\theta} \mid \mathbf{x}) = \frac{1}{Z}P(\mathbf{x} \mid \boldsymbol{\theta})P(\boldsymbol{\theta}), \tag{1.11}$$

where Z is a normalization constant, can then be obtained by multiplying the likelihood by a suitable prior. I have used a separable prior, such that

$$P(\boldsymbol{\theta}) = P(r) \cdot P(v_{\rm tan}) \cdot P(\phi). \tag{1.12}$$

For the distance, I have used the exponentially decreasing space density prior

$$P(r) = \begin{cases} \dfrac{1}{2L^3}\, r^2 e^{-r/L} & \text{if } \; r > 0 \\ 0 & \text{otherwise}\ , \end{cases} \tag{1.13}$$

where the scale length L is chosen according to the line of sight, or a single value is adopted for all sources (see Chapter 3.). For the velocity prior I have used a Beta ($\alpha = 2$, $\beta = 3$) distribution

$$P(v_{\rm tan}) = \frac{1}{B(\alpha,\beta)}\left(\frac{v_{\rm tan}}{v_{\rm max}}\right)^{\alpha-1}\left(1-\frac{v_{\rm tan}}{v_{\rm max}}\right)^{\beta-1}, \tag{1.14}$$

where $B(\alpha,\beta)$ is the beta function, and the maximum velocity was set to $v_{\rm max} = 500\ {\rm km\,s^{-1}}$. The prior for the direction of the movement was chosen to be uniform:

$$P(\phi) = \frac{1}{2\pi}. \tag{1.15}$$

The posterior does not have a simple form, so it needs to be characterized via Monte Carlo sampling. After getting posteriors for the distance and velocities, it is possible to obtain the peculiar tangential velocity by accounting for the Galactic rotation and peculiar velocity of the Sun (e.g., Johnson and Soderblom, 1987; Mdzinarishvili and Chargeishvili, 2005).

1.8.3 Bow shocks

The ISM is intertwined with many complex structures with different morphologies created by a complex interplay of various physical processes, such as stellar winds, SN explosions, effects of radiation, and large-scale matter flows. These structures exhibit all imaginable scales, ranging from sub-pc sizes to vast structures in the intergalactic medium.

One of such structures are stellar bow shocks (or bow shock nebulae). These are arc-shaped nebular structures with a driving star located near its axis of symmetry. They are created by the strong wind of the driving star which has a high velocity

FIGURE 1.7: A bow shock generated by a prototype runaway star ζ Oph as seen by the *Spitzer* Space Telescope (Werner et al., 2004). Blue color represents 3.6, green 4.5, and red 24 μm light (image made by the author).

with respect to the surrounding ISM. Since their first identification by Gull and Sofia (1979) as arcuate optical emission nebulae around LL Ori and ζ Oph (for instance, see Fig. 1.7), a lot of such structures have been identified. Bow shocks can be generated around various fast-moving objects, but here I will concentrate on the ones associated with the runaway early-type stars.

Massive stars have strong stellar winds ($\dot{M} \sim 10^{-8}$–10^{-6} $\mathrm{M_\odot\,yr^{-1}}$, $v_\infty \sim 1000$–2500 $\mathrm{km\,s^{-1}}$, e.g., Mokiem et al., 2007; Vink and Sander, 2021). If these stars move supersonically with respect to their environment, a bow shock will be formed at the stand-off distance R_0 from the star (the bow shock apsis), where the momentum flux of the stellar wind and ISM balance each other. Hence, we can write (e.g., Wilkin, 1996):

$$\frac{1}{2}\rho_\mathrm{w} v_\mathrm{w}^2 = \frac{1}{2}\rho_\mathrm{ISM} v_\mathrm{ISM}^2, \tag{1.16}$$

where ρ_w is the stellar wind density, v_w is the stellar wind velocity, ρ_ISM stands for the density of ambient ISM, and v_ISM is the velocity of the star relative to the ambient ISM.

The density of the stellar wind can be rewritten as

$$\rho_\mathrm{w} = \frac{\dot{M}_\mathrm{w}}{4\pi R^2 v_\mathrm{w}}, \tag{1.17}$$

where $\dot{M}_\mathrm{w}$ is the stellar mass loss rate and R is the distance from the star. By rearranging, we can write for R:

$$R_0 = \left(\frac{\dot{M}_\mathrm{w} v_\mathrm{w}}{4\pi \rho_\mathrm{ISM} v_\mathrm{ISM}^2}\right)^{1/2}. \tag{1.18}$$

The projection of R_0 can be measured from the bow shock images, as the swept-up material in the bow shock is heated by the radiation of the OB star, making these structures visible in either shocked gas (Kaper et al., 1997; Brown and Bomans, 2005) or through the emission of warm dust at mid-infrared wavelengths (van Buren and

McCray, 1988; Peri et al., 2012; Peri, Benaglia, and Isequilla, 2015).

Bow shocks can be separated into two classes:

- The structures formed around stars with high peculiar velocities that sweep up ambient ISM gas and dust as they move. In this case, we can substitute $v_{\rm ISM} = v_{\rm pec}$ in Eq. 1.18 (e.g., Kaper et al., 1997; Comerón and Pasquali, 2007; Gvaramadze et al., 2011).
- The structures formed around slowly moving stars encountering large-scale ISM flows (from an expanding HII region, e.g., Povich et al., 2008).

The largest catalog of Galactic bow shocks includes more than 1000 objects, the great majority of which are driven by OB stars and are in isolated locations far from known star-forming regions, suggesting high peculiar velocities (e.g. Kobulnicky et al., 2016; Jayasinghe et al., 2019). Since bow shocks are parsec-scale structures that tie together the properties of stellar wind, the velocity of the star with respect to the surrounding ISM, and the ISM density, they can be used for detecting distant runaway stars, estimating stellar mass-loss rates, and probing the properties of the ISM (e.g., Povich et al., 2008; Gvaramadze, Kroupa, and Pflamm-Altenburg, 2010; Gvaramadze, Pflamm-Altenburg, and Kroupa, 2011; Kobulnicky, Gilbert, and Kiminki, 2010; Kobulnicky et al., 2016; Kobulnicky, Chick, and Povich, 2019).

1.9 Neutron stars

Neutron stars (NSs) are stellar remnants of stars with initial masses above $\sim$8 $M_\odot$, resulting from the compression of stellar cores to atomic-nuclei densities during CCSN explosions. They are very small – most have a radius of the order of 10 km and a mass of about 1.4 $M_\odot$. NSs are supported against further collapse by neutron degeneracy pressure and repulsive nuclear forces. The maximum NS mass, where these processes start to be insufficient to stabilize the NS is called Tolman–Oppenheimer–Volkoff limit which is around 2.16 $M_\odot$ (Rezzolla, Most, and Weih, 2018). From the observational point of view, we observe NSs with masses up to 2.14 $M_\odot$ (Cromartie et al., 2020). As the core collapses into an NS, it retains a large part of its angular momentum. Therefore, NSs are rapid rotators (see, e.g., Lattimer and Prakash, 2004, for a general NS review).

The vast majority of known isolated NSs are observed as pulsars in the radio band, but some young isolated NSs, despite being radio-quiet, are still hot enough to be detectable at X-ray and optical wavelengths due to their thermal emission (e.g., Petre, Becker, and Winkler, 1996; Chakrabarty et al., 2001; Haberl, 2007). Pulsars are rotating NSs that emit beams of radiation. This radiation is thought to be primarily emitted from regions near their magnetic poles. Therefore, if the magnetic poles do not coincide with the rotational axis of the NS, and the observer is somewhere in the path of the beam, they may be detected as pulsating objects, with pulses that repeat with a periodicity equal to the rotation period of the NS. This pulsed emission is observed in radio, therefore we also term such systems as 'radio pulsars' (as opposed to 'X-ray pulsars' for accreting NSs). They are powered by the rotational energy of the NS, and the mechanism of energy release is related to their strong magnetic field, $B \sim 10^{12}$ G (e.g., Beskin et al., 2015, for a general review). More than 3300 pulsars of various types are known[4] (Manchester et al., 2005).

Pulsar pulse periods range between 1.4 ms and 12 s and fall into two main groups. The so-called 'normal' or 'classical' pulsars have periods longer than about 30 ms and

[4] https://www.atnf.csiro.au/research/pulsar/psrcat/

the 'millisecond' pulsars (MSPs) have shorter periods. Around 15% of the known pulsar population are MSPs. Classical pulsars and MSPs are evolutionarily different. Most classical pulsars are formed in SN explosions. They age with relatively constant surface dipole magnetic field strength until the pulse emission mechanism begins to fail $\sim 10^6$ yr after their formation. Most of these pulsars lie relatively close to the Galactic Plane, some of them even in their parent SNRs, which is consistent with their massive star origins. MSPs are more widely distributed in the Galaxy. They are believed to originate from old, slowly rotating NSs that get rejuvenated by accreting matter and angular momentum from an evolving binary companion. This 'recycling' process speeds up their rotation so that they have periods in the millisecond range and also re-energizes the beamed emission (e.g. Bhattacharya and van den Heuvel, 1991; Manchester, 2015).

Classical young pulsars can originate from multiple evolutionary pathways. According to theoretical models, about one-third of them originate from single massive stars or close binaries that have merged during the main sequence evolution. However, most classical pulsars originate from SNe in massive binary systems. The frequency of surviving binaries and the relative number of pulsars that are released during the first and second SN explosion depends on the distribution of SN velocity kicks. Due to typically large SN velocity kicks, most classical pulsars are isolated (binary fraction $\lesssim$5%, Antoniadis, 2020; Antoniadis, 2021)

Isolated NSs are, in general, high-velocity objects – darting throughout the Galaxy with speeds on average $\sim$350 $\mathrm{km\,s^{-1}}$, many of them exceeding 1000 $\mathrm{km\,s^{-1}}$ (e.g., Arzoumanian, Chernoff, and Cordes, 2002; Verbunt, Igoshev, and Cator, 2017). Due to their high-velocity nature, the chances of observing an NS in a star cluster are very slim. Due to a substantial velocity imparted to NSs at formation, even by SNe that eject little mass with weak NS kicks, NSs are not retained by star clusters. Considering even a modest imparted velocity of 50 $\mathrm{km\,s^{-1}} \sim 50\ \mathrm{pc\,Myr^{-1}}$, a newly-formed NS would escape its parent OC core in less than 0.1 Myr. Therefore, finding one still within its parent star cluster would be very fortuitous.

Notable exceptions are GCs. Due to their large masses, the escape velocities from GCs are significant. It was shown by Igoshev et al. (2021), that the shape of the velocity distribution of NSs born from low-kick SNe suggests that a small fraction of these NSs ($\lesssim$5 %) should have velocities that are not high enough to escape from GCs. Taking into consideration a large number of GC member stars, this translates to a significant number. Also, the high binary fraction among early-type stars and the fact that some binaries are not disrupted by SN explosions (which means that the velocity kick imparted to an NS is dampened by the presence of a secondary, as the NS has to drag its massive secondary along), means that the number of NSs retained by GCs is further increased. The NSs are then available to form many types of exotic binary systems with other GC stars, as the dense environments of GCs make dynamical formations of new binary systems possible. One of these objects are MSPs, and GCs are hosting a large number of them (e.g., Davies and Hansen, 1998; Ransom, 2008). Due to the high stellar densities within the GC central regions (between 10^3 to $10^5\,\mathrm{M_\odot\,pc^{-3}}$) stellar interactions may produce dynamically-formed binaries that can spin-up NSs. Also, these dynamical interactions can produce MSPs in unusual and eccentric orbits. Because of the frequent occurrence of MSPs in GCs, and their potential for many astrophysical applications, GCs have been the subjects of many dedicated pulsar studies, and as of January 2022, there are 234 known pulsars in 34 GCs[5]. Similarly, low-mass X-ray binaries, the predecessors of MSPs, are also

[5]According to the list of pulsars in GCs from http://www.naic.edu/~pfreire/GCpsr.html

overabundant in GCs for the same reasons as MSPs (e.g., Liu, van Paradijs, and van den Heuvel, 2007)

Except for the case above, it is hard to find any NSs within clusters. However. it is possible to use the NS kinematics to backtrack their trajectories back to their presumed sites of origin (e.g., parent star clusters, geometric centers of the associated SNRs, or positions of historical SNe). This can be done through optical astrometry (Jennings et al., 2018) if the pulsar has a luminous binary companion (or for the Crab pulsar, which is bright enough for *Gaia*), or through radio VLBI astrometry (e.g., Deller et al., 2019). The Australia Telescope National Facility (ATNF) Pulsar Catalogue (Manchester et al., 2005) lists more than 400 pulsars with measured proper motions – some of them with accuracies comparable to the *Gaia* proper motion measurements. The kinematic age of the pulsar derived in relation to its putative parent cluster can be potentially compared to the spin-down age t_{sd} of the pulsar – even if this age is unreliable and often does not reflect the true age of the pulsar. The spin-down age is defined using $t_{sd} \equiv P/2\dot{P}^{\cdot}$, where P and $\dot{P}^{\cdot}$ are the period and its time derivative, respectively (e.g., Page et al., 2004). Unfortunately, due to the nature of NSs, the radial velocities are often not known for isolated NSs, the exception being when they drive a bow shock. The inclination of a bow shock can yield an estimate of the radial velocity (e.g., Tetzlaff, Neuhäuser, and Hohle, 2009).

Young pulsars can be tracked to their parent SNRs (e.g., Tetzlaff et al., 2013). For a small number of NSs parent clusters have been suggested (e.g. Bobylev, 2008; Bobylev and Bajkova, 2009). Due to large uncertainties in the NS distances and the unknown radial velocities, the results are often not unambiguous (e.g., Tetzlaff et al., 2010). For the same reasons, their flight paths can only be traced back up to a maximum of a few Myr. Additional indicators, for instance, the identification of a possible former companion that is now a runaway star and also shows signs of the former binary evolution, are usually needed to reach firmer conclusions. Some of the NSs for which their parent clusters and associations have been proposed are:

- The Guitar pulsar (PSR B2224+65) was traced to the Cyg OB3 association, with a likely initial progenitor mass of 21–37 $M_{\odot}$ (Tetzlaff, Neuhäuser, and Hohle, 2009).
- The radio-quiet NS RX J1856.5-3754 has probably originated in Upper Scorpius, which is a subgroup of the nearby Scorpius-Centaurus association. Its progenitor had an initial mass of about 40–60 $M_{\odot}$ (Tetzlaff et al., 2011).
- The isolated NS RX J1605.3+3249 was probably born in the Octans association, with an initial progenitor mass of ∼11 $M_{\odot}$ (Tetzlaff et al., 2012).
- The young pulsar PSR J0826+2637 was tracked back to the cluster Stock 7. The initial mass of its progenitor was between 12–30 $M_{\odot}$ (Tetzlaff et al., 2014).

More recently, Neuhäuser, Gießler, and Hambaryan (2020) determined that the radio pulsar PSR B1706-16 and the well-known runaway zeta Oph have originated from a binary system in Upper-Centaurus-Lupus, a subgroup of the Scorpius-Centaurus association (e.g. Wright, 2020), that got disrupted by an SN, releasing both the runaway star and the pulsar. The age of the association and the kinematic ages suggest that the pulsar progenitor had an initial mass of 16–18 $M_{\odot}$.

1.10 Neutron star high-mass X-ray binaries

While NSs can be detected as radio sources (radio pulsars), they also reveal themselves when they accrete matter coming from a companion star in a binary system, as X-ray sources. Such systems are often termed X-ray binaries. In a very broad sense, an X-ray binary is a system that consists of a compact object that accretes material from a stellar companion, which results in the emission of X-ray radiation. In most literature, the systems hosting an accreting WD (cataclysmic variables, novae, etc.) are excluded from this category, since they have been known from optical astronomy already, before the advent of space-born X-ray astronomy. A book by Lewin and van der Klis (2006) provides a comprehensive review of the various aspects of X-ray binaries.

Due to their intrinsic faintness, NSs and BHs are notoriously difficult to study in the field. However, X-ray binaries are a potent tool for studying the formation and evolution of NSs and BHs, as their presence in these systems is revealed by their interactions with their stellar companions and the resulting bright X-ray emission (Tauris and van den Heuvel, 2006). X-ray binaries are excellent laboratories of exotic matter and physical processes under extreme gravity, temperature, pressure, rotation speeds, and magnetic fields (e.g., Arnason et al., 2021, and the references therein). Understanding evolutionary channels and the formation rate of X-ray binaries is important for understanding the X-ray component of the emission from distant, high-z galaxies and constraining the effects of feedback by X-ray binaries in the early universe. Population synthesis models predict that the formation rate of X-ray binaries depends on the age of the stellar population and its metallicity (Fragos et al., 2013b; Fragos et al., 2013a). However, this is not well tested, because both of these quantities have been difficult to determine for the stellar populations within our Galaxy, though some progress has been achieved by studying the systems in Magellanic Clouds (Antoniou et al., 2010; Antoniou and Zezas, 2016; Antoniou et al., 2019).

The fact that NSs and BHs can exist in binary systems with other stars has been puzzling. The initially more massive star in a binary system should evolve faster and explode as an SN first. However, as a consequence of the virial theorem, this would most likely lead to the disruption of the binary system post-SN, when more than half of the total mass of the binary is suddenly ejected (Blaauw, 1961). However, it was found that the effects of large-scale mass transfer can often flip the mass ratio for close interacting binary components prior to the first SN (e.g., Tauris and van den Heuvel, 2006, and the references therein).

For this reason, X-ray binaries are also inherently biased sources for SN studies. Due to the previous mass transfer phases, the SN mechanism and outcome can be very different compared to the isolated stars of the same mass and metallicity. The effects of close binarity are hard to quantify, as we do not have a reliable sample of NSs and BHs that resulted from the SN explosions of isolated stars (e.g., Podsiadlowski et al., 2004). Therefore, some properties such as the resulting NS magnetic field and the NS mass can be different for the NSs born from SNe in isolated stars compared to the NSs born in close binaries. Also, Renzo et al. (2019) showed that most binaries get disrupted after the first SN explosion. Therefore, most observed X-ray binaries (with the exception of dynamically-formed sources) formed from the systems where the compact object natal kick was weak, and the systems experiencing higher compact object natal kicks were more likely to get disrupted. Another possible source of bias is that the observed X-ray binaries are more likely to have relatively short orbital periods. It is possible that the energy released at the SN of the first star did not

significantly widen the binary orbit but instead contributed mostly to the kinetic energy of the system (Renzo et al., 2019).

NS and BH-hosting X-ray binaries are typically classified according to the mass of the non-degenerate companion star as high-mass X-ray binaries (HMXBs, $M \gtrsim 8\,\mathrm{M}_\odot$) and low-mass X-ray binaries (LMXBs, $M \lesssim 2\,\mathrm{M}_\odot$). HMXBs and LMXBs are very different types of sources. HMXBs contain early-type (O or B) companions, while the spectral type of the optical star in LMXBs is later than A. This also makes LMXBs much older than HMXBs, which have lifetimes only of a couple of dozen Myr (at most) and they never stray far from the Galactic plane. LMXBs can be several Gyr old and are more widely distributed throughout the Galaxy, especially towards the Galactic bulge and GCs. LMXBs are powered by mass transfer via Roche-lobe overflow, and accretion of matter always occurs through the formation of an accretion disc. While some HMXBs are also fed by Roche-lobe overflow, other mass transfer mechanisms are more common in most HMXBs (e.g., Tauris and van den Heuvel, 2006; Liu, van Paradijs, and van den Heuvel, 2006; Liu, van Paradijs, and van den Heuvel, 2007).

While some LMXBs have been used to investigate SNe and the formation of compact objects in binaries (e.g., Jonker and Nelemans, 2004; Repetto, Igoshev, and Nelemans, 2017; Atri et al., 2019; Gandhi et al., 2019), the properties of HMXBs make them more suited to this task. The main factor is their lifetime. Since LMXBs have long lifetimes (>1 Gyr), their encounters with giant molecular clouds, their movement through changing Galactic gravitational potential, and other effects mean that the currently observed peculiar velocities of LMXBs are significantly different from what they were just after the SN in the system. On the other hand, the lifetimes of HMXBs are very short, so their peculiar velocities do not have the time to change appreciably from their values just after the SN explosion. Also, NS masses and magnetic fields in LMXBs are significantly modified by accretion over long periods of time (accretion timescales ∼0.01–1 Gyr), while NSs in HMXBs have little time to be modified by accretion and their magnetic field strengths and masses are expected to lie close to their natal values (accretion timescales ∼0.1 Myr). The intrinsic faintness of LMXB optical counterparts also poses difficulty for obtaining precise astrometry and radial velocity measurements. A lot of LMXBs do not even have visible optical counterparts (e.g., Tauris and van den Heuvel, 2006; Liu, van Paradijs, and van den Heuvel, 2007).

Generally, HMXBs are further divided into two main subgroups according to the nature of the luminous companion – supergiant HMXB systems (sgHMXBs; or sometimes also called 'standard' HMXB systems) and Be/X-ray binaries (BeXRBs).

1.10.1 Supergiant X-ray binaries

In supergiant HMXBs (sgHMXBs), the compact object orbits an O or early B-type supergiant donor star. These secondary stars emit a strong stellar wind, with mass-loss rates of 10^{-6}–10^{-8} $\mathrm{M}_\odot\,\mathrm{yr}^{-1}$ with a terminal velocity up to 2000 $\mathrm{km\,s}^{-1}$. According to the mass transfer mechanism, we distinguish two types of systems: Roche lobe overflow and wind-fed systems. In some objects, both of these mass transfer mechanisms might be taking place.

The wind-fed systems comprise the majority of sgHMXBs, Vela X-1 being the best-known member of this group. They are close systems (P_{orb}<15 d) with low eccentricities. Despite the inefficiency of the capture of matter from a high-velocity stellar wind, large mass-loss rates can result in an appreciable mass accretion rate onto an NS that is sufficient to power the X-ray emission. This accretion results in

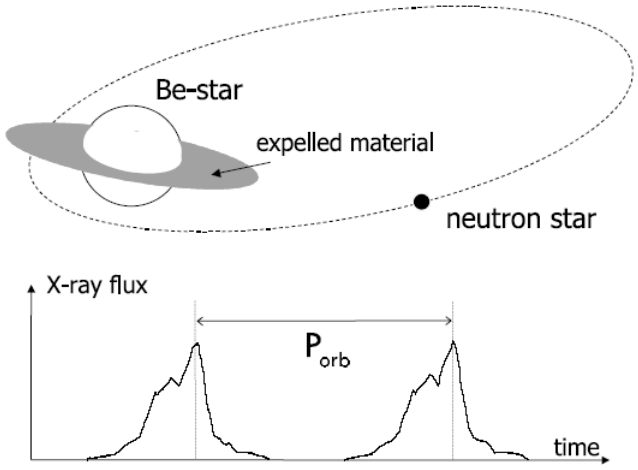

FIGURE 1.8: Schematic model of a typical BeXRB system. The secondary is a main sequence Be star with a decretion disk. The NS moves around in an eccentric orbit and accretes matter from the disk near its periastron, resulting in periodic X-ray outbursts lasting several days. Figure reproduced from Tauris and van den Heuvel (2006).

a persistent X-ray luminosity of of 10^{35}–10^{36} erg s^{-1}. Due to stellar wind inhomogeneities, these systems may exhibit large variations in brightness on relatively short timescales (e.g., Liu, van Paradijs, and van den Heuvel, 2006; Chaty, 2018).

If the secondary star fills its Roche lobe, this can lead to a transfer of material to the compact object via the first Lagrange point and the formation of an accretion disk around it. Such a process results in a mass transfer rate that is much larger than by the capture of the stellar wind alone. Therefore, much higher X-ray luminosity is produced ($\sim 10^{38}$ erg s^{-1}) during outbursts. These systems are very rare and only a handful of them are known, an example being SMC X-1, situated in the Small Magellanic Cloud (e.g., Liu, van Paradijs, and van den Heuvel, 2006; Chaty, 2018).

1.10.2 Be/X-ray binaries

The majority of the known HMXBs are Be/X-ray binary systems (BeXRBs) (e.g., Liu, van Paradijs, and van den Heuvel, 2006). In the BeXRBs the donor stars are rapidly rotating Be stars situated on, or close to, the main sequence (luminosity class III–V), with masses in the range of about 8—20 $M_\odot$ (spectral types O9–B3). These secondaries are deep inside their Roche-lobes, as is indicated by long orbital periods of BeXRBs (>15 d up to 4 yr) and by the absence of X-ray eclipses and ellipsoidal light variations. These stars possess a circumstellar 'decretion' disk, which is believed to be related to the rapid, but sub-critical, rotation of the star. There is also a possible link with non-radial stellar pulsations (e.g., Rivinius, Carciofi, and Martayan, 2013, and the references therein).

With the possible exception of the BH in MWC 656, only NSs have been successfully identified as compact objects in BeXRBs (Casares et al., 2014). In general, NSs move in eccentric orbits, and the accretion onto the NS mostly occurs close to the periastron, which is thought to be the cause of the BeXRB X-ray outbursts (see Fig. 1.8). Most BeXRBs are detected as X-ray transients. The outbursts are generally classified into two categories. First, Type I outbursts recur with the orbital period and are expected to occur near periastron passage. Type II outbursts are more luminous,

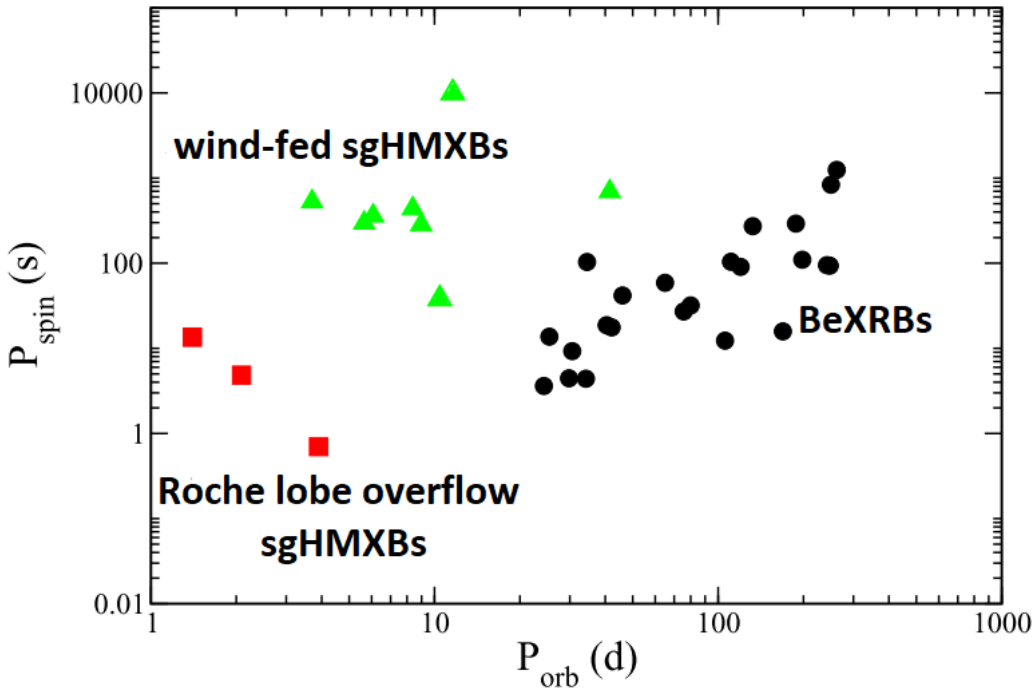

FIGURE 1.9: Corbet diagram (NS P_s versus system P_{orb}), showing the three HMXB populations: Roche lobe overflow (or disk-fed) sgHMXBs as red squares, wind-fed sgHMXBs as green triangles, and BeXRBs as black circles. Figure adapted from Reig (2011).

irregular, and occur less frequently. These outbursts have no obvious relation with the orbital phase and can have longer durations than Type I outbursts. The cause of Type II outbursts is not known (e.g., see review by Reig, 2011).

1.10.3 X-ray pulsars

A large portion of the HMXB systems hosts accreting pulsars. In these systems, the plasma approaching the NS is stopped by the pressure of the dipolar magnetic field and forced to move along the field lines toward the magnetic poles, where the captured matter releases its gravitational energy in the form of X-rays. The pulses of X-ray radiation are due to a misalignment of the NS's rotation axis and its magnetic axis. Therefore, such systems are often called X-ray pulsars. The detection of coherent pulsations from an accreting X-ray source provides one of the strongest pieces of evidence that the compact object is an NS. These pulsars occupy well-defined positions in the spin period (P_s) versus orbital period (P_{orb}) diagram (the Corbet diagram; Corbet, 1984; Corbet, 1986), according to the HMXB subtype they belong to, which also reflects the different types of mass transfer (see Fig 1.9). This diagram is a useful tool for studying the interaction and feedback between the NS and accreted matter, and the influence of the local absorbing matter. The location of the different systems in the Corbet diagram is determined by the equilibrium period reached by the rotation of the NS accreting matter on its surface (e.g., Chaty, 2018).

Roche lobe overflow sgHMXBs pulsars are clustered towards short orbital periods and short spin periods and display an anticorrelation in the Corbet diagram. Wind-fed sgHMXBs show long spin periods and short orbital periods, occupying the upper-left

part of the diagram. The lack of correlation for wind-fed sgHMXBs suggests that in this case, wind accretion is very inefficient to transfer angular momentum.

It is clear from this diagram that a strong correlation exists for BeXRBs ($P_s \propto (P_{orb})^2$). This can be understood in terms of the equilibrium period, which is the period at which the outer edge of the NS magnetosphere rotates with the Keplerian velocity. This equilibrium period depends on the NS rotation period, its mass, the magnetic field strength, and the properties of the stellar wind (Waters and van Kerkwijk, 1989; Tauris and van den Heuvel, 2006). If the NS (and hence the magnetosphere) spin period is smaller than the equilibrium period, then matter is ejected away by the propeller mechanism. Only if the spin period is larger than the equilibrium period can matter be accreted onto the NS. This results in angular momentum transfer to the NS, increasing its rotation velocity and therefore decreasing the spin period. The equilibrium period depends mainly on the accretion rate because it determines the size of the magnetosphere which is assumed to corotate with the NS. In turn, the accretion rate depends on the separation of the two components of the binary systems, hence on the orbital period (e.g., Reig, 2011).

As can be seen in the more detailed Corbet diagram for the Galactic, SMC, and LMC BeXRB pulsars (see Fig. 1.10), the one-dimensional projections of the data onto the $\log(P_{orb})$ and $\log(P_s)$ axes both suggest that the BeXRB population might be bimodal (Knigge, Coe, and Podsiadlowski, 2011). The short-period subpopulation has a characteristic $P_{orb} \approx 40$ d and $P_s \approx 10$ s, and the long-period subpopulation has $P_{orb} \approx 100$ d and $P_s \approx 200$ s, with the division between them more pronounced in P_s.

Knigge, Coe, and Podsiadlowski (2011) propose that these two subpopulations represent two distinct BeXRB formation channels, associated with two distinct SN types. Specifically, they hypothesize that the short-period subpopulation is produced by electron capture SNe (ECSNe), and the long-period subpopulation is created in iron-core-collapse SNe (CCSNe). ECSNe are also expected to form BeXRBs systems with lower orbital eccentricities, NS masses, and lower peculiar velocities.

1.10.4 HMXB birth sites

Finding an HMXB in its parent SNR implies a very young binary system, as the visibility time of SNRs is only a few 10^4 yr, much less than the lifetimes of HMXBs. However, several such associations exist.

- In the SMC, the BeXRB pulsar SXP 1062 was found to be associated with an SNR (Hénault-Brunet et al., 2012). Gvaramadze, Kniazev, and Oskinova (2019) also discovered an SNR shell probably associated with SXP 1323, also a BeXRB.

- There are also three HMXB-SNR associations in the LMC. Maitra et al. (2019) discovered a very young (<6000 yr) HMXB LXP 4.4 associated with an SNR. XMMU 050722.1-684758 might be also linked to an SNR (Maitra et al., 2021). DEM L241 is another HMXB with an uncertain primary (might be a BH) that is linked to the projected SNR (Seward et al., 2012).

- In the Galaxy, SS 433 and Circinus X-1 are linked to SNRs (Geldzahler, Pauls, and Salter, 1980; Heinz et al., 2013). However, it is unclear whether Circinus X-1 is an HMXB or an LMXB, and SS 433 is a microquasar prototype hosting a BH primary.

The association of an HMXB to its parent SNR presents a puzzle. The duration of the Ejector and Propeller phases (see, e.g., Reig, 2011) is expected to be far longer

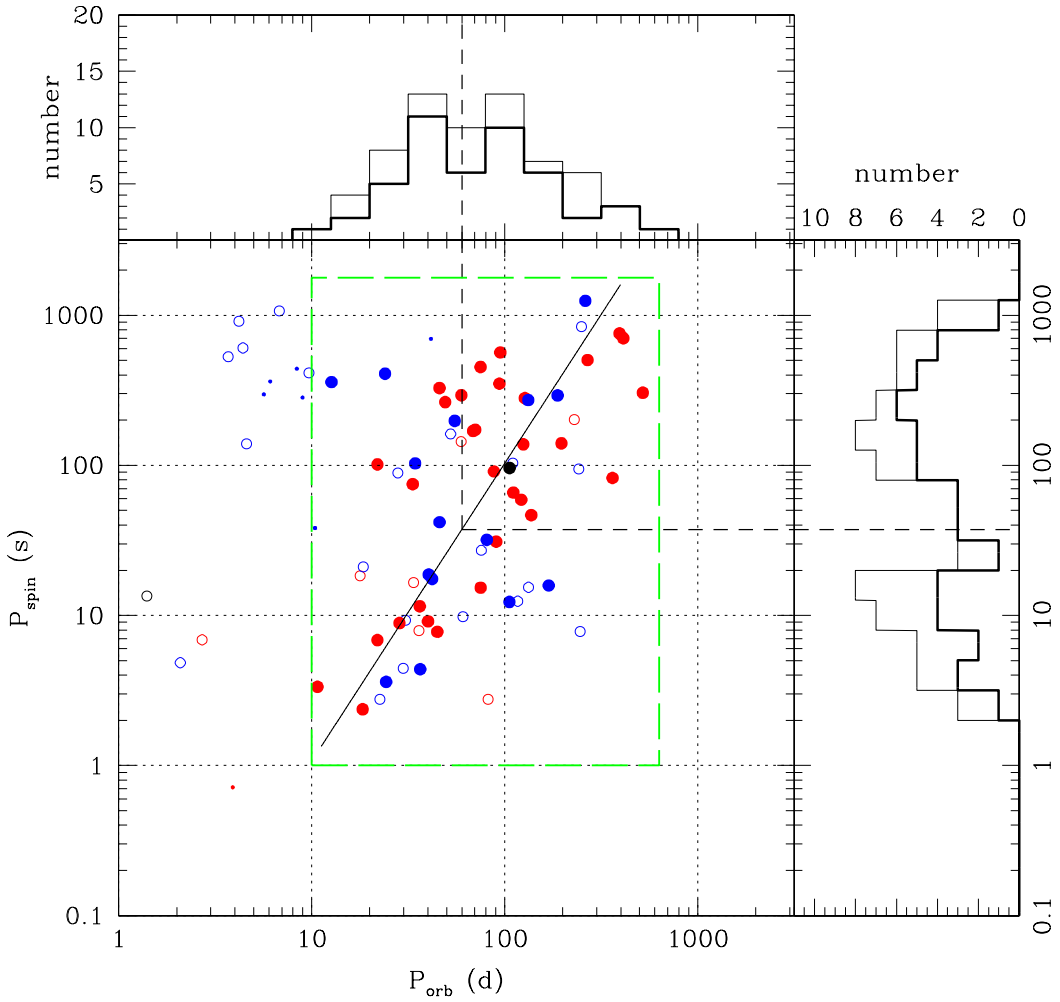

FIGURE 1.10: The Corbet diagram for MW, SMC, and LMC BeXRBs with measured $P_{\rm orb}$ and $P_{\rm s}$. The figure is composed of three parts. The inner panel shows the Corbet diagram ($\log(P_{\rm orb})$–$\log(P_{\rm s})$ distribution) for NS hosting BeXRBs. Filled circles denote spectroscopically confirmed BeXRBs, open circles BeXRB candidates, and small dots confirmed non-BeXRBs. The color indicates the host galaxy: blue corresponds to the MW, red to SMC, and black to LMC. The dashed green box selects the approximate parameter space occupied by the confirmed BeXRBs and used for the analysis in Knigge, Coe, and Podsiadlowski (2011). The histograms in the top and right-hand panels show the distribution of $P_{\rm orb}$ and $P_{\rm s}$ of the systems within the selection box. In both panels, the thick line corresponds to the confirmed BeXRBs only, while the thin line corresponds to both the confirmed and candidate BeXRBs. The horizontal and vertical dashed lines indicate apparent dips in the distributions of $P_{\rm s}$, and $P_{\rm orb}$, respectively.
Figure reproduced from Knigge, Coe, and Podsiadlowski (2011).

than the typical SNR lifetimes. Therefore, these associations should not be observed, as the HMXB is expected to 'switch on' long after the SNR has dispersed. However, Khokhriakova and Popov (2022) have demonstrated that after an NS experiences a fallback episode, and with certain realistic NS spin periods, magnetic field strengths,

and stellar wind properties of the secondary it is possible to avoid the Ejector stage. This speeds up the HMXB evolution which results in relatively rapid initiation of accretion, making the HMXB detectable.

Owing to the past SN explosion of one of its components, a significant portion of HMXBs possess high (runaway) peculiar velocities (e.g., van den Heuvel et al., 2000). Therefore, they do not remain in their parent cluster for long after the formation of a compact object. However, due to their luminous early-type secondaries, it is possible to obtain relatively precise parallaxes and proper motions for many of them, especially with *Gaia*. Therefore, it is possible to use their astrometric parameters to trace back their parent cluster.

The Vela X-1 system is one of the most well-known and best-studied X-ray binaries. It was reported by van Rensbergen, Vanbeveren, and De Loore (1996) that the system originated in the Vela OB1 association. Based on its astrometry, they conclude that Vela X-1 is a runaway system that was probably expelled from the association by the velocity kick imparted to the system during the SN explosion. The association was revisited in Kaper et al. (1997), who also discovered a bow shock associated with the system. Using the symmetry axis of the bow shock, they proposed a different direction of the peculiar velocity of the system than in van Rensbergen, Vanbeveren, and De Loore (1996). The system kinematics was further refined in Gvaramadze et al. (2011) and Gvaramadze et al. (2018) using the HIPPARCOS and *Gaia* DR1 data. The revised systemic trajectory suggested that Vela X-1 might have originated in Vela X-1. Kretschmar et al. (2021) (who also provided a recent review and synthesis of the knowledge about Vela X-1) derived a new distance to Vela OB1 association based on the EDR3 data, which places it at a distance that is consistent with the distance of Vela X-1, however, this distance estimate has a significant uncertainty, which makes it impossible to firmly conclude that Vela X-1 is indeed associated with Vela OB1.

There are other examples of HMXBs being ejected from their birth sites. Ankay et al. (2001) used the HIPPARCOS astrometry to propose that the HMXB 4U 1700-37 originates in the OB association Sco OB1. More recently, van der Meij et al. (2021) revisited this pair and determined that the HMXB originates from NGC 6231, which is the nucleus of Sco OB1. Using the kinematic age of the HMXB and the age of the cluster, they determined that the progenitor must have been a star with a mass in excess $\gtrsim$ 60 $M_\odot$. Another pairing was recently identified by Hambaryan et al. (2022), who traced back the motion of the HMXB 4U 2206+54 to the Cepheus OB1 association, and determined that the NS progenitor must have had an initial mass of $\gtrsim$ 32 $M_\odot$. Also, the HMXB candidate 1H 11255-567 was recently tracked back to the Lower-Centaurus-Crux group by Neuhäuser, Gießler, and Hambaryan (2020), where it could have originated up to ∼1.8 Myr ago.

1.11 HMXB population of the Magellanic Clouds

The Magellanic Clouds provide unique opportunities to study X-ray binary population, star formation, and their links.

Despite its small size, the SMC hosts more than 140 HMXBs and HMXB candidates – almost all of them BeXRBs (with the exception of SMC X-1). Approximately half of them show pulsations in the X-ray band, indicating the spin period of the NS (Haberl and Sturm, 2016). Gravitational interaction with the LMC and the Milky Way are believed to have triggered recent bursts of star formation about 25–60 Myr ago, which is a time scale consistent with the evolutionary age of the Be phenomenon

($\sim$ 40 Myr; Antoniou et al., 2010). The spin periods of the SMC BeXRBs have a bimodal distribution peaking at around 10 s and 250 s (Haberl and Sturm, 2016). The investigations of X-ray pulsars and their population studies in the SMC have several advantages over the equivalent studies done in the Milky Way:

- In the Milky Way, where most X-ray pulsars are located in the Galactic Plane, a large amount of absorption by the ISM poses problems for the detection and analysis of these sources. On the other hand, the SMC lies well above the Galactic Plane, so the sources within it are only moderately affected by the Galactic absorption ($N_H \approx 6 \times 10^{20}\mathrm{cm}^{-2}$; Dickey and Lockman, 1990). The line-of-sight extinction across the SMC has also been well-studied (Zaritsky et al., 2002).

- Due to the observational problems, it is difficult to derive precise distances to the X-ray pulsars in the Milky Way. This impacts the precision of the derived parameters as they are sensitive to distance. For the SMC objects and certain science cases, it is reasonable to assume that all sources lie at the same well-known distance of about 60 kpc (Graczyk et al., 2020). However, it should be noted that the SMC is significantly extended along the line of sight and the line of sight depth is also significant (see e.g. Tatton et al., 2021, for a recent overview).

- In order to conduct a population study for a given object type, it is necessary to conduct an all-sky survey, whereas the angular size of the SMC of a couple of degrees allows complete coverage of the entire galaxy using just a few observations.

Due to the lower metallicity of the SMC, the comparison between the SMC and Milky Way provides an important insight into the effects of metallicity on the evolutionary pathways of the X-ray pulsars and their progenitors.

While the Large Magellanic Cloud (LMC) is significantly more massive than the SMC, the number of HMXBs in the LMC is a lot smaller. Including the recent new discoveries, the total tally is $\sim$60 LMC HMXB candidates, with 25 of them being X-ray pulsars (Haberl and Sturm, 2016; Maitra et al., 2021; Haberl et al., 2021; Haberl et al., 2022). The fraction of sgHMXBs is higher in the LMC as compared to the SMC (Antoniou and Zezas, 2016; Vasilopoulos et al., 2018). This, together with the lower overall number of LMC HMXBs relative to the SMC is probably related to the different star formation history of the two galaxies (Antoniou et al., 2010; Antoniou and Zezas, 2016).

As in the SMC, studying HMXBs in the LMC also has advantages, and the points outlined in the text above still apply. However, its larger projected angular size in the sky hinders extensive monitoring observations, as deep X-ray observations with the modern observatories can only cover a small part of the LMC (e.g., Maggi et al., 2016). This probably partly contributes to the lower number of known LMC HMXBs as well.

Unlike in the SMC, the BeXRB pulsar population in the LMC does not show evidence of the bimodality of the spin periods as in the SMC and MW, despite the recent discoveries of new BeXRB pulsars. However, the LMC is still not adequately covered in X-rays. It can be expected that the continuation of targeted and serendipitous observations will likely uncover more of the LMC HMXB population and allow us to reach more definite conclusions (Haberl et al., 2022).

1.12 Black holes and black hole binaries

Black holes (BHs) are formed when massive stars fail to explode as SNe and undergo direct collapse. The alternative is the delayed collapse channel, where an explosion can occur, but its energy is not sufficient to completely unbind the stellar envelope, and a large fraction of matter falls back onto the nascent NS (the so-called fallback), leading to the formation of a BH (e.g., Mirabel, 2017, for a review). Theory shows that there could be certain ranges in the property space of massive stellar progenitors in which the stars are less likely to explode and instead collapse straight into a BH (e.g., Pejcha and Thompson, 2015; Sukhbold et al., 2016).

The Galaxy is believed to host $\sim 10^8$ quiescent stellar-mass BHs (Shapiro and Teukolsky, 1983). However, these are practically invisible so their detection is very hard and not much is known about them. However, as they are very massive, they can potentially be detected using gravitational microlensing – photometric or astrometric (e.g., Paczynski, 1996; Bramich, 2018). Here, a BH can act as a massive lens, distorting the positions and brightness of the stars that are projected close to it in the sky but lying at much further distances than the BH. Despite the advent of microlensing surveys including the Optical Gravitational Lensing Experiment (OGLE), the Microlensing Observations in Astrophysics (MOA), and *Gaia* (which also collects epoch astrometry that is expected to be included in the future data releases), these events are expected to be very elusive, as the invisible nature of isolated BHs makes it impossible to predict microlensing events in advance using the astrometric information. Nevertheless, two teams (Lam et al., 2022; Sahu et al., 2022), working independently, recently reported the detection of a compact object OGLE-2011-BLG-0462/MOA-2011-BLG191 (OB110462) using a combination of photometric data and HST astrometry. However, the reported properties of the lens object were significantly different in each study. Lam et al. (2022) reported a lens mass between 1.6–4.2 $M_\odot$, consistent with either a NS or a BH, while Sahu et al. (2022) inferred a more tightly constrained mass of 7.1 ± 1.3 $M_\odot$, consistent with a BH. The reported kinematics were also different – in Lam et al. (2022) OB110462 has a transverse velocity $\lesssim 25$ km s^{-1}, while in Sahu et al. (2022) it is $\sim$45 km s^{-1}. By modeling the population of isolated Galactic BHs, Vigna-Gómez and Ramirez-Ruiz (2022) concluded that this object most likely originates from a disrupted binary system. Future detections of BH microlensing events can be useful to understand the isolated and binary evolution of massive stars.

A logical choice would be observing BHs in binary systems with luminous stars. A presence of a luminous companion would allow determining the distance, the radial velocity, and the proper motion of the system, from which it is possible to derive its systemic velocity, which can provide information on the formation of the BH, and in some cases even to determine its birthsite (potentially a star cluster or an SNR). This can lead to the determination of the mass and the metallicity of the BH progenitor. If the binary system is wide and detached (so the components have never interacted), the properties of the secondary can also be used to constrain the mass and metallicity of the BH progenitor. Recently, several studies with detailed orbital motion analysis have identified a number of such systems with a BH component. However, the BH binary interpretations for most of these systems identified to date are controversial. Further work by independent groups proposed non-BH explanations for many of these systems (see, e.g., Stevance, Parsons, and Eldridge, 2022; El-Badry et al., 2022, and the references therein for a more detailed discussion).

Tight binaries hosting BHs that interact with their secondaries are more suitable for constraining BH kicks (at least for now), despite the inherent bias that arises when

considering such a sample, as such binaries are formed through a very specific formation channel. These BH X-ray Binaries (BHXRBs) are interacting binary systems where X-rays are produced by material accreting from a secondary companion star onto a BH primary. We know of ∼70 BHXRB systems and candidates in the Milky Way (Corral-Santana et al., 2016; Tetarenko et al., 2016). These systems provide useful test sites for investigating BH formation channels. Atri et al. (2019) and Gandhi et al. (2019) studied the kinematics of BHXRBs and discovered that the majority of the studied sources have received significant BH kick ($\gtrsim$ 50 km s^{-1}). The same conclusion was reached by studying the height of the BHXRBs above the Galactic plane (e.g., Repetto, Igoshev, and Nelemans, 2017). The typical lifetimes of BHXRBs are very long, since they are mostly hosting low-mass secondary donor stars. For this reason, aside from the velocity imparted during the BH formation, most of them have also acquired some additional velocity by dynamic diffusion and encounters with giant molecular clouds. Therefore, in general, we do not expect to find them near their parent star clusters. A notable exception is GCs, which have significant escape velocities that are sufficient to capture low-kick BHs and BH binaries. For this reason, many GCs retain a significant BH population, and these BHs often form various exotic binaries through dynamical interactions, but they are also present in directly undetectable configurations. This makes GCs prime sites for hosting compact object mergers and gravitational wave events (e.g., Kulkarni, Hut, and McMillan, 1993; Maccarone et al., 2007; Strader et al., 2012; Peuten et al., 2016; Hénault-Brunet et al., 2020; Weatherford et al., 2020; Gieles et al., 2021).

For BHXRBs with massive secondaries and therefore limited lifetimes, it is also possible to search for parent clusters. Perhaps the most well-known object from this class is the X-ray binary Cygnus X-1, which contains the first BH ever discovered. According to Mirabel and Rodrigues (2003), Cygnus X-1, which hosts a ∼10 M$_\odot$ BH with a more massive O supergiant donor star, is moving in the OB association Cygnus OB3, with a very small relative velocity to it, consistent with the random velocity dispersion of the association members. Since the most massive star in the association has a mass of ∼40 M$_\odot$, this is also the lower mass limit for the BH progenitor. The low peculiar velocity of the system implies that the BH was formed through a low-energy SN explosion (with little mass loss from the system and weak velocity kick) or even by prompt implosion without an SN. Recently, Miller-Jones et al. (2021) reassessed the distance to Cyg X-1 to about 2.22 kpc, which changed the inferred BH mass to ∼21 M$_\odot$, making it more massive than any previously observed BH in BHXRBs. This new distance is also consistent with the revised distance to Cygnus OB3 of 2.0±0.3 kpc (Rao et al., 2020). This distance revision only slightly increased its relative velocity to the association to ∼11 km s^{-1}. Another BHXRB that can be traced back to its parent cluster is LMC X-1, which also drives a bow shock. Hyde et al. (2017) investigated the cluster N159-O1 as a likely site of origin of this system and derived a BH progenitor mass ∼60 M$_\odot$.

The first observed BH formation candidate was observed in the galaxy NGC 6946 (Gerke, Kochanek, and Stanek, 2015; Adams et al., 2017). The analysis of the stellar population in the vicinity of the disappearing star yielded the progenitor lifetime of ∼10.6 Myr and the progenitor initial mass of ∼18 M$_\odot$ (Murphy et al., 2018). Another candidate was recently identified in the galaxy M 101 (Neustadt et al., 2021).

Chapter 2

Occurrence of bow shocks around high-mass X-ray binaries

2.1 Paper summary

High-mass X-ray binaries (HMXBs) are systems containing a compact object – a neutron star (NS) or a black hole (BH) – and a massive, early-type companion of spectral class O or B. As the name suggests, they are strong emitters of X-ray radiation, which is produced as the result of the accretion of matter from the stellar companion onto the compact object (e.g., Lewin and van der Klis, 2006; Liu, van Paradijs, and van den Heuvel, 2006; Reig, 2011).

Due to the past supernova (SN) explosion that has occurred within the system, a significant portion of HMXBs are runaway systems, possessing large peculiar (systemic) velocities (e.g. van Oijen, 1989; van den Heuvel et al., 2000). Normally, in order to identify a runaway star and obtain its peculiar velocity, high-quality astrometry (i.e. parallaxes and proper motions) and radial velocity measurements from spectroscopy are needed. However, a lot of HMXBs are very distant, affected by heavy extinction, and lie in the fields with very high source densities (Liu, van Paradijs, and van den Heuvel, 2006; Walter et al., 2015). This means that a lot of HMXBs only have an infrared or a very faint optical counterpart, which poses a challenge even for the contemporary modern missions such as *Gaia* (Gaia Collaboration et al., 2016b). Radial velocities of HMXBs are also often unreliable because the optical lines of OB stars are formed in atmospheric layers that have variable outflow velocities of several tens of $\mathrm{km\,s^{-1}}$ (van Oijen, 1989).

Another possible method of searching for runaway star candidates is through the detection of bow shocks associated with these objects (e.g., Peri et al., 2012; Kobulnicky et al., 2016). This method does not rely on the knowledge of the astrometry of the star or parameters of its local standard of rest (LSR). Stellar bow shocks are also parsec-scale structures and are prominent in the mid-infrared, which makes them discernible even at large distances (Gvaramadze, Kroupa, and Pflamm-Altenburg, 2010; Gvaramadze, Pflamm-Altenburg, and Kroupa, 2011).

The presence of a stellar bow shock associated with an HMXB is potentially very valuable, as the bow shock properties depend on the density of the ambient ISM, properties of stellar wind of the companion, and the velocity of the system with respect to the ISM. Only 11 HMXBs have been studied for the presence of stellar bow shocks possibly associated with these systems (Huthoff and Kaper, 2002). Despite this limited sample, two bow shock-hosting HMXBs have been identified among these objects – one around Vela X-1 and the second one around 4U 1907+09 (Kaper et al., 1997; Gvaramadze et al., 2011). Therefore, with more than a hundred Galactic HMXBs and HMXB candidates known, and the advent of the modern missions operating in the mid-infrared, such as the *Spitzer* Space Telescope (Werner et al., 2004) and

the Wide-field Infrared Survey Explorer (WISE; Wright et al., 2010) – the former providing a high mid-infrared resolution and the latter a mid-infrared all-sky survey – it was reasonable to expect that many bow shocks associated with HMXBs await discovery.

Therefore, for the HMXBs listed in Liu, van Paradijs, and van den Heuvel (2006) and Walter et al. (2015), I searched for all available mid-infrared data. The retrieved WISE images from WISE Image Service[1] covered all HMXBs and could be used in their retrieved form. In order to obtain *Spitzer* science-grade images, I retrieved the relevant observations (if available) and processed them using the mission software MOPEX (Makovoz and Khan, 2005). The fields around the studied HMXBs were visually examined for the presence of the extended emission, with the focus on the WISE 22 μm and *Spitzer*-MIPS (Rieke et al., 2004) 24 μm images. These wavelengths have proven to be especially suitable for the bow shock searches (e.g., Kobulnicky et al., 2016). The flux cuts and the scaling of the studied images were changed manually depending on the particular field. If a diffuse emission, potentially linked with an HMXBs, was identified in the images, I searched for possible counterparts in other wavebands as well.

This search yielded diffuse structures projected around 12 HMXBs. The structures could be broadly categorized into several classes: arc-like structures (around γ Cas, GX 304-01, EXO 1722-363), wispy circumstellar nebulae (EXO 051910+3737.7, 1H 1255-567), cavities/bubbles (IGR J11435-6109, AX J1841.0-0536, XTE J1855-026), and partial cavities/bubbles (GX 301-2, 4U 1700-37, XTE J1739-302). The relevant images can be found in the accompanying paper.

I have utilized the data outside the mid-infrared and the *Gaia* data release 2 astrometry (GDR2; Gaia Collaboration et al., 2018; Lindegren et al., 2018) to compute HMXB peculiar velocities in order to investigate the alignment between the symmetry of the diffuse structures (if present) and the direction of the peculiar motion, which can be instrumental in determining whether the projected structures and HMXBs are physically associated.

Only one of these detections can be regarded as a bow shock candidate, namely GX 304-01, where the unusual dimpled structure near the arc apex prevents its classification as a secure bona fide stellar bow shock. Despite the ambiguity, the system possesses a moderate runaway velocity, and, if the bow shock is real, it would be the first such object identified around a Be/X-ray binary (BeXRB).

The absence of bow shocks around the studied HMXBs is puzzling. Even if the structure around GX 304-01 was regarded as a stellar bow shock, the incidence of observable bow shocks associated with HMXBs would be $\sim$2%. This is noticeably lower than the bow shock incidence around OB runaway stars (ranging from around 40% to 6%, depending on the study van Buren, Noriega-Crespo, and Dgani, 1995; Huthoff and Kaper, 2002; Peri et al., 2012; Peri, Benaglia, and Isequilla, 2015). The paucity of other circumstellar structures that could result from the stellar feedback, which can be directly linked with the studied HMXBs, is also unexpected. A possible explanation for this lack of bow shocks and other associated objects might be a hypothesis proposed by Huthoff and Kaper (2002), who suggest that HMXBs and OB runaways have, in general, different kinematic ages. HMXBs are thought to be kinematically younger, attaining their large peculiar velocities when one of the binary components explodes in an SN. Therefore, they are still enclosed within the hot and rarefied regions (hot bubbles) around their parent OB associations and star clusters – unable to form an observable bow shock even if their velocity is high. OB runaways

[1] https://irsa.ipac.caltech.edu/applications/wise/

have predominantly escaped their parent associations or clusters early on when the cluster was dense and the probability of dynamical ejections was high. Thus they are more likely to have already escaped from the zone of influence of their parent clusters and associations and are more likely to form bow shocks. Some supporting evidence for this can be found in Bodaghee et al. (2012), who studied the clustering between HMXBs and OB association and also suggest that the massive binary progenitors of HMXBs tend to remain gravitationally bound to their birth sites prior to the SNe explosions in these systems.

This also implies that if the progenitors to HMXBs are not usually expelled from their birth sites by dynamical interactions early in the cluster lifetimes, the two-step ejection process – when the system is first dynamically ejected and later on experiences another kick in a random direction during an SN explosion (Pflamm-Altenburg and Kroupa, 2010) – is not at work for a number of HMXBs. This should make it possible to backtrack some HMXBs to their parent clusters and associations using the HMXB astrometry. This opens several possibilities for further research, such as determining precise kinematic ages of HMXBs, compact object velocity kicks, and masses of the compact object progenitors.

2.2 Paper I

A&A 621, A37 (2019)
https://doi.org/10.1051/0004-6361/201832682

Astronomy & Astrophysics

Concerning the occurrence of bow shocks around high-mass X-ray binaries*

M. Prišegen

Department of Theoretical Physics and Astrophysics, Masaryk University, Kotlářská 2, 611 37 Brno, Czech Republic
e-mail: michalprisegen@gmail.com

Received 22 January 2018 / Accepted 1 November 2018

ABSTRACT

Context. We investigate the occurrence of stellar bow shocks around high-mass X-ray binaries (HMXBs) in the Galaxy.
Aims. We seek to conduct a survey of HMXBs in the mid-infrared to search for the presence of bow shocks around these objects.
Methods. Telescopes operating in the mid-infrared, such as the *Spitzer* Space Telescope or Wide-field Infrared Survey Explorer (WISE), are potent tools for searching for the stellar bow shocks. We used the available archival data from these telescopes to search for bow shock candidates around the confirmed and candidate HMXBs in the Galaxy.
Results. We detected extended mid-infrared structures around several surveyed confirmed and candidate HMXBs. Two of these structures, associated with Vela X-1 and 4U 1907+09, are genuine bow shocks that have been studied previously. However, there are no new unambiguous bow shocks among the rest of the objects. The paucity of bow shocks around HMXBs suggests that the majority of these systems still reside within hot, low-density bubbles around their parent star clusters or associations. This also implies that the dynamical ejection of massive binaries is apparently less efficient than the ejections caused by the supernova explosions inside a binary.

Key words. proper motions – binaries: general – stars: early-type – stars: kinematics and dynamics – infrared: ISM

1. Introduction

High-mass X-ray binaries (HMXBs) are systems consisting of a massive, early-type star (spectral class O or B) in the process of stellar evolution and a compact object, neutron star, or black hole, revolving around their common center of mass. The compact object accretes mass from the stellar wind of its companion or, if the companion star fills its Roche lobe, the matter flows directly onto the compact object (e.g., Lewin et al. 1997; Lewin & van der Klis 2006; Liu et al. 2006).

Owing to the past supernova explosion of one of its components, possibly combined with close dynamical encounters of the system with other stars in its parent cluster as well, a significant portion of HMXBs possess high (runaway) space velocities (e.g., van Oijen 1989; Kaper et al. 2004). Furthermore, their galactic height distribution also implies their runaway nature (van Oijen 1989).

Traditionally, runaway stars can be revealed via measurements of their proper motions, yielding their tangential velocities. However, this method requires the distance to the object to be determined and the proper motion to be measured with sufficient precision. Determination of the radial velocities via spectroscopic measurements is also a viable method. Nevertheless, these methods are only applicable to a portion of relatively close HMXBs, having sufficiently large proper motion to be reliably measured and/or bright optical counterpart for the spectroscopic studies. With the advent of modern high-energy missions, there has been a sharp increase in the number of confirmed and candidate HMXB systems that are detected at considerable distances, are often highly absorbed, and only have weak infrared counterparts. As they are hard objects to study with the above methods, the kinematics of these objects is poorly known.

Another means of searching for runaway star candidates is through the detection of bow shocks associated with these objects (e.g., van Buren & McCray 1988; van Buren & Noriega-Crespo 1995; Gvaramadze & Bomans 2008; Gvaramadze et al. 2011a; Peri et al. 2012). This method does not rely on the knowledge of the star's proper motion, precise distance, or the characteristics of the local standard of rest (LSR) of the studied system. Stellar bow shocks are also parsec-scale structures, manifesting strongly in the mid-infrared, so they can be detected at considerable distances due to their size and low levels of extinction at these wavelengths (e.g., Gvaramadze et al. 2010, 2011b). Thus, this method could be especially potent when studying distant HMXBs, as most of them do not have their proper motions and distances determined or they are measured with low significance.

The peculiar radial velocity of HMXBs, their Galactic height distribution, and low OB association memberships provides a strong evidence that HMXBs are a subclass of high-velocity stars (van Oijen 1989). This conclusion was verified by the peculiar tangential velocity measurements by Chevalier & Ilovaisky (1998) and van den Heuvel et al. (2000). Both studies also note a disparity between the peculiar tangential velocities of OB-supergiant X-ray binaries and Be/X-ray binaries; the former group has a mean peculiar tangential velocity $\langle v_{\rm pec,tan}\rangle = 42 \pm 14\,{\rm km\,s^{-1}}$, while the latter only has a modest $\langle v_{\rm pec,tan}\rangle = 15 \pm 6\,{\rm km\,s^{-1}}$ (van den Heuvel et al. 2000). Despite the considerable difference in the peculiar velocity between the two subgroups, the faster members of the Be/X-ray binary subgroup

* *Herschel* is an ESA space observatory with science instruments provided by European-led Principal Investigator consortia and with important participation from NASA.

should have sufficient peculiar velocity to produce an observable bow shock (Meyer et al. 2017).

The first detection of a bow shock associated with a HMXB was reported by Kaper et al. (1997), who discovered a faint arcuate structure around a well-known HMXB Vela X-1 in a Hα image obtained with the 1.54 m Danish telescope at the European Southern Observatory. The first bow shock survey of HMXBs was conducted by Huthoff & Kaper (2002), choosing a sample of 11 HMXBs for which the conditions for bow shock formation seemed favorable: a large peculiar velocity and an OB companion with a strong stellar wind and a high luminosity. Using high-resolution IRAS maps, Huthoff & Kaper (2002) detected an infrared counterpart to the already known bow shock generated by Vela X-1. Another survey was conducted by Gvaramadze et al. (2011c) on the same sample of HMXB systems. They utilized the data from the *Spitzer* Space Telescope, which were of higher quality but they covered only 5 of 11 HMXB from the original sample. Nevertheless, these authors were able to discover a new bow shock around 4U 1907+09 and provided a more detailed view of Vela X-1 bow shock as well.

We are currently aware of more than a hundred HMXBs or HMXB candidates in the Galaxy and their numbers are increasing (Liu et al. 2006). Together with the advent of space infrared missions such as *Spitzer* Space Telescope (Werner et al. 2004) and Wide-field Infrared Survey Explorer (WISE; Wright et al. 2010), this presents an opportunity to have a more detailed look at the bow shock occurence around HMXBs. In this paper, we have undertaken a search for bow shocks around the Galactic HMXBs from the fourth edition of the Catalog of High Mass X-ray binaries in the Galaxy (Liu et al. 2006) and around systems listed in Walter et al. (2015), which are not listed in Liu et al. (2006).

The paper is organized as follows. The rationale, observations, and general data processing are described in Sect. 2. A detailed description of the selected targets and supplementary astrometry is given, respectively, in Sects. 3 and 4. We discuss the nature of the emission around the studied objects in Sect. 5. Finally, the summary and conclusions are provided in Sect. 6.

2. Rationale and methods

A number of past successful studies of bow shocks conducted in the mid-infrared (e.g., Peri et al. 2012, 2015; Kobulnicky et al. 2016 and the references therein) and extensive computational work (e.g., Meyer et al. 2016, 2017) suggest that this part of the electromagnetic spectrum is the most suited for bow shock searches.

To search for bow shocks around HMXBs, we used data obtained by Multiband Imaging Photometer for *Spitzer* (MIPS; Rieke et al. 2004) extracted from the *Spitzer* Space Telescope archive and data obtained from WISE Image Service. The available *Spitzer* data cover the fields containing less than a half of catalogued HMXBs, the data from WISE cover all surveyed HMXB systems. To obtain science-grade images, the *Spitzer* data was processed by Mosaicking and Point source Extraction (MOPEX; Makovoz & Khan 2005). Visual inspection of *Spitzer* and WISE images was used to search for the extended emission possibly associated with the HMXBs. To search for the possible counterparts of the detected emission, we used the SuperCOSMOS H-alpha Survey (SHS; Parker et al. 2005), data obtained by the Photodetector Array Camera and Spectrometer (PACS; Poglitsch et al. 2010), and the Spectral and Photometric Imaging Receiver (SPIRE; Griffin et al. 2010) on board the *Herschel* Space Observatory (Pilbratt et al. 2010), and data obtained by the InfraRed Array Camera (IRAC; Fazio et al. 2004) on board the *Spitzer* Space Telescope.

3. Remarks on individual objects

Owing to the short lifetimes of HMXBs, these objects cannot travel far from the Galactic plane where they formed. This means that they are often projected onto a region with complex diffuse infrared emission and it is often hard to conclude whether the emission is actually physically related to the system or is of a foreground/background origin. However, a physical relation is likely if the diffuse emission is centered at the system or exhibits some degree of symmetry wherein the HMXB lies on or near the axis of symmetry. Below, we briefly describe the systems with such infrared emission.

3.1. γ Cas

γ Cas has attracted a lot of attention since its discovery as the first of what became known as Be stars (Secchi 1866). Despite considerable interest, the origin of X-ray emission from the object is still highly debated. The proposed scenarios include the accretion onto a neutron star or a white dwarf and a magnetic star–disk interaction (see review by Smith et al. 2016 and the references therein). The nature of this system is so peculiar that it has become a prototype of a separate class of X-ray emitters knowns as "γ Cas analogs". While the recent study by Postnov et al. (2017) reconciles the peculiar X-ray properties of γ Cas by invoking a fast spinning neutron star as a companion, their results are disputed (Smith et al. 2017). Because of its atypical properties and the disputed nature, we consider γ Cas as a HMXB candidate only.

γ Cas is a relatively nearby object. Both Perryman et al. (1997) and Coleiro & Chaty (2013) put it at a similar distance of 0.19 and 0.17 kpc, respectively. Megier et al. (2009) estimated a lower distance of 0.12 kpc. We adopt a distance of 0.15 kpc as a compromise for the subsequent analysis.

WISE 22 μm image (Fig. 1) reveals a faint arc-like nebula to the north of the system. Unfortunately, the system is not covered by the *Herschel* data and *Spitzer* data are limited to the first two IRAC channels, taken in the post-cryo mode, which do not show any discernable diffuse emission. The system is slightly offset from the axis of the symmetry of the arc. The system is also embedded in a fainter 22 μm diffuse emission.

3.2. EXO 051910+3737.7 (V420 Aur)

The X-ray source was discovered by Uhuru satellite (Forman et al. 1978) and associated with a Be star V420 Aur by Polcaro et al. (1984). No X-ray pulses have been detected from the system (Liu et al. 2006).

The system does not have a significant HIPPARCOS parallax, Chevalier & Ilovaisky (1998) estimated the distance to be approximately 1.05 kpc using a typical luminosity of a B0 subgiant. Astraatmadja & Bailer-Jones (2016) estimated the distance to be 1.5 ± 0.5 kpc utilizing *Tycho-Gaia* astrometric solution (TGAS; Lindegren et al. 2016) parallaxes and Milky Way prior. A more recent catalog by Bailer-Jones et al. (2018), employing the second *Gaia* data release (hereafter GDR2; Gaia Collaboration 2018), puts the system at $1.29^{+0.11}_{-0.09}$ kpc.

The system appears to be a center of an irregular wispy infrared nebula (Fig. 2), readily apparent on WISE 12 μm, 22 μm, and MIPS 24 μm images. The central, brighter part of the nebula, is divided into two filaments, aligned in the Galactic

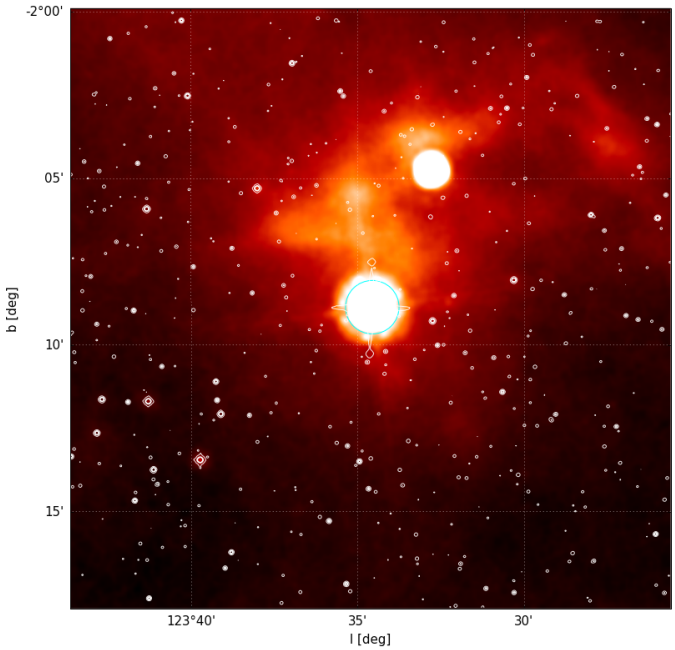

Fig. 1. WISE 22 μm image of the field around γ Cas with 2MASS Ks contours (sensitive to starlight) overlaid on top. The system position is indicated by the cyan circle.

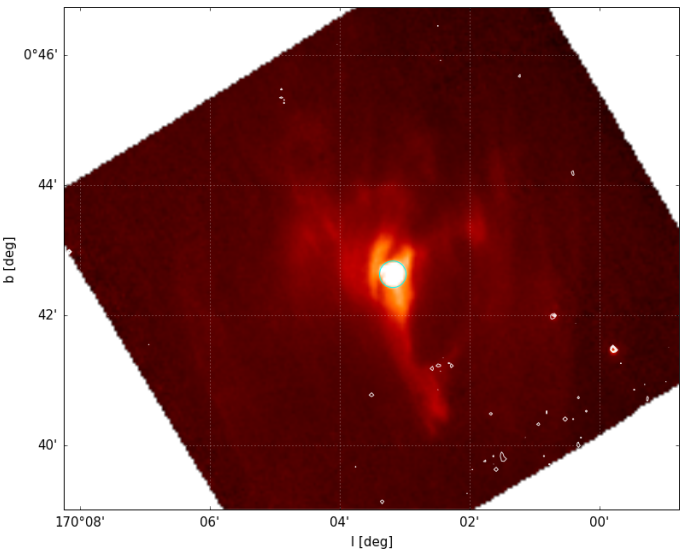

Fig. 2. *Spitzer* MIPS 24 μm image of the field around EXO 051910+3737.7 (V420 Aur) with *Spitzer* IRAC 3.6 μm contours (mainly sensitive to starlight) overlaid on top. The system position is indicated by the cyan circle.

north–south direction: one apparently connected with the system and one slightly ahead of it. The nebula also possesses four fainter arms; the most dominant arm extends toward the Galactic south and the fainter three point to the Galactic north, northwest, and northeast.

3.3. IGR J11435-6109

IGR J11435-6109 is a HMXB discovered by Grebenev et al. (2004) via INTEGRAL mission. The system is an X-ray pulsar with a pulse period of about 162 s and orbital period of 52.5 days

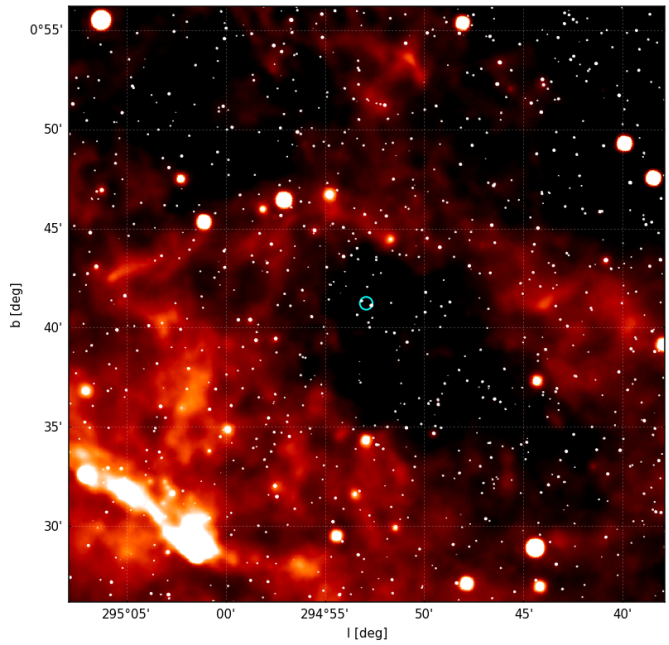

Fig. 3. WISE 22 μm image of the field around IGR J11435-6109 with 2MASS K band contours (sensitive to starlight) overlaid on top. The system position is indicated by the cyan circle.

(in't Zand & Heise 2004; Corbet & Remillard 2005). The optical counterpart was determined by Tomsick et al. (2007) and confirmed by Negueruela et al. (2007). Coleiro et al. (2013) refined the spectral classification to B0.5Ve, confirming the system as a Be/X-ray binary.

The system is a distant X-ray binary (>6 kpc; Negueruela et al. 2007). Masetti et al. (2009) estimated the distance to be about 8.6 kpc. Coleiro & Chaty (2013) derived a slightly higher distance, $d = 9.8 \pm 0.86$ kpc. Bailer-Jones et al. (2018) confirmed the distant nature of this HMXB, placing it at $8.59^{+2.54}_{-1.81}$ kpc.

Figure 3 shows the enviroment around the system. IGR J11435-6109 appears to be projected onto the eastern part of a large cavity.

3.4. GX 301-02

GX 301-2 is an obscured HMXB system that is very bright in X-rays, thanks to the slow and very dense stellar wind of its massive, hyper giant companion (Kaper et al. 2006). The system contains a pulsar with a period of around 700 s in 41.5 days, highly eccentric orbit (Sato et al. 1986).

The distance to GX 301-2 was estimated by Kaper et al. (2006) to be in a range of 3–4 kpc. Coleiro & Chaty (2013) estimated the distance to be 3.1 ± 0.64 kpc via a spectral energy distribution procedure. The system is covered in TGAS, however, the measured parallax is not significant (0.34 ± 0.75), so the distance estimates by Astraatmadja & Bailer-Jones (2016) vary significantly based on the prior used. The distance estimate was refined after GDR2; Bailer-Jones et al. (2018) estimated the distance to the system $d = 3.53^{+0.52}_{-0.40}$ kpc, confirming the previous estimates.

The system lies in a region of very bright and complex infrared emission (see Fig. 4). This system is embraced by a region of bright 24 μm emission to the Galactic south and a bright ridge of extended emission to the north. The PACS and SPIRE data suggest that the system could be enclosed in a partial far-infrared bubble, open at one side.

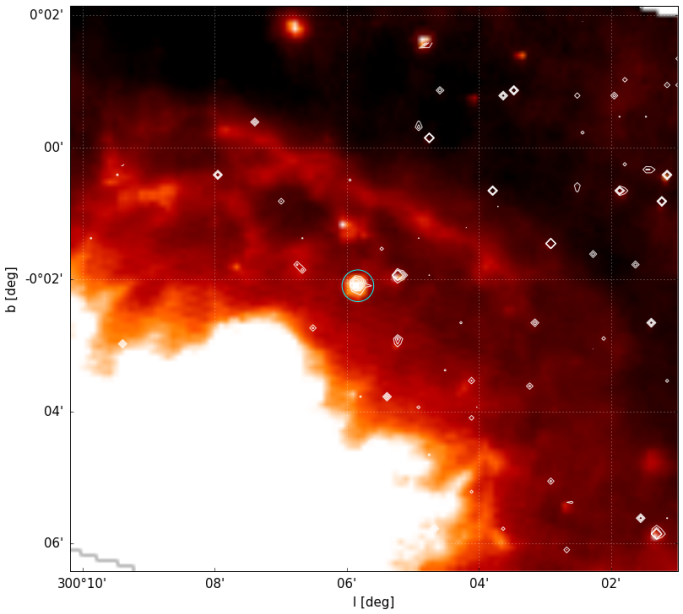

Fig. 4. *Spitzer* MIPS 24 μm image of the field around GX 301-2 (BP Cru) with *Spitzer* IRAC 3.6 μm contours (mainly sensitive to starlight) overlaid on top. The system position is indicated by the cyan circle.

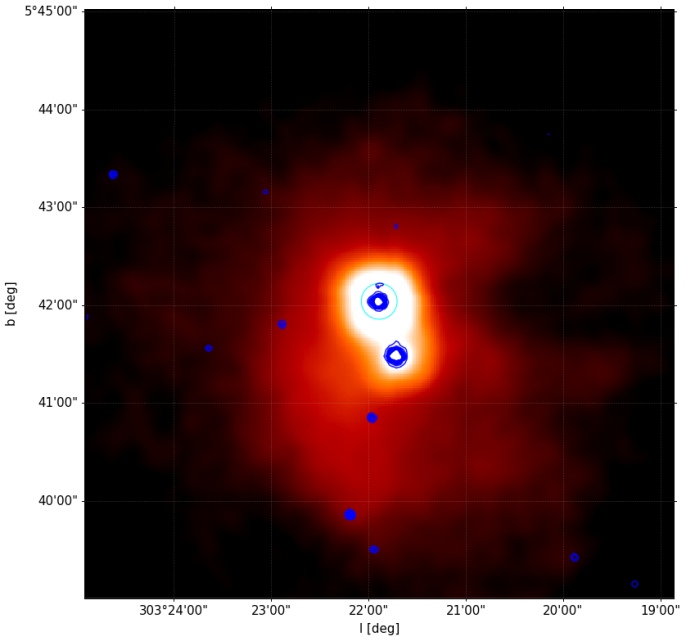

Fig. 5. WISE 22 μm image of the field around 1H 1255-567 (μ^2 Cru) with 2MASS Ks contours (sensitive to starlight) overlaid on top. The system position is indicated by the cyan circle.

3.5. 1H 1255-567

Listed as a HMXB candidate in Liu et al. (2006), but as a Be star in Simbad (Levenhagen & Leister 2006), the system is a part of a visual double with μ^1 Cru (Hoffleit & Jaschek 1982).

1H 1255-567 appears to be a close system. Chevalier & Ilovaisky (1998) estimated its distance to be about 111 ± 8 pc. Chen et al. (2012) listed a slightly larger value of 125 ± 5 pc. More recently, Bailer-Jones et al. (2018) estimated the distance to be 112^{+2}_{-3} pc.

Figure 5 shows a WISE 22 μm image of the visual double with both members visible in far-infrared emission, enshrouded in a fine extended nebula. The nebula bears a complex shape and has a system of fine filaments and wisps, emanating from μ^1 Cru (the prominent unmarked source to the Galactic south of 1H 1255-567) and 1H 1255-567 as well.

3.6. GX 304-01

The HMXB GX 304-01 (4U 1258-61) was discovered by balloon X-ray observations in 1970 (McClintock et al. 1971). The optical counterpart of the X-ray source was identified by Mason et al. (1978), making V850 Cen the most likely counterpart. A subsequent spectral analysis by Parkes et al. (1980) showed the presence of a strong double-peaked emission in Hα and deep sharp absorption lines indicating a Be star. The most recent measurements give a more precise spectral classification that indicates the secondary is a B0.7 Ve star (Ziolkowski 2002). Using the data from Vela satellite, Priedhorsky & Terrell (1983) found a periodicity in the X-ray flux of 133 days and interpreted this as being the orbital period of a neutron star in an orbit around the Be star, the variability in the X-ray flux being caused by enhanced accretion onto the neutron star as it passes through the periastron. This establishes GX 304-01 as a HMXB with a Be star companion (i.e., a Be/X-ray binary).

Parkes et al. (1980) estimated the distance of the system to be 2.4 ± 0.5 kpc. Coleiro & Chaty (2013) provided an estimate of the distance of 1.3 kpc. Using GDR2, Bailer-Jones et al. (2018) derived a larger distance of $2.01^{+0.15}_{-0.13}$ kpc.

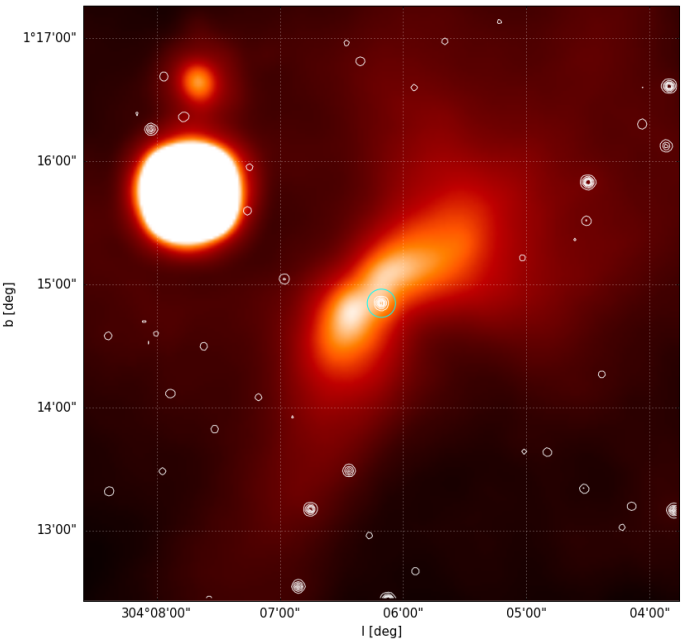

Fig. 6. WISE 22 μm image of the field around GX 304-01 (V850 Cen) with 2MASS Ks contours (sensitive to starlight) overlaid on top. The system position is denoted by the cyan circle.

The 22 μm WISE image of the system (see Fig. 6) reveals a fine arcuate nebula that has a noticable dimple at the apex of the arc, close to the HMXB. Unfortunately, the system is not covered by the *Spitzer* data. The arc is also visible in PACS 70 μm image; no Hα counterpart was detected. The arc exhibits a clear symmetric morphology without any discernable clumps or finer structure. The infrared counterpart of GX 304-01 lies along the axis of symmetry of the arc, making it likely that this

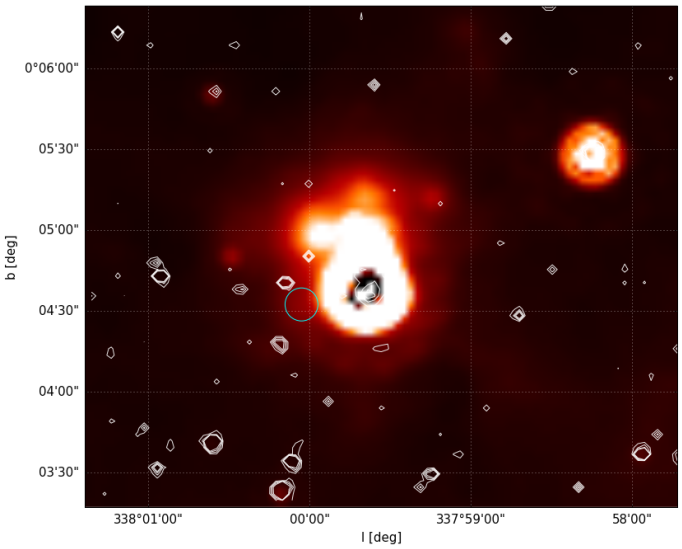

Fig. 7. *Spitzer* MIPS 24 μm image of the field around AX J1639.0-4642 with *Spitzer* IRAC 3.6 μm contours (mainly sensitive to starlight) overlaid on top. The system position is denoted by the cyan circle.

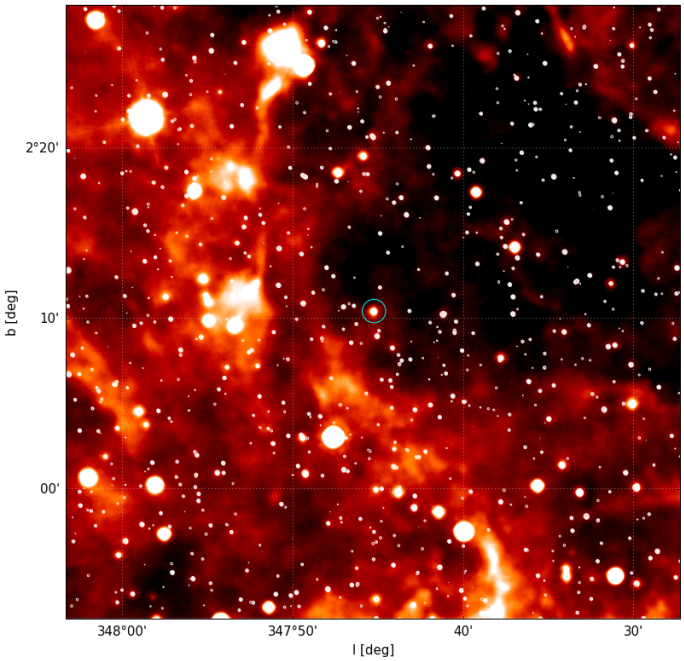

Fig. 8. WISE 22 μm image of the field around 4U 1700-37 (V884 Sco) with WISE 3.4 μm contours (mainly sensitive to starlight) overlaid on top. The system position is denoted by the cyan circle.

emission is associated with the HMXB system. Because of the apex dimple, limited resolution of WISE 22 μm channel, and close proximity of the nebula to the system, the HMXB seems to be immersed in the nebula.

3.7. AX J1639.0-4642

The X-ray source AX J1639.0-4642 was discovered by the Advanced Satellite for Cosmology and Astrophysics (ASCA) observatory (Sugizaki et al. 2001). The system is likely a supergiant HMXB. It is highly absorbed X-ray pulsar with a spin period of 911 s (Bodaghee et al. 2006). The infrared counterpart identification has been problematic. 2MASS J16390535-4642137 was proposed as a possible counterpart (Chaty et al. 2008). Further refinement of the system position by Bodaghee et al. (2012a) suggested another close, faint, and blended star as the most probable counterpart. The precise orbital period of the system is disputed, but is most likely around 4.2 days (e.g., Corbet et al. 2010; Corbet & Krimm 2013). These values of pulse and orbital period place the system among the other wind-fed HMXBs in Corbet's diagram of pulse versus orbital period (Corbet 1986).

The faintness of the infrared counterpart hampers the distance determination. Assuming a luminosity typical for an accretion-driven X-ray pulsar, Bodaghee et al. (2006) estimated the distance of the source to be approximately 10 kpc.

Figure 7 shows the field around the system. The HMXB is adjacent to a bright 24 μm nebula, centered on the group of faint infrared stars. The HMXB is immersed into the fainter outskirts of this nebula. The nebula also dominates the field at IRAC and *Herschel* wavelengths.

3.8. 4U 1700-37

4U 1700-37 is an eclipsing HMXB with a very massive companion of O6Iafcp spectral class (Jones et al. 1973; Sota et al. 2014). The nature of the compact object is unclear. The absence of pulsation suggests the presence of a low-mass black hole, but a neutron star seems more likely (e.g., Reynolds et al. 1999; Boroson et al. 2003).

Ankay et al. (2001) estimated the distance to be about 1.9 kpc. Megier et al. (2009) and Coleiro & Chaty (2013) adopted 2.12 ± 0.34 and 1.8 ± 0.15 kpc, respectively. Depending on the adopted prior, Astraatmadja & Bailer-Jones (2016) derived vastly different distances from the TGAS data (approximately from 0.7 to 3.3 kpc), which also suffer from large uncertainties. Utilizing GDR2, Bailer-Jones et al. (2018) derived a more precise distance estimate of $1.75^{+0.24}_{-0.19}$ kpc.

Figure 8 shows that the system lies on the axis of symmetry of an arcuate cavity that is excavated into a nearby bright cloud of 24 μm.

3.9. EXO 1722-363

EXO 1722-363 was discovered in the Galactic ridge by EXOSAT observations in 1984 (Warwick et al. 1988). Analysis of Ginga observations by Tawara et al. (1989) suggested the presence of a dense envelope of circumstellar matter around the system. Takeuchi et al. (1990) placed a 9 days lower limit for the orbital period, which was later refined by Corbet et al. (2005) and Thompson & Tomsick (2007) to be 9.74 days. Using INTEGRAL observations, Zurita Heras et al. (2006) found a probable infrared counterpart to the system, 2MASS J17251139-3616575, 1″ away from the best position of the source as given by INTEGRAL. Subsequent observations of the counterpart by Rahoui et al. (2008) and Mason et al. (2009) supported the earlier assumptions that the system is a HMXB containing an early supergiant B star, which produces strong stellar wind that fuels the accretion onto the neutron star.

The absence of the visual counterpart and the location of the system in the Galactic ridge region make the distance determination difficult. Zurita Heras et al. (2006), considering a typical luminosity of an active accretion pulsar, estimated the distance to the system to be 7 kpc. Thompson & Tomsick (2007) placed the system between 5.3 and 8.7 kpc. Using the broadband data, Rahoui et al. (2008) derived a slightly smaller distance to the

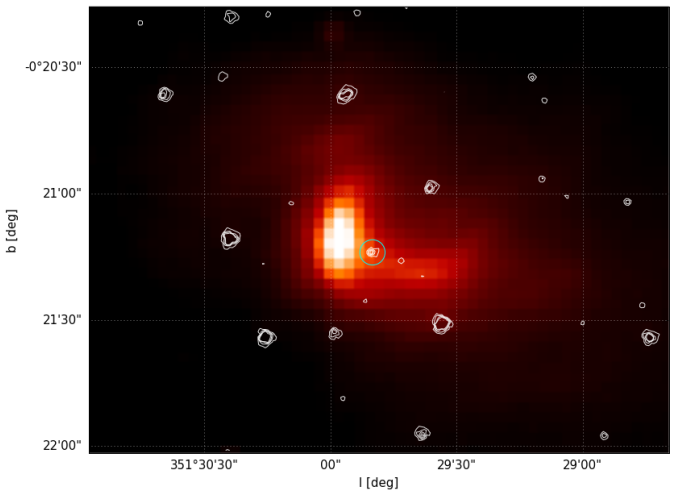

Fig. 9. *Spitzer* MIPS 24 μm image of the field around EXO 1722-363 with *Spitzer* IRAC 3.6 μm contours (mainly sensitive to starlight) overlaid on top. The system position is indicated by the cyan circle.

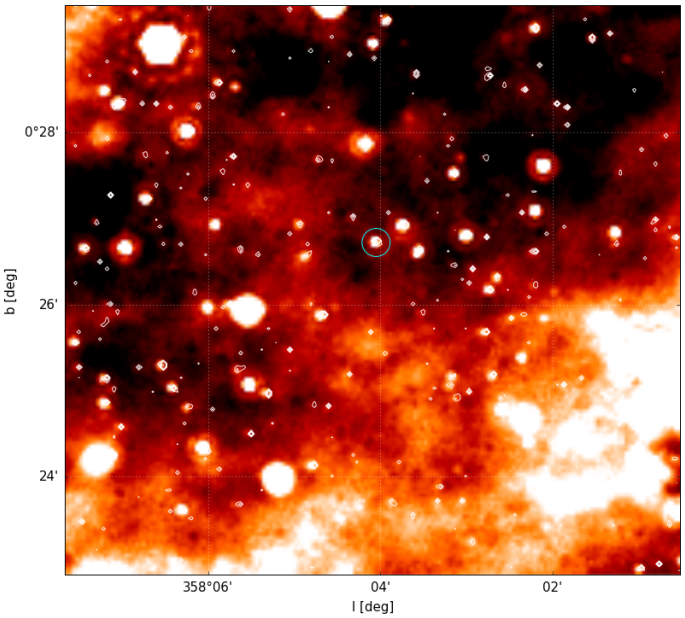

Fig. 10. *Spitzer* MIPS 24 μm image of the field around XTE J1739-302 with *Spitzer* IRAC 3.6 μm contours (mainly sensitive to starlight) overlaid on top. The system position is indicated by the cyan circle.

system of 6.1 kpc. Distance determinations were also made by Mason et al. (2009), later refined by Mason et al. (2010), placing the system to be $7.1 \leq d \leq 7.9$ kpc.

The nebula around EXO 1722-363 is visible in both the *Spitzer* MIPS 24 μm (see Fig. 9) and 22 μm WISE images. The arc is also visible in the PACS 70 μm image and a gleam of emission possibly associated with the arc is also visible in the IRAC 8 μm image. No Hα counterpart was detected. The *Spitzer* MIPS 24 μm image reveals an irregular, curved morphology, where the part of the nebula to the Galactic east of the system appears to be brighter and more prominent. This seems to be a feature of the structure itself, as our inspection of this area in the different bands does not reveal any possible background or foreground sources that could be responsible for the enhanced emission. The infrared counterpart of EXO 1722-363 appears to lie within the nebula. If we consider the outer boundary of the nebula tracing an arc, the system lies along the approximate symmetry axis of this arc. This, together with the lack of any notable brighter point sources within the nebula, suggests that the structure is likely associated with the HMXB.

3.10. XTE J1739-302

XTE J1739-302 (IGR J17391-3021) is a supergiant X-ray transient (SFXT) discovered with the proportional counter array on board the Rossi X-Ray Timing Explorer (RXTE; Smith et al. 1998). The system consists of a neutron star on an eccentric 51.47 days orbit (Drave et al. 2010) around a O8 Iab(f) supergiant companion (Negueruela et al. 2006a, Rahoui et al. 2008).

The source lies in the direction of the Galactic center. Using spectroscopy and photometry of the counterpart, Negueruela et al. (2006a) estimated its distance to be 2.3 ± 0.6 kpc. The subsequent analysis by Rahoui et al. (2008) derived a slightly larger distance of about 2.7 kpc. The distance estimate from GDR2 seems to be less constraining. Bailer-Jones et al. (2018) provided an estimate for the distance of $5.32^{+3.92}_{-2.12}$ kpc. It is therefore questionable whether the HMXB is a foreground source, as suggested by the earlier studies, or is, potentially, a Galactic center object.

Figure 10 shows that the system lies in a region of complicated mid-infrared emission, typical for Galactic center region. The system could be lying on the axis of symmetry of a faint arc of extended emission or a partial bubble.

3.11. AX J1841.0-0536

AX J1841.0-0536 was discovered as a variable X-ray source by ASCA (Bamba et al. 2001) while undergoing two bright flares lasting approximately 1 h each. The flaring activity of the system puts it into a SFXT class of HMXBs (e.g., Romano et al. 2011). *Chandra* observations by Halpern et al. (2004) pinpointed the infrared counterpart. Negueruela et al. (2006b) provided constraints on the spectral type of the secondary, being of a luminous B0-1 type. This is further refined by the infrared spectroscopy done by Nespoli et al. (2008), who derived the spectral type B1Ib for the secondary. The orbital period of the system of 6.45 days was reported by González-Galán (2015).

The distance estimates of the system vary. Nespoli et al. (2008) provided a broad estimate of the distance of $3.2^{+2}_{-1.5}$ kpc. A more recent analysis by Coleiro & Chaty (2013) put the system further away, at 7.8 ± 0.74 kpc. This is in agreement with the distance estimated from GDR2, $d = 7.60^{+3.06}_{-2.16}$ kpc (Bailer-Jones et al. 2018).

Figure 11 shows that the system lies in the center of the region of reduced 24 μm emission. The cavity does not feature bright rims of mid-IR emission and the evidence of the reduced emission can be seen on the PACS and SPIRE wavebands as well.

3.12. XTE J1855-026

XTE J1855-026 is a HMXB discovered by RXTE. The system showed pulsations with a period of about 361 s and a flux modulation with a period of 6.1 days, which was interpreted as the orbital period of the system (Corbet et al. 1999). This was confirmed by Negueruela et al. (2008). The optical counterpart of the system was pinpointed by Verrecchia et al. (2002) and its spectral type was determined to be B0Iaep (Negueruela et al. 2008).

Corbet et al. (1999) proposed a distance of approximately 10 kpc. The analysis by Coleiro & Chaty (2013) derived a consistent distance estimate of 10.8 ± 1.0 kpc. The distance given by Bailer-Jones et al. (2018) is slightly smaller, $8.14^{+2.58}_{-1.79}$ kpc.

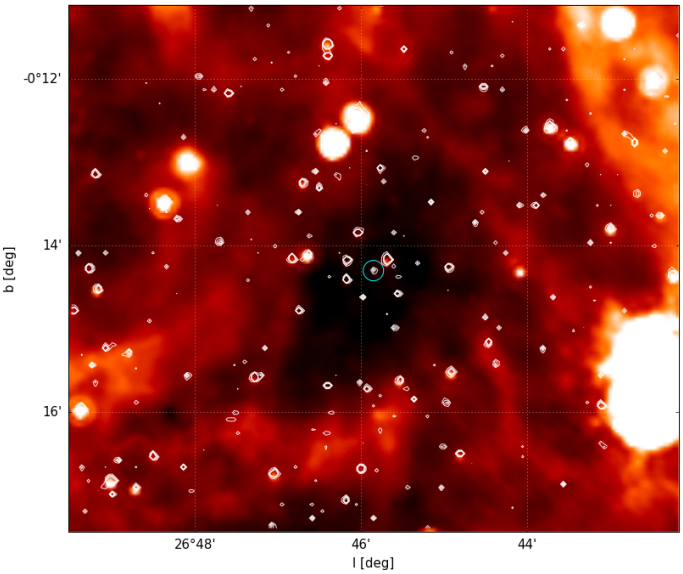

Fig. 11. *Spitzer* MIPS 24 μm image of the field around AX J1841.0-0536 with *Spitzer* IRAC 3.6 μm contours (mainly sensitive to starlight) overlaid on top. The system position is indicated by the cyan circle.

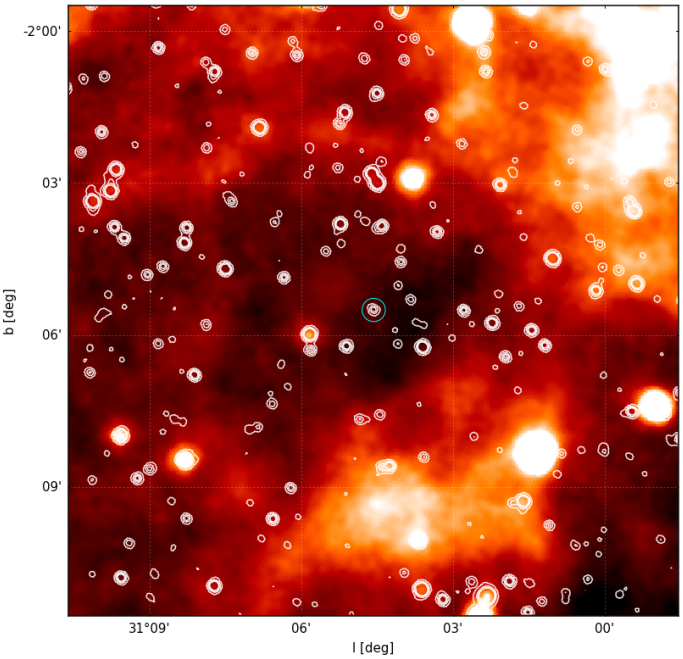

Fig. 12. WISE 22 μm image of the field around XTE J1855-026 with WISE 3.4 μm contours (mainly sensitive to starlight) overlaid on top. The system position is indicated by the cyan circle.

This system also appears to be associated with a region of reduced 24 μm emission (Fig. 12). The paucity of emission is not that well pronounced as is the case with the previous system, however, the region appears to be surrounded by a bright partial mid-infrared shell, most noticable to the Galactic south and northwest of the system.

4. Kinematics of the studied systems

The kinematics of the studied HMXBs is of significant interest, as it can provide constraints for several interesting system characteristics, such as the origin of the system or the properties of the progenitor binary. However, studying it has been difficult owing to considerable distances of these sources and insufficient accuracy of the past astrometric surveys. This resulted in the proper motions measured with a low significance, often varying significantly depending on the survey, making them hard to utilize. Only a few, very close sources did not suffer from these issues. The situation improved somewhat with the advent of the first *Gaia* data release (GDR1; Gaia Collaboration 2016). While TGAS, part of GDR1 (Lindegren et al. 2016), contained only a small number of HMXBs, re-reductions of past catalogs using GDR1, such as UCAC5 (Zacharias & Finch 2017) and Hot Stuff for One Year (HSOY; Altmann et al. 2017) provided more precise proper motions for many more sources. However, the issue of discrepant proper motions depending on the catalog used still persisted.

We used the parallaxes and proper motions from GDR2 (Gaia Collaboration 2018) to compute peculiar tangential velocities, which are especially interesting for systems associated with an arcuate structure in their vicinity. For our objects, we followed the approach outlined in Luri et al. (2018). The distances and tangential velocities were jointly estimated from the parallaxes and proper motions via Bayesian inferrence and the prior scale lengths are adopted from Bailer-Jones et al. (2018). To obtain the peculiar tangential velocities, we adopted the Galactic constants $R_0 = 8.2$ kpc, $\Theta_0 = 238\,\mathrm{km\,s^{-1}}$ and the solar peculiar motion $(U_\odot, V_\odot, W_\odot) = (10.0, 11.0, 7.0)\,\mathrm{km\,s^{-1}}$ from Bland-Hawthorn & Gerhard (2016). Table 1 lists the computed peculiar velocity medians with the errors obtained from 68% credibility intervals. The only exception was γ Cas, as it is too bright for *Gaia*. In this case, we used the proper motion given in HSOY with an adopted distance of 0.15 kpc as discussed above. It must be noted that we computed the errors in the peculiar velocity for γ Cas from the errors of the proper motion measurements only, so they should be considered as low-limit approximations.

Unfortunately, for the rest of the systems not listed in Table 1, the choice of catalogs is limited. Because of the significant distance of these sources or faint optical/infrared counterparts, they are not listed in any proper motion catalogs or they exhibit no measurable proper motion.

A number of the studied objects exhibit increased values of the astrometric flags, such as the astrometric excess noise and goodness-of-fit statistic, possibly indicating problems with the astrometric solution in GDR2. Issues with the astrometry may arise when dealing with the regions with large source densities, such as the Galactic plane and center regions, where HMXBs are predominantly situated. Another caveat is that the astrometric solution in GDR2 does not take the binarity into account, which may have an impact on the astrometry and its quality (Lindegren et al. 2018). To investigate these effects, we queried GDR2 for stars of similar magnitude and color ($\Delta G = \pm 0.5$ mag, $\Delta(\mathrm{BP} - \mathrm{RP}) = \pm 0.2$ mag) within a 10° radius cone centered on each source. For each source we also constructed an equivalent query, extracting the sources from the opposite side of the sky to study the effects of crowding. Comparison of the studied HMXBs with the extracted stars from the source vicinity and the opposite side of the sky showed that, except for AX J1841.0-0536, none of the HMXBs are significant outliers, despite some sources having astrometric flag values indicating problems with the single-star astrometric solution. It is, however, unlikely that the measured parallaxes and proper motions are corrupted by the unmodeled orbital motion. The longest orbital period among our sources is approximately

Table 1. Proper motions and derived peculiar tangential velocities for selected HMXBs.

ID	pmRA (mas yr^{-1})	pmDE (mas yr^{-1})	Parallax (mas)	$v_{\rm l,pec}$ (km s^{-1})	$v_{\rm b,pec}$ (km s^{-1})
EXO 051910+3737.7	1.44 ± 0.12	-4.12 ± 0.07	0.753 ± 0.057	$15.5^{+2.3}_{-2.0}$	$-0.4^{+1.0}_{-1.0}$
IGR J11435–6109	-5.982 ± 0.059	1.089 ± 0.056	0.026 ± 0.042	-10^{+55}_{-63}	-13^{+5}_{-5}
GX 301-02	-5.303 ± 0.051	-2.166 ± 0.049	0.253 ± 0.035	34^{+25}_{-23}	-45^{+7}_{-8}
1H 1255-567	-28.15 ± 0.22	-10.34 ± 0.34	8.95 ± 0.23	$1.7^{+0.4}_{-0.5}$	$1.9^{+0.2}_{-0.2}$
GX 304-01	-4.235 ± 0.043	-0.316 ± 0.043	0.470 ± 0.033	24^{+6}_{-5}	$4.9^{+0.5}_{-0.5}$
4U 1700-37	2.220 ± 0.087	4.954 ± 0.073	0.0549 ± 0.064	65^{+7}_{-6}	$17.3^{+1.8}_{-1.4}$
XTE J1739-302	-0.89 ± 0.22	3.49 ± 0.17	0.12 ± 0.16	161^{+425}_{-80}	99^{+48}_{-32}
AX J1841.0-0536	-2.66 ± 0.25	-5.36 ± 0.21	-0.29 ± 0.13	18^{+122}_{-124}	4^{+7}_{-8}
XTE J1855-026	-2.605 ± 0.063	-6.788 ± 0.056	0.039 ± 0.044	-10^{+83}_{-93}	-26^{+6}_{-7}
ID	pmRA (mas yr^{-1})	pmDE (mas yr^{-1})	Distance (kpc)	$v_{\rm l,pec}$ (km s^{-1})	$v_{\rm b,pec}$ (km s^{-1})
γ Cas	24.950 ± 0.167	-3.890 ± 0.231	0.15	6.5 ± 0.1	5.0 ± 0.2

Notes. γ Cas is separated from the rest of the systems owing to its questionable nature and not having a solution in GDR2. In this case, the distance estimate is used instead of the parallax.

133 days for GX 304-01 (Priedhorsky & Terrell 1983). Even this orbital period is small compared to the 22-month observing time of GDR2. For such periods, it is expected that the orbital motion should average out and should not significantly impact the parallax and proper motion measurements (Jennings et al. 2018). Interestingly, AX J1841.0-0536, the system with elevated astrometric flags as compared to the extracted sources from the queries, only has an orbital period of 6.45 days (González-Galán 2015).

5. Discussion

The infrared survey of the HMXB sample yielded a variety of extended emission that may suggest the influence of the HMXBs on the surrounding interstellar medium (ISM). This emission, its presence or absence, has important implications not only for the particular system, but also for the HMXB population as a whole.

5.1. Extended emission

The studied objects are projected against complex infrared structures, which are not only arcs bending outward from the HMXB, possibly indicating a bow shock, but also infrared filaments that appear to emanate from the system and emission cavities.

5.1.1. γ Cas arc

Figure 1 shows the arcuate nebulosity in the vicinity of γ Cas. While the infrared arcs around early-type stars are traditionally interpreted as stellar bow shocks, various phenomena can produce morphologies resembling bow shocks, including partial infrared bubbles and H II regions with density gradients. The infrared arcs may also be interpreted as dust waves or bow waves that may form around late-type OB main sequence stars, which may drive weaker stellar winds than expected (the weak wind problem; Ochsendorf et al. 2014a,b). These structures can be attributed to the interaction of radiation pressure from the star with dust carried along by a photoevaporative flow of ionized gas from a dark cloud or inside an evolved interstellar bubble. The structures are very similar in morphology to genuine stellar bow shocks.

The position of the arc is approximately consistent with the position of GCRV 309 E, a H II region, however, we were unable to confirm its presence on the image data in the INT Photometric H-Alpha Survey (IPHAS; Barentsen et al. 2014) Hα images. The absence of other infrared data makes it hard to establish the exact nature of the nebula. However, given the peculiar velocity of the source, its spectral type, a bow or a dust wave interpretation is more likely than a stellar bow shock. Adding to this, the arc approximately points to the infrared pillars, associated with two clouds, IRAS 00560+6037 and IC 59, which may be sources of a material flow toward the system. While the nature of the arc is debatable, it is, most likely, not a stellar bow shock.

5.1.2. EXO 051910+3737.7 nebula

The wispy nebula, fanning approximately in the Galactic north–south direction, may suggest a dusty outflow indicating a systemic mass loss. The nebula bears some resemblance to circumstellar nebulae observed around some B[e] and Be stars in the infrared images (Mayer et al. 2016). The literature on the enviroments around Be stars is sparse, but at least one Be star, SX Aur, also shows the presence of a mid-infrared nebula (Deschamps et al. 2015), however, this nebula is more compact and shows a blob-like morphology instead of fine wispy jets.

There also exists a possibility that the dusty structure is not associated with the system and the system is just passing in its vicinity, heating the dust. However, the position of the system in the central knot of the emission hints at the association. Moreover, the system has a significant peculiar velocity to the Galactic east. If the outflows emanate from the system, it would be expected to observe some bending of the structure toward the west, as the system plows through the surrounding ISM. This bending is apparent in the bright part of the nebula and also in the fainter south wisp.

The nature of the easternmost rim of the nebula is puzzling. It is leading the star in the direction of its peculiar motion, so it cannot be related to the past mass-loss episode. It also exhibits

the same degree of bending as the bright bar centered on the system. A bending toward the system due to its systemic peculiar motion would be expected for a stellar bow shock, however, the bar does not seem to be completely detached from the system, which is not expected. The bar may be a part of an infrared filament, locally heated by the system as it passes in its vicinity.

5.1.3. IGR J11435-6109 cavity

The system lies in a large infrared cavity that is apparent in WISE 12, 22 μm images and in SPIRE wavebands. Coleiro et al. (2013) discussed the cavity briefly and noted that it could be a result of the feedback of the system on the surrounding ISM. The physical relation of the system to the cavity is difficult to prove because of the inherent inaccuracy of the distance determination to both infrared cavities and distant HMXBs. Moreover, the system lies significantly off-center of the cavity. This could be reconciled if the system has a significant peculiar velocity pointing away from the cavity center. The system has proper motion data available but they are of a low quality. However, the peculiar motion component in the Galactic latitude is sufficiently well constrained to suggest that the system is moving to the Galactic south, which is at odds with its supposed origin near the center of the cavity. Considering the points above, it seems that the HMXB and the cavity it is projected against are unrelated.

5.1.4. GX 301-02 nebula

The system is surrounded by an extended infrared emission. Huthoff & Kaper (2002) and Servillat et al. (2014) discussed the possibility of a bow shock or a cavity associated with the system. The peculiar velocity obtained from the proper motion suggests that the system is moving predominantly to the Galactic southeast toward the bright extended emission, so the bright rim of infrared emission to the north of the system is unlikely to be a stellar bow shock. The surrounding emission is most likely related to the infrared bubble [SPK2012] MWP1G300134-001035 to the south of the system. No bow shock is apparent despite the considerable peculiar velocity of the system.

5.1.5. 1H 1255-567 nebula

The system is enshrouded in a fine wispy nebula, similar to the wispy nebula associated with EXO 051910+3737.7, but less prominent. Moreover, it is hard to determine if the emission is instead associated with μ^1 Cru. The system exhibits no significant peculiar motion, yet the filaments seem to exhibit some curvature, as is evident in Fig. 5. However, also the southern star, μ^1 Cru, does not exhibit any significant peculiar systemic motion.

5.1.6. GX 304-01 arc

The HMXB appears to be associated with a mid-infrared smooth arc pointing approximately to the Galactic northeast. The proper motion of the system from the GDR2 data yields a mildly runaway peculiar velocity primarily to the Galactic east, which deviates about 30° from the approximate symmetry axis of the arc. The arcuate mid-infrared nebula upstream of the system could be interpreted as a stellar bow shock. However, there are several problems with this interpretation. The arc does not bear a classical bow shock shape and does not seem to be fully detached from the system. The most puzzling feature of the nebula is its apex dimple, pointing toward the system. Recently, Meyer et al. (2017) conducted a series of simulations of stellar bow shocks of early-type stars in a magnetized medium. Their modeling suggests that in a magnetized ambient medium, the classic bow shock shape gets distorted and compressed, increasing its opening angle and becoming much blunter around the apex, as the stand-off distance decreases significantly. Interestingly, an apex dimple may form. This bow shock morphology change is especially prominent for stars having a modest space velocity, matching that of GX 304-01. This makes the bow shock interpretation appealing, however, the apparent attachment of the emission onto the system still remains an issue despite the expected decreased stand-off distance expected for such system. The mentioned misalignment between the peculiar velocity vector and the symmetry axis of the arc also poses a problem for the bow shock hypothesis, however, this can be reconciled by the presence of a large-scale flow in the ISM. An alternative origin of the emission might be due to the system encountering an infrared filament along its way, locally heating and compressing it. An example of such system is HD 49662, as discussed in Kalas et al. (2002). This system appears to be embedded in an infrared filament, heating it locally. This produces a blister-like infrared emission, visible in WISE 12 and 22 μm images, bulging ahead of the system while the system is embedded in the diffuse emission. However, the peak of the diffuse emission is centered directly on the system, which is not the case for the HMXB. Also, the diffuse emission around GX 304-01 does not bear a blister-like shape. Thus, we classify the emission around GX 304-01 as ambiguous.

5.1.7. Blob near AX J1639.0-4642

AX J1639.0-4642 is adjacent to a blob of strong mid-infrared emission. The emission is very concentrated, however, its outskirts reach the HMXB, which is the most apparent in the longer IRAC wavebands. Several infrared point sources are present in the central part of the blob. This region is designated IRAS 16353-4636 and is a site of star formation (Benaglia et al. 2010). The point sources within the blob make up a protostellar cluster. Benaglia et al. (2010) derived a distance of ~8 kpc to the embedded protocluster. Owing to the inherent evolved nature of HMXBs, and because this protocluster is about 2 kpc closer than the HMXB, this cluster is not related to AX J1639.0-4642.

5.1.8. 4U 1700-37 cavity

The system seems to be centered on an arcuate cavity protruding into a nearby mid-infrared cloud to the Galactic southeast. Toalá et al. (2017) suggested that this structure is a stellar bow shock driven by the HMXB. The HMXB has a well-measured proper motion, which yields a runaway peculiar velocity at the adopted distance. The inferred direction of the peculiar motion deviates by about 60° from the approximate axis of symmetry of the cavity. This difference cannot be attributed to the errors in the peculiar velocity, as it is well constrained. Also, considering the magnitude of the peculiar velocity of the system of about 70 km s^{-1}, the peculiar ambient medium velocity would have to be considerably large to produce such deviation. Another point to consider is the absence of the emission enhancement along the boundary of the cavity. The brightness along the rim of the tentative bow shock is practically the same as in the surrounding cloud to the Galactic southeast. This poses problems for the bow shock interpretation. A possible alternative could be a partial cavity, possibly shaped by the feedback from the system, or a chance alignment of a foreground/background structure.

5.1.9. EXO 1722-363 nebula

The system is projected atop a crescent-shaped irregular mid-infrared nebula. Owing to a considerable distance to the system, there is no proper motion information available, so it is not possible to investigate whether there exists a connection with the orientation of the nebula and the systemic peculiar motion. The nebula is not evenly bright; as can be seen in Fig. 9, the east part of the nebula is significantly brighter. The brightening could be related to the systemic motion, however, it is impossible to ascertain given the lack of data. The system may be passing through a larger ISM cloud and shock only a part of it, while heating some of the unshocked material as well, which could explain the fainter filament that is projected downstream of the tentative bow shock. The nebula could be interpreted as a partial wind-blown bubble, however, the system is lying significantly off center. Another possibility is that the filament projected onto the system is a part of an interstellar cloud crossing behind or in front of the HMXB, passing closest to the system on its east-projected side. We classify this structure as ambiguous.

5.1.10. XTE J1739-302 filament

The system is adjacent to a fine mid-infared arc or filament, situated to the Galactic east, and its approximate axis of symmetry is oriented in the same direction. The proper motion data for the system yield a runaway peculiar velocity in the direction approximately to the Galactic northeast, albeit with considerable errors (see Table 1). For this reason, it is not meaningful to investigate the alignment of the peculiar velocity vector with the symmetry axis of the arc. Adding to this, the arcuate filament is not significantly brighter than the surrounding emission to the Galactic south that it seems to be linked with, as would be expected for the heated dust piled at the bow shock front. This implies that the filament cannot be interpreted as a stellar bow shock, and is, most likely, not related to the HMXB system.

5.1.11. AX J1841.0-0536 cavity

The system is projected into a cavity of a reduced 24 μm emission. Taking the peculiar velocity at face value, the system moves rather slowly for a supergiant-hosting HMXB. However, because of its uncertain distance, its peculiar velocity is ill-determined. Interestingly, the system seems to be a part of a small star group, possibly making up a star cluster. The distance to the cavity is not known, as it is not catalogued. However, the presence of a HMXB together with the surrounding stars in its center, make it possible that the cavity is shaped by stellar feedback.

5.1.12. XTE J1855-026 structure

The system seems to be located in a region of reduced 24 μm emission, bracketed by regions of stronger emission to the Galactic south and northwest, possibly making up a partial bubble. The system is a likely runaway owing to its position away from the Galactic plane. The precise kinematics of the system is hard to constrain because of the errors in the parallax measurement, however, none of the bright rims on the either side of the HMXB can be interpreted as stellar bow shocks.

5.2. Paucity of bow shocks around HMXBs

Our search for bow shocks driven by HMXBs yielded only one questionable new detection. Even if we consider the structure around GX 304-01 as a bona fide stellar bow shock, together with the bow shocks associated with Vela X-1 and 4U 1907+09, there are only three known HMXB bow shocks (only about 2% of the HMXBs drive detectable bow shocks). This is considerably lower than the bow shock occurrence around OB runaway stars, although this number has been fluctuating over the years (about 13%, van Buren & Noriega-Crespo 1995; ∼40%, Huthoff & Kaper 2002; ∼10%, Peri et al. 2012; and ∼6%, Peri et al. 2015). This discrepancy can be explained by the hypothesis proposed by Huthoff & Kaper (2002) suggesting different ejection scenarios for HMXBs and OB runaways. OB runaways have predominantly escaped their parent associations or clusters at a relatively early stage, when the cluster was dense and the probability of close encounters and ejections of stars was high. On the other hand, a lot of HMXBs became runaways only after the occurrence of a supernova within the system. Thus, the kinematical age and the distance to their parent clusters should be lower for HMXBs. Therefore, HMXBs are more likely to be still enclosed in the hot and rarefied regions (hot bubbles) that surround OB associations and clusters while the OB runaways have already escaped from these regions. The (isothermal) speed of sound in the ISM increases with temperature, thus, the hotter the medium is, the less likely are runaways moving through it supersonically. Together with the lower ISM density in these regions, this means a smaller chance of bow shock detection. At the time, Huthoff & Kaper (2002) were only able to study the difference in bow shock occurrence between the OB runaways and HMXBs on a sample of 11 HMXB systems. The analysis of the clustering between HMXBs and OB associations by Bodaghee et al. (2012b) also reinforced this notion, suggesting that the massive binaries that are the progenitors of HMXBs tend to remain gravitationally bound to their birth sites until the supernova explosion in the system. Thus, they acquire their runaway velocity only later on, leaving the association or cluster after it has evolved considerably, evacuating cavities in their surroundings, making the formation of an observable bow shock less likely.

Moreover, in addition to bow shocks associated with stars having large peculiar velocities, the young stars in a star cluster can drive significant outflows, causing the local ISM velocities to deviate from the LSR. Thus, bow shocks can also be generated around neighboring stars or stars at cluster outskirts without necessarily having large peculiar velocities (e.g., Povich et al. 2008). These bow shocks are often coined "in situ bow shocks" and their axes of symmetry point predominantly toward the source of outflows. The effects of outflows abates as the cluster ages and thus by the time the first supernova explosions start to occur in a cluster, possibly giving rise to HMXBs or their progenitiors, the outflows are weaker and the ISM around the cluster is more rarified because of feedback effects. This suggests that the in situ bow shock generation is also less likely for HMXBs as compared to other OB stars.

All this points to the scenario in which massive binaries, which are progenitors to HMXBs, are not efficiently expelled from star clusters and associations during the early stages of a cluster lifetime. This also implies that the two-step ejection process (Pflamm-Altenburg & Kroupa 2010) is not at work for a considerable number of HMXBs, making it possible to determine their birth sites via the peculiar velocity measurements.

6. Summary and conclusions

We have searched for bow shocks around HMXBs using WISE and MIPS *Spitzer* Space Telescope archival data. Apart from the

already known bow shocks (associated with Vela X-1 and 4U 1907+09), we found only one new structure resembling a bow shock, but even this structure cannot be conclusively interpreted as a bona fide bow shock.

The detection of the bow shock candidate around GX 304-01 suggests that this system possesses at least a moderate runaway velocity. The proper motion measurements also seem to support the runaway interpretation of GX 304-01. The bow shock around GX 304-01, if real, would be the first bow shock detected associated with a Be/X-ray binary.

The relative paucity of bow shocks associated with HMXBs as compared to OB runaway stars supports the hypothesis that HMXBs are kinematically younger objects than OB runaways, meaning that most of them are still moving within hot and tenuous medium near their parent cluster or association and thus unable to form an observable bow shock.

We expect that future releases of proper motion and paralax measurements obtained by the mission *Gaia* will considerably improve our knowledge of kinematics of these HMXBs. The planned *James Webb* Space Telescope will also be able to obtain more detailed images of bow shock candidates and nebulosities, allowing us to gain more insight into both the diffuse structures and the HMXBs that are associated with them.

Acknowledgements. The author acknowledges support from grant MUNI/A/0789/2017. This research has made use of the NASA/IPAC Infrared Science Archive, which is operated by the Jet Propulsion Laboratory, California Institute of Technology, under contract with the National Aeronautics and Space Administration. This work is based (in part) on observations made with the *Spitzer* Space Telescope, which is operated by the Jet Propulsion Laboratory, California Institute of Technology under a contract with NASA. This publication makes use of data products from the Wide-field Infrared Survey Explorer, which is a joint project of the University of California, Los Angeles, and the Jet Propulsion Laboratory/California Institute of Technology, funded by the National Aeronautics and Space Administration. This work has made use of data from the European Space Agency (ESA) mission *Gaia* (https://www.cosmos.esa.int/gaia), processed by the *Gaia* Data Processing and Analysis Consortium (DPAC; https://www.cosmos.esa.int/web/gaia/dpac/consortium). Funding for the DPAC has been provided by national institutions, in particular the institutions participating in the *Gaia* Multilateral Agreement. This research has made use of the SIMBAD database and the VizieR catalog access tool, both operated at CDS, Strasbourg, France. This publication makes use of data products from the Two Micron All Sky Survey, which is a joint project of the University of Massachusetts and the Infrared Processing and Analysis Center/California Institute of Technology, funded by the National Aeronautics and Space Administration and the National Science Foundation. This paper makes use of data obtained as part of the INT Photometric Hα Survey of the Northern Galactic Plane (IPHAS; www.iphas.org) carried out at the Isaac Newton Telescope (INT). The INT is operated on the island of La Palma by the Isaac Newton Group in the Spanish Observatorio del Roque de los Muchachos of the Instituto de Astrofisica de Canarias. All IPHAS data are processed by the Cambridge Astronomical Survey Unit, at the Institute of Astronomy in Cambridge. The band-merged DR2 catalog was assembled at the Centre for Astrophysics Research, University of Hertfordshire, supported by STFC grant ST/J001333/1. This research made use of Montage. It is funded by the National Science Foundation under Grant Number ACI-1440620, and was previously funded by the National Aeronautics and Space Administration's Earth Science Technology Office, Computation Technologies Project, under Cooperative Agreement Number NCC5-626 between NASA and the California Institute of Technology. This research made use of Astropy, a community-developed core Python package for Astronomy (Astropy Collaboration 2018).

References

Altmann, M., Roeser, S., Demleitner, et al. 2017, A&A, 600, L4
Ankay, A., Kaper, L., de Bruijne, J. H. J., et al. 2001, A&A, 370, 170
Astraatmadja, T. L., & Bailer-Jones, C. A. L. 2016, ApJ, 833, 119
Astropy Collaboration (Price-Whelan, A. M., et al.) 2018, AJ, 156, 123
Bailer-Jones, C. A. L., Rybizki, J., Fouesneau, M., et al. 2018, AJ, 156, 58
Bamba, A., Yokogawa, J., Ueno, M., et al. 2001, PASJ, 53, 1179
Barentsen, G., Farnhill, H. J., Drew, J. E., et al. 2014, MNRAS, 444, 3230
Benaglia, P., Ribó, M., Combi, J. A., et al. 2010, A&A, 523, A62
Berger, D. H., & Gies, D. R. 2001, ApJ, 555, 364
Bland-Hawthorn, J., & Gerhard, O. 2016, ARA&A, 54, 529
Bodaghee, A., Walter, R., Zurita Heras, J. A., et al. 2006, A&A, 447, 1027
Bodaghee, A., Rahoui, F., Tomsick, J. A., et al. 2012a, ApJ, 751, 113
Bodaghee, A., Tomsick, J. A., Rodriguez, J., et al. 2012b, ApJ, 774, 108
Boroson, B., Vrtilek, S. D., Kallman, T., et al. 2003, ApJ, 592, 516
Chaty, S., Rahoui, F., Foellmi, C., et al. 2008, A&A, 484, 783
Chen, C. H., Pecaut, M., Mamajek, E. E., et al. 2012, ApJ, 756, 133
Chevalier, C., & Ilovaisky, S.A. 1998, A&A, 330, 201
Coleiro, A., & Chaty, S. 2013, ApJ, 764, 185
Coleiro, A., Chaty, S., Zurita Heras, J. A., et al. 2013, A&A, 560, A108
Corbet, R. H. D. 1986, MNRAS, 220, 1047
Corbet, R. H. D., & Krimm, H. A. 2013, ApJ, 778, 45
Corbet, R. H. D., & Remillard, R. 2005, ATel, 377
Corbet, R. H. D., Marshall, F. E., Peele, A. G., et al. 1999, ApJ, 517, 956
Corbet, R. H. D., Markwardt, C. B., & Swank, J. H. 2005, ApJ, 633, 377
Corbet, R. H. D., Krimm, H. A., Barthelmy, S. D., et al. 2010, ATel, 2570
Deschamps, R., Braun, K., Jorissen, A., et al. 2015, A&A, 577, A55
Drave, S. P., Clark, D. J., Bird, A. J., et al. 2010, MNRAS, 409, 1220
Fazio, G. G., Hora, J. L., Allen, L. E., et al. 2004, ApJS, 154, 10
Forman, W., Jones, C., Cominsky, L., et al. 1978, ApJS, 38, 357
Gaia Collaboration (Brown, A. G. A., et al.) 2016, A&A, 595, A2
Gaia Collaboration (Brown, A. G. A., et al.) 2018, A&A, 616, A1
Grebenev, S. A., Ubertini, P., Chenevez, J., et al. 2004, ATel, 350
González-Galán, A. 2015, ArXiv e-prints [arXiv:1503.01087]
Griffin, M. J., Abergel, A., Abreu, A. et al. 2010, A&A, 518, L3
Gvaramadze, V. V., & Bomans, D. J. 2008, A&A, 490, 1071
Gvaramadze, V. V., Kroupa, P., & Pflamm-Altenburg, J. 2010, A&A, 519, A33
Gvaramadze, V. V., Kniazev, A. Y., Kroupa, P., et al. 2011a, A&A, 535, A29
Gvaramadze, V. V., Pflamm-Altenburg, J., & Kroupa, P. 2011b, A&A, 525, A17
Gvaramadze, V. V., Roser, S., Scholz, R. -D., et al. 2011c, A&A, 529, A14
Halpern, J. P., Gotthelf, E. V., Helfand, D. J., et al. 2004, ATel, 289, 1
Hoffleit, D., & Jaschek, C. 1982, Bright Star Catalogue (New Haven: Yale University)
Huthoff, F., & Kaper, L. 2002, A&A, 383, 999
in't Zand, J., & Heise, J. 2004, ATel, 362
Jennings, R. J., Kaplan, D. L., Chatterjee, S., et al. 2018, ApJ, 864, 26
Jones, C., Forman, W., Tananbaum, H., et al. 1973, ApJ, 181, L43
Kalas, P., Graham, J. R., Beckwith, S. V. W., et al. 2002, ApJ, 567, 999
Kaper, L., van Loon, J.Th., Augusteijn, T., et al. 1997, ApJ, 475, L37
Kaper, L., van der Meer, A., & Tijani, A.H. 2004, The Environment and Evolution of Double and Multiple Stars, Proc. IAU Colloq. 191, 21, 128
Kaper, L., van der Meer, A., & Najarro, F. 2006, A&A, 457, 595
Kobulnicky, H. A., Chick, W. T., Schurhammer, D. P. et al. 2016, ApJS, 2, 18
Levenhagen, R. S., & Leister, N. V. 2006, MNRAS, 371, 252
Lewin, W.H.G., & van der Klis, M. 2006, Compact Stellar X-ray Sources (Cambridge, UK: Cambridge University Press)
Lewin, W.H.G., van Paradijs, J., van den Heuvel, E.P.J., et al. 1997, X-ray Binaries (Cambridge, UK: Cambridge University Press)
Lindegren, L., Lammers, U., Bastian, U., et al. 2016, A&A, 595, A4
Lindegren, L., Hernandez, J., Bombrun, A., et al. 2018, A&A, 616, A2
Liu, Q.Z., van Paradijs, J., & van den Heuvel, E.P.J. 2006, A&A, 455, 1165
Luri, X., Brown, A. G. A., Sarro, L. M., et al. 2018, A&A, 616, A9
Makovoz, D., & Khan, I. 2005, in Astronomical Data Analysis Software and Systems XIV, eds. P. Shopbell, M. Britton, & R. Ebert, ASP Conf. Ser., 347, 81
Manousakis, A., & Walter, R. 2011, A&A, 526, A62
Masetti, N., Parisi, P., Palazzi, E., et al. 2009, A&A, 495, 121
Mason, K. O., Murdin, P. G., Parkes, G. E., et al. 1978, MNRAS, 184, 45P
Mason, A. B., Clark, J. S., Norton, A. J., et al. 2009, A&A, 505, 281
Mason, A. B., Norton, A. J., Clark, J. S., et al. 2010, A&A, 509, A79
Mayer, A., Deschamps, R., & Jorissen, A. 2016, A&A, 587, A30
McClintock, J.E., Ricker, G.R., & Lewin, W.H.G. 1971, ApJ, 166, L73
Megier, A., Strobel, A., Galazutdinov, G. A., et al. 2009, A&A, 507, 833
Meyer, D. M. -A., van Marle, A. -J., Kuiper, R. et al. 2016, MNRAS, 459, 1146
Meyer, D. M. -A., Mignone, A., Kuiper, R. et al. 2017, MNRAS, 464, 3229
Negueruela, I., Smith, D. M., Harrison, T. E., et al. 2006a, ApJ, 638, 982
Negueruela, I., Smith, D. M., Reig, P., et al. 2006b, ESA SP, 604, 165
Negueruela, I., Torrejón, J. M., & McBride, V. 2007, ATel, 1239
Negueruela, I., Casares, J., Verrecchia, F., et al. 2008, ATel, 1876
Nespoli, E., Fabregat, J., & Mennickent, R. E. 2008, A&A, 486, 911
Ochsendorf, B. B., Cox, N. L. J., Krijt, S., et al. 2014a, A&A, 563, A65
Ochsendorf, B. B., Verdolini, S., Cox, N. L. J., et al. 2014b, A&A, 566, A75
Parker, Q. A., Phillipps, S., Pierce, M. J., et al. 2005, MNRAS, 362, 689
Parkes, G.E., Murdin, P.G., & Mason, K.O. 1980, MNRAS, 190, 537
Peri, C.S., Benaglia, P., Brookes, D.P., et al. 2012, A&A, 538, A108
Peri, C. S., Benaglia, P., & Isequilla, N. L. 2015, A&A, 578, A45
Perryman, M. A. C., Lindegren, L., Kovalevsky, J., et al. 1997, A&A, 323, L49

Pflamm-Altenburg, J., & Kroupa, P. 2010, MNRAS, 404, 1564
Pilbratt, G.L., Riedinger, J.R., Passvogel, T., et al. 2010, A&A, 518, L1
Poglitsch, A., Waelkens, C., Geis, N., et al. 2010, A&A, 518, L2
Polcaro, V. F., Bazzano, A., La Padula, C., et al. 1984, A&A, 131, 229
Postnov, K., Oskinova, L., & Torrejón, J. M. 2017, MNRAS, 465, L119
Povich, M. S., Benjamin, R. A., Whitney, B. A., et al. 2008, ApJ, 689, 242
Priedhorsky, W.C., & Terrell, J. 1983, ApJ, 273, 709
Rahoui, F., Chaty, S., Lagage, P. O., et al. 2008, A&A, 484, 801
Reynolds, A. P., Owens, A., Kaper, L., et al. 1999, A&A, 349, 873
Rieke, G.H., Young, E.T., Engelbracht, C.W., et al. 2004, ApJS, 154, 25
Romano, P., Mangano, V., Cusumano, G., et al. 2011, MNRAS, 412, L30
Sato, N., Nagase, F., Kawai, N., et al. 1986, ApJ, 304, 241
Secchi, A. 1866, Astron. Nachr., 68, 6
Servillat, M., Coleiro, A., Chaty, S., et al. 2014, ApJ, 797, 114
Smith, D. M., Main, D., Marshall, F., et al. 1998, ApJ, 501, L181
Smith, M. A., Lopes de Oliveira, R., & Motch, C. 2016, Adv. Space Res., 58, 782
Smith, M. A., Lopes de Oliveira, R., & Motch, C. 2017, MNRAS, 469, 1502
Sota, A., Maíz Apellániz, J., Morrell, N. I., et al. 2014, ApJS, 211, 10
Sugizaki, M., Mitsuda, K., Kaneda, H., et al. 2001, ApJS, 134, 77
Takeuchi, Y., Koyama, K., & Warwick, R. S. 1990, PASJ, 42, 287
Tawara, Y., Yamauchi, S., Awaki, H., et al. 1989, PASJ, 41, 473
Thompson, T.W.J., Tomsick, J.A., in 't Zand, J.J.M., et al. 2007, ApJ, 661, 447
Toalá, J. A., Oskinova, L. M., & Ignace, R. 2017, ApJ, 838, L19
Tomsick, J. A., Chaty, S., Rodriguez, J., et al. 2007, ATel, 1231
van Buren, D., & McCray, R. 1988, ApJ, 329, L93
van Buren, D., Noriega-Crespo, A., & Dgani, R. 1995, AJ, 110, 2914
van den Heuvel, E.P.J., Portegies Zwart, S.F., Bhattacharya, D., et al. 2000, A&A, 364, 563
van Oijen, J.G.J. 1989, A&A, 217, 115
Verrecchia, F., Negueruela, I., Covino, S., et al. 2002, ATel, 102
Walter, R., Lutovinov, A.A., Bozzo, E., et al. 2015, A&ARv, 23, 2
Warwick, R.S., Norton, A.J., Turner, M.J.L., et al. 1988, MNRAS, 232, 551
Werner, M., Roellig, T., Low, F., et al. 2004, ApJS, 154, 1
Wright, E. L., Eisenhardt, P. R. M., Mainzer, A. K., et al. 2010, AJ, 140, 1868
Zacharias, N., Finch, C., & Frouard, J. 2017, AJ, 153, 166
Ziolkowski, J. 2002, Mem. Soc. Astron. It., 73, 1038
Zurita Heras, J.A., De Cesare, G., Walter, R., et al. 2006, A&A, 448, 261

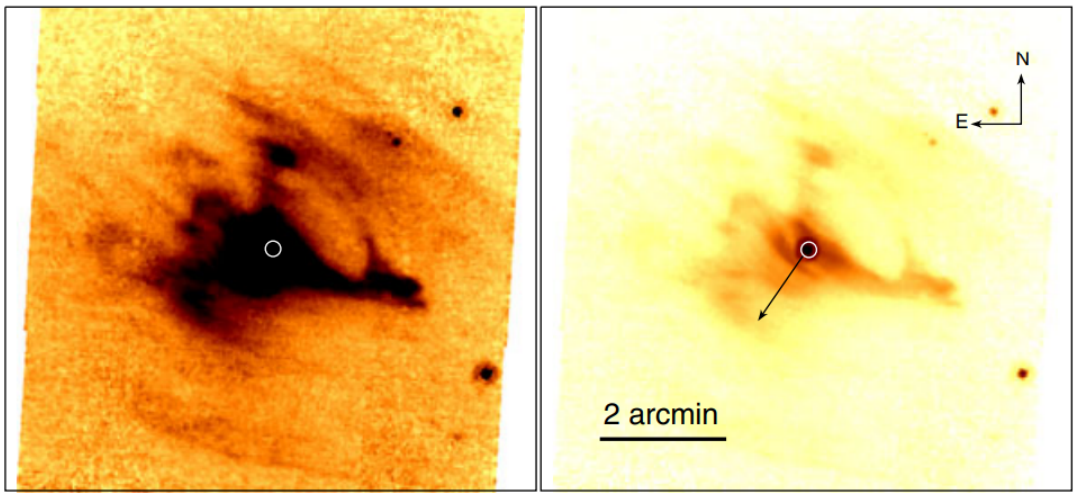

FIGURE 2.1: *Spitzer* MIPS 24 μm image of the nebula around EXO 051910+3737.7 (V420 Aur) in two intensity scalings. The position of the system is indicated by white circles, and the arrow shows the peculiar velocity direction of the system. Figure reproduced from Gvaramadze (2019).

2.3 Further developments

Since the publishing of the accompanying paper dealing with the bow shocks and other circumstellar structures around HMXBs, there have not been any new detections of bow shocks around HMXBs. Nevertheless, there has been some progress in this field.

Gvaramadze (2019) discussed some of the nebulae that were also found in the paper presented in this chapter. He ruled out the bow shock interpretation of the nebula associated with EXO 1722-363 and proposed that the most likely explanation is that the emission arises from the local ISM that is heated by radiation from the supergiant companion star in EXO 1722-363. However, it is also possible that the nebula is produced by collimated outflows or jets produced by this system.

In addition to this, Gvaramadze (2019) also briefly discussed the nature of the nebula around EXO 051910+3737.7 (V420 Aur). Similarly to me, he noted that the eastern arc is leading the system in the direction of its peculiar velocity and that the complex shape of the nebula makes it impossible to interpret it as a classical bow shock (see Fig. 2.1).

Gvaramadze (2019) also noted the bow-like structure around GX 304-01 (V850 Cen) and interpreted it as a bow wave driven by radiation pressure, although other interpretations involving jets or illumination of the local ISM cannot be excluded as well. It can be seen clearly in Fig. 2.2 that the dimpled structure of the arc is visible also in the *Herschel* PACS 70 μm image.

Furthermore, Gvaramadze (2019) discussed the case of IGR J16327-4940, a HMXB candidate (Masetti et al., 2010). I did not investigate this object as it is not included in the sample of Liu, van Paradijs, and van den Heuvel (2006) and Walter et al. (2015). Using *Spitzer* data, Gvaramadze, Kniazev, and Fabrika (2010) discovered a circular nebula around the presumed optical counterpart of IGR J16327-4940 (see Fig. 2.3). The spectral and variability analysis determined that the counterpart is a luminous blue variable (Gvaramadze, Kniazev, and Berdnikov, 2015). Interestingly, the GDR2 astrometry indicates that this star is a fast runaway ejected from the massive star cluster Westerlund 1 (Gvaramadze, 2018). It is therefore puzzling that

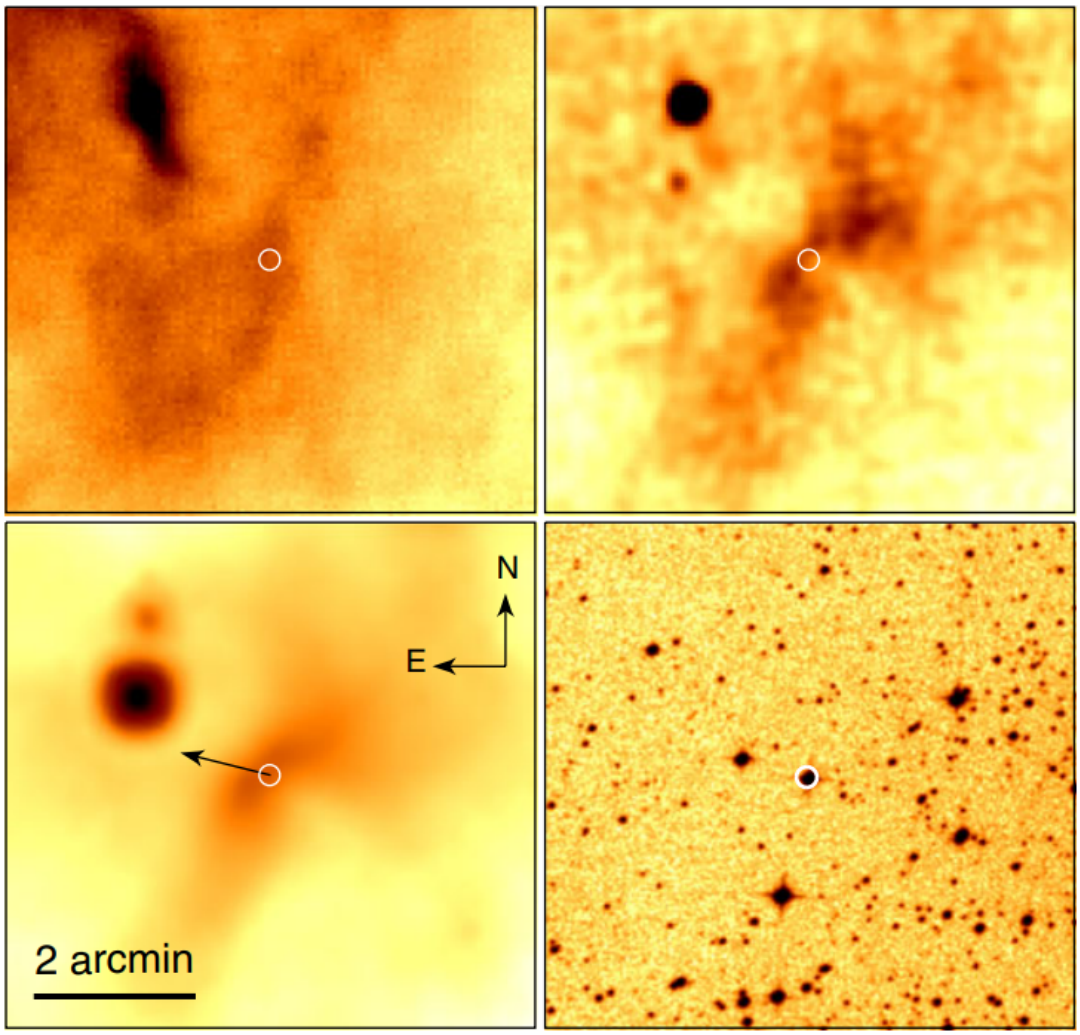

FIGURE 2.2: From left to right and from top to bottom: *Herschel* PACS 160 μm and *Herschel* PACS 70 μm (Pilbratt et al., 2010; Poglitsch et al., 2010), WISE 22 μm, and Digitized Sky Survey (DSS-2-red) images of the GX 304-01 vicinity. The position of the system is indicated by a circle, and the arrow shows the peculiar velocity direction of the system. Figure reproduced from Gvaramadze (2019).

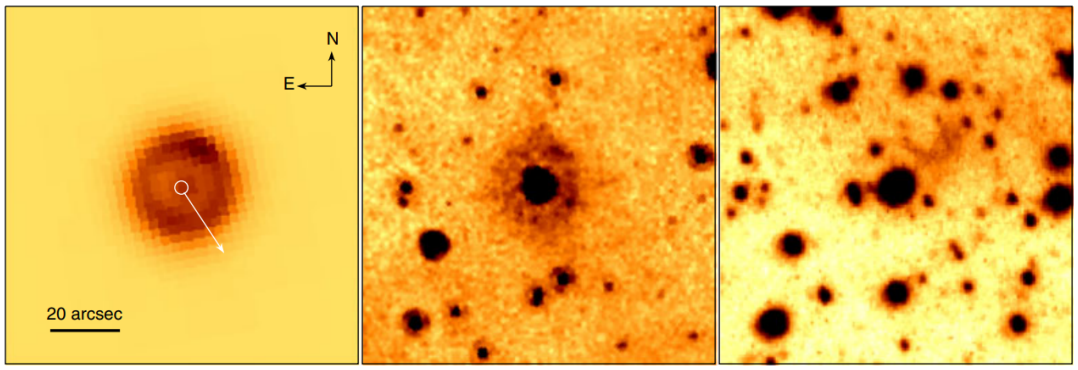

FIGURE 2.3: From left to right: *Spitzer* MIPS 24 μm, *Spitzer* IRAC 8 μm (Fazio et al., 2004), and SHS Hα (Parker et al., 2005) image of the circumstellar structure associated with IGR J16327-4940. The position of the system is indicated by a circle, and the arrow shows the peculiar velocity direction of the system. Figure reproduced from Gvaramadze (2019).

the high peculiar velocity with respect to the local ISM has no apparent effect on the shape of the nebula. Gvaramadze (2019) theorizes that the nebula is created due to stellar wind interacting with a co-moving dense material lost by the star during the preceding evolutionary stage. Another possibility is that this material was produced in a recent binary interaction.

Overall, Gvaramadze (2019) also arrived at the same conclusion concerning the paucity of bow shocks around HMXBs – that most of HMXBs are still moving through a hot and low-density medium, where the bow shocks do not form due to the sound speed in the local ISM being higher than the peculiar velocity of the HMXB, or that the bow shocks in this rarefied ISM are very faint, leading to a low fraction of HMXBs driving bow shocks as compared to OB runaways. Moreover, this lower fraction can also be partly attributed to the fact that a lot of HMXBs are BeXRBs, where the Be secondaries are suspected to not have strong stellar winds and may also be moving with lower peculiar velocities than the typical bow shock-driving OB runaways (e.g., van den Heuvel et al., 2000).

Independently of the study presented in this chapter, Bodensteiner et al. (2018) investigated the occurrence of mid-infrared nebulae around bright massive early-type stars. They constructed a sample of bright OBA stars, classical Be stars, Be+sdO systems (Be stars with a hot subdwarf companion), and 72 BeXRBs taken from the compilation by Raguzova and Popov (2005). Similarly to this work, they based their search around the visual examination of the WISE 22 μm images for potential nebulae in the vicinity of all objects of their sample. They identified more than 200 possible nebulae associated with the studied objects. Based on the shape of the nebula, its position with respect to the studied object, and the direction of the peculiar velocity of the object with respect to the nebula, they broadly classified their detections into 5 groups:

- clear bow shocks with the diffuse emission separated from the star and its symmetry aligned with the stellar peculiar velocity direction,
- clear bow shocks with the diffuse emission separated from the star but with the peculiar velocity direction not aligned with the symmetry of the nebula,
- centered nebulae,

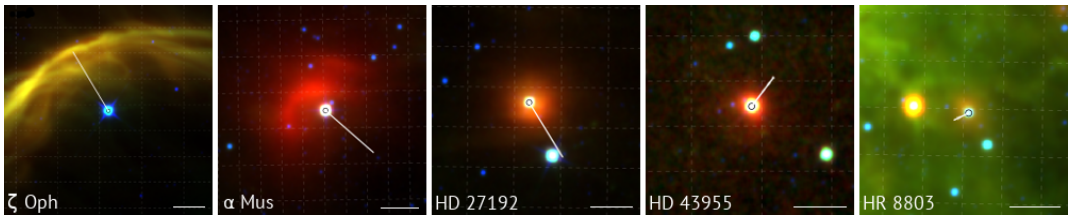

FIGURE 2.4: Morphological groups of Bodensteiner et al. (2018) and their examples. From left to right: bow shocks aligned with the peculiar velocity direction, bow shocks unaligned with the peculiar velocity direction, centered, unresolved and unclassified nebulae. The white lines show the direction of the peculiar velocity and its relative magnitude. The white line at the bottom right of each panel corresponds to 2 arcmin. Figure reproduced from Bodensteiner et al. (2018).

- unresolved nebulae,
- unclassified nebulae (see Fig. 2.4).

They found that ∼28% of all O stars are associated with infrared nebulae and that the occurrence of nebulae decreases rapidly when moving to the later spectral classes, as only ∼13% of the B and ∼0.4% of the A stars show possible associations with nebulae.

While they reported no detections of aligned bow shocks associated with BeXRBs, they found four associations of BeXRBs with infrared nebulae. Among them is the nebula around γ Cas, which falls among the unclassified objects, and the nebula around μ^2 Cru, which displays centered morphology. I recovered both objects in my study (see Fig. 1 and Fig. 5 of the paper included in this chapter). The other two objects reportedly also exhibit the unclassified morphology, but Bodensteiner et al. (2018) did not provide their identifiers or discussed them in more detail as their optical counterparts are not bright enough to be considered in their study. It is interesting to note that the BeXRB nature of both γ Cas and μ^2 Cru is disputed. γ Cas is a prototype of a separate class of peculiar objects, γ Cas analogs (e.g., Smith, Lopes de Oliveira, and Motch, 2016), while μ^2 Cru might be an ordinary star (Arnason et al., 2021). The exclusion of these two objects from the bona fide HMXBs further exacerbates the absence of mid-infrared nebulae around HMXBs.

Bodensteiner et al. (2018) also proposed an explanation for the origin of some centered nebulae (such as the one associated with μ^2 Cru) around massive early-type stars and binaries. A fraction of them might be an observational signature of dust formed in the material that has been lost during non-conservative mass transfer (i.e., in a Roche lobe overflow or a stellar merger, e.g., Packet, 1981; Shu and Lubow, 1981; Wellstein, Langer, and Braun, 2001) heated by the star (and the compact companion – if present). These nebulae should be very short-lived as they expand rapidly into the local ISM.

γ Cas and its circumstellar nebula have also been briefly discussed in Langer et al. (2020). They investigate several models for γ Cas analogs, including the propeller model, which assumes the presence of an NS in the system – as in a classical BeXRB. Due to the presence of an NS, the system should have gained some peculiar velocity as a consequence of an SN explosion. Langer et al. (2020) search for the presence of stellar bow shocks around γ Cas analogs that would indicate a high velocity of the system with respect to the local ISM. They find two nebulae – one associated with

γ Cas and the second one around π Aqr. They briefly comment that the morphological evidence for a bow shock around γ Cas is weak, but the nebula may be related to the system.

Recently, Chen et al. (2021) discovered a large $\sim 2.0^\circ \times 1.4^\circ$ (or 6.0 pc $\times$ 4.2 pc) cavity toward γ Cas in the H I radio data. The scale of this structure is much bigger than the scale of the diffuse nebula that I have detected around γ Cas. Through multiwavelength analysis Chen et al. (2021) concluded that the cavity is opened by a strong stellar wind from the system. The presence of strong stellar wind opens a possibility to explain the peculiar X-ray emission of γ Cas analogs. They theorized that if the binary scenario for these systems is invoked, a strong interaction between the winds of the primary and the secondary can be expected, creating a much harder X-ray emission than that from isolated massive stars (e.g., Rauw and Nazé, 2016). The multiple thermal components detected in the X-rays for γ Cas analogs would then be explained by wind–wind and wind–disk interactions in the context of a binary system (Langer et al., 2020). The other characteristics of these objects, such as the short-term and phase-dependent X-ray variability could then be explained by the high intrinsic instability of the wind, changes in the stellar separation, wind absorption, and/or stellar occultation (Rauw and Nazé, 2016; Pittard and Dawson, 2018).

Very recently, van den Eijnden et al. (2022) presented the discovery of 1.3-GHz radio emission from the Vela X-1 bow shock with the MeerKAT telescope. This makes it the second radio bow shock detected around a massive runaway star, the first being BD+43°3654 (Benaglia et al., 2010; Benaglia et al., 2021). Therefore, it is also the first radio bow shock detected around an HMXB. The investigation presented in van den Eijnden et al. (2022) suggests that the bow shock emission is dominated by optically thin free-free emission and that a high density of the local ISM around Vela X-1 is essential for the detection of radio emission.

Chapter 3

Kinematic distinction of the two subpopulations of X-ray pulsars

3.1 Paper summary

High-mass X-ray binaries (HMXBs) are systems comprising of a compact object (an NS or a BH) and a luminous, massive ($\gtrsim 10\,M_\odot$) companion, providing matter to it. One of the HMXB subclasses, known as Be/X-ray binaries (BeXRBs), consists of a compact object (normally an NS) with a Be star secondary with a decretion disk, which is formed as a consequence of its rapid rotation, as the material is being ejected from the Be star's surface (e.g. Reig, 2011; Casares, Jonker, and Israelian, 2017).

Due to the various physical processes and interactions within the system, the observations of BeXRBs show considerable variability on a wide range of time scales across various wavelengths. Most of the mass accretion occurs as the NS passes through, or close to, the decretion disk of the Be companion. During these passes, the system undergoes bright and periodic Type I outbursts. They are modulated by the BeXRB orbital periods, which typically span from about 10 to 400 d (Liu, van Paradijs, and van den Heuvel, 2006; Reig, 2011).

Another important class of periodic BeXRB variability is X-ray pulsations, which also have the shortest timescales from all types of periodic variabilities observed in these systems. They are typically of the order of a few seconds to ∼1000 s (Liu, van Paradijs, and van den Heuvel, 2006; Walter et al., 2015). The X-ray pulsations arise due to a misalignment of the rotation and magnetic axes of the NS. When the matter is accreted from the secondary and is channeled by the NS's magnetic field onto the magnetic poles, it can produce two or more localized X-ray hot spots. As the NS rotates, these hot spots periodically come into view, producing periodic X-ray pulses. Thus, by analyzing the pulsations, the NS spin (pulse) period can be obtained. Almost all BeXRBs show X-ray pulsations (we term such objects here as X-ray pulsars), and their presence is one of the strongest indications that the compact object present in the system is indeed an NS (Reig, 2011).

The orbital ($P_{\rm orb}$) and the spin periods ($P_{\rm s}$) of the BeXRBs are found to be linearly correlated in the $\log(P_{\rm orb})$–$\log(P_{\rm s})$ plane (Corbet diagram; Corbet, 1984; Corbet, 1986). Knigge, Coe, and Podsiadlowski (2011) observed that, aside from this correlation, the BeXRBs seem to be split into two groups, a short $P_{\rm s}/P_{\rm orb}$ subpopulation and a long $P_{\rm s}/P_{\rm orb}$ subpopulation, where the spin period divide is at $P_{\rm s}/P_{\rm orb} \approx 40$ s and the orbital period divide is at $P_{\rm orb} \approx 60$ d (see Fig. 1.10). After considering several possible reasons for this bimodality, they concluded that the most plausible one is that the two subpopulations arise from two distinct BeXRB formation channels, corresponding to two different types of SN events in these systems. Specifically, electron-capture SNe (hereafter ECSNe) are the result of the collapse of an oxygen-neon-magnesium core of an intermediate-mass star (with initial masses lower than

10 $M_\odot$ and perhaps as low as 6 $M_\odot$, especially if in tight, low-metallicity binaries) as it loses pressure support owing to the sudden capture of electrons by neon or magnesium nuclei (Nomoto, 1984; Nomoto, 1987), whereas iron-core collapse SNe (hereafter CCSNe) occur after a degenerate iron core form inside higher mass stars (e.g. Cerda-Duran and Elias-Rosa, 2018, and the references therein). The possibility of the presence of two distinct BeXRB subpopulations from different SN types has been noted before as well, where it has been theorized that a subclass of BeXRBs with low eccentricities and low X-ray luminosities could be the result of an ECSN or some other type of a weak SN that imparts a low kick to the nascent NS (Pfahl et al., 2002; Podsiadlowski et al., 2004; van den Heuvel, 2004).

Knigge, Coe, and Podsiadlowski (2011) theorize, that ECSNe give rise to the systems falling into the short $P_\mathrm{s}/P_\mathrm{orb}$ BeXRB subpopulation, and CCSNe are responsible for the systems found in the long $P_\mathrm{s}/P_\mathrm{orb}$ subpopulation. Aside from this, ECSNe should produce slightly less massive NSs than CCSNe (Nomoto, 1984). Also, ECSNe eject less mass during the explosion and impart smaller kicks to the nascent NSs than CCSNe. This translates to the smaller peculiar (systemic) velocities and orbital eccentricities in the systems where the NS was born in an ECSN. Then, if the hypothesis by Knigge, Coe, and Podsiadlowski (2011) is correct, the short $P_\mathrm{s}/P_\mathrm{orb}$ should also exhibit lower NS masses, orbital eccentricities, and peculiar velocities, which is testable. There is also an alternative hypothesis for the origin of the bimodality in P_s. Cheng, Shao, and Li (2014) proposed that this bimodality is caused by different accretion modes of NSs in BeXRBs.

Unfortunately, the number of the systems with the measured NS masses and orbital eccentricities is too low for meaningful statistics. This was also the case for the peculiar velocities, but the situation changed with the advent of the *Gaia* mission (Gaia Collaboration et al., 2016b), especially its second data release (GDR2; Gaia Collaboration et al., 2018; Lindegren et al., 2018), which provided very precise astrometry for the unprecedented number of sources, including many BeXRBs. This enabled us to study the kinematics of a sufficient number of BeXRBs for the first time.

I have collated a sample of Galactic BeXRBs from Liu, van Paradijs, and van den Heuvel (2006) and Walter et al. (2015), where the systems have optical counterparts bright enough to have the full astrometric solution in *Gaia* and have measured P_s values. After discarding some sources with unreliable astrometric solutions, 27 sources were retained for the analysis. Using the divide $P_\mathrm{s,split} = 40$ s between the subpopulations, as adopted in Knigge, Coe, and Podsiadlowski (2011), the sample was split into a short-spin subpopulation, containing 7 sources, and a long-spin subpopulation with 20 sources.

The derivation of distances and velocities from astrometry is not straightforward, mainly because the measured parallaxes (especially those with relatively high uncertainties) have a non-linear relationship to distances. Distances are also constrained to be positive, which is not the case for *Gaia* parallaxes, especially of distant objects. A lot of the sample BeXRBs have parallaxes with relative errors higher than 20%, and three of them have negative parallaxes. Therefore, distances and tangential velocities of the studied BeXRBs were jointly estimated from parallaxes and proper motions via Bayesian inference (see e.g. Luri et al., 2018), using the prior scale lengths adopted from Bailer-Jones et al. (2018) and the common empirically determined scale length, calculated from the BeXRBs distances collected from the literature. The tangential peculiar velocities were derived by accounting for and removing the kinematic components stemming from the Galactic rotation and the peculiar movement of the Sun relative to its LSR (i.e. relative to the expected motion in the Galaxy; e.g. van den

Heuvel et al., 2000; Gvaramadze et al., 2011). This yielded that the short-spin subpopulation possesses a mean tangential peculiar velocity of approximately 29±11 $\mathrm{km\,s^{-1}}$, while for the long-spin subpopulation it is about 16±8 $\mathrm{km\,s^{-1}}$. This kinematic difference is robust and statistically significant according to a number of different statistical tests.

I have also investigated the kinematics of the BeXRBs in the Small Magellanic Cloud (SMC), which contains an unexpectedly high number of them. However, due to its distance and the irregular nature of this galaxy, it was not possible to adopt the same method as for the Galactic BeXRBs. Instead, I have made use of the projected separations between the SMC BeXRBs and the nearby young star clusters and associations (hereafter just 'clusters') closest to them under the assumption they have, most likely, originated there. These separations can serve as a proxy for the peculiar velocities (Coe, 2005). I have used the SMC BeXRBs from the catalog of Haberl and Sturm (2016) and SMC cluster catalogues of Rafelski and Zaritsky (2005), Nayak et al. (2018), and Piatti (2018). The BeXRBs with no optical counterpart, unknown spin period, and the ones that lie outside the region covered by the cluster catalogs, have been discarded. Using all SMC cluster catalogs, the split between the short-spin subpopulation and the long-spin subpopulation is observed as in the Milky Way. For instance, given the distance to the SMC of 62.44 kpc (Graczyk et al., 2020), and using the catalog of Rafelski and Zaritsky (2005), the BeXRBs in the short-spin subpopulation are approximately 120±73 pc from the nearest cluster, while for the long-spin subpopulation it is 80±42 pc.

Combining the results obtained from the analysis of BeXRBs in both galaxies, it seems there is strong evidence for kinematic bimodality of these systems, where the short-spin subpopulation has larger peculiar velocities than the long-spin population. This trend is opposite the one predicted by Knigge, Coe, and Podsiadlowski (2011). This can be reconciled if the scenario proposed by Podsiadlowski et al. (2004) is adopted instead, where the systems with short orbital periods (and therefore short spin periods, as these two quantities are correlated for BeXRBs) are expected to arise from CCSNe.

Several interesting trends are visible if the calculated peculiar velocities are investigated together with orbital periods and eccentricities of the Galactic BeXRBs. Notably, there is no observable correlation between the orbital periods and the peculiar velocities, contrary to the expected anticorrelation in the simulations by Brandt and Podsiadlowski (1995). There is also a tentative anti-correlation between the eccentricities and the peculiar velocities. While several hypotheses for these relations can be proposed, the number of sources studied is still too low for a meaningful inference, and the sample is likely biased by selection effects. Clearly, there is a lot of observational and theoretical work to be done. Particularly, the future *Gaia* data releases will provide improved astrometry that will further constrain the kinematics of Galactic BeXRBs.

3.2 Paper II

A&A 640, A86 (2020)
https://doi.org/10.1051/0004-6361/201935642

Astronomy & Astrophysics

Kinematic distinction of the two subpopulations of X-ray pulsars

M. Prišegen

Department of Theoretical Physics and Astrophysics, Masaryk University, Kotlářská 2, 611 37 Brno, Czech Republic
e-mail: michalprisegen@gmail.com

Received 8 April 2019 / Accepted 4 June 2020

ABSTRACT

Context. The population of Be/X-ray binaries shows strong evidence of bimodality, especially in the spin period of neutron stars. Several physical mechanisms may produce this bimodality. The most favored candidate mechanisms are two distinct supernova channels or different accretion modes of the neutron stars in Be/X-ray binaries. Investigating the kinematics of these systems may provide some additional insight into the physics of this bimodality.
Aims. If the two Be/X-ray binary subpopulations arise from two distinct supernova types, then the two subpopulations should have different peculiar (systemic) velocities. This can be tested either directly, by measuring the velocity of the system, or indirectly, by measuring the position of the system with respect to its birthplace. A difference in the peculiar velocity magnitude between the subpopulations would favor the supernova hypothesis, and the lack of this difference would suggest that the accretion hypothesis is a more favorable option to explain the bimodality.
Methods. Using the most recent *Gaia* dataset and the newest catalogs of Small Magellanic Cloud (SMC) star clusters, we analyzed the tangential peculiar velocities of Be/X-ray binaries in the Galaxy and the positions of Be/X-ray binaries in the SMC. We used the distance of the system from the nearest young star cluster as a proxy to the tangential velocity of the system. We applied statistical testing to investigate whether the two subpopulations that are divided by the spin of the neutron star are also kinematically distinct.
Results. There is evidence that the two subpopulations are indeed kinematically distinct. However, the tangential peculiar velocities of the two subpopulations are the reverse from what is expected from the distinct supernova channel hypothesis. We find some marginal evidence ($p \approx 0.005$) that the Galactic Be/X-ray binaries from the short-spin subpopulation have systematically higher peculiar velocities than the systems from the long-spin subpopulation. The same effect, but weaker, is also recovered for the SMC Be/X-ray binaries for all considered cluster catalogs. The unexpected difference in the peculiar velocities between the two subpopulations of Be/X-ray binaries contradicts these two hypotheses, and an alternative physical explanation for this may be needed.

Key words. binaries: general – stars: neutron – X-rays: binaries

1. Introduction

Be/X-ray binaries (BeXRBs) are the most numerous subclass of high-mass X-ray binaries in the Galaxy. They are systems containing a neutron star with a mass-losing Be-type main-sequence companion that is surrounded by a circumstellar decretion disk (e.g., Rivinius et al. 2013). These objects are typically revealed by X-ray activity that is fueled by mass accretion. Most of the mass accretion takes place during periastron passages, when the neutron star passes in the vicinity, in some cases, even through, the decretion disk of the Be star (e.g., Ziolkowski 2002; Reig 2011; Casares et al. 2017).

A supernova explosion occurring in a massive binary leads to a disruption of the system in the majority of cases (see, e.g., Brandt & Podsiadlowski 1995; De Donder et al. 1997; Eldridge et al. 2011; Renzo et al. 2019). For the systems that remain bound, BeXRBs provide a valuable but inherently biased laboratory for studying the physics of the supernova explosions that formed their neutron stars. BeXRBs provide a well-defined and simple population: each hosts a neutron star primary with a mass of $\sim$1.4 $M_\odot$ (with the notable exception of MWC 656, which hosts a black hole; Casares et al. 2014) and a secondary star from a relatively narrow spectral distribution that peaks at B0 (Reig 2011). This population nevertheless exhibits a wide variety of properties that encode the information about the past supernova event in the system and the massive binary progenitor. Moreover, the short lifetime of the BeXRB phase, typically $\sim$10 Myr (van den Heuvel et al. 2000), does not allow parameters such as the neutron star masses, orbital periods, and peculiar velocities to change significantly. These parameters are therefore close to their birth values just after the supernova explosion.

The original idea that there might be subpopulations in the BeXRB population was proposed by Pfahl et al. (2002), who reported a subclass of BeXRBs with low eccentricities and low X-ray luminosities. They proposed that this subclass originates from the binaries where the initially more massive star undergoing a supernova explosion has a rapidly rotating core, which results in a neutron star that has received only a small natal kick. Podsiadlowski et al. (2004) and van den Heuvel (2004) proposed that this low-eccentricity subpopulation might be explained if the neutron stars in these systems underwent an electron-capture supernova (ECSN). The ECSNe are the result of the collapse of an oxygen-neon-magnesium core of a lower mass star (possibly with an initial mass as low as 6 $M_\odot$ if it is in a tight binary, especially at lower metallicities; Podsiadlowski et al. 2004) as it loses pressure support owing to the sudden capture of electrons by neon or magnesium nuclei (Nomoto 1984, 1987), ejecting little mass in the supernova explosion (normally $\lesssim$1 $M_\odot$) and imparting little to no kick to the nascent neutron star (Podsiadlowski et al. 2004; van den Heuvel 2004). The classical high-eccentricity BeXRB population would then be a result of iron-core-collapse supernovae (CCSNe),

which occur after a degenerate iron core forms inside a higher mass star (e.g., Cerda-Duran & Elias-Rosa 2018 and the references therein). CCSNe eject more mass and might impart a substantial kick to the newly formed neutron stars as well. The evidence supporting the existence of two distinct explosion mechanisms is not limited to BeXRBs. Observations of double neutron stars, the bimodal velocity distribution of young pulsars, and a high number of neutron stars retained in globular clusters can be attributed to two supernova explosion mechanisms (Beniamini & Piran 2016; Verbunt et al. 2017; Pfahl et al. 2002).

Examining the spin–orbital period diagram of BeXRBs, Knigge et al. (2011; hereafter KCP) also noted that the BeXRB population consists of two subpopulations, a short-period subpopulation with a characteristic orbital period of $P_{\rm orb} \approx 40$ d and spin period $P_{\rm s} \approx 10$ s, and a long-period subpopulation with $P_{\rm orb} \approx 100$ d and $P_{\rm s} \approx 200$ s. The histogram of $P_{\rm orb}$ and $P_{\rm s}$ was used to estimate an approximate threshold dividing the subpopulations. This threshold lies at 60 d and 40 s, respectively. Especially in the case of spin periods, the dip in the histogram is considerably wide, therefore these values need to be considered with caution. The two subpopulations are more clearly separated in the spin period than in the orbital period. KCP theorized that these two subpopulations are also a consquence of two different supernovae types that occur in these binaries, where the ECSNe reportedly produce the short-period subpopulation and the CCSNe produce the long-period subpopulation. The observed BeXRB spin periods are not a direct result of the supernova explosion itself, rather, they evolve during the BeXRB phase toward some equilibrium spin period $P_{\rm eq}$. This $P_{\rm eq}$ is dependent on the orbital period of the BeXRBs, which produces the well-known correlation in the spin–orbital period diagram, but it also depends on other parameters that are expected to be different for ECSNe and CCSNe (e.g., resulting neutron star magnetic field and neutron star mass; Waters & van Kerkwijk 1989).

Cheng et al. (2014) proposed an alternative explanation for the two subpopulations in $P_{\rm s}$, where the bimodality in $P_{\rm s}$ can be ascribed to different accretion modes of the neutron stars in BeXRBs. Here, the BeXRB systems that exhibit giant outbursts tend to have shorter spins. During giant outbursts, the neutron star accretes from a thin disk with a relatively long lifetime, which efficiently transfers mass and angular momentum to the neutron star, so that its spin period reaches $P_{\rm s} \sim 10$ s. For the BeXRBs, which undergo predominantly normal outbursts or have no outbursts at all, the accretion torques are smaller. The accretion flows around the neutron stars within these systems are in the form of advection-dominated accretion flows, meaning that the spin-up is infrequent and ineffective. The sources from this subpopulation then exhibit spin periods of about $P_{\rm s} \sim 100$ s. While the supernova mechanism has some effect on the occurrence and type of outbursts and thus spin periods, it is unclear how dominant it is and what other processes are relevant in this case.

These two competing hypotheses can be tested using the BeXRB parameters that do not depend, or depend only negligibly, on the accretion processes, such as the neutron star mass, orbital eccentricity, and peculiar velocity. ECSNe should produce less massive neutron stars than CCSNe (Nomoto 1987; Podsiadlowski et al. 2004). Thus, provided that the BeXRB subpopulations originate from different types of supernovae, we should be able to observe two subpopulations with different neutron star masses. Unfortunately, this cannot be investigated as the long orbital periods and scarcity of eclipsing BeXRBs means that there are only a handful of systems for which the neutron star mass can be determined. ECSNe are also expected to impart smaller kicks to the neutron stars and expel less matter in the explosion, producing systems with lower eccentricities and lower peculiar velocities (Podsiadlowski et al. 2004). It is expected that the observed eccentricities are still close to the original values just after the supernova explosion because the timescales for tidal circularization for the BeXRBs with orbital periods $P_{\rm orb} \geq 10$ d are significantly higher than the secondary lifetime. As a result, tidal effects should have little effect on the orbit of a typical BeXRB, which has an orbital period well above 10 d (van den Heuvel et al. 2000; Reig 2011). KCP noted that there is a trend toward lower eccentricities in the short-period BeXRB subpopulation, in line with their hypothesis, but this trend is not significant. A small number of systems for which the eccentricity values are available makes it difficult to investigate this using this parameter.

Studying the kinematics of BeXRBs has also been problematic. Many of them have only a weak optical counterpart and/or lie at a considerable distance. Thus, their distances and proper motions have been unreliable, often with different astrometric catalogs giving disparate values of the parallaxes and proper motions for the same system (e.g., Ankay et al. 2001; Gvaramadze et al. 2011). This has made the determination of their peculiar velocities difficult and viable only for the close systems. The situation has changed with the advent of the second *Gaia* data release (GDR2; Gaia Collaboration 2018; Lindegren et al. 2018), which contains the parallaxes and proper motions for the majority of the confirmed and candidate BeXRBs in the Galaxy. This enables us to derive the peculiar velocities of the Galactic population of BeXRBs in a consistent way. However, at the time of writing, the kinematics of BeXRBs situated in the Magellanic Clouds still has to be studied indirectly.

In this work, we investigate whether kinematic subpopulations of BeXRBs exist and what their origin is. We compute the tangential peculiar velocities of Galactic BeXRBs and conduct statistical tests to determine whether they comprise two distinct subpopulations. For the population in the Small Magellanic Cloud (SMC), we use the distances from the closest star cluster that is assumed to be the birthplace of that particular BeXRB as a proxy for the tangential peculiar velocity and conduct equivalent tests.

2. Milky Way Be/X-ray binary population

To construct our sample of Galactic BeXRBs, we selected the systems classified as such in Walter et al. (2015) and the systems listed in the fourth edition of the Catalogue of High Mass X-ray binaries in the Galaxy (Liu et al. 2006). To select a population of the confirmed BeXRBs, we only selected sources with measured $P_{\rm s}$. Sources without an optical counterpart or those without a match in GDR2 were also removed from the analysis. This selection yielded 24 systems out of the total of 32 listed in Walter et al. (2015). Another 11 sources satisfying the same criteria were added from Liu et al. (2006). We chose to discard 4U 1901+03 because its optical counterpart is unknown (Reig & Milonaki 2016; Walter et al. 2015), although it is matched to *Gaia* DR2 4268774695647764352 in Simbad[1]. We also removed SAX J0635.2+0533 because of its rotation-powered (rather than accretion-powered) nature (La Palombara & Mereghetti 2017). The relevant properties of

[1] http://simbad.u-strasbg.fr/simbad/

Table 1. Galactic BeXRB pulsars.

Name	P_{orb} (d)	P_s (s)	GDR2 ID	d_{lit} (kpc)	d_{BJ} (kpc)	d_{lit} ref
4U 0115+63	24.3	3.61	524677469790488960	5.3 ± 0.44	$7.2^{+1.5}_{-1.1}$	Coleiro & Chaty (2013)
V 0332+53	34.67	4.375	444752973131169664	6.9 ± 0.71	$5.13^{+1}_{-0.76}$	Coleiro & Chaty (2013)
GS 0834-430	105.8	12.3	5523448270462666880 [(a)]	$3.0 < d < 5.0$	$5.5^{+2.5}_{-1.7}$	Israel et al. (2000)
IGR J19294+1816	117.2	12.4	4323316622779495680	11.0 ± 1.0	$2.93^{+2.5}_{-1.5}$	Rodes-Roca et al. (2018)
XTE J1946+274	169.2	15.8	2028089540103670144	6.2 ± 3.0	$12.6^{+3.9}_{-2.9}$	Coleiro & Chaty (2013)
4U 1416-62	42.12	17.64	5854175187680510336 [(b)]	7.0 ± 0.74	$5.21^{+2.6}_{-1.6}$	Coleiro & Chaty (2013)
KS 1947+300	40.415	18.7	2031939548802102656	8.5 ± 2.3	$15.2^{+3.7}_{-2.7}$	Coleiro & Chaty (2013)
GS 1843+00		29.5	4278536022438800640	12.5 ± 2.5	$2.28^{+1.9}_{-0.95}$	Israel et al. (2001)
RX J0812.4-3114	81.3	31.8851	5548261400354128768	8.6 ± 1.8	$6.76^{+1.2}_{-0.91}$	Coleiro & Chaty (2013)
EXO 2030+375	46.016	42	2063791369815322752	3.1 ± 0.38	$3.64^{+1.3}_{-0.88}$	Coleiro & Chaty (2013)
IGR J22534+6243		46.67	2207277877757956352	$4.0 < d < 5.0$	$8.06^{+2.3}_{-1.6}$	Esposito et al. (2013)
AX J1700.2-4220	44.0	54	5966213219190201856	$1.7 < d < 2.6$	$1.56^{+0.18}_{-0.14}$	Negueruela & Schurch (2007)
Cep X-4		66.2	2178178409188167296	3.7 ± 0.52	$10.2^{+2.1}_{-1.6}$	Coleiro & Chaty (2013)
XTE J1906+090	26–30	89.17	4310649149314811776 [(c)]	$d > 4$	$2.77^{+2.3}_{-1.4}$	Göğüş et al. (2005)
GRO J1008-57	249.46	93.6	5258414192353423360 [(d)]	4.1 ± 0.59	$3.65^{+0.51}_{-0.4}$	Coleiro & Chaty (2013)
3A 0535+262	111.1	103	3441207615229815040	3.8 ± 0.33	$2.13^{+0.26}_{-0.21}$	Coleiro & Chaty (2013)
4U 0728-25	34.5	103.2	5613494119544761088	5.0 ± 0.82	$9.51^{+3.1}_{-2.1}$	Coleiro & Chaty (2013)
2E 0655.8-0708	101.2	160.7	3052677318793446016	3.9 ± 0.1	$5.11^{+1.4}_{-0.93}$	McBride et al. (2006)
IGR J11435-6109	52.46	161.76	5335021664274920576	9.8 ± 0.86	$8.59^{+2.5}_{-1.8}$	Coleiro & Chaty (2013)
GRO J2058+42	55.03	198	2065653598916388352	9.0 ± 1.3	$8.04^{+1.2}_{-0.94}$	Wilson et al. (2005)
RX J0440.9+4431	155	202.5	252878401557369088	2.9 ± 0.37	$3.25^{+0.62}_{-0.45}$	Coleiro & Chaty (2013)
GX 304-1	132.5	272	5863533199843070208	1.3 ± 0.1	$2.01^{+0.15}_{-0.13}$	Coleiro & Chaty (2013)
4U 1145-619	187.5	292	5334823859608495104	4.3 ± 0.52	$2.23^{+0.19}_{-0.16}$	Coleiro & Chaty (2013)
SAX J2103.5+4545	12.68	358.6	2162805896614571904	8.0 ± 0.78	$6.43^{+0.86}_{-0.69}$	Coleiro & Chaty (2013)
1A 1118-615	24.0	406	5336957010898124160	3.2 ± 1.4	$2.93^{+0.26}_{-0.22}$	Coleiro & Chaty (2013)
IGR J01583+6713		469.2	518990967445248256	4.1 ± 0.63	$7.4^{+1.1}_{-0.9}$	Coleiro & Chaty (2013)
2RXP J130159.6-635806		700	5862285700835092352	$4.0 < d < 7.0$	$5.54^{+2.8}_{-1.7}$	Chernyakova et al. (2005)
4U 0352+309	250	835	168450545792009600	1.2 ± 0.16	$0.793^{+0.037}_{-0.034}$	Coleiro & Chaty (2013)
3U 1022-55		860	5352018121173519488	~ 5	$5.04^{+1}_{-0.75}$	Motch et al. (1997)
SAX J2239.3+6116	262	1247	2201091578667140352	4.9 ± 0.8	$8.03^{+1.3}_{-1}$	Reig et al. (2017)
RX J0146.9+6121		1400	511220031584305536	2.3 ± 0.5	$2.5^{+0.2}_{-0.2}$	Reig et al. (1997)
4U 2206+543	9.57	5559	2005653524280214400	3.4 ± 0.35	$3.34^{+0.39}_{-0.32}$	Coleiro & Chaty (2013)
1H 1249-637		14200	6055103928246312960	0.392 ± 0.055	$0.416^{+0.023}_{-0.021}$	Megier et al. (2009)

Notes. Names, orbital periods (P_{orb}), and spin periods (P_s) are obtained from Liu et al. (2006) and Walter et al. (2015). GDR2 ID is the source id of the counterpart in GDR2. d_{lit} are the distances of the BeXRBs collected from the literature used to estimate the scale length (Sect. 2.2). The typical uncertainty for P_{orb} and P_s is <1 d and $\ll$1 s, respectively (see references in Liu et al. 2006 and Walter et al. 2015), although higher errors may be present for higher P_{orb} and P_s values.
References. [(a)]Israel et al. (2000), [(b)]Grindlay et al. (1984), [(c)]Göğüş et al. (2005), [(d)]Coe et al. (1994).

the 33 selected sources are summarized in Table 1 without these two systems. Because we relied on the P_s values to divide the subpopulations, we refer to them as the short-spin subpopulation and the long-spin subpopulation.

We emphasize here that we only studied the tangential (transverse) components of the peculiar velocities. To obtain complete information about the kinematics of the source, the radial component of the velocity is necessary as well. However, there are literature radial velocity measurements for only a handful of the sources from the sample, and *Gaia* does not provide radial velocity measurements for the early-type stars. Moreover, the measured radial velocities of OB stars are, in general, not accurate because the optical lines are formed in atmospheric layers that have outflow velocities of 20–30 km s^{-1} (e.g., van Oijen 1989). We show below that this value is comparable to the typical tangential peculiar velocities of the BeXRB population. It is also not feasible to correct for this effect because the outflow velocities are variable: nonradial pulsations and wind fluctuations change them. This means that the measured radial velocities of BeXRB do not reflect the true radial motion of the system. We therefore did not consider the radial velocities and assumed that the peculiar velocity distribution of BeXRBs is isotropic.

Many possible methods can be employed to study the kinematics of BeXRBs. First, it is possible to measure the

peculiar velocities by accounting for and removing the kinematic components stemming from the Galactic rotation and the peculiar movement of the Sun relative to its local standard of rest (i.e., relative to the expected motion in the Galaxy; e.g., van den Heuvel et al. 2000; Gvaramadze et al. 2011). This method was adopted to compute the peculiar tangential velocities in this paper. More precise and accurate results might be obtained if it were possible to establish the birthplace of the studied system, such as the parent star cluster or association. In this case, the birthplace can be used to anchor a local standard of rest of the system, and the peculiar velocity of the system can then be obtained by subtracting the proper motion of the birthplace from the proper motion of the system (Ankay et al. 2001; Drew et al. 2018; Lennon et al. 2018; Kalari et al. 2019). This normally results in more precise and accurate results than the previous method, as it is not dependent on us knowing the Galactic rotation curve, the distance to the Galactic center, and the peculiar movement of the Sun, and thus is not affected by the uncertainties in these parameters. However, the census of Galactic open clusters and associations beyond 1–2 kpc is incomplete, particularly because of high interstellar extinction in the Galactic plane where the majority of these objects are located. This is also evident considering the high number of newly discovered star clusters using the GDR2 data (e.g., Castro-Ginard et al. 2018; Cantat-Gaudin et al. 2018; Liu & Pang 2019). Because most of the sample BeXRBs lie at much larger distances, using this method was not practical for the vast majority of sources and therefore was not used. Another possible method to obtain an estimate of the peculiar velocity is to estimate the local standard of rest by averaging the proper motions of the stars that are close in projection on the sky to the studied source and approximately at the same distance as the studied source (Kochanek et al. 2019). Similarly, the resulting peculiar velocity estimate can then be obtained by subtracting this mean local proper motion from the proper motion of the studied source.

An alternative way for studying the kinematical properties of the BeXRB sample is indirectly, by studying the locations of BeXRBs and the sites of recent massive star formation, such as the young open clusters and associations. On the premise that the closest young cluster or association to the particular BeXRB system is its birthplace, the separation between the two can then serve as a proxy for the peculiar velocity. This method was used to study the kinematics of BeXRBs in the SMC (Coe 2005), but it is ill-suited for the Milky Way systems because the cluster and association catalogs are incomplete, as mentioned above.

2.1. Peculiar velocities using the Bailer-Jones scale length

Going from the noisy parallax and proper motion measurements to distances and velocities is non-trivial. The most notable problems are the nonlinearity of the transformation and the positivity constraint of the distance. The parallax measurements often exhibit high relative uncertainties and can even be negative, which is often the case when distant objects such as BeXRBs are considered. The naive methods fail and give unphysical results when these measurements are used. However, these measurements are perfectly valid and still hold informational value, therefore it would be a mistake to discard them. The only viable way to handle these measurements is to use a probabilistic analysis (see Luri et al. 2018 and Bailer-Jones et al. 2018 for a more detailed discussion).

Here we used the parallaxes and proper motions from GDR2 (Gaia Collaboration 2018; Lindegren et al. 2018) to compute the tangential peculiar velocities. We followed the approach outlined in Luri et al. (2018), using the workflow from Bailer-Jones (2017). The distances and tangential velocities were jointly estimated from the parallaxes and proper motions by Bayesian inference, with the prior scale lengths for each object adopted from Bailer-Jones et al. (2018). To obtain the peculiar tangential velocities, we adopted the solar Galactocentric distance $R_0 = 8.2\,\mathrm{kpc}$, the circular Galactic rotation velocity $\Theta_0 = 238\,\mathrm{km\,s^{-1}}$, and the solar peculiar motion $(U_\odot, V_\odot, W_\odot) = (10.0, 11.0, 7.0)\,\mathrm{km\,s^{-1}}$ from Bland-Hawthorn & Gerhard (2016).

2.2. Peculiar velocities using an empirically determined scale length

BeXRBs are predominantly discovered in X-rays, which means that it is possible to detect them at significant distances and/or obscured by several tens of magnitudes of extinction. They are then subject to deep follow-up observations to determine and characterize the stellar counterpart. This may result in their selection function being different from the other field stars. However, we do not expect this to affect our results as significantly as in Gandhi et al. (2019), who studied low-mass X-ray binaries hosting black holes. BeXRBs have significantly shorter lifetimes, therefore it is not possible for them to escape far from their parent populations near the Galactic plane, even at runaway speeds. Considering a runaway velocity of $30\,\mathrm{km\,s^{-1}} \sim 30\,\mathrm{pc\,Myr^{-1}}$ (informed by the measured tangential peculiar velocities of BeXRBs by van den Heuvel et al. 2000 and theoretical peculiar velocity predictions from Eldridge et al. 2011 and Renzo et al. 2019) and a BeXRB lifetime after the supernova of 10 Myr, we obtain a migration distance estimate of 300 pc. There is also evidence that BeXRB progenitors tend to remain bound within their parent cluster or associations and only acquire high peculiar velocities later on after the supernova explosion of one of its components (Bodaghee et al. 2012). This further limits the possible displacement from the Galactic-plane massive star population. On the other hand, Treuz et al. (2018) found that there might be problems with the distances determined using the scale lengths from Bailer-Jones et al. (2018), where these distances appear to be an underestimation when compared to the distance values obtained using the conventional methods for sources closer than ~5 kpc. For sources that lie farther away than this, the trend seems to be reversed.

To investigate this, we determined a new scale length for the selected BeXRBs using the distance measurements collected from the literature. These measurements come from a number of sources and thus were collected using various methods, sometimes applied in conjunction. For some sources, more distance estimates exist, in which case we then preferred to use the estimates from the most recent works. These estimates, together with their errors (if available), are listed in Table 1.

These distances were then fit with the exponentially decreasing space density prior probability model,

$$P(d) = \frac{1}{2L^3} d^2 \mathrm{e}^{-d/L} \qquad \text{if} \quad d > 0, \tag{1}$$

where d is the distance to the source and L is the scale length, as discussed in Bailer-Jones (2015).

Similarly to Gandhi et al. (2019), an unbinned maximum likelihood algorithm was used for the fit. To quantify the uncertainty of L, we generated randomized ensembles of d_{lit} values by resampling from a suitable distribution for each object. In most cases, for the objects with a published distance estimate d_{lit} and its uncertainty, a normal distribution was used for resampling,

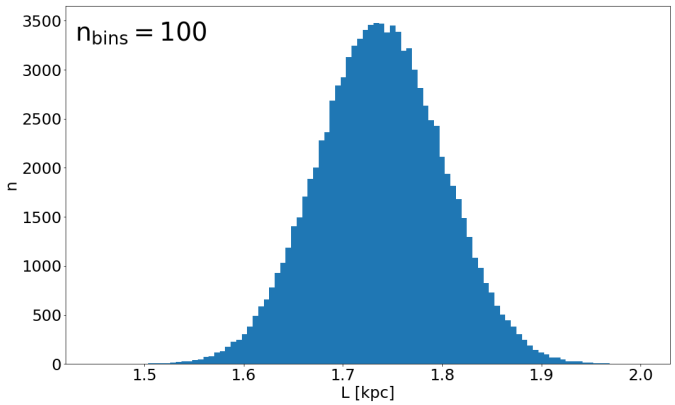

Fig. 1. Histogram of the scale lengths L resulting from the resampling.

with the assumed mean and standard deviation corresponding to $d_{\rm lit}$ and its uncertainty, respectively. For four sources with distance limits, random values were drawn from a uniform distribution characterized by the lower and upper distance limit (GS 0834-430, IGR J22534+6243, AX J1700.2-4220, and 2RXP J130159.6-635806). In the case of XTE J1906+090, where only the lower limit on $d_{\rm lit}$ is known, we also drew from a uniform distribution, where we assumed the upper limit to be $d_{\rm lit} + 5$ kpc. One object in our sample, 3U 1022-55, has no uncertainty on $d_{\rm lit}$. In this case, we assumed the uncertainty to be 20 % of the published $d_{\rm lit}$. We then resampled from a normal distribution as above.

A total of 100 000 ensembles were randomized, resulting in a mean value of the characteristic scale length of $L = 1.74 \pm 0.06$ kpc (this is somewhat higher than the scale height of the thick disk of 0.7–1.2 kpc; Siegel et al. 2002), with the uncertainty quoted here being the standard deviation of the randomized ensambles. The scale length distribution is plotted in Fig. 1. We then adopted this scale length for all the objects in our sample and followed the same procedure as outlined in Sect. 2.1.

2.3. Quality of GDR2 data and astrometric fits

While GDR2 provides astrometric measurements of unprecedented quality and quantity, which allows insight into the kinematics of many BeXRBs for the first time, it still contains some sources for which the solutions are ill-behaved. The astrometric parameters of these sources should be considered suspect and be flagged or filtered out from the analysis. Problems with the astrometry may arise for sources that are located in regions with high source densities, for instance, in the Galactic plane. Another potential caveat is that all GDR2 sources are treated as single stars in the astrometric solution, where binaries do not receive any special treatment (Gaia Collaboration 2018; Lindegren et al. 2018). Owing to the binary and early-type nature of BeXRBs, they might be affected by this problem. It is therefore necessary to examine the quality of the astrometric parameters of the BeXRB sample.

Unreliable astrometric solutions can be empirically identified by considering the distributions of the parallax and proper motion errors at the relevant magnitudes and colors and comparing them to the errors for the objects of interest, or by using the recommended astrometric quality indicators that are included or can be computed from the parameters that are part of GDR2. Informed by Gaia Collaboration (2018), Lindegren et al. (2018), and Lindegren (2018), we retained the systems that satisfied

- `duplicated_source = False`
- `astrometric_excess_noise` < 1 mas or `astrometric_excess_noise_sig` < 2
- `ruwe` < 1.4 or `u` $< 1.2 \times \max(1, \exp(-0.2(G - 19.5)))$.

The flag `duplicated_source=True` indicates observational, cross-matching, or processing problems, or stellar multiplicity, probably leading to problems in the astrometric solution. The `astrometric_excess_noise` (ϵ_i) is an angular measure of the astrometric goodness of fit, indicating the additional scatter that may arise from the movement of the emission centroid that in turn is due to the motion of the components inside a binary. Last, the cuts based on `ruwe` and `u`, which stand for renormalized unit weight error and unit weight error, respectively, ensured the removal of ill-behaved astrometric solutions. The `ruwe` is obtained by dividing `u` by a normalization factor that is a function of the source magnitude and color and is included in the GDR2 archive. The `u` values are obtained through

$$u = \sqrt{\chi^2/(N-5)}, \tag{2}$$

where χ^2 is `astrometric_chi2_al` and N is `astrometric_n_good_obs_al`, which can both be queried in the GDR2 archive. Cuts based on `u` were applied to the objects with no color information in GDR2, for which the `ruwe` values were not available.

The relevant quantities and quality flags for the objects in the Galactic BeXRB sample are listed in Table 2. Based on these quality cuts, we discarded five objects from the subsequent analysis. Table 2 shows that the unmodeled orbital motion due to the binary nature of the BeXRBs does not seem to affect the astrometric solutions for the majority of sources in a significant way. The longest $P_{\rm orb}$ in the sources is about 262 d for SAX J2239.3+6116 (in't Zand et al. 2000), which has an astrometric solution well below all considered cut limits. This $P_{\rm orb}$ is still considerably shorter than the 22-month observing time of GDR2. For periods such as this and shorter, any orbital motion will therefore largely average out (Jennings et al. 2018).

The five discarded sources (4U 0728-25, GX 304-1, GS 1843+00, XTE J1906+090, and IGR J19294+1816) are not outstanding in the BeXRB sample in $P_{\rm orb}$, distance, or optical brightness. The last three sources, which were discarded due to the increased ϵ_i, lie relatively close to each other in the same region of the sky. They also have lower values of `visibility_periods_used`, ranging from 10 to 13, while the mean value for the studied BeXRB sample is 15. We opted to list the computed velocities of these sources in the subsequent tables, but we did not consider them in the statistical analysis as their velocities cannot be considered reliable.

2.4. Kinematics of Galactic BeXRBs

We obtained the peculiar velocities for 33 Galactic BeXRBs showing pulsations (see Table 3). In addition to the five sources we discarded because the astrometry was unreliable, we also decided to remove 1H 1249-637 because of its uncertain nature as a γ Cas analog (these are systems that most likely do not host a neutron star, where the X-ray emission is generated by interactions between magnetic fields on the Be star and its decretion disk; e.g., Smith et al. 2016), yielding a final sample of 27 sources. However, this did not affect the results of the following analysis in any significant way. We split the sample according to the dip in $P_{\rm s}$ adopted from KCP, which is $P_{\rm s,split} = 40$ s. The short-spin subpopulation comprises 7 sources, and the long-spin subpopulation is more numerous, with 20 sources. The

Table 2. Relevant GDR2 parameters and flags pertaining to the quality of the astrometric solution.

System	Parallax (mas)	parallax_error (mas)	Gmag (mag)	ϵ_i (mas)	ϵ_i sig	u	ruwe	duplicated_source
4U 0115+63	0.091	0.027	14.44	0.13	3.51	1.20	1.00	False
V 0332+53	0.14	0.04	14.22	0.20	8.28	1.40	1.01	False
GS 0834-430	−0.16	0.15	20.52	0.75	5.96	1.34	0.96	False
IGR J19294+1816	−0.38	1.06	20.39	4.47	5.55	1.36	1.23	False
XTE J1946+274	−0.072	0.044	15.71	0.25	6.88	1.27	0.96	False
4U 1416-62	0.0046	0.1352	17.77	0.33	2.13	1.10	–	False
KS 1947+300	0.0056	0.0189	13.84	0	0	0.78	0.96	False
GS 1843+00	0.41	0.35	18.68	1.06	4.0	1.26	–	False
RX J0812.4-3114	0.10	0.02	12.48	0	0	1.27	1.02	False
EXO 2030+375	0.15	0.11	16.91	0.64	13.43	1.70	1.05	False
IGR J22534+6243	0.053	0.037	14.60	0.23	8.53	1.35	1.03	False
AX J1700.2-4220	0.62	0.06	8.68	0	0	1.08	0.87	False
Cep X-4	0.051	0.020	13.82	0	0	0.92	1.08	False
XTE J1906+090	0.066	0.726	19.73	2.85	9.35	1.38	–	False
GRO J1008-57	0.24	0.03	13.90	0.25	13.41	1.54	1.02	False
3A 0535+262	0.44	0.05	8.68	0	0	1.34	1.05	False
4U 0728-25	0.028	0.039	11.62	0	0	1.23	0.94	True
2E 0655.8-0708	0.15	0.04	12.03	0	0	1.19	1.10	False
IGR J11435-6109	0.03	0.04	15.67	0.10	0.90	1.07	0.99	False
GRO J2058+42	0.077	0.018	14.19	0	0	0.99	1.06	False
RX J0440.9+4431	0.27	0.05	10.43	0	0	1.00	0.80	False
GX 304-1	0.47	0.03	12.65	0	0	1.69	0.99	True
4U 1145-619	0.42	0.04	8.63	0	0	1.33	0.88	False
SAX J2103.5+4545	0.12	0.02	13.0	0	0	0.90	1.08	False
1A 1118-615	0.31	0.03	11.60	0	0	1.19	0.94	False
IGR J01583+6713	0.098	0.018	13.70	0	0	0.95	0.97	False
2RXP J130159.6-635806	0.063	0.108	17.34	0.52	6.66	1.28	0.95	False
4U 0352+309	1.23	0.06	6.25	0.16	16.39	2.29	1.32	False
3U 1022-55	0.16	0.03	11.25	0	0	1.55	1.06	False
SAX J2239.3+6116	0.084	0.019	14.15	0.08	1.17	1.18	1.11	False
RX J0146.9+6121	0.37	0.03	11.21	0	0	1.70	1.21	False
4U 2206+543	0.27	0.03	9.74	0	0	1.44	0.90	False
1H 1249-637	2.38	0.13	5.12	0.62	148.90	4.82	0.99	False

distribution of the tangential peculiar velocities, derived using the scale lengths from Bailer-Jones et al. (2018; $v_{\rm pec,BJ}$) and the empirically determined scale length from Sect. 2.2 ($v_{\rm pec,iso}$), with respect to $P_{\rm s}$ is shown in Fig. 2.

Although only a few BeXRBs fall into the short-spin subpopulation, it is apparent that this subpopulation seems on average to be moving with a higher peculiar velocity than the long-spin subpopulation. Using the means of the tangential peculiar velocity posteriors of the individual BeXRBs, we can estimate the characteristics of the two BeXRB subpopulations. The short-spin subpopulation possesses a mean tangential peculiar velocity of approximately $29 \pm 11\,\mathrm{km\,s^{-1}}$, which for the long-spin subpopulation is about $16 \pm 8\mathrm{km\,s^{-1}}$. The reported errors are the standard deviations of the velocity mean distributions. The results obtained using the empirically determined scale length derived in Sect. 2.2 are similar, but individual velocity measurements exhibit higher uncertainties. In this case, we obtained $28 \pm 11\,\mathrm{km\,s^{-1}}$ and $16 \pm 8\,\mathrm{km\,s^{-1}}$ for the short- and long-spin subpopulation, respectively.

To test the significance of this difference between the populations, we conducted a two-sample Anderson-Darling test (e.g., Scholz & Stephens 1987). The result is that the two populations are indeed distinct. We also used bootstrap testing to estimate the velocity difference between the populations and quantified the effect size through Cohen's d (Cohen 1988), which is the difference in subpopulation means $\bar{X}_1$ and $\bar{X}_2$, standardized by dividing by the standard deviation:

$$d_C = \frac{\bar{X}_1 - \bar{X}_2}{S}, \tag{3}$$

where S is the pooled standard deviation:

$$S = \sqrt{\frac{(n_1 - 1)s_1^2 + (n_2 - 1)s_2^2}{n_1 + n_2 - 2}}, \tag{4}$$

where n_i and s_i are the size and standard deviation of the subpopulation i, respectively. The results of this testing are summarized in Table 4.

Here and throughout this paper, the quoted p-values have the usual statistical meaning: they represent the probability of obtaining a test statistic at least as extreme as the observed one when the null hypothesis is correct. In the case of the peculiar velocities of Galactic BeXRBs, the null hypothesis is that the data are drawn from the same underlying distribution. We adhered to the classical threshold of $p < 0.05$ for a significant result.

Table 3. Derived tangential peculiar velocities and orbital eccentricity values compiled from the literature.

Name	$v_{\rm pec,BJ}$ (km s^{-1})	$v_{\rm pec,iso}$ (km s^{-1})	e	e ref
4U 0115+63	22^{+6}_{-3}	23^{+8}_{-4}	0.342 ± 0.004	Raichur & Paul (2010)
V 0332+53	15^{+3}_{-2}	16^{+3}_{-2}	0.417 ± 0.007	Raichur & Paul (2010)
GS 0834-430	50^{+9}_{-11}	48^{+11}_{-15}	0.14 ± 0.04	Wilson et al. (1997)
IGR J19294+1816	73^{+81}_{-45}	99^{+93}_{-60}		
XTE J1946+274	26^{+17}_{-14}	26^{+16}_{-14}	0.33 ± 0.05	Wilson et al. (2003)
4U 1416-62	39^{+13}_{-8}	41^{+16}_{-9}	0.417 ± 0.003	Raichur & Paul (2010)
KS 1947+300	27^{+39}_{-18}	24^{+36}_{-16}	0.033 ± 0.013	Galloway et al. (2004)
GS 1843+00	17^{+16}_{-9}	23^{+65}_{-13}		
RX J0812.4-3114	22^{+5}_{-8}	20^{+6}_{-9}		
EXO 2030+375	9^{+8}_{-4}	16^{+22}_{-9}	0.412 ± 0.001	Wilson et al. (2008)
IGR J22534+6243	12^{+6}_{-5}	12^{+8}_{-6}		
AX J1700.2-4220	17^{+1}_{-1}	17^{+2}_{-1}		
Cep X-4	42^{+26}_{-16}	45^{+28}_{-17}		
XTE J1906+090	51^{+79}_{-36}	86^{+98}_{-60}	$0.03 < e < 0.06$	Wilson et al. (2002)
GRO J1008-57	16^{+1}_{-2}	16^{+1}_{-2}	0.68 ± 0.02	Coe et al. (2007)
3A 0535+262	20^{+4}_{-3}	21^{+4}_{-3}	0.47 ± 0.02	Finger et al. (1994)
4U 0728-25	13^{+10}_{-8}	13^{+10}_{-8}		
2E 0655.8-0708	$5.9^{+4.7}_{-2.3}$	$6.5^{+6.6}_{-2.7}$	$e \sim 0.4$	Yan et al. (2012)
IGR J11435-6109	17^{+14}_{-5}	18^{+23}_{-5}		
GRO J2058+42	23^{+5}_{-6}	20^{+6}_{-5}		
RX J0440.9+4431	12^{+5}_{-4}	12^{+6}_{-4}	$e > 0.4$	Yan et al. (2016)
GX 304-1	23^{+1}_{-1}	23^{+1}_{-1}	$e \sim 0.5$	Sugizaki et al. (2015)
4U 1145-619	$9.6^{+0.6}_{-0.6}$	$9.6^{+0.6}_{-0.6}$	$e \sim 0.8$	Watson et al. (1981)
SAX J2103.5+4545	24^{+4}_{-2}	25^{+5}_{-2}	0.406 ± 0.004	Baykal et al. (2007)
1A 1118-615	22^{+1}_{-1}	22^{+1}_{-1}	$0 < e < 0.16$	Staubert et al. (2011)
IGR J01583+6713	$4.8^{+1.9}_{-2.1}$	$4.7^{+2.0}_{-2.1}$		
2RXP J130159.6-635806	17^{+6}_{-6}	17^{+6}_{-6}		
4U 0352+309	$10.6^{+0.4}_{-0.4}$	$10.6^{+0.4}_{-0.4}$	0.111 ± 0.018	Delgado-Martí et al. (2001)
3U 1022-55	12^{+10}_{-5}	14^{+12}_{-6}		
SAX J2239.3+6116	15^{+3}_{-2}	15^{+3}_{-2}		
RX J0146.9+6121	$9.6^{+0.9}_{-0.8}$	$9.7^{+0.9}_{-0.8}$		
4U 2206+543	18^{+3}_{-2}	19^{+3}_{-2}	$e \sim 0.15$	Ribó et al. (2006)
1H 1249-637	$2.2^{+1.0}_{-0.8}$	$2.1^{+1.0}_{-0.8}$		

Notes. $v_{\rm pec,BJ}$ denotes the velocities obtained using the priors adopted from Bailer-Jones et al. (2018), and $v_{\rm pec,iso}$ are the velocities obtained using the empirically determined scale length derived in Sect. 2.2.

The divide of $P_{\rm s,split}$ = 40 s adopted here to split the two subpopulations was estimated from the histogram of log $P_{\rm s}$ values of the BeXRB pulsar sample studied by KCP. The dip in the log $P_{\rm s}$ histogram in Fig. 1. of KCP is rather wide, ranging from approximately $P_{\rm s}$ = 20–80 s. To test the robustness of the above results, we repeated the above analysis for the $P_{\rm s,split}$ of 20, 60, and 80 s using the $v_{\rm pec,BJ}$ velocities. The recomputed p-values from the Anderson-Darling test, credibility intervals of the velocity differences between the subpopulations, and Cohen's d for each $P_{\rm s,split}$ are listed in Table 5. While for $P_{\rm s,split}$ = 20 s and 80 s the velocity difference is still significant, at $P_{\rm s,split}$ = 60 s the significance disappeared.

We also tested an alternative approach of estimating the peculiar velocities by determining the local standard of rest through the proper motions of stars near the estimated distance of the studied system. For each BeXRB in the sample, we queried GDR2 for stars within 30 arcmin radius whose parallax was within 1 σ of the system parallax. This ensured that we obtained $\gtrsim$1000 stars in the vicinity of each BeXRB that satisfied the parallax criterion. Using the GDR2 proper motions of these stars, we established a local standard of rest by computing the mean and dispersion of these values. Normally, these "field" proper motion values would be subtracted from the proper motion of the binary, and with a distance estimate, this would be used to compute a peculiar velocity estimate, such as in Kochanek et al. (2019). However, upon inspection of the field parameters, we found that in general, the dispersions of the proper motion obtained from the stars near the studied systems

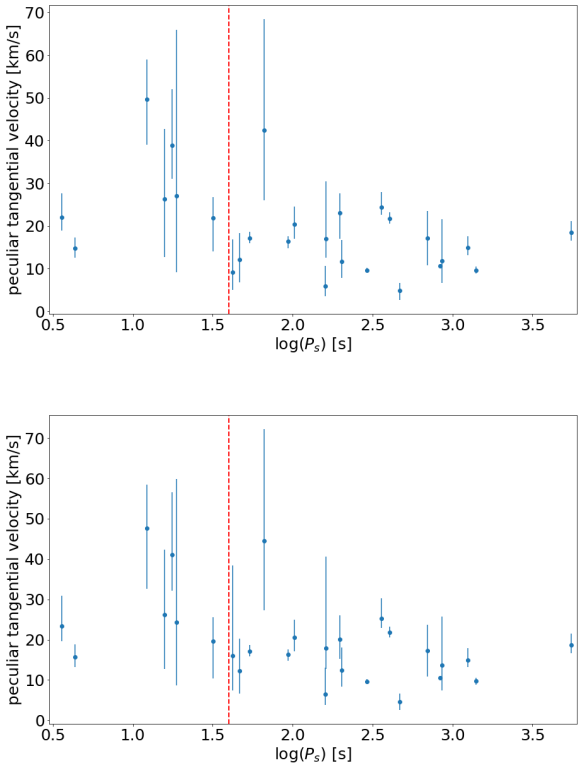

Fig. 2. Peculiar tangential velocities of Galactic BeXRBs with respect to P_s. The red vertical line delineates the approximate divide ($P_{s,split}$ = 40 s) between the two BeXRB subpopulations according to KCP. *Top*: tangential peculiar velocities computed using the scale lengths from Bailer-Jones et al. (2018). *Bottom*: same as above, but with the scale length L resulting from the resampling we used.

Table 4. Summary of the statistical properties of the Galactic BeXRB sample.

	Short P_s pop.	Long P_s pop.
Mean $v_{pec,BJ}$ (km s^{-1})	29 ± 11	16 ± 8
Mean $v_{pec,iso}$ (km s^{-1})	28 ± 11	16 ± 8
p	0.004	
p_{iso}	0.007	
Pop. $v_{pec,BJ}$ difference	(4.4, 22.0)	
Pop. $v_{pec,iso}$ difference	(3.5, 20.9)	
d_C	1.43	
$d_{C,iso}$	1.32	

Notes. p indicates the significance of the subpopulation split as obtained from the Anderson-Darling test, pop. v_{pec} difference is the difference between the short-spin and long-spin subpopulation velocity means obtained from bootstrapping, and d_C is the value of Cohen's d, indicating the effect size. The difference between the subpopulation velocity means, pop. v_{pec}, is characterized using a 95% credibility interval as resulting from the bootstrap testing.

are too high for any velocity estimates to be meaningful. This was verified when we estimated the peculiar velocity of each BeXRB by drawing 40 000 random samples from the proper motion of its surrounding field, the BeXRB distance distribution, and the BeXRB proper motion distribution (which was assumed to be the normal distribution centered on the GDR2 proper motion value, with the standard deviation being the proper motion error) while also taking the correlations between the proper motions in RA and Dec into account. This yielded peculiar velocity estimates that also supported the hypothesis that there are two kinematic subpopulations of BeXRBs, separated by P_s = 40 s threshold ($p \sim 0.01$). However, large errors on the parameters of the field population caused these velocities to be overestimated and to be affected by much larger errors than the velocities obtained using the previous method. As a result, these peculiar velocity estimates were discarded and were not considered in the analysis.

Table 5. Statistical properties of the Galactic BeXRB sample for varying values of $P_{s,split}$.

$P_{s,split}$ (s)	20	60	80
n short P_s	6	10	11
n long P_s	21	17	16
p	0.006	0.12	0.019
pop. $v_{pec,BJ}$ difference	(4.2, 23.7)	(−0.6, 16.2)	(3.2 , 18.9)
d_C	1.54	0.75	1.18

3. Small Magellanic Cloud Be/X-ray binary population

The SMC contains an unexpectedly high number of BeXRBs. Interestingly, all SMC high-mass X-ray binaries, with the exception of SMC X-1, are BeXRB systems. Therefore and because of its relative proximity, the SMC provides a unique laboratory for studying BeXRBs in a homogeneous and consistent manner (Coe & Kirk 2015; Haberl & Sturm 2016).

Still, the SMC distance poses problems for the current astrometric missions. Because of this and its nature as an irregular galaxy, it is not possible to investigate the peculiar velocities of a sufficient number of BeXRBs directly. Using GDR2, Oey et al. (2018) studied the kinematics of early-type SMC runaways, including 14 BeXRBs. However, the P_s for only seven of them is listed in the HMXB catalog of Haberl & Sturm (2016). It is interesting to note that the mean peculiar tangential velocity of these BeXRBs is $v_{tan,pec} \sim 30$ km s^{-1}, which is higher than the observed mean peculiar tangential velocity of Galactic BeXRB ($v_{tan,pec} = 15 \pm 6$ km s^{-1}; van den Heuvel et al. 2000). The same result is obtained regardless of the method that is used, and it remains the same whether all BeXRBs are considered or only the X-ray pulsars. A possible reason for this higher velocity may be that the metalicity of the SMC is lower than that of the Milky Way (Renzo et al. 2019). Unfortunately, only one BeXRB with $P_s < 40$ s is included in their analysis. While this system has the lowest peculiar residual velocity of all the sources they studied (not just the BeXRBs), its peculiar velocity as determined locally (using the kinematics of the nearby OB stars) is substantial. Nevertheless, using only one system to characterize a subpopulation is not meaningful.

Therefore, the velocities of a large sample of SMC BeXRBs need to be studied indirectly. In this section we investigate the mutual positions of BeXRBs in the SMC and nearby young star clusters where they might have formed and are now running away after acquiring a high peculiar velocity after the supernova explosion within the progenitor binary. This approach was adopted by Coe (2005), who computed a mean peculiar peculiar velocity arising from the supernova explosion for the BeXRBs in the SMC. Using 17 BeXRB pulsars, their value $v_{tan,pec} \sim 16$ km s^{-1} is in line with the mean tangential peculiar velocity

of Galactic BeXRBs (van den Heuvel et al. 2000). Interestingly, the mean age of the clusters associated with the BeXRB pulsars in Coe (2005) is rather high, 130 ± 140 Myr ($\log(t/\mathrm{yr}) \sim 8.1$). While no firm conclusions can be drawn from a value with such an uncertainty, at face value, this seems much higher than the main-sequence lifetime of a B0 V star (the system secondary), even when we consider that the star would be rejuvenated (i.e., its evolutionary clock will be reset) by the mass transfer within the binary, which would still only yield a maximum lifetime of ~40 Myr. A possible explanation would be that the cluster ages are only poorly determined, which is common when young star clusters are considered (e.g., Netopil et al. 2015). This would also account for the high uncertainty of the mean cluster age derived in Coe (2005). Another possibility is that the component masses of the SMC BeXRB progenitors may initially be as low as 7–8 $M_\odot$. It is possible for stars in this mass range to explode as ECSNe, especially if they have lower metallicities, as is the case for the stars in the SMC (Podsiadlowski et al. 2004) During the binary progenitor evolution, the initially more massive star can transfer a substantial amount of mass to the secondary through Roche-lobe overflow, increasing its mass by several $M_\odot$. Its subsequent evolution will be very similar to the evolution of an isolated star with higher mass (e.g., Podsiadlowski et al. 1992; Pfahl et al. 2002). This would then account for the fact that the spectral distribution of SMC BeXRBs is consistent with that of the Milky Way (Reig 2011).

3.1. Clusters from Rafelski & Zaritsky

Recently, there has been a sharp increase in the number of SMC BeXRBs (Coe & Kirk 2015; Haberl & Sturm 2016). Therefore, it is worthwhile to repeat the analysis done by Coe (2005) on a larger sample size and also look for possible BeXRB subpopulations. We used the catalog of high-mass X-ray binaries in the SMC by Haberl & Sturm (2016), listing 147 BeXRBs, where we selected all pulsating BeXRBs with precisely determined positions for the further analysis. This selection resulted in a list of 56 sources. Similarly to Coe (2005), the SMC clusters comes from the list of Rafelski & Zaritsky (2005; hereafter RZ clusters).

We compared the projected positions of BeXRBs and the RZ clusters. The position of every BeXRB was compared to all RZ clusters and the distance to the closest cluster was obtained. After this, we removed all BeXRBs that lay in the regions that are not covered by the RZ clusters catalog (objects with distances to the closest cluster >25 arcmin). After this cut, we retained 53 BeXRBs for the analysis.

We caution that this method, while being simple, has significant drawbacks. First, it is in general not possible to establish whether the matched BeXRB/cluster pairs are really equidistant, that is to say, to determine the radial distance offset between them. It is also difficult to determine whether the matched cluster is really the birthplace of the BeXRB, especially when two or more clusters have similar separations from the particular BeXRB. Therefore, automatically picking the closest cluster may not necessarily be correct. Filtering out the old clusters that cannot be the birthplaces of the currently observed BeXRBs alleviates the problem somewhat, but it is apparent that the results obtained using this method need to be interpreted with caution. More precise proper motions from the future *Gaia* data releases may allow us to confirm the relative system-cluster positions with the peculiar velocities, which would help eliminate some spurious pairings.

Figure 3 shows the distances of the studied BeXRBs from the nearest RZ star cluster. The dashed line indicates the approximate boundary between the two subpopulations, where KCP observed a dip in the spin distribution. The subpopulations appear to be marginally kinematically distinct: the short-spin subpopulation have on average larger distances from the star clusters than the long-spin subpopulation. The mean distance from the nearest cluster of the short-spin subpopulation is approximately 6.6 ± 4.0 arcmin, while for the long-spin subpopulation, it is 4.4 ± 2.3 arcmin. The reported error values are the standard deviations of the distance distributions. The effect size is significant; the Cohen d is 0.75 between the two subpopulations.

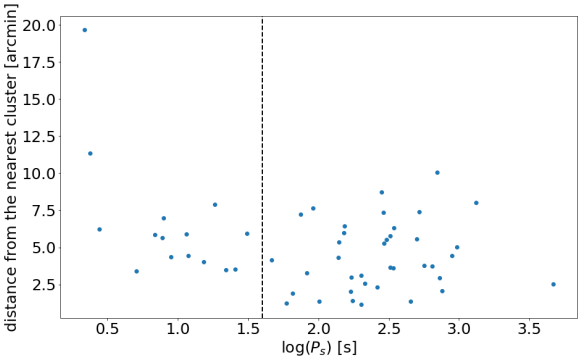

Fig. 3. Distances of the SMC BeXRBs from the nearest cluster in the RZ catalog. The conservative estimate of the distance error is 0.7 arcmin, corresponding to twice the median SMC cluster radius listed in the catalog by Glatt et al. (2010). Error bars are omitted for clarity.

To test the significance of this split in the subpopulations, we conducted a two-sample Anderson-Darling test. The test confirmed that the populations are significantly distinct ($p = 0.039$). The bootstrap testing yielded comparable results: the populations are distinct at a credibility better than 95% (but lower than 99%).

The values we obtained above are sensitive to the inclusion of the two BeXRBs with the shortest P_s, which also exhibit the highest separation from the closest cluster. Excluding them would affect the significance of the subpopulation split, lowering it to $p \approx 0.1$. We also used the same cluster catalog as Coe (2005), but it can be expected that the results might change if a different cluster catalog were used. Netopil et al. (2015) studied the inferred parameters of Galactic open clusters in different catalogs and found significant dispersion in the ages of open clusters, with the mean standard deviation of approximately 0.5 dex. Even though the open clusters in the SMC are easier to study in some aspects (the distance to the SMC is known, and the reddening is less variable) than the Galactic open clusters, it is likely that there are significant differences between the SMC cluster catalogs. These differences between the star cluster catalogs that are used are likely to have a significant effect on the results of this analysis. We therefore determined the reliability of this result using the more recent SMC star clusters catalogs.

3.2. Clusters from Nayak et al. (2018)

Nayak et al. (2018) estimated the parameters, including ages, of 174 SMC star clusters. They also collected the parameters of star clusters that were not included in their studied sample, producing a combined catalog of 468 clusters in total, which they used to study the spatio-temporal cluster distribution. We used this catalog to repeat the workflow outlined in the previous section. Because the catalog contains reliable cluster ages, it is possible to study the statistics of clusters/BeXRBs distributions after the age cuts are applied to exclude clusters of a particular age.

To determine the cluster age range in which it is worthwhile to study BeXRB/cluster pairings, we need to estimate the maximum age of the cluster that can be associated with a currently observed BeXRB. This age corresponds to the maximum age of the BeXRB secondary, where it is possible to make a conservative estimate. A star with a mass of 6 $M_{\odot}$, which is considered to be a low-mass limit for supernovae if the star is in a binary (Podsiadlowski et al. 2004), has a main-sequence lifetime of ∼110 Myr. If it accretes mass from the primary near the end of its lifetime, it rejuvenates, meaning that it will subsequently evolve like a more massive star, but its evolutionary clock will be reset. As discussed above, we also need to consider the potential uncertainty in estimated cluster ages of approximately 0.5 dex. Thus, in order to include as many viable clusters as possible, it is necessary to include clusters as old as $\log(t/\mathrm{yr}) = 8.6$. Clusters older than this age cut contaminate the analysis.

We therefore studied cluster age ranges from $\log(t/\mathrm{yr}) = 8$ to 9 because the number of clusters younger than this is lower than or comparable to the number of the studied BeXRBs and the clusters older than $\log(t/\mathrm{yr}) > 8.6$ are too evolved for a BeXRBs to be associated with them, even after possible age uncertainties are considered. However, in order to investigate the effect of the contamination by the older clusters, the considered age range was expanded somewhat. We conducted a series of statistical tests in which we applied an age cut every time, starting from $\log(t/\mathrm{yr}) = 8$ in 0.1 dex increments and omitted clusters with ages older than this value. As in the previous section, for each BeXRB we searched for the closest cluster within 25 arcmin, collected the distances between them, and compared the BeXRB–closest cluster distance distributions between the spin subpopulations using the $P_{\mathrm{s,split}} = 40$ s as listed in KCP. The number of retained clusters for the analysis, the significance of the difference between the two BeXRB populations resulting from the two-sample Anderson-Darling test, and the effect size estimated using Cohen's d are shown in Fig. 4.

3.3. Clusters from Piatti

Piatti (2018) also compiled a large catalog of SMC star clusters, 411 in total, that includes cluster ages. We repeated the same analysis using this catalog. The results are also included in Fig. 4 to facilitate comparison with the clusters from Nayak et al. (2018).

The catalogs of Nayak et al. (2018) and Piatti (2018) are not completely independent. This is shown in Fig. 4, where they follow similar trends, which is most clearly visible around $\log(t/\mathrm{yr}) = 8.3$, where the statistics for both catalogs degrade strongly. For both catalogs, the subpopulations appear to be the most distinct overall when only clusters younger than $\log(t/\mathrm{yr}) = 8.2$–8.6 are considered, which is reasonable considering the BeXRB lifetimes and likely errors associated with the cluster ages. When older star clusters are included, the statistics degrade, as is expected when clusters are introduced that are unlikely birthplaces of BeXRBs; they contaminate the sample.

The evidence for the BeXRB subpopulation difference is stronger in Piatti (2018) catalog, where the p-value is near the 0.05 level throughout $\log(t/\mathrm{yr}) = 8.2$–8.6, and below it at $\log(t/\mathrm{yr}) = 8.2$, and 8.4 to 8.5. The subpopulation split is less clear using the sample from Nayak et al. (2018), but even then, for both of the catalogs and the entire age range considered, we always observed the trend that the short-spin subpopulation has higher separations at face value, even though the difference is not always statistically significant.

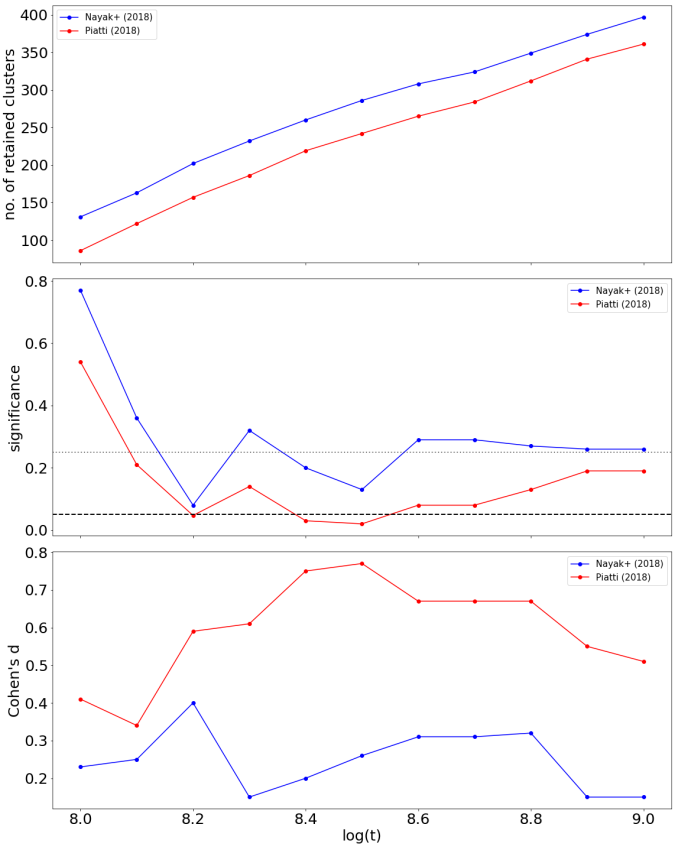

Fig. 4. *Top*: number of retained star clusters when clusters older than a particular age limit from the catalogs of Nayak et al. (2018) and Piatti (2018) are excluded. *Middle*: significance of the BeXRB–closest cluster distance bimodality as obtained from a two-sample Anderson-Darling test with respect to the applied age cutoff. The horizontal dashed line indicates the classical significance threshold of $p = 0.05$. The p-values that exceed 0.25 need to be considered as approximate because they are computed by extrapolation. This threshold is indicated by the horizontal dotted black line. *Bottom*: effect size of the bimodality quantified using Cohen's d as a function of the applied age cutoff.

4. Discussion

The hypothesis proposed by KCP predicts that the long-spin subpopulation of BeXRBs possesses higher peculiar velocities owing to a higher mass-loss and a stronger kick that is exhibited by a CCSN. On the other hand, if the spin bimodality is caused by different accretion modes, as proposed by Cheng et al. (2014), we are less likely to observe any difference in the kinematics of the BeXRB subpopulations. The observed trends, although marginal, challenge both hypotheses.

Overall, we found that the mean peculiar tangential velocity for the Galactic BeXRBs is $v_{\mathrm{tan,pec}} = 19 \pm 11\,\mathrm{km\,s^{-1}}$, which is consistent with but somewhat higher than the previous estimates of Chevalier & Ilovaisky (1998) and van den Heuvel et al. (2000). We observed that the short-spin subpopulation of the Galactic BeXRBs exhibits higher tangential peculiar velocities than the long-spin subpopulation. This also holds if the divide between the subpopulations $P_{\mathrm{s,split}}$ is shifted within 20–80 s, but we caution that if $P_{\mathrm{s,split}} = 60$ s is adopted, the difference between the populations is not statistically significant. Using the distances of SMC BeXRBs from the nearest star cluster, we observed marginal evidence of the same effect in the SMC, but the size and reliability of the effect depends on the star

cluster catalog that is used for the analysis. While some problems affect the method we used to investigate the kinematics of SMC BeXRBs, which makes the result less reliable, it appears possible to conclude that there is some evidence that the BeXRB subpopulations are kinematically distinct when we also consider the result we obtained for the Galactic BeXRBs,.

4.1. BeXRBs as runaway systems

We considered the origins of the peculiar velocity of a BeXRB. Two mechanisms induce this additional velocity in BeXRBs: the ejection of a high amount of mass by the supernova explosion, and the asymmetries in the explosion that cause the natal kick for the neutron star. The latter of the two is a consequence of the supernova explosion itself and is thought to be highly stochastic and impossible to describe by a simple analytical prescription. However, scaling relations exist that link the neutron star kick velocity to the mass of the neutrino-heated ejecta, explosion energy, and asymmetry, and the progenitor structure (Janka 2017; Bray & Eldridge 2016). The first of the two mechanisms is a consequence of a rapid mass loss from a binary. During the explosion, the primary loses a considerable amount of mass in a very short time, as compared to the orbital period of the binary. Even if the explosion is spherically symmetric with respect to the remnant neutron star, there is a strong asymmetry with respect to the center of mass of the system. This causes the system to recoil, and it can be described analytically (Zwicky 1957; Blaauw 1961; Cerda-Duran & Elias-Rosa 2018 and references therein).

In a symmetric supernova explosion, the post-supernova binary only remains bound if the system loses less than half of its mass, in other words, when the supernova ejecta $M_{\rm ej}$ comprises less than a half of the system's pre-supernova mass, $M_{ej} < (1/2)(M_1 + M_2)$, where M_1 and M_2 are the masses of the primary and secondary components, respectively (Blaauw 1961; Boersma 1961). When we consider the mass loss at the supernova to be instantaneous, the binary system gains a peculiar velocity, given by

$$v_{\rm sym} = \left(\frac{GM_2}{a_{\rm pre-SN}}\right)^{1/2}\left(\frac{M_2}{M_1+M_2}\right)^{1/2}\left(\frac{M_1-M_{\rm co}}{M_2+M_{\rm co}}\right), \tag{5}$$

where $M_{\rm co} = M_1 - M_{\rm ej}$ is the mass of the compact object (a neutron star in the studied BeXRBs), G is the gravitational constant, and $a_{\rm pre-SN}$ is the pre-supernova semimajor axis of the binary. The last term on the right-hand side of the equation,

$$\frac{M_1 - M_{\rm co}}{M_2 + M_{\rm co}} = e, \tag{6}$$

is the eccentricity of the remnant BeXRB (Iben & Tutukov 1997).

The acquired peculiar velocity (and eccentricity) can be higher when the supernova explosion was asymmetric and the compact object received a kick at birth. Depending on the orientation and magnitude of the kick, the acquired peculiar velocity is

$$v_{\rm asym} = \left(v_{\rm sym}^2 - 2v_{\rm sym}v_{\rm k}\cos\psi + v_{\rm k}^2\right)^{1/2}, \tag{7}$$

with

$$v_{\rm k} = \frac{M_{\rm co}w}{M_{\rm co}+M_2}, \tag{8}$$

where $v_{\rm sym}$ is given by Eq. (5), w is the kick velocity of the nascent neutron star, and ψ is the angle between the kick velocity and the pre-supernova relative orbital velocity. Equation (7) shows that the highest peculiar velocity is attained if $\cos\psi = -1$, that is, if the direction of the kick at the supernova explosion was opposite to the direction of the relative orbital velocity (Stone 1982; Gvaramadze et al. 2011). In this case, Eq. (7) can be rewritten simply as

$$v_{\rm max} = v_{\rm sym} + v_{\rm k} = v_{\rm sym} + \frac{M_{\rm co}w}{M_{\rm co}+M_2}. \tag{9}$$

Equation (5) shows that the BeXRB attains the highest peculiar velocity if the binary is as tight as possible before the supernova explosion. Higher relative mass-loss from the supernova explosion will also yield higher peculiar velocities. Another way to increase the peculiar velocity is by the natal kick of the neutron star (however, these kicks can also counteract the kick resulting from a symmetric explosion; Kalogera 1998). The magnitude of this natal kick can potentially be very high (as evidenced by the high velocities of isolated radio pulsars; e.g., Hobbs et al. 2005), but given its random orientation to the pre-supernova relative orbital velocity and the canonical mass of the nascent neutron star of about $M_{\rm co} = 1.4\,M_\odot$, its impact on the attained systemic velocity is reduced because the neutron star has to drag its massive secondary along, provided that the system has remained bound after the supernova. The contribution of the neutron star kick to the systemic velocity abates with the increasing mass of the secondary component as $M_{\rm co}/(M_{\rm co}+M_2) \ll 1$.

We caution that BeXRBs are fundamentally a biased population and cannot, in general, be used to make inferences about the general properties of neutron stars and supernovae. Renzo et al. (2019) estimated that about ~86% of the binary systems are disrupted at the moment of the first supernova that occurs within the system, primarily because of the high natal kick that is imparted to the nascent compact object. Eldridge et al. (2011) estimated a similar disruption rate of ~80%. The majority of the surviving binaries comes from relatively tight pre-supernova orbits, which are less vulnerable to disruption. The majority of these sources is expected to evolve through a phase when they might be detectable as X-ray sources. When Renzo et al. (2019) also included ECSNe in the modeling, allowing for smaller natal kicks imparted to the neutron star, the fraction of bound systems increased significantly from ~14% to ~35%.

As outlined above, if a binary survives the supernova, then its velocity relative to the pre-supernova center of mass changes. Here we make a general and approximate brief estimate of the velocity that is expected to be imparted to the system in the case of the CCSN and ECSN. Podsiadlowski et al. (2004) postulated that the main factor determining the type of the supernova that the system will undergo is the initial orbital period (or equivalently, the binary separation) of the system at the start of its evolution (see their Fig. 2). Using the pre-supernova parameters of their prototype binaries and Eq. (5), we derive an approximate attained peculiar velocity of the surviving binary system for the CCSN scenario of $\sim 80\,{\rm km\,s^{-1}}$ and $\lesssim 10\,{\rm km\,s^{-1}}$ for the ECSN scenario. In the CCSN scenario, the attained peculiar velocity of the surviving binary system is predominantly due to the mass loss from the binary after a supernova explosion (the "Blaauw kick"). However, the impact of the SN asymmetry and neutron star kick also significantly supplements the attained peculiar velocity. If the kick velocity w is drawn from a Maxwellian with $\sigma \sim 265\,{\rm km\,s^{-1}}$ (motivated by the high peculiar velocities of isolated pulsars; e.g., Arzoumanian et al. 2002; Hobbs et al. 2005; Verbunt et al. 2017), this would correspond to a mean kick velocity[2] of $w \sim 420\,{\rm km\,s^{-1}}$. Even after

[2] The mean of a Maxwellian distribution is given by $\sigma\sqrt{8/\pi}$.

rescaling w to v_k using Eq. (8), as the impulse of the kick is shared by the entire system (provided that the binary remains bound; van den Heuvel et al. 2000), this velocity is comparable to $v_{\rm sym}$. However, a kick of this magnitude can lead to the disruption of the binary (Renzo et al. 2019), therefore the kick magnitude was likely far lower for the surviving BeXRBs, which in turn decreases its likely contribution to the attained peculiar velocity. In the latter case, we considered the effect of the lower natal neutron star kick of $w \sim 50\,{\rm km\,s^{-1}}$ (a mean velocity resulting from a Maxwellian velocity distribution with $\sigma \sim 30\,{\rm km\,s^{-1}}$; Pfahl et al. 2002; Renzo et al. 2019), which when "diluted" by the total mass of the system, is also comparable to the velocity imparted by the binary mass loss due to the supernova.

To facilitate the comparison with the measured tangential peculiar velocities, it is necessary to project these velocity estimates onto a plane, assuming that the velocity distribution is isotropic. This can be done by multiplying the velocities by a factor of $\sim\pi/4$ (e.g., van den Heuvel et al. 2000). This resulted in approximate expected tangential peculiar velocities of $\sim$60 km s^{-1} and $\sim$6 km s^{-1} for CCSN and ECSN scenarios, respectively. Furthermore, it is also necessary to correct for the frame of reference because the estimated velocities are in the rest frame of the pre-supernova binaries and the observed velocities are measured using a frame that corotates with the Galactic disk. When we assume that the BeXRB progenitors have formed in OB associations and clusters, we need to account for the velocity dispersion inside these structures, which is typically $\sim$5 km s^{-1} (e.g. Mel'nik & Dambis 2017). The velocity of the pre-supernova binary inside an OB association and the velocity acquired after the supernova explosion are both randomly oriented, therefore it is necessary to convolve the theoretical velocity distribution by the velocity dispersion. This does not have any significant effect except to smear out the theoretical velocity distribution (see Renzo et al. 2019) and slightly increase the expected velocity of the systems that underwent an ECSN. Moreover, Reid et al. (2014) noted that star-forming regions may be lagging by about $\sim$5 km s^{-1} behind the rotation of the Galactic disk. When the frame of reference tied to the Galactic disk is used, the peculiar velocities derived in this way are therefore slightly overestimated compared to their true values. However, this systematic shift affects all studied Galactic BeXRB in the same way and is also quite small. For the purpose of our analysis, it can be neglected.

It needs to be noted that these general and approximate analytic estimates depend heavily on the previous binary evolution. The simulations reported by Renzo et al. (2019) showed that the neutron star natal kick w is the dominant factor affecting the attained peculiar velocity, not the effect of the sudden mass loss from a binary at supernova explosion. The average effective natal kick for compact objects in systems that remained bound after the supernova was $w \sim 66\,{\rm km\,s^{-1}}$ for their simulation, where the kicks were drawn from the Maxwellian with $\sigma \sim 265\,{\rm km\,s^{-1}}$. This is far lower than the average w that would be expected, even when supernova fallback is accounted for. The systems experiencing higher compact object natal kicks were more likely to be disrupted.

When we consider the points above, if the CCSNe and ECSNe both occur in the BeXRB progenitors, we expect according to our analytic estimates to observe two subpopulations with tangential peculiar velocities of about $\sim$60 km s^{-1} and $\sim$10 km s^{-1}. Brandt & Podsiadlowski (1995) and Eldridge et al. (2011) also derived a similar value for the CCSN subpopulation, but Renzo et al. (2019) and Kochanek et al. (2019) both derived significantly lower values with a median of $\sim$20 km s^{-1} ($\sim$16 km s^{-1} if projected). For systems that underwent an ECSN, both Renzo et al. (2019) and Kochanek et al. (2019) derived very low peculiar velocities.

A reference frame that corotates with the Galactic disk is prone to many uncertainties. It should still be feasible for modern astrometric missions such as *Gaia*, however, to distinguish between these two subpopulations.

4.2. Relationship between the peculiar velocity, eccentricity, and orbital period

The orbital solutions available for some of the systems from the Galactic BeXRB population enables us to investigate the relationships between the peculiar velocities, eccentricities and $P_{\rm orb}$. The top part of Fig. 5 shows the $P_{\rm orb}$–eccentricity dependence for the studied BeXRBs, similar to Fig. 6 of Townsend et al. (2011). The plot shows two populations, a low-eccentricity (with $e \lesssim 0.2$) and a high-eccentricity population, which contains most of the remaining systems. Excluding the low-eccentricity subpopulation from the analysis, Townsend et al. (2011) reported a weak correlation between the $\log(P_{\rm orb})$ and eccentricity. It is not meaningful for us to perform a detailed correlation analysis because our sample is smaller because we lack the SMC systems. The middle part of Fig. 5 shows the $P_{\rm orb}$ and peculiar velocity relationship. These two parameters appear to be uncorrelated or independent of each other. This contradicts the result of the simulations by Brandt & Podsiadlowski (1995), who predicted an anticorrelation between the peculiar velocity and post-supernova $P_{\rm orb}$.

Recently, Bray & Eldridge (2016) proposed a simple relation for the neutron star natal kick velocity, which is defined as a function of the ratio of the supernova ejecta to the neutron star mass. When the resulting neutron star mass is considered to be about identical for all supernova scenarios, this would mean that the resulting velocity, which is a function of the ejected mass, would in general be proportional to the neutron star natal kick, which affects the post-supernova eccentricity. Moreover, the scaling relations from Janka (2017) suggest the same outcome: a more powerful explosion results in higher peculiar velocities and eccentricities. Therefore, we expect to observe that in general, a high-eccentricity system also exhibits high peculiar velocity. The relation between the orbital eccentricities and peculiar velocities of the systems we studied is shown in the bottom part of Fig. 5. The expected relation is clearly not confirmed observationally, and it may even show the opposite trend to what would be expected if the data were taken at face value. This is puzzling, unless some post-supernova orbital circularization mechanism operates in these objects. This is not expected because as outlined above, the timescale for tidal circularization for main-sequence binaries with $P_{\rm orb} > 16$ d is at least a few tens of Myr, which is significantly longer than the BeXRB phase lifetime (typically $\sim$10 Myr; van den Heuvel et al. 2000). However, for the systems with $P_{\rm orb} \lesssim 16$ d, the orbits might be partially circularized, especially if we observe the system near the end of its lifetime. Alternatively, it is possible that the orbit circularizes when the neutron star interacts with the decretion disk of the Be star at periastron passage (e.g., Martin et al. 2009). Therefore, it is prudent to regard the observed eccentricities as the lower limits of the post-supernova eccentricities.

However, there is also a high scatter in the data, and possible selection effects also need to be taken into account. Furthermore, we also need to consider (see Eqs. (5) and 6 and also Maccarone et al. 2014) that the eccentricity induced on a system by a spherically symmetric mass-loss event alone is normally

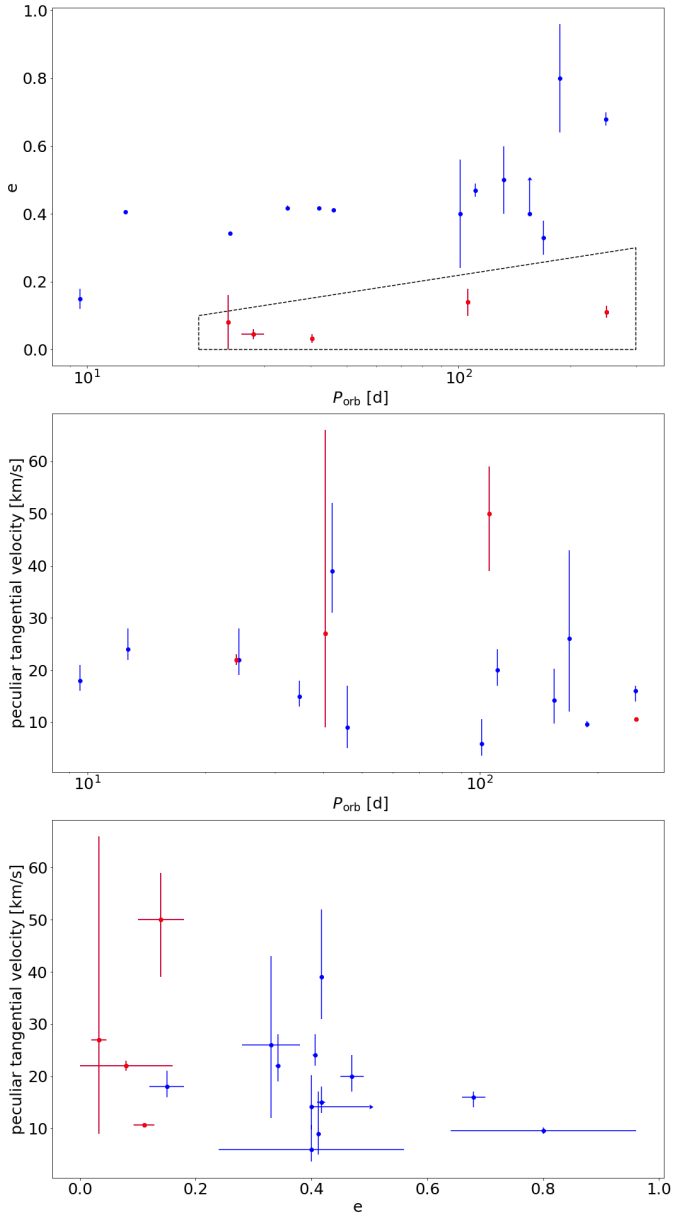

Fig. 5. Relations between the eccentricities e, orbital periods P_{orb} , and peculiar tangential velocities ($v_{pec,BJ}$) for the sample of Galactic BeXRBs. *Top*: P_{orb} vs. e plot for the Galactic BeXRB sample. The region that contains the low-eccentricity class of BeXRBs (Pfahl et al. 2002; the region adopted from Townsend et al. 2011) is marked by dashed lines. These systems are marked in red in the current and subsequent graphs for clarity. GX 304-01 and XTE J1906+090 are omitted from the subsequent figure panels because of their unreliable peculiar velocity that is a result of unreliable astrometry. *Middle*: P_{orb} vs. tangential peculiar velocity. *Bottom*: e vs. peculiar tangential velocity.

rather low for BeXRBs ($e < 0.2$ and far below this value in most cases), while the effect of the neutron star natal kicks is thought to have more impact on the orbital eccentricity, if it is present (van den Heuvel 2004). When the contribution of the neutron star natal kick w to the attained peculiar velocity is significant, it can be expected for a given w that systems with higher eccentricities exhibit lower peculiar velocities and vice versa, as the energy released by the neutron star natal kick can go either into the kinetic energy of the binary system or into the orbit of the system, which would cause the orbit to become larger and/or more eccentric. Therefore, the orbital energy of the binary and its kinetic energy as a whole would be anticorrelated, meaning that the peculiar velocity, eccentricity, and orbital period are linked. This also connects to the previous part of Fig. 5, where it seems that the $\log(P_{orb})$ is not correlated with peculiar velocity, therefore the orbital energy seems to be increased by pumping the eccentricity rather than widening the binary system. It is not realistic to expect that all sample systems have received a kick of equal magnitude. Moreover, the quality of the current measurements, the low significance of the correlation, and the number of the systems in the sample are not sufficient to reach any firm conclusions at this point.

While the majority of BeXRBs attained their peculiar velocities at the supernova explosion, as indicated by their young kinematic age compared to the OB runaway stars (Huthoff & Kaper 2002; Bodaghee et al. 2012), it is possible that the sample contains some systems that attained some peculiar velocity prior to the supernova explosion, when their progenitors were dynamically ejected from their parent clusters or associations (Poveda et al. 1967). This two-step ejection scenario (Pflamm-Altenburg & Kroupa 2010) may be responsible for the higher observed peculiar velocities of some systems, possibly accounting for some outliers.

4.3. Origins of the kinematic bimodality

When we consider the points above, there are two possible ways to explain the higher peculiar velocities of the short-spin subpopulation, still within the framework of the different supernovae hypothesis. They might arise from tighter binary progenitors or experience greater relative mass-loss and kicks during the supernova explosion than their counterparts in the long-spin subpopulation. However, this is at odds with the current supernova models, where the ECSNe are not expected to cause high mass-loss and neutron star kicks.

In the previous sections, we assumed that the short-spin subpopulation arises from the ECSNe and the long-spin subpopulation arises from systems that underwent a CCSN, which is the hypothesis put forward by KCP. This disagrees with the scenario proposed by Podsiadlowski et al. (2004), where the short-orbit subpopulation (therefore the short-spin subpopulation because P_{orb} and P_s are correlated, see, e.g., Fig. 1 in KCP) is instead expected to arise from CCSN. The higher peculiar velocities of the short-spin subpopulation would therefore be explained if this model were adopted instead: the opposite of the hypothesis put forward by KCP. However, we note that the predicted peculiar velocities for the CCSN BeXRB subpopulation, derived from the prototype binaries of Podsiadlowski et al. (2004; which are simplifications of the reality), seem to be notably higher than what is observed.

The implications are interesting when we assume that the bimodality in the spin period is caused by different accretion modes of the neutron stars in BeXRBs. According to Cheng et al. (2014), the bimodal distribution of the spin period is not directly linked to the two supernova channels, but the supernova mechanism can still be one of the factors that can modulate it, through its influence on the orbital period, eccentricity, and misalignment of the Be star disk, which are some of the factors that then probably affect the occurrence of the giant outbursts. Haberl & Sturm (2016) used the SMC BeXRB census to investigate which mechanism is responsible for the bimodal spin distribution. They reported higher long-term variability for the short-spin subpopulation, favoring the accretion mode model of Cheng et al. (2014) as the mechanism behind the

bimodality. For a BeXRB to show giant outbursts, the right combination of eccentricity and orbital period is apparently needed (Sidoli & Paizis 2018; Cheng et al. 2014). The relative contribution of other factors is also unclear, such as the activity of the Be star, to the frequency of giant outbursts (e.g., Ziolkowski 2002; Reig 2011). Because the effect of the supernova explosion mechanism is only indirect, it is probably unlikely that any kinematic bimodality is observable at all. If giant outbursts (producing the systems with shorter spin periods) dominate in low-eccentricity systems, which are thought to have an ECSN origin, it is expected that the short-spin subpopulation also has a lower peculiar velocity than the rest of the population, which is not observed. However, this changes when the contribution of the neutron star natal kick to the peculiar velocity is significant because we would expect the systems with low eccentricities to exhibit higher peculiar velocities in general.

5. Summary and conclusions

We investigated the kinematics of BeXRB subpopulations that arise from the neutron star spin bimodality in order to test the supernovae hypothesis proposed by KCP and the accretion mode hypothesis of Cheng et al. (2014). We used the GDR2 astrometry to derive the tangential peculiar velocities for the Galactic BeXRBs. In the SMC we used an indirect approach, where we analyzed the distances of the individual BeXRBs from the nearest star cluster as a proxy for the tangential peculiar velocities.

KCP predicted that the short-spin subpopulation, which arises from ECSNe, has systematically lower peculiar velocities than the long-spin subpopulation, which is produced by CCSNe. However, we found some evidence that the subpopulations are kinematically distinct, but in the opposite way as predicted by KCP. The kinematics of the BeXRB subpopulations is difficult to explain within the supernova hypothesis framework because all possible explanations for the increased peculiar velocity of the short-spin subpopulation are hard to reconcile with the current understanding of the ECSNe and CCSNe. Alternatively, adopting the scenario proposed by Podsiadlowski et al. (2004), which reverses the hypothesis of KCP, appears to resolve the discrepancy between the BeXRB kinematics and the supernova mechanisms.

Although the results derived here are statistically significant, they should be regarded with caution because the sample sizes and the methods we used are limited. Clearly, more reliable determinations of the star cluster parameters in the SMC will provide a more solid base for the type of analysis conducted in this paper. Furthermore, the future *Gaia* data releases will provide an improved astrometry that can further constrain the kinematic properties of Galactic BeXRBs.

Acknowledgements. I would like to thank the anonymous referee for their helpful comments that led to a significant improvement of the paper. This work has made use of data from the European Space Agency (ESA) mission *Gaia* (https://www.cosmos.esa.int/gaia), processed by the *Gaia* Data Processing and Analysis Consortium (DPAC, https://www.cosmos.esa.int/web/gaia/dpac/consortium). Funding for the DPAC has been provided by national institutions, in particular the institutions participating in the *Gaia* Multilateral Agreement. This research made use of the Python language (van Rossum 1995) and the following packages: NumPy (Oliphant 2006); SciPy (Jones et al. 2001); Astropy, a community-developed core Python package for Astronomy (Astropy Collaboration 2018) and matplotlib (Hunter 2007). This research has made use of the SIMBAD database, operated at CDS, Strasbourg, France.

References

Ankay, A., Kaper, L., de Bruijne, J. H. J., et al. 2001, A&A, 370, 170
Arzoumanian, Z., Chernoff, D. F., & Cordes, J. M. 2002, ApJ, 568, 289
Astropy Collaboration (Price-Whelan, A. M., et al.) 2018, AJ, 156, 123
Bailer-Jones, C. A. L. 2015, PASP, 127, 994
Bailer-Jones, C. A. L. 2017, IA-C8-TN-MPIA-CBJ-081, https://www.mpia.de/4287840/3D_astrometry_inference.pdf
Bailer-Jones, C. A. L., Rybizki, J., Fouesneau, M., et al. 2018, AJ, 156, 58
Baykal, A., Inam, S. Ç., Stark, M. J., et al. 2007, MNRAS, 374, 1108
Beniamini, P., & Piran, T. 2016, MNRAS, 456, 4089
Bland-Hawthorn, J., & Gerhard, O. 2016, ARA&A, 54, 529
Blaauw, A. 1961, Bull. Astron. Inst. Neth., 15, 265
Bodaghee, A., Tomsick, J. A., Rodriguez, J., et al. 2012, ApJ, 744, 108
Boersma, J. 1961, Bull. Astron. Inst. Neth., 15, 291
Brandt, N., & Podsiadlowski, P. 1995, MNRAS, 274, 461
Bray, J. C., & Eldridge, J. J. 2016, MNRAS, 461, 3747
Cantat-Gaudin, T., Jordi, C., Vallenari, A., et al. 2018, A&A, 618, A93
Casares, J., Negueruela, I., Ribó, M., et al. 2014, Nature, 505, 378
Casares, J., Jonker, P. G., & Israelian, G. 2017, Handbook of Supernovae, 1499
Castro-Ginard, A., Jordi, C., Luri, X., et al. 2018, A&A, 618, A59
Cerda-Duran, P., & Elias-Rosa, N. 2018, Astrophys. Space Sci. Lib., 1
Cheng, Z.-Q., Shao, Y., & Li, X.-D. 2014, ApJ, 786, 128
Chevalier, C., & Ilovaisky, S. A. 1998, A&A, 330, 201
Chernyakova, M., Lutovinov, A., Rodríguez, J., et al. 2005, MNRAS, 364, 455
Coe, M. J. 2005, MNRAS, 358, 1379
Coe, M. J., & Kirk, J. 2015, MNRAS, 452, 969
Coe, M. J., Roche, P., Everall, C., et al. 1994, MNRAS, 270, L57
Coe, M. J., Bird, A. J., Hill, A. B., et al. 2007, MNRAS, 378, 1427
Cohen, J. 1988, Statistical Power Analysis for the Behavioral Sciences (Routledge)
Coleiro, A., & Chaty, S. 2013, ApJ, 764, 185
De Donder, E., Vanbeveren, D., & van Bever, J. 1997, A&A, 318, 812
Delgado-Martí, H., Levine, A. M., Pfahl, E., et al. 2001, ApJ, 546, 455
Drew, J. E., Herrero, A., Mohr-Smith, M., et al. 2018, MNRAS, 480, 2109
Eldridge, J. J., Langer, N., & Tout, C. A. 2011, MNRAS, 414, 3501
Esposito, P., Israel, G. L., Sidoli, L., et al. 2013, MNRAS, 433, 2028
Finger, M. H., Wilson, R. B., & Hagedon, K. S. 1994, IAU Circ., 5931, 1
Gaia Collaboration (Brown, A. G. A., et al.) 2018, A&A, 616, A1
Galloway, D. K., Morgan, E. H., & Levine, A. M. 2004, ApJ, 613, 1164
Gandhi, P., Rao, A., Johnson, M. A. C., et al. 2019, MNRAS, 485, 2642
Glatt, K., Grebel, E. K., & Koch, A. 2010, A&A, 517, A50
Göğüş, E., Patel, S. K., Wilson, C. A., et al. 2005, ApJ, 632, 1069
Grindlay, J. E., Petro, L. D., & McClintock, J. E. 1984, ApJ, 276, 621
Gvaramadze, V. V., Röser, S., Scholz, R.-D., et al. 2011, A&A, 529, A14
Haberl, F., & Sturm, R. 2016, A&A, 586, A81
Hobbs, G., Lorimer, D. R., Lyne, A. G., et al. 2005, MNRAS, 360, 974
Hunter, J. D. 2007, Comput. Sci. Eng., 9, 90
Huthoff, F., & Kaper, L. 2002, A&A, 383, 999
Iben, I., & Tutukov, A. V. 1997, ApJ, 491, 303
in't Zand, J. J. M., Halpern, J., Eracleous, M., et al. 2000, A&A, 361, 85
Israel, G. L., Covino, S., Campana, S., et al. 2000, MNRAS, 314, 87
Israel, G. L., Negueruela, I., Campana, S., et al. 2001, A&A, 371, 1018
Janka, H.-T. 2017, ApJ, 837, 84
Jennings, R. J., Kaplan, D. L., Chatterjee, S., et al. 2018, ApJ, 864, 26
Jones, E., Oliphant, T., & Peterson, P. 2001, http://www.scipy.org/
Kalari, V. M., Vink, J. S., de Wit, W. J., et al. 2019, A&A, 625, L2
Kalogera, V. 1998, ApJ, 493, 368
Knigge, C., Coe, M. J., & Podsiadlowski, P. 2011, Nature, 479, 372
Kochanek, C. S., Auchettl, K., & Belczynski, K. 2019, MNRAS, 485, 5394
La Palombara, N., & Mereghetti, S. 2017, A&A, 602, A114
Lennon, D. J., Evans, C. J., van der Marel, R. P., et al. 2018, A&A, 619, A78
Lindegren, L. 2018, GAIA-C3-TN-LU-LL-124-01, www.rssd.esa.int/doc_fetch.php?id=3757412
Lindegren, L., Hernández, J., Bombrun, A., et al. 2018, A&A, 616, A2
Liu, L., & Pang, X. 2019, ApJS, 245, 32
Liu, Q. Z., van Paradijs, J., & van den Heuvel, E. P. J. 2006, A&A, 455, 1165
Luri, X., Brown, A. G. A., Sarro, L. M., et al. 2018, A&A, 616, A9
Maccarone, T. J., Girard, T. M., & Casetti-Dinescu, D. I. 2014, MNRAS, 440, 1626
Martin, R. G., Tout, C. A., & Pringle, J. E. 2009, MNRAS, 397, 1563
McBride, V. A., Wilms, J., Coe, M. J., et al. 2006, A&A, 451, 267
Megier, A., Strobel, A., Galazutdinov, G. A., et al. 2009, A&A, 507, 833
Mel'nik, A. M., & Dambis, A. K. 2017, MNRAS, 472, 3887
Motch, C., Haberl, F., Dennerl, K., et al. 1997, A&A, 323, 853
Nayak, P. K., Subramaniam, A., Choudhury, S., et al. 2018, A&A, 616, A187
Negueruela, I., & Schurch, M. P. E. 2007, A&A, 461, 631
Netopil, M., Paunzen, E., & Carraro, G. 2015, A&A, 582, A19
Nomoto, K. 1984, ApJ, 277, 791
Nomoto, K. 1987, ApJ, 322, 206

Oey, M. S., Dorigo Jones, J., Castro, N., et al. 2018, ApJ, 867, L8
Oliphant, T. 2006, A Guide to NumPy (USA: Trelgol Publishing), 1
Pfahl, E., Rappaport, S., Podsiadlowski, P., et al. 2002, ApJ, 574, 364
Pflamm-Altenburg, J., & Kroupa, P. 2010, MNRAS, 404, 1564
Piatti, A. E. 2018, MNRAS, 478, 784
Podsiadlowski, P., Joss, P. C., & Hsu, J. J. L. 1992, ApJ, 391, 246
Podsiadlowski, P., Langer, N., Poelarends, A. J. T., et al. 2004, ApJ, 612, 1044
Poveda, A., Ruiz, J., & Allen, C. 1967, Boletin de los Observatorios Tonantzintla y Tacubaya, 4, 86
Rafelski, M., & Zaritsky, D. 2005, AJ, 129, 2701
Raichur, H., & Paul, B. 2010, MNRAS, 406, 2663
Reid, M. J., Menten, K. M., Brunthaler, A., et al. 2014, ApJ, 783, 130
Reig, P. 2011, Ap&SS, 332, 1
Reig, P., & Milonaki, F. 2016, A&A, 594, A45
Reig, P., Fabregat, J., Coe, M. J., et al. 1997, A&A, 322, 183
Reig, P., Blay, P., & Blinov, D. 2017, A&A, 598, A16
Renzo, M., Zapartas, E., de Mink, S. E., et al. 2019, A&A, 624, A66
Ribó, M., Negueruela, I., Blay, P., et al. 2006, A&A, 449, 687
Rivinius, T., Carciofi, A. C., & Martayan, C. 2013, A&ARv, 21, 69
Rodes-Roca, J. J., Bernabeu, G., Magazzù, A., et al. 2018, MNRAS, 476, 2110
Scholz, F. W., & Stephens, M. A. 1987, J. Am. Stat. Assoc., 82, 918
Sidoli, L., & Paizis, A. 2018, MNRAS, 481, 2779
Siegel, M. H., Majewski, S. R., Reid, I. N., et al. 2002, ApJ, 578, 151
Smith, M. A., Lopes de Oliveira, R., & Motch, C. 2016, Adv. Space Res., 58, 782
Staubert, R., Pottschmidt, K., Doroshenko, V., et al. 2011, A&A, 527, A7
Stone, R. C. 1982, AJ, 87, 90
Sugizaki, M., Yamamoto, T., Mihara, T., et al. 2015, PASJ, 67, 73
Townsend, L. J., Coe, M. J., Corbet, R. H. D., et al. 2011, MNRAS, 416, 1556
Treuz, S., Doroshenko, V., Santangelo, A., et al. 2018, A&A, submitted [arXiv:1806.11397]
van den Heuvel, E. P. J. 2004, 5th INTEGRAL Workshop on the INTEGRAL Universe, 185
van den Heuvel, E. P. J., Portegies Zwart, S. F., Bhattacharya, D., et al. 2000, A&A, 364, 563
van Oijen, J. G. J. 1989, A&A, 217, 115
van Rossum, G. 1995, Python tutorial, Report CS-R9526, pub-CWI:adr
Verbunt, F., Igoshev, A., & Cator, E. 2017, A&A, 608, A57
Walter, R., Lutovinov, A. A., Bozzo, E., et al. 2015, A&ARv, 23, 2
Waters, L. B. F. M., & van Kerkwijk, M. H. 1989, A&A, 223, 196
Watson, M. G., Warwick, R. S., & Ricketts, M. J. 1981, MNRAS, 195, 197
Wilson, C. A., Finger, M. H., Harmon, B. A., et al. 1997, ApJ, 479, 388
Wilson, C. A., Finger, M. H., Göüş, E., et al. 2002, ApJ, 565, 1150
Wilson, C. A., Finger, M. H., Coe, M. J., et al. 2003, ApJ, 584, 996
Wilson, C. A., Weisskopf, M. C., Finger, M. H., et al. 2005, ApJ, 622, 1024
Wilson, C. A., Finger, M. H., & Camero-Arranz, A. 2008, ApJ, 678, 1263
Yan, J., Zurita Heras, J. A., Chaty, S., et al. 2012, ApJ, 753, 73
Yan, J., Zhang, P., Liu, W., et al. 2016, AJ, 151, 104
Ziolkowski, J. 2002, Mem. Soc. Astron. It., 73, 1038
Zwicky, F. 1957, Morphological Astronomical Kaleidoscope (Berlin: Springer)

3.3 Further developments

The study of the kinematics of NS and NS-hosting binaries offers great opportunities to expand our knowledge of the terminal stages of the stellar evolution of the massive stars and binaries. Therefore, as our understanding of these objects increases due to the advent of new instruments and techniques, it is reasonable to expect that we will see significant advancements in this field of study. Most notably, since the publishing of the paper that is the base of this chapter, there have been major improvements in the astrometry, where *Gaia* EDR3 (Gaia Collaboration et al., 2021; Lindegren et al., 2021b) can provide greatly improved kinematics of these objects.

In this section, I summarize the subsequent developments relevant to the kinematics of BeXRB pulsars and take advantage of the *Gaia* EDR3 data to test that the kinematic bimodality of the Galactic BeXRB pulsars is still present using the current (as of writing this thesis) *Gaia* EDR3 astrometry.

3.3.1 Revisiting the kinematic bimodality using the *Gaia* EDR3 data

The goal of this section is to establish whether the observed kinematic bimodality in the paper is still present in the light of the new *Gaia* EDR3 data. The new release provides more reliable astrometry, with reduced uncertainties on parallaxes and proper motions, and better treatment of systematic errors, as compared to GDR2. In order to get the correct astrometry, I re-checked the identifiers of the optical counterparts. This was necessary because not all objects retain the same source identifier (`source_id`) going from GDR2 to EDR3. Secondly, due to the new data being released in the time between the writing of the paper and this dissertation, it was worthwhile to check the validity of the optical counterparts, especially for the faint sources in the fields with high source density.

By doing this, I have identified two cases where the identifiers changed. The first affected object is 4U 0728-25 where the identifier changed from 5613494119544761088 in GDR2 to 5613494119551805184 in EDR3. The second one is XTE J1906+090, where the identifier changed from 4310649149314811776 in GDR2 to 4310649153642824320 in EDR3. For 4U 1416-62, I have decided to revise the counterpart from 5854175187680510336 in the original paper to 5854175187710795136 in the light of the Chandra observation of the system (Observation ID 14640; PI: Wijnands). The new optical counterpart better matches the X-ray counterpart of the system. The previous mismatch of the optical counterpart does not affect the overall conclusions of the published paper.

After querying the relevant astrometry for the studied sources, I have applied a correction for the parallax zero point to all sources[1]. Unlike the fixed recommended correction used in GDR2, the zero-point in EDR3 is dependent on the position, the color, the magnitude, and the type of the astrometric solution (Lindegren et al., 2021a). Therefore, it slightly differs for each source. After that, I filtered out the sources with unreliable astrometric solutions using the same criteria as listed in Sect. 2.3 of the paper. This resulted in the exclusion of 4U 0352+309 due to the high renormalized unit weight error (`ruwe`), IGR J19294+1816 and XTE J1906+090 due to the high astrometric excess noise, and 4U 0728-25 which might be duplicated.

To conduct a direct comparison, I have calculated the peculiar velocities using the same methods and the empirically determined scale length in the paper – the

[1]The correction has been applied using the Python package from `https://gitlab.com/icc-ub/public/gaiadr3_zeropoint`

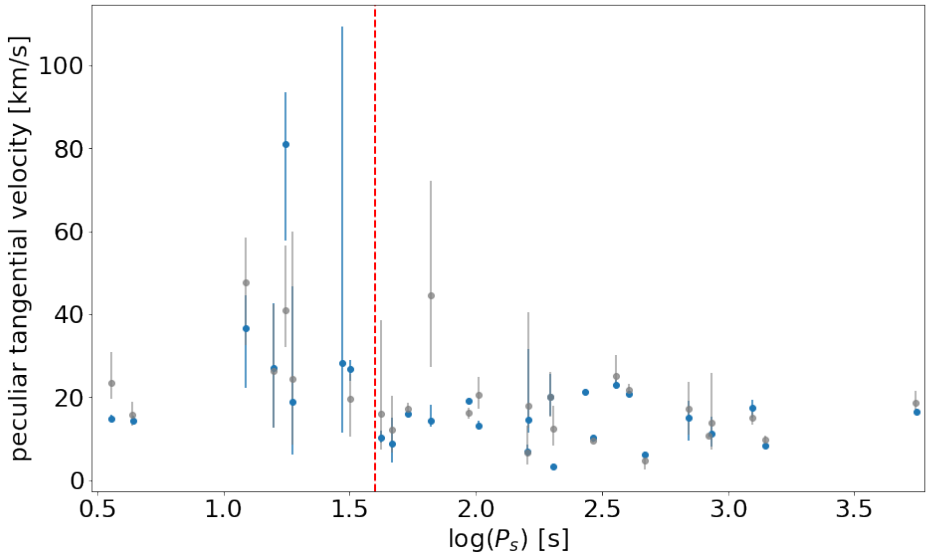

FIGURE 3.1: Peculiar tangential velocities of Galactic BeXRBs with respect to spin periods (P_s). The vertical red line ($P_{s,split} = 40$ s) divides the subpopulations as in Knigge, Coe, and Podsiadlowski (2011). To facilitate comparisons, the velocity data from the lower panel of Fig.2. in the accompanying paper, based on the GDR2 astrometry, are overplotted in gray.

only difference being the updated astrometry of the studied BeXRBs. The resulting plot of the calculated tangential peculiar velocities and spin periods P_s is in Fig. 3.1 (compare also with the lower panel of Fig.2. in the paper). According to the two-sample Anderson-Darling test (Scholz and Stephens, 1987), the significance of the population split is $p \approx 0.002$, which is more significant than $p \approx 0.007$ obtained by the GDR2 analysis in the paper. This is also the case for the rest of the statistical markers in the paper. Therefore, it can be concluded that using the improved astrometry in EDR3, the subpopulation split still seems to be present.

3.3.2 Subsequent studies and comments

The evidence supporting the existence of two distinct SN explosion mechanisms is not limited to only BeXRBs. Observations of double NSs, the bimodal velocity distribution of young pulsars, and a high number of NSs retained in GCs can be understood if two SN mechanisms are invoked (e.g., Pfahl et al., 2002; Beniamini and Piran, 2016; Verbunt, Igoshev, and Cator, 2017). However, combining the observations and analyses of different nature into a more unified picture has been challenging.

Recently, Igoshev et al. (2021) investigated SN explosions and NS natal kicks in massive binaries using population synthesis models and compared different model outcomes to the observed kinematic properties of young isolated NSs and Galactic BeXRBs. This combination is a major improvement as it allows to simultaneously study the systems disrupted by the SN and the ones remaining bound, removing several biases that would be present if the isolated NSs and BeXRBs were studied on their own. They made use of the updated astrometry provided by *Gaia* EDR3 to investigate the kinematics of the Galactic BeXRBs and obtained results similar to

the ones in my paper, having identified two populations of BeXRBs with different velocities. Ultimately, by the joint analysis of the isolated NSs and BeXRBs, they derived that around $\sim 20\%$ of NSs are imparted a weak kick (described by a Maxwellian distribution with $\sigma \approx 45\,\mathrm{km\,s^{-1}}$), and the remaining objects being imparted a strong kick (a Maxwellian distribution with $\sigma \approx 336\,\mathrm{km\,s^{-1}}$).

Arnason et al. (2021) used GDR2 distances to compare the reliability of other distance estimators commonly used for HMXBs and studied the positions of the Galactic HMXBs with respect to the Galactic spiral arms. The comparisons between different distance diagnostics are especially useful, as a lot of HMXBs do not have a bright and reliable optical counterpart, especially the distant and heavily absorbed systems – meaning that the *Gaia*-based distances are not available for a number of HMXBs. It was determined that the distances based on the GDR2 agree well with objects whose parallaxes have been previously measured by HIPPARCOS or radio interferometry. Furthermore, they found no significant association of HMXBs with spiral arms. This is unexpected, since in other galaxies, the bright X-ray sources, many of them HMXBs, are concentrated in spiral arms. The possible reasons for the absence of a correlation between the Galactic HMXBs and spiral arms include an incomplete understanding of star formation in the context of spiral arms, a large time delay between the star formation and the onset of the HMXB phase, large HMXB natal kicks, small HMXB sample size, and imperfect knowledge of the spiral arms structure.

Also, Bodaghee et al. (2021) studied the spatial correlation between the SMC HMXBs (which are almost exclusively BeXRBs) and their likely birthplaces – OB associations. Assuming a range of migration timescales, they derive average values of the peculiar velocities inherited by the SMC HMXBs in the range of 2–34 $\mathrm{km\,s^{-1}}$. This is consistent with the observed velocities of the Galactic BeXRBs.

Chapter 4

White dwarfs associated with open clusters based on Gaia DR2

4.1 Paper summary

White dwarfs (WDs) are the ultimate product of stellar evolution of low and intermediate-mass stars ($\lesssim 8$ $M_\odot$), which make up more than 97 % of all stars (Fontaine, Brassard, and Bergeron, 2001). These abundant stellar remnants serve numerous purposes in modern astrophysics, such as, tracing the Galactic formation history, understanding the physics of extreme conditions, type Ia SNe, and stellar evolution. However, the study of WDs has been hampered by their low intrinsic brightness (see, e.g., Althaus et al., 2010, for a general review).

WDs associated with open clusters (OCs) are extremely valuable. OCs are groups of gravitationally bound stars born in the same star-forming event, thus sharing the same age, initial metallicity, distance from the observer, and kinematics in the context of the Galaxy (e.g., Lada and Lada, 2003). Since OC WDs must also share these properties, this opens multiple research avenues. Firstly, by establishing that a particular WD is a member of an OC, it is possible to obtain its distance to a much higher precision through the analysis of the OC as a whole. The precise distance of a WD is crucial to studying its fundamental properties. While there is a sizeable sample of nearby WDs, where the individual distance measurements are highly informative (Tremblay et al., 2020), WD-OC associations are invaluable for more distant WDs.

One of the most fundamental questions that can be studied using WDs in OCs is the initial-final mass relation (IFMR). For the objects that have undergone stellar evolution in isolation, the IFMR links the final mass of a WD to the initial mass of its progenitor, and therefore it represents the total mass lost by a star during its entire evolution from the zero-age main sequence to the WD stage. An association between a WD and an OC allows us to use the WD cooling age to estimate the progenitor mass as the cooling age can be subtracted from the OC age, yielding the lifetime of the WD progenitor. This lifetime can then be converted to the progenitor mass using stellar evolutionary models. The knowledge of the IFMR has far-reaching applications, for instance, modeling stellar feedback in galaxy evolution, and predicting rates of type Ia SNe (e.g., Greggio, 2010; Agertz and Kravtsov, 2015).

The potential to use WDs in OCs for this has been realized early on (e.g., van den Heuvel, 1975), and since then, a large number of studies addressed this topic and a lot of progress has been made. A recent compilation of OC WDs can be found in Cummings et al. (2018). However, past studies were limited by the narrow fields of view of OC photometric studies, the high field WD contamination of OC fields, and the absence of WD astrometry essential to establish secure OC memberships. The research topic has been revolutionized since the publication of GDR2 (Gaia Collaboration et al., 2016b; Gaia Collaboration et al., 2018; Lindegren et al., 2018), which provided,

for the first time, proper motions and parallaxes precise enough for these faint objects, so their OC memberships could be firmly established. Also, using the GDR2 data, a large number of previously unknown WDs and WD candidates have been discovered and characterized (Gentile Fusillo et al., 2019). The GDR2 data has also provided improvements to the Galactic OC census (Cantat-Gaudin et al., 2018).

In this work, we crossmatch the known WDs and WD candidates listed in the catalog of Gentile Fusillo et al. (2019) with the OCs from Cantat-Gaudin et al. (2018), using positional, parallax, and proper motion criteria. The physical reality of the recovered OC-WD associations is then further studied using other OC and WD parameters.

To be considered OC members, WDs were required to:

- Have their positions, proper motions, and parallaxes consistent with their potential parent OC.
- Have their intrinsic brightness and colors consistent with lying on the WD cooling sequence when the measured WD brightness and colors are corrected using the distance and reddening of the tentative parent OC.
- Have cooling ages that are shorter than the OC age.

We start the candidate preselection by considering the WDs within $\theta_{\rm max} < 4.5\times$`r_50` from the OC centers in the sky, where `r_50` is the radius expected to contain half of the OC members (Cantat-Gaudin et al., 2018). This large selection radius $\theta_{\rm max}$ guarantees to encompass a highly complete population of the potential OC WDs, even for extremely loose OCs. The preselected WD-OC pairs were also required to have their proper motions and parallaxes within 3σ of each other. This preselection yielded $\sim$4000 distinct WD-OC pairs, a lot of them being low-probability ones.

To further filter the preselected WDs and obtain a clean IFMR, precise OC parameters, mainly ages, are essential. A lot of the parameters of our OC sample are cataloged in the literature (Dias et al., 2002; Kharchenko et al., 2013; Röser, Schilbach, and Goldman, 2016; Bossini et al., 2019). We validated these OC parameters by inspecting individual OC color-magnitude diagrams (CMDs) and how well they match with the theoretical isochrones that correspond to these OC parameters. It was discovered that many OCs were assigned parameters that correspond to isochrones that do not match these OCs well enough. In such cases, we fit the isochrones of all these clusters, using the photometry of the stars with membership probabilities larger than 50%, as listed in Cantat-Gaudin et al. (2018), to derive new sets of OC parameters.

For the preselected putative WD-OC pairs, we derived the absolute magnitudes and dereddened colors of the WDs using the OC parameters. This makes it possible to apply additional filtering to the preselected pairs. First, if the considered object is indeed a bona fide WD and the WD-OC match is not spurious, then, after correcting the WD photometry using the OC distance and reddening, the WD must lie within a specific region of the CMD. This CMD region is delineated by the cooling tracks of the most and least massive WDs. If this is not the case, the WD-OC pair is discarded, because either the object is not a WD, the WD-OC match is not physically real, or the object in question is a binary of some sort (either WD+WD or WD+MS star). The binary systems, while interesting, are not considered in this work because we aimed to investigate the stellar evolution of isolated stars for the IFMR derivation. Additionally, the astrometry of binaries may be unreliable because the GDR2 uses single-star astrometric solutions, and it is impossible to derive photometric WD cooling ages and masses since the precise contribution of the secondary to the combined light of

the binary is generally not known. Further filtering was done using the preliminary calculation of the WD cooling ages. Obviously, the cooling age of a WD associated with an OC cannot exceed the total age of the OC.

Overall, we identified WDs and WD candidates in over 20 OCs. A significant number of them are recovered for the first time. For the WD-hosting OCs, we also searched the literature for the previously identified WDs that were identified as members of these OCs in past works. It turned out that a significant number of these literature WD-OC associations have WD proper motions or parallaxes inconsistent with OC memberships and are therefore spurious matches.

After these selection steps, the remaining OC WD candidates were cleaned using the astrometric and photometric quality flags and indicators, removing the sources where the astrometry and/or photometry may not be reliable. The sources with problematic photometry were kept as OC members but were not considered for the derivation of WD cooling ages and masses.

The cooling models are slightly different for WDs with different atmosphere types. Therefore, to establish precise cooling ages and WD masses, it is necessary to know the WD atmospheric composition, which is normally determined using spectroscopic information or UV photometry. However, these are not available for most of the objects in our sample. Therefore, we assume that the detected WDs belong to the DA spectral class, meaning that they are covered in an opaque, nearly pure hydrogen atmosphere. This is true for the vast majority ($\gtrsim 80\%$) of all WDs (Kepler et al., 2016; Kepler et al., 2021). However, the fraction of DA WDs in OCs seems to be even higher than this (e.g., Kalirai et al., 2005; Salaris and Bedin, 2019).

The WD masses and cooling ages were calculated using the models from Renedo et al. (2010) for the intermediate-mass WDs, and from Camisassa et al. (2019) for the WDs with masses $M_{\rm WD} \gtrsim 1.0$ M$_\odot$, employing the tool from Cheng (2020). In order to compute the errors of the WD masses and the cooling ages, we used 10^4-element Monte Carlo simulations, each time drawing an absolute magnitude and color sample value from normal distributions, which are centered on the measured values and 1σ errors. The obtained masses and cooling ages are presented in terms of their median values and the quoted errors are derived from the 68% confidence intervals.

We detected mostly intermediate-mass WDs that are OC members and it seems there is an apparent lack of massive WDs ($M_{\rm WD} \gtrsim 0.9$ M$_\odot$). This is understandable when the properties of WDs, the distribution of OCs in the solar neighborhood, and the limitations of *Gaia* are taken into account. Firstly, due to their nature, the high-mass WDs are less luminous and cool more rapidly than their low-mass counterparts. For this reason, they remain bright enough for *Gaia* only for the closest and youngest OCs. However, there is a notable lack of young OCs in the solar neighborhood (see, e.g., Cantat-Gaudin et al., 2018). Moreover, it is possible that the high-mass WDs can get ejected from their parent OC due to the potential velocity kicks imparted on them upon formation or by dynamical interactions with other OC stars (Fellhauer et al., 2003; Tremblay et al., 2012).

Using the obtained WD cooling ages and the ages of the OCs that they are associated with, we computed the progenitor lifetimes and masses. For this, we utilized PARSEC version 1.2S (Bressan et al., 2012) and COLIBRI S_35 (Pastorelli et al., 2019) isochrones and Monte Carlo simulations, each time drawing a value from the normal distribution of the WD cooling time, OC age and its metallicity.

By examining the IFMR (the progenitor mass M_i vs. the final WD mass M_f, see Fig. 6 of the paper attached to this chapter), it can be seen that the newly characterized WDs are consistent with the nonlinear IFMR of Marigo et al. (2020) with a kink in located over 1.65 M$_\odot \lesssim M_i \lesssim$ 2.1 M$_\odot$, which can be interpreted as a

signature of the lowest-mass stars in the Galaxy that become carbon stars during the thermally-pulsing AGB phase.

Apart from this IFMR kink, there is a visible offset between the theoretical and the observed masses from approximately $M_i \gtrsim 3.0$ $M_\odot$, where the observed WD masses are ~ 0.1 $M_\odot$ more massive than predicted, as has been also noted by Cummings et al. (2018). Cummings et al. (2019) later attributed this offset mainly to the effects of convective-core overshoot and rotational mixing in the main sequence progenitors, where the rotational effects are not taken into consideration in the theoretical IFMR models.

Clearly, the advantages of the precise astrometry brought by *Gaia* to WD studies are palpable. It can be expected that further improvements in the data quality in the subsequent *Gaia* data releases and further work on the OC census have a potential to advance this research topic even further.

4.2 Paper III

A&A 645, A13 (2021)
https://doi.org/10.1051/0004-6361/202039276

Astronomy & Astrophysics

White dwarf-open cluster associations based on *Gaia* DR2

M. Prišegen, M. Piecka, N. Faltová, M. Kajan, and E. Paunzen

Department of Theoretical Physics and Astrophysics, Faculty of Science, Masaryk University, Kotlářská 2, 611 37 Brno, Czech Republic
e-mail: michalprisegen@gmail.com

Received 27 August 2020 / Accepted 13 October 2020

ABSTRACT

Context. Fundamental parameters and physical processes leading to the formation of white dwarfs (WDs) may be constrained and refined by discovering WDs in open clusters (OCs). Cluster membership can be utilized to establish the precise distances, luminosities, ages, and progenitor masses of such WDs.
Aims. We compile a list of probable WDs that are OC members in order to facilitate WD studies that are impractical or difficult to conduct for Galactic field WDs.
Methods. We use recent catalogs of WDs and OCs that are based on the second data release of the *Gaia* satellite mission (GDR2) to identify WDs that are OC members. This crossmatch is facilitated by the astrometric and photometric data contained in GDR2 and the derived catalogs. Assuming that most of the WD members are of the DA type, we estimate the WD masses, cooling ages, and progenitor masses.
Results. We have detected several new likely WD members and reassessed the membership of the literature WDs that had been previously associated with the studied OCs. Several of the recovered WDs fall into the recently reported discontinuity in the initial-final mass relation (IFMR) around $M_i \sim 2.0\,M_\odot$, which allows for tighter constrains on the IFMR in this regime.

Key words. open clusters and associations: general – white dwarfs – catalogs – surveys

1. Introduction

White dwarfs (WDs) are the evolutionary endpoint of low- and intermediate-mass stars, which constitute a vast majority of all stars in the Galaxy. Their nature as compact and dense stellar remnants has been an important test bed for many areas of fundamental physics and stellar evolution theories. However, the study of WDs has been hampered by their low brightness, meaning that only observations of the closest objects could yield reliable results (see, e.g., Liebert 1980; Althaus et al. 2010; Córsico et al. 2019, for a general review).

White dwarfs associated with star clusters are extremely valuable. Star clusters are groups of gravitationally bound stars born in the same star-forming event, thus sharing the same age, metallicity, distance from the Sun, and proper motion. Since the WD cluster members also share these characteristics, this allows for a number of interesting questions to be addressed. Perhaps the most fundamental is the initial-final mass relation (IFMR), which links the final mass of a WD to the initial mass of its progenitor, hence also providing the total amount of mass lost during the stellar evolution. The progenitor mass can be estimated by determining the cooling age of a WD and subtracting it from the total age of the cluster as determined from the observations of the non-WD cluster members. This yields the lifetime of the WD progenitor, which can then be converted into the progenitor initial mass. Knowledge of the IFMR has applications in many areas of astrophysics. Perhaps one of the most fundamental applications of the high-mass end of the IFMR is determining the minimum main sequence stellar mass for a core-collapse supernova (SN) to occur. The IFMR is also an important ingredient in the modeling of stellar feedback in galaxy simulations and predicting SN type Ia rates (e.g., Greggio 2010; Agertz & Kravtsov 2015; Cummings 2017). Aside from the IFMR, other possible avenues of research utilizing cluster WDs include studying the effects of metallicity and binarity on WD evolution and measuring WD masses using gravitational redshift (Pasquini et al. 2019). Such studies are impossible or very challenging to conduct for Galactic field WDs.

While isolated WDs in globular clusters are very faint due to the considerable distances of these objects, the impetus for discovering WDs in open clusters (OCs) in the solar neighborhood is clear, as these OCs usually have well-determined parameters such as distance, reddening, age, and metallicity, providing a unique laboratory for studying the WDs associated with them and the related physical processes. This potential was realized early on when the Hyades cluster was studied by Tinsley (1974) and van den Heuvel (1975). More WD-cluster pairs were investigated by Weidemann (1977) and Romanishin & Angel (1980). Follow-up studies by Koester & Reimers (1981, 1985, 1993), Reimers & Koester (1982, 1988, 1989, 1994) obtained the spectroscopy of the WD candidates from Romanishin & Angel (1980), confirming some of them as bona fide cluster WDs and deriving their physical parameters. Since then, several other WD-OC pairs have been discovered and investigated by various authors and working groups (e.g., Anthony-Twarog 1982; Richer et al. 1998; Claver et al. 2001; Williams 2002). A recent compilation of OC WDs can be found in Cummings et al. (2018).

Past studies were limited by the small fields of view of the photometric surveys, which usually only covered the core OC regions. Another caveat was significant field WD contamination. To differentiate between the cluster and field WDs in the same area of the sky, accurate parallax and proper motion measurements of WDs were needed. The situation has

improved since the publication of the second data release of the *Gaia* mission (GDR2; Gaia Collaboration 2016, 2018b), which contains precise astrometry (positions, parallaxes, and proper motions) as well as photometry in three bands (G, G_{BP}, and G_{RP}). Since the advent of *Gaia*, the knowledge and census of Galactic OCs have also been substantially furthered (e.g., Gaia Collaboration 2017; Cantat-Gaudin et al. 2018a,b). Furthermore, a large number of new WDs have been discovered and characterized (Gentile Fusillo et al. 2019), including WDs in OCs (e.g., Salaris & Bedin 2018, 2019; Richer et al. 2019).

Due to recent increases in the number of known WDs and OCs with reliable parameters and astrometry, it has become possible to conduct a systematic search for WDs that are members of nearby OCs. In this paper, we crossmatch the known WDs and WD candidates listed in the catalog of Gentile Fusillo et al. (2019) with the OCs from Cantat-Gaudin et al. (2018a), using positional, parallax, and proper motion criteria. The physical reality of the putative WD-OC pairs are then further investigated using the cluster parameters (distance modulus, age, and reddening) and the position of the WD on the corresponding cooling sequence.

This paper is structured as follows. In Sect. 2, we describe the catalogs used in this study, the star cluster parameters, and the workflow leading to the selection of the WD OC member candidates. In Sect. 3, we discuss the recovered OCs hosting WDs and compare our detections with the literature, where available. The quality of GDR2 astrometric solutions and photometry for the recovered WDs are examined in Sect. 4. The WD masses and cooling ages are estimated in Sect. 5, and their application for the IFMR is addressed in Sect. 6. Finally, we summarize and add concluding remarks in Sect. 7.

2. Data analysis

The WD and OC catalogs that form the basis of this work are based on GDR2; therefore, they should be directly comparable, with no systematic offsets between them. The catalog of WD and WD candidates of Gentile Fusillo et al. (2019) lists over 480 000 objects, approximately 260 000 of which are high-probability WDs. Due to the intrinsic faintness of many isolated WDs, the majority of them are found within 1 kpc of the Sun, as can be seen in Fig. 1. This is in contrast with the distance distribution of the OCs from Cantat-Gaudin et al. (2018a; containing 1229 OCs), which is approximately uniform in the interval from 0.5 to 4 kpc; however, there is a notable paucity of OCs with distances $\lesssim$0.5 kpc. More than half of the cataloged WDs lie within this distance, with their distance distribution peaking at ~170 pc.

As can be seen in Fig. 1, the distribution of the parallax and proper motion errors of WDs and OC member stars listed in Cantat-Gaudin et al. (2018a) is also markedly different. The reason for this is two-fold. Firstly, the stars utilized to compute overall cluster astrometric parameters, which are also listed in Cantat-Gaudin et al. (2018a), are all brighter than $G > 18$ mag, whereas WDs from Gentile Fusillo et al. (2019) are much fainter by comparison, with a median brightness of $G_{\rm WD} \approx 20$ mag. Such a jump in G leads to considerably larger errors for WDs (Lindegren et al. 2018). The second reason is that WDs are typically bluer in color than most stars in the GDR2. Blue objects observed by *Gaia* also exhibit increased errors in proper motion and parallax[1].

[1] https://www.cosmos.esa.int/web/gaia/science-performance

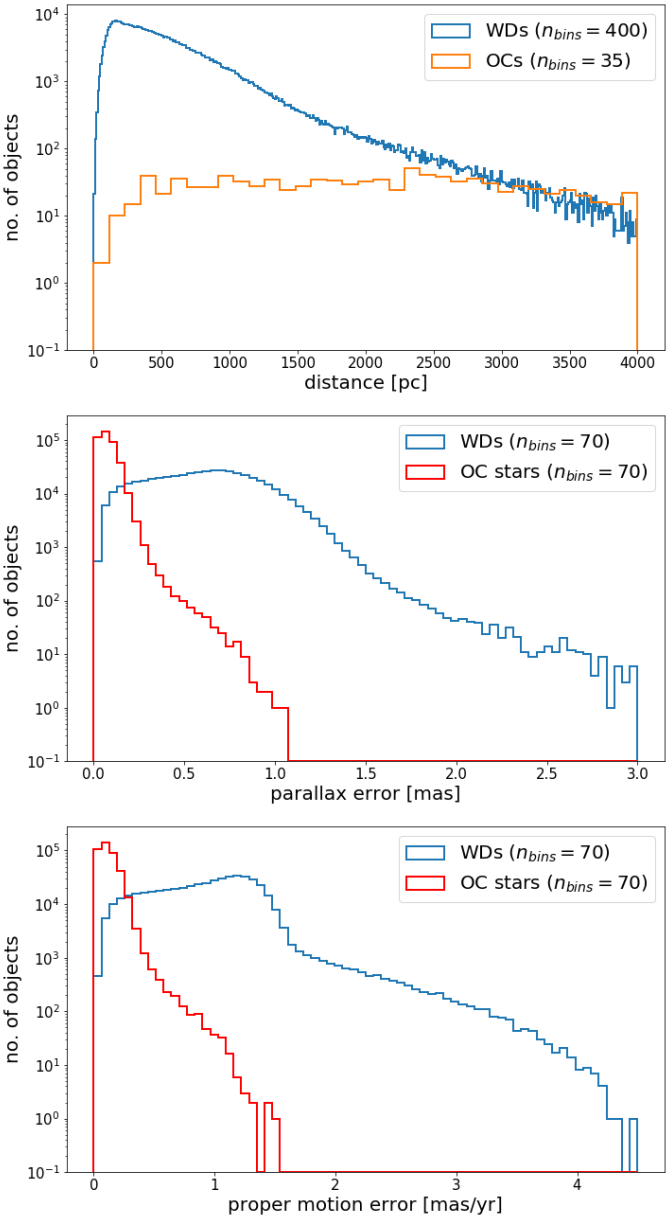

Fig. 1. *Top*: distance distribution of WDs from the catalog of Gentile Fusillo et al. (2019) compared to the distribution of OCs listed in Cantat-Gaudin et al. (2018a). *Middle*: comparison of the parallax error distribution of the WDs and OC member stars listed in Cantat-Gaudin et al. (2018a). *Bottom*: comparison of the average proper motion error (average of the RA and Dec components) of the WDs and OC members.

Due to these factors, using only the astrometric criteria (relying on positions, parallaxes, and proper motions) will yield a lot of low-confidence or spurious WD-OC matches. The most common such case is erroneous matches where a nearby WD gets matched with a more distant OC.

2.1. WD-OC pair preselection

Despite the shortcomings discussed above, the astrometric data are still potent when assigning potential WD members to OCs, especially when no such data of this quality and scope were available before GDR2. In order to make a rough preliminary preselection of potential cluster WDs, we utilized the

positional, proper motion, and parallax information contained in Cantat-Gaudin et al. (2018a) and Gentile Fusillo et al. (2019). The matching criteria are as follows:

$$\theta < 4.5 \times r50 \tag{1}$$

$$(plx - 3 \times s\_plx;\ plx + 3 \times s\_plx)_{\rm OC} \cap (Plx - 3 \times e\_Plx;\ Plx + 3 \times e\_Plx)_{\rm WD} \neq \emptyset \tag{2}$$

$$(pmRA - 3 \times s\_pmRA;\ pmRA + 3 \times s\_pmRA)_{\rm OC} \cap (pmRA - 3 \times e\_pmRA;\ pmRA + 3 \times e\_pmRA)_{\rm WD} \neq \emptyset \tag{3}$$

$$(pmDE - 3 \times s\_pmDE;\ pmDE + 3 \times s\_pmDE)_{\rm OC} \cap (pmDE - 3 \times e\_pmDE;\ pmDE + 3 \times e\_pmDE)_{\rm WD} \neq \emptyset. \tag{4}$$

Equation (1), where θ is the angular distance from a WD to a center of the cluster, represents the positional condition. Cantat-Gaudin et al. (2018a) list *r50*, which is the cluster radius that contains half of the cluster members, as the dimension of the studied clusters. In order to ensure search completeness, we considered WDs with projected separations up to $4.5 \times r50$ from the given cluster center. Next, Eq. (2) represents the parallax (distance) constraint. We considered every WD-cluster pair that satisfies this condition, where the WD has a parallax value of *Plx* and an associated error *e_Plx* from Gentile Fusillo et al. (2019; adopted directly from the GDR2) and the OC has a mean parallax of *plx* and a standard deviation of parallax of OC members *s_plx* from Cantat-Gaudin et al. (2018a). Lastly, Eqs. (3) and (4) are proper motion constraints. Again, Gentile Fusillo et al. (2019) adopt proper motion values and errors directly from the GDR2. For OCs, *pmRA* (*pmDE*) is the mean proper motion along the right ascension (declination) of OC members, and *s_pmRA* (*s_pmDE*) is its standard deviation.

Such a selection yields almost 4000 distinct WD-OC pairs. Naturally, due to the problems with the WD astrometry outlined in Sect. 2 and the generous selection criteria applied, most of these pairs are low-probability and are only spurious pairings. Given the nature of the WD astrometry, it is normally not sufficient to rely on astrometric data alone to determine membership. Further investigations can be conducted using cooling models in conjunction with cluster ages.

2.2. Isochrones and white dwarfs

One of the most important parameters describing stellar clusters is their age. With the use of photometric data available for the cluster members, the age of the cluster is usually found with the help of an isochrone fitting method. First, isochrones need to be calculated, which can be done with evolutionary models for stars of different masses. In the case that a correct age and metallicity are chosen (together with the distance and the extinction), the resulting isochrone should coincide with the distribution of cluster members in the color-magnitude diagram (CMD). Due to its dependence on all four cluster parameters, this method is very useful for improving distance and extinction while determining age and metallicity (although metallicity is often ignored and assumed to be solar). This whole process is a necessary step because of the fact that we are attempting to assign WDs to clusters. In this section, our goal is to show the quality of the cluster parameters derived from isochrone fitting techniques that have (mostly) been published in recent years. Furthermore, the method used to compute values for the WDs displayed in the CMD (in *Gaia* magnitudes) is described.

Table 1. Sources for cluster parameters.

Source of parameters	Number of OCs
Bossini et al. (2019)	67
Kharchenko et al. (2013)	81
Dias et al. (2002)	2
Röser et al. (2016)	3
Custom fit	98

To verify our assignment of WDs to the sample of OCs, we need to take a look at the CMDs that show both the cluster members and the WDs. Moreover, we need to acquire cluster parameters (distance, extinction, and age, excluding metallicity) for all clusters in our sample. The newest data set provided by Bossini et al. (2019) contains the required parameters for 269 clusters, which are based on the data from the GDR2. Unfortunately, not all of these clusters coincide with those from our sample. For this reason, we decided to also make use of the data provided by Kharchenko et al. (2013) We took parameters from Dias et al. (2002) and Röser et al. (2016) as secondary sources of data if a cluster is not present in either of the two previous data sets.

Closer inspection of the individual CMDs then helped us determine which of the data sets gives a better isochrone fit to a given cluster. For our purposes, we decided to use CMD 3.3, the isochrone data from Evans et al. (2018), an assumed solar metallicity ($Z = 0.02$), and a chosen time-step $\Delta \log T = 0.05$. We favored this metallicity value because it has been shown to be consistent with recent results of helioseismology (Vagnozzi 2019). Together with information about cluster members from Cantat-Gaudin et al. (2018a) and the sets of cluster parameters, we can make a comparison between the corresponding isochrones. It is immediately clear from the plots that many of the clusters were assigned parameters that correspond to isochrones that do not match these clusters well enough. Our criterion for picking the parameters from the available data was to get the best isochrone fit. For the most part, values from Bossini et al. (2019) and Kharchenko et al. (2013) provide the best descriptions of the clusters (for example, Fig. 2), with parameters of only five clusters being taken from the secondary data sets. However, there are also many examples (about one-third of the whole sample) of clusters for which it was impossible to get an acceptable fit using data from any of the mentioned works.

For these cases, we fit the isochrones of all the individual clusters, using the photometric data of stars with membership probabilities larger than 50%. This was done without any black box algorithm. The metallicity was again assumed to be solar and kept fixed. Then, the reddening was determined using the shape of the main sequence. As a last step, the distance modulus was chosen so that the main sequence and turnoff point fit satisfyingly within the isochrone grid. The total final result for cluster parameters can be seen in Table 1.

The next task was fairly simple: determine the position of the WDs in the CMDs. To do this properly, we had to be able to subtract the extinction from the *Gaia* magnitudes. Since the extinction is usually described by either the A_V or R_V parameters (we assumed that $A_V = \frac{E(B-V)}{0.324}$) and we want to make use of GDR2 data, we needed to know the transformations between extinction in A_G (A_{BP}, A_{RP}) and A_V. It is not viable to use the simple approach $A_G = 0.835\,A_V$ due to the width of the *Gaia*

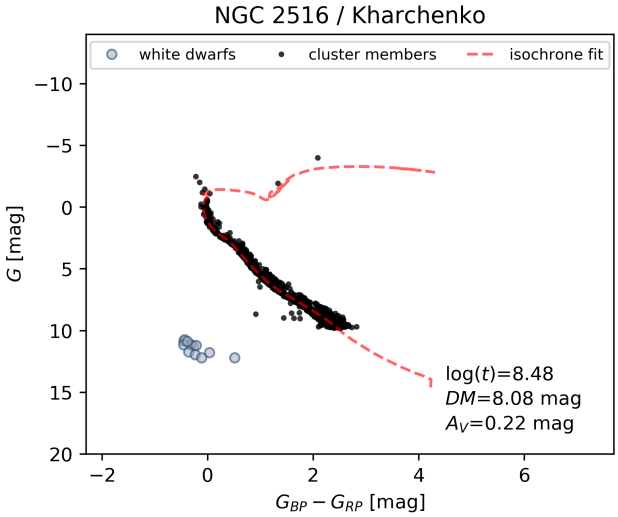

Fig. 2. Example of a cluster (NGC 2516) in the CMD with members taken from Gentile Fusillo et al. (2019) and fit with an isochrone (parameters from Kharchenko et al. 2013). Our initial candidate WDs are displayed in the plot together with the cluster parameters (age, reddened distance modulus, and extinction).

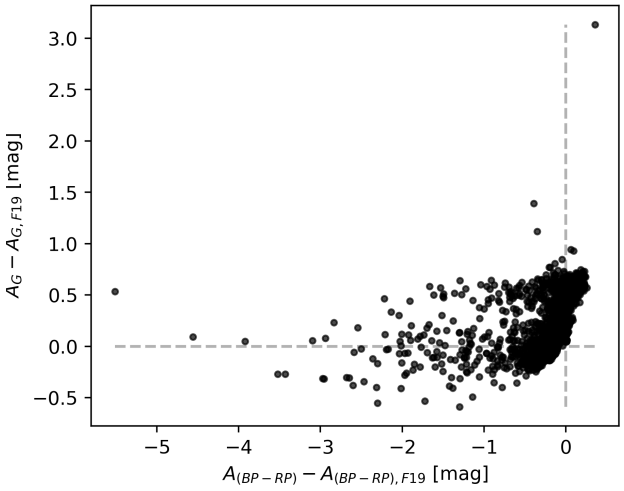

Fig. 3. Comparison of the extinction values A_G and $A_{B_P-R_P}$ between this work and Gentile Fusillo et al. (2019).

passbands. For our purposes, we decided to use the polynomial combination of $(G_{BP} - G_{RP})$ and A_V values that is described in Gaia Collaboration (2018a).

As mentioned before, we only employed isochrones with solar metallicity (i.e., $Z = 0.02$). To investigate the effect of the metallicity on the cluster parameters derived from isochrone fitting, the range of the metallicity in the solar vicinity has to be assessed. Netopil et al. (2016) present homogenized metallicities for 172 OCs on the basis of photometric and spectroscopic data. More recent studies using optical (Pancino et al. 2017) or infrared (Donor et al. 2018) spectroscopy have not added a significant number of new investigated OCs. Furthermore, theses results are very much in line with those from Netopil et al. (2016). These last authors have showed that almost all OCs within 2 kpc of the Sun have [Fe/H] = ±0.2 dex. There are hardly any known Galactic OCs that exceed a [Fe/H] value of ±0.5 dex. The isochrones up to [M/H] = ±1.0 dex are shifted in the distance modulus only. This means that, for the same color, stars become fainter for lower metallicities. We used the turnoff points for the whole isochrone grid to investigate the concrete values. As a conclusion, it can be said that for [M/H] up to ±1.0 dex, the differences of the distance modulus scales are one-to-one with metallicity (i.e., Δ[M/H] $\approx \Delta DM$). This shift is negligible compared to the width of the main sequence and the intrinsic errors of the parallaxes. Therefore, using an isochrone grid with solar metallicity is a justifiable approach.

Finally, we wanted to compare the calculated extinction values A_G with those provided by Gentile Fusillo et al. (2019). Assuming that $A_G^{'} = 0.835\, A_V$, they give

$$A_G = A_G^{'}\left(1 - \exp\left(-\frac{\sin|b|}{200\varpi}\right)\right),$$

$$A_{(BP-RP)} = 0.586\, A_G^{'}\left(1 - \exp\left(-\frac{\sin|b|}{200\varpi}\right)\right),$$

as the effective values of the extinction coefficients, where b is the Galactic latitude of the WD and ϖ is its parallax (in arcseconds). We can see that the relation between the two results is not one-to-one (Fig. 3). However, this is to be expected since both approaches use a different version of the extinction law. What remains uncertain in our case is the applicability of the transformation described in Gaia Collaboration (2018a) since their coefficients were derived with the use of stars with estimated effective temperatures $T_{\rm eff} \lesssim T_{\rm eff,WD}$ and it is unknown what order of magnitude of errors is produced at the higher temperature regime (>10 000 K).

2.3. CMD and cooling age–based filtering

Provided that accurate cluster ages, distances (parallaxes), and extinction values are available, it is possible to use photometry to filter out spurious WD-OC pairings. In order to do this, we used the cluster parameters as obtained in the previous section and Montreal WD cooling tracks[2] (Fontaine et al. 2001).

For our initial sample of several hundred putative WD-OC pairings, we used the distance moduli and extinctions of the matched OCs to compute the dereddened absolute magnitudes and colors for the corresponding WDs. We plot these quantities with the theoretical cooling tracks for the lowest- ($0.2\, M_\odot$) and highest-mass ($1.2\, M_\odot$) WDs in Fig. 4. In order for a WD-OC pairing to be physical (provided that the WD is not in a binary), it is necessary (but not sufficient) for a WD to lie in the CMD region delineated by the lowest- and highest-mass cooling tracks. It is apparent that the majority of the potential OC WDs lie above the lowest-mass cooling track, being more luminous than what would be expected if they were OC members. This was expected (see the discussion in Sect. 2), as these WDs tend to be in the foreground of the OCs and are spuriously matched to them due to the generous selection criteria and substantial errors in parallax and proper motions.

Further constraints can be made using the age of the OC matched with a WD. Obviously, the cooling age of the WD cannot be higher than the age of the OC it is associated with, provided that the association is real. Using this, other spurious WD-OC pairs can be filtered out on an individual basis using additional cuts in the CMD diagrams. If the cluster age is known, a WD that is associated with the cluster should lie in the CMD region delineated by the lowest- and highest-mass cooling track (as discussed above), the zero-age cooling isochrone, and the cooling isochrone corresponding to the cluster age.

[2] http://www.astro.umontreal.ca/~bergeron/CoolingModels

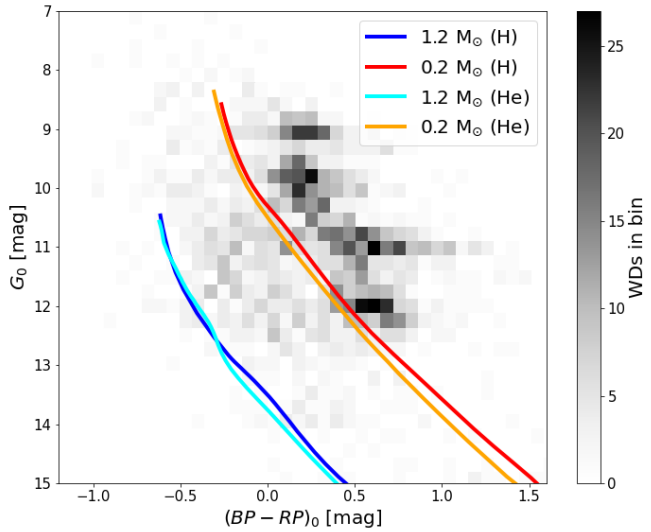

Fig. 4. 2D density WD histogram obtained from the initial WD sample in the absolute magnitude-color space. The absolute magnitudes and colors for each WD are calculated using the parameters of the cluster of which the WD is a member candidate. Overlaid are the Montreal WD cooling tracks for low-mass and high-mass WDs with H and He atmospheres.

3. Notes on the individual WD-OC pairs

In this section, we list and discuss the obtained OC-WD candidate pairs that passed the astrometric, photometric, and cooling age criteria as described in the previous sections. The figures that illustrate the placement of the WD candidates in the cluster CMD and astrometric phase space are included in the appendix; however, some of the more interesting examples are discussed in this section.

3.1. ASCC 73, ASCC 79, and ASCC 97

ASCC 73, ASCC 79, and ASCC 97 are three OCs discovered in Kharchenko et al. (2005). Due to their relatively recent discovery and sparse nature, they have been studied very little in the literature. No studies of WDs potentially hosted by these clusters have been conducted to date.

Our analysis has recovered one potential cluster WD: GDR2 5856401252012633344 for ASCC 73. On face value, it seems to be a mild outlier from the other cluster members as cataloged by Cantat-Gaudin et al. (2018a), both in terms of proper motion and parallax. However, considering the astrometric uncertainties of the WD candidate, it is still consistent with cluster membership.

For ASCC 79, we have found three possible cluster WDs: GDR2 5825203021908148480, 5826384584601681152, and 5825187834899772160. However, it needs to be noted that the probability of the last object being a WD, as given in Gentile Fusillo et al. (2019), is only $P_{wd} = 0.59$.

Gaia DR2 4092407537313874048 has been identified as a viable candidate for ASCC 97. While its astrometric properties are consistent with cluster membership, its WD nature is ambiguous ($P_{wd} = 0.47$ in Gentile Fusillo et al. 2019).

3.2. Alessi 3

Alessi 3 is a sparse evolved OC (or OC remnant; Angelo et al. 2019). Its WD content has not been studied before.

We have identified one cluster WD candidate: GDR2 5508976051738818176. Its astrometric properties are consistent with cluster membership, but its parallax puts it into the cluster background if taken at face value. However, the parallax error is very high, and a number of cluster members lie within 1σ of the cluster WD candidate's parallax.

3.3. Alessi 13

Alessi 13 (χ^{01} For moving group) is a sparse nearby stellar association. Its WD content has never been studied.

We have identified one possible WD cluster member: GDR2 4853382867764646912. Its astrometric properties are consistent with cluster membership.

3.4. Alessi 62

Alessi 62 is another unstudied old OC. No WDs that are potential members of this cluster are known.

Our analysis has yielded one cluster WD candidate: GDR2 4519349757791348480. Its proper motion is consistent with cluster membership; however, its parallax is more problematic as it suffers from a large uncertainty, and, if taken at face value, it puts the member candidate into the background. However, some of the cluster members are still contained with its 1σ uncertainty interval. Its nature as a bona fide WD is ambiguous since Gentile Fusillo et al. (2019) gives a lower $P_{wd} = 0.56$ for this object.

3.5. IC 4756

IC 4756 is a close, intermediate-age OC. Though IC 4756 has been heavily studied, WDs potentially hosted in the cluster have never been investigated in detail in the literature. However, it needs to be noted that by looking at the CMD of the cluster stars listed in Cantat-Gaudin et al. (2018a), one can readily identify a potential WD candidate on the cluster WD sequence. The WD is bright enough to not be excluded in the magnitude cutoff of $G = 18$ mag adopted there.

Our analysis has identified only one viable cluster WD candidate, and it is the same one as discussed above (GDR2 4283928577215973120). Its proper motion and parallax make it a very likely cluster member.

3.6. Mamajek 4

Mamajek 4 is a poorly studied OC. No WD studies targeting this cluster have been conducted.

Our search has identified one potential cluster WD: GDR2 6653447981289591808. Its proper motion is consistent with cluster membership, though its parallax indicates that it may be a background object. However, its parallax error is quite high and a significant portion of the cluster members lie within a 1σ error of the candidate parallax.

3.7. Melotte 22

Melotte 22 (Pleiades) is one of the closest, best-studied, and, arguably, most well-known OCs. Despite its proximity, only one cluster WD has been identified so far: EGGR 25 (GDR2 66697547870378368; Eggen & Greenstein 1965; Lodieu et al. 2019).

Our analysis recovered EGGR 25. However, it failed to identify any new potential cluster WD candidates.

3.8. NGC 2422

NGC 2422 is a rather young (~150 Myr) OC with a current turnoff age of about 5.4 $M_{\odot}$ (Richer et al. 2019). The potential WD content of the cluster was first investigated by Koester & Reimers (1981), who found a potential WD candidate (GDR2 3030026344167186304) that may also be a cluster member. However, they were not able to fully ascertain its nature; while it may be a massive WD that is a member of the cluster, it may also be a field WD behind the cluster or a subdwarf O-type star. Richer et al. (2019) find a massive cluster WD with a helium-rich atmosphere and large magnetic field, probably in a binary with a late-type companion (GDR2 3029912407273360512).

Our analysis only recovered the WD found by Richer et al. (2019), as the other one is not included in the catalog by Gentile Fusillo et al. (2019). However, taking advantage of GDR2 astrometry, it can clearly be seen that the WD member candidate of Koester & Reimers (1981) is most certainly not a cluster member and that it lies in the foreground.

3.9. NGC 2516

NGC 2516 is also a young OC that likely started forming WDs relatively recently. Reimers & Koester (1982) first identified three probable cluster WDs and later added a fourth, the nature of which was previously uncertain (Koester & Reimers 1996). Recently, Holt et al. (2019) have added two more candidate WD members, which were identified using the GDR2.

Our analysis of this cluster identified three sources, one of which was already identified in Reimers & Koester (1982) and the two others in Holt et al. (2019). Thus, no novel detections were made. The other three WDs from Reimers & Koester (1982) and Koester & Reimers (1996) are also included in Gentile Fusillo et al. (2019), but their cluster membership is not solid. GDR2 5290720695823013376 seems to lie in the foreground and GDR2 5290719287073728128 in the background; GDR2 5290834387897642624 is a proper motion outlier but just narrowly did not make the cut.

3.10. NGC 2527

NGC 2527 is an older (~800 Myr) OC with a turnoff mass of ≈2.2–3.5 $M_{\odot}$ (Raddi et al. 2016). A WD that is also a likely cluster member was reported in Raddi et al. (2016).

We did not recover this WD (GDR2 5597874285564810880) as it is not listed in Gentile Fusillo et al. (2019). However, we identified a new candidate. Using the GDR2 astrometry, it can clearly be seen that the WD identified as a cluster member in Raddi et al. (2016) is a significant outlier in both parallax and proper motion, making it a likely field object.

3.11. NGC 2632

NGC 2632 (Praesepe) is a close and well-known OC with a large number of published WDs. It is considered to be a "benchmark" cluster for WD studies, and it is likely that the observed cluster single WD population is complete due to its proximity.

Our analysis recovered all 12 known cluster WDs with no new detections, as expected. A comprehensive analysis of these WDs in the context of their parent cluster is available in a recent analysis by Salaris & Bedin (2019) and the references therein.

3.12. NGC 3532

This rich, ~300 Myr old OC is believed to host a number of WDs. Reimers & Koester (1989) identified seven candidate cluster WDs and confirmed the degenerate nature of three of them. Their subsequent extended survey added three more candidate WD members later on (Koester & Reimers 1993). However, a more detailed analysis by Dobbie et al. (2009) put two of these WDs in the background of the cluster. An expanded survey by Dobbie et al. (2012) identifies several more WD candidates, including another four bona fide WDs in the direction of the cluster, three of which are reportedly cluster members. Furthermore, Raddi et al. (2016) add an additional, very massive WD cluster member.

A combined tally of seven cluster WDs, as obtained from the literature, makes the cluster appealing as one of the benchmark clusters, together with Hyades and Praesepe. However, our detection of only three WD candidate members is seemingly at odds with these reported WD numbers. Crossmatching these literature WDs with the GDR2 and querying them in the WD catalog by Gentile Fusillo et al. (2019), we found that only two of them are listed there: GDR2 5340219811654824448 and GDR2 5338718261060841472; the latter is also a cluster member according to our analysis. Our second identified cluster WD candidate is also among the cluster members reported in Cantat-Gaudin et al. (2018a) – GDR2 5340220262646771712 – with a reported membership probability of 1.0; it actually lies at the beginning of the WD cooling sequence. This makes it a solid WD candidate that must have formed very recently. The last detected source – GDR2 5338685962923467136 – is a new candidate cluster WD.

All of the reported cluster WDs, with the exception of the massive WD identified in Raddi et al. (2016), have a GDR2 counterpart with a full five-parameter solution. Despite them not being in the catalog of Gentile Fusillo et al. (2019), we can still assess their cluster membership. Figure 5 shows that the literature WDs have astrometric properties that are consistent with the cluster membership. The only exception is GDR2 5340148691289324416 (reported as a member in Dobbie et al. 2012), whose cluster membership, which is based on its astrometric properties, can be disputed. Another interesting case is GDR2 5338650984675000448 (cluster member according to Reimers & Koester 1989; also listed in Gentile Fusillo et al. 2019), which seems too luminous and red to be a cluster member.

3.13. NGC 6633

NGC 6633 is a loose OC with various age estimates, ranging from 430 Myr (Dias et al. 2002) to 800 Myr (our estimate from isochrone fitting). Reimers & Koester (1994) investigated possible WD candidates in the field of the cluster and found one (GDR2 4477214475044842368) that may be a cluster member, but they were not able to confirm its cluster membership. A later study by Williams & Bolte (2007) found two more WDs at the cluster distance modulus (GDR2 4477166581862672256 and GDR2 4477253202776118016) and another two (GDR2 4477214475044842368 and GDR2 4477168746525464064) that appear too bright to be cluster members if single, but could potentially be double degenerate systems belonging to the cluster. One of them had already been identified as a WD member candidate in Reimers & Koester (1994).

Our analysis yielded two WD member candidates: GDR2 4477214475044842368 and GDR2 4476643725433841920; one

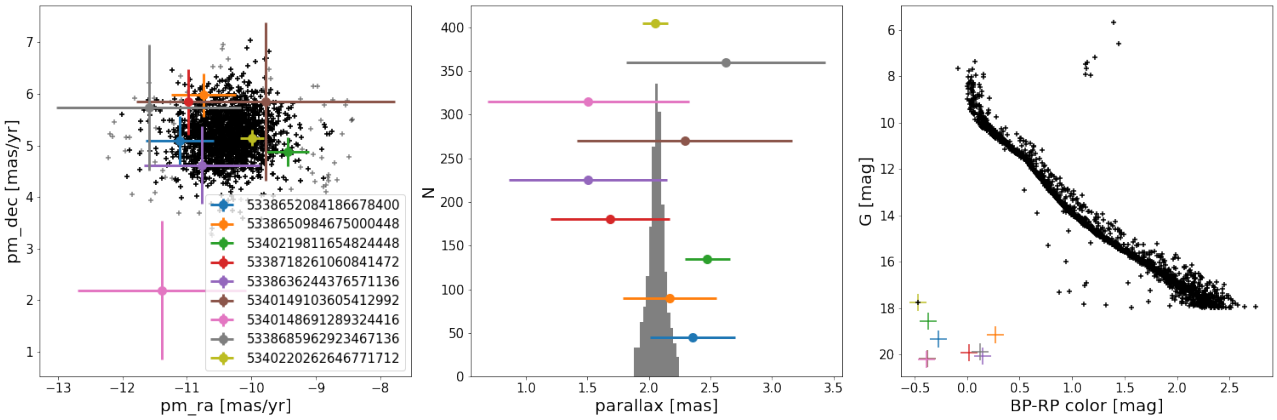

Fig. 5. *Left*: proper motion diagram of the NGC 3532 stars with the recovered and literature WD proper motion overlaid. Cluster stars with cluster membership probability <0.5 are marked using gray crosses, while black crosses indicate likely cluster members. Here, and in the subsequent graphs, the errorbars indicate a 1σ uncertainty, as reported in the GDR2. Errorbars for the cluster stars are omitted for clarity. *Middle*: parallax histogram of the cluster member stars (membership probability ≥0.5) with WD parallaxes overlaid. *Right*: cluster member star CMD with WDs overlaid.

was already known and one is a novel detection. Out of the two WD member candidates identified in Williams & Bolte (2007), we identified one as a cluster member in our analysis. Neither of them is included in Gentile Fusillo et al. (2019). *Gaia* DR2 4477166581862672256 has a parallax and proper motion consistent with cluster membership. The other, which was thought to be a rare DB cluster WD, is a clear outlier in terms of both parallax and proper motion. Out of the two potential double degenerate systems (both listed in Gentile Fusillo et al. 2019), only one of them (GDR2 4477214475044842368) has astrometric parameters consistent with cluster membership.

3.14. NGC 6991

NGC 6991 is a relatively unstudied sparse OC. Our literature search for cluster WDs and candidates did not yield any objects that may be associated with this cluster.

We present the identification of a possible cluster WD (GDR2 2166915179559503232). It is a high-confidence WD in Gentile Fusillo et al. (2019), and its proper motion is consistent with other members of the cluster. On face value, its parallax puts it in the foreground of NGC 6991, but the parallax error is rather large so its cluster membership cannot be conclusively assessed this way.

3.15. NGC 7092

NGC 7092 (M 39) is a well-known and well-studied cluster. At the time of writing, Caiazzo et al. (2020) have identified and characterized one cluster WD (GDR2 2170776080281869056).

Our analysis yielded a high-confidence WD that is a possible member of this cluster, the same object as in Caiazzo et al. (2020). The parallax and proper motion of this object matches well with those of the cluster members.

3.16. RSG 7 and RSG 8

RSG 7 and RSG 8 are two of the sparse, close OCs discovered in Röser et al. (2016). The literature on these clusters is very limited, and there are no WDs associated with them.

Our search resulted in three WD candidates that can potentially be assigned to RSG 7, as well as one that could be a member of either RSG 7 or RSG 8 (the double match resulted from a combination of the close proximity of the clusters in the projection on the sky as well as the proper motion space and large parallax uncertainty of the member candidates). However, upon analysis of the proper motion diagram, parallax distribution, and CMDs of the cluster members in Cantat-Gaudin et al. (2018a), we concluded that the parameters of these clusters listed there are erroneous. The issue seems to be a heavy contamination from the members of the adjacent cluster, which is clearly visible and presents as multiple populations in the cluster CMDs. Taking the quality of the astrometric parameters of the candidate WD members into consideration as well, we thus discarded these OC-WD pairs.

3.17. Ruprecht 147

Ruprecht 147 (NGC 6774) is one of the oldest star clusters in the solar neighborhood. Its proximity and age make it attractive as one of the potential benchmark clusters for stellar evolution studies, and WDs in particular. This has been demonstrated by Gaia Collaboration (2018a), who identified ten cluster WDs. A subsequent comprehensive study by Olivares et al. (2019) has added five more, for a total WD tally of 15. A recent study of the cluster by Marigo et al. (2020) rules out the membership of several previously associated WDs based on conflicting spectroscopic and photometric luminosities, but it adds one new cluster WD not listed in Gentile Fusillo et al. (2019)

Our analysis identified nine cluster WD candidates, none of which are new detections; this is not surprising given the depth of the previous studies. However, we decided to discard three member candidates – GDR2 4183847562828165248, GDR2 4184148073089506304, and GDR2 4184196073644880000 – which are all members according to Gaia Collaboration (2018a) and Olivares et al. (2019) but are found to be non-members in Marigo et al. (2020). Therefore, we retained six potential WD members. One of the WDs from Olivares et al. (2019) is not included in Gentile Fusillo et al. (2019), and five of them are slight proper motion outliers with respect to the cluster members of Cantat-Gaudin et al. (2018a), with one of the WDs just narrowly inside the margin delineated by our selection criteria.

3.18. Stock 2

Stock 2 is a nearby OC. Despite its proximity, it is relatively unstudied due to its large angular size and the variable reddening in its direction (Spagna et al. 2009). Its age is disputed, so we estimated the cluster age to be $\log(t) = 8.5$. Stock 2 was one of the clusters studied in Gaia Collaboration (2018a), who identify eight cluster WD candidates.

Our analysis managed to identify 16 WD candidates with parameters consistent with cluster membership. Out of these, ten are new detections, while the remaining six were identified in Gaia Collaboration (2018a). There are two extra cluster WD candidates contained in Gaia Collaboration (2018a) that were not recovered in our analysis, despite them being listed in Gentile Fusillo et al. (2019): GDR2 508400329710144896 and GDR2 506848643933335296. The parallaxes of these two objects are not consistent with cluster membership.

3.19. Stock 12

Stock 12 is a poorly studied cluster, the WD content of which has never been studied before. We uncovered only one novel WD member candidate: GDR2 1992469104239732096.

4. Reliability of the GDR2 solution

The GDR2 provides high-quality astrometric and photometric measurements for an unprecedented number of sources. However, it still contains some solutions that are ill-behaved and need to be accounted for or removed from the analysis. Problems with the astrometry and photometry can arise for sources that are located in regions with high source densities, for instance in the Galactic plane and star clusters. Binary systems can also be problematic because GDR2 sources are treated as single stars in the astrometric solution, whereas binaries do not receive any special treatment (Gaia Collaboration 2018b; Lindegren et al. 2018). We therefore examined the quality of the GDR2 solutions for the recovered WD member candidates.

Gentile Fusillo et al. (2019) have conducted some cleaning of their WD sample, identifying many potentially spurious sources. However, in order to obtain a reliable list of WD member candidates, we further cleaned the WD sample based on the recommended astrometric and photometric flags. Informed by Gaia Collaboration (2018b), Lindegren et al. (2018) and Lindegren (2018; GAIA-C3-TN-LU-LL-124-01[3]), we retained the sources that satisfied the following three conditions: (a) duplicated_source = False; (b) astrometric_excess_noise < 1 mas or astrometric_excess_noise_sig < 2; and (c) ruwe < 1.4.

Specifically, the flag `duplicated_source=True` implies observational problems, crossmatching problems, processing problems, or stellar multiplicity, potentially leading to problems in the astrometric solution. The `astrometric_excess_noise` (ϵ_i) is the excess astrometric noise of the source postulated to explain the scatter of residuals in the astrometric solution. When it is high and significant, it can mean that the astrometric solution has failed for that source. Another possibility is that the observed source is a binary system, where the additional scatter can arise from the movement of the emission centroid due to the motion of the binary components. Finally, the cuts based on `ruwe`, which stands for renormalized unit weight error, ensured the removal of ill-behaved astrometric solutions.

[3] http://www.rssd.esa.int/doc_fetch.php?id=3757412

None of the selected WD candidates exhibited increased astrometric noise or `ruwe` values; however, three of them (GDR2 4519349757791348480, GDR2 5338685962923467136, and GDR2 511159317926025600) were possible duplicated sources. These objects were then removed from the candidate list.

In order to identify the cases where the photometry is unreliable, we applied the following two quality indicators, as given in Gaia Collaboration (2018a): (a) phot_bp_rp_excess_factor $>1.0 + 0.015(G_{BP} - G_{RP})^2$ and (b) phot_bp_rp_excess_factor $<1.3 + 0.06(G_{BP} - G_{RP})^2$. The WDs that did not satisfy the above criteria were retained as member candidates, but we did not estimate their characteristics as the photometry cannot be considered reliable.

5. Parameter estimates for the recovered WD member candidates

In order to establish precise WD parameters, spectroscopic studies are usually needed. In addition to atmospheric parameters such as effective temperature, surface gravity, and chemical composition, spectroscopic data provide an additional check for cluster membership by comparing the WD spectroscopic-based luminosity with the luminosity derived from photometry when the cluster distance and extinction is adopted. Furthermore, spectroscopy is required to ascertain the WD atmospheric composition (unless ultraviolet photometry is available) and binarity status. Unfortunately, most of the new WD member candidates lack the needed spectroscopic data. However, we can assume that most of the recovered WDs are of the DA type, which is overwhelmingly the most dominant WD type found in OCs due to their typical ages, while only a handful of DB cluster WDs are known in the literature (e.g., Kalirai et al. 2005; Salaris & Bedin 2019; Marigo et al. 2020). Under this assumption, the GDR2 photometry enables us to compute the WD absolute magnitudes and colors, adopting the cluster distance and reddening. From these, the photometric-based estimates of WD parameters, such as mass $M_{\rm WD}$ and cooling age $t_{\rm cool}$, can be derived.

While the Montreal WD cooling tracks were used for the photometric selection of viable OC WDs and can, in principle, be used to compute $M_{\rm WD}$ and $t_{\rm cool}$ estimates, they suffer from several shortcoming that can affect these estimates. Notably, they do not include the effects of residual nuclear burning, which can have a significant impact on the derived $t_{\rm cool}$ (Iben & Tutukov 1984; Camisassa et al. 2015; Althaus et al. 2010). Additionally, the Montreal WD cooling tracks assume unrealistic WD core compositions and do not include the impact of the energy release resulting from phase separation on crystallization, which also affects the derived $t_{\rm cool}$. Then, to compute $M_{\rm WD}$ and $t_{\rm cool}$, we used a combination of models, employing the tool from Cheng (2020). For the WDs with masses of $0.45\,M_\odot \lesssim M_{\rm WD} \lesssim 1.0\,M_\odot$, we used the model from Renedo et al. (2010) with a metallicity of $Z = 0.01$, which is suitable for the solar neighborhood. For the high-mass WDs ($M_{\rm WD} \gtrsim 1.0\,M_\odot$), we adopted the model from Camisassa et al. (2019), in which such WDs are expected to be harboring O-Ne cores. In order to account for the errors in absolute magnitude and color, we performed a 10^4-element Monte Carlo simulation for each WD, interpolating the $M_{\rm WD}$ and $t_{\rm cool}$ from the cooling tracks each time. For the simulations, we drew absolute magnitude and color samples from normal distributions (assumed to be independent), which are centered around the measured values and 1σ errors. We defined our 1σ absolute magnitude and color errors by adding in quadrature the error from the distance modulus (in the case of absolute magnitude), reddening, and instrumental errors. Resulting

Table 2. Novel or newly characterized WD-OC pairs recovered in this analysis.

GDR2 source ID	Associated cluster	$P_{\rm WD}$	$\log t_{\rm cl}$ (yr)	[Fe/H]	[M/H]	$M_{\rm WD}$ ($M_\odot$)	$t_{\rm cool}$ (Gyr)
5856401252012633344	ASCC 73	0.867	8.190			$0.64^{+0.12}_{-0.11}$	$0.097^{+0.037}_{-0.03}$
5825203021908148480	ASCC 79	0.961	6.950			$0.37^{+0.13}_{-0.08}$	$0.007^{+0.004}_{-0.004}$
5826384584601681152	ASCC 79	0.916	6.950			$0.33^{+0.09}_{-0.06}$	$0.008^{+0.002}_{-0.005}$
5825187834899772160	ASCC 79	0.594	6.950			$0.29^{+0.07}_{-0.03}$	$0.01^{+0.002}_{-0.003}$
4092407537313874048	ASCC 97	0.465	7.900		0.129 ± 0.166	$0.24^{+0.06}_{-0.04}$	$0.035^{+0.023}_{-0.01}$
5508976051738818176	Alessi 3	0.995	8.870		-0.275 ± 0.065	$0.81^{+0.09}_{-0.09}$	$0.638^{+0.128}_{-0.109}$
4853382867764646912	Alessi 13	0.998	8.720		0.06 ± 0.15	$0.57^{+0.08}_{-0.08}$	$0.568^{+0.076}_{-0.07}$
4283928577215973120	IC 4756	0.986	8.987	-0.02 ± 0.01		$0.34^{+0.14}_{-0.07}$	$0.011^{+0.005}_{-0.006}$
6653447981289591808	Mamajek 4	0.990	8.824	0.09 ± 0.08		$0.85^{+0.11}_{-0.12}$	$0.282^{+0.073}_{-0.061}$
5289447182180342016	NGC 2516 [a]	0.999	8.475	0.08 ± 0.01		$0.71^{+0.21}_{-0.17}$	$0.149^{+0.069}_{-0.052}$
5294015515555860608	NGC 2516 [a]	0.998	8.475	0.08 ± 0.01		$0.98^{+0.11}_{-0.11}$	$0.077^{+0.027}_{-0.025}$
5597682038533250304	NGC 2527	0.996	8.910	-0.1 ± 0.04		–	–
5340220262646771712	NGC 3532	0.989	8.650	-0.07 ± 0.10		$0.5^{+0.12}_{-0.12}$	$0.3^{+0.061}_{-0.063}$
4476643725433841920	NGC 6633	0.532	8.900	-0.098 ± 0.037		$0.58^{+0.17}_{-0.16}$	$0.157^{+0.061}_{-0.055}$
2166915179559503232	NGC 6991	0.998	9.100	0.0 ± 0.03		$0.56^{+0.14}_{-0.12}$	$0.023^{+0.013}_{-0.012}$
4183928888026931328	Ruprecht 147	0.996	9.330	0.16 ± 0.08		$0.49^{+0.27}_{-0.19}$	$0.162^{+0.091}_{-0.078}$
4183926006112672768	Ruprecht 147	0.955	9.330	0.16 ± 0.08		$0.49^{+0.11}_{-0.12}$	$0.481^{+0.076}_{-0.066}$
5065149077856230 40	Stock 2	0.939	8.500	-0.06 ± 0.03		$0.37^{+0.11}_{-0.08}$	$0.306^{+0.046}_{-0.045}$
5082767033717249 28	Stock 2	0.980	8.500	-0.06 ± 0.03		$0.39^{+0.48}_{-0.19}$	$0.169^{+0.159}_{-0.117}$
5070548066570429 44	Stock 2	0.999	8.500	-0.06 ± 0.03		$0.83^{+0.07}_{-0.08}$	$0.069^{+0.023}_{-0.018}$
5071051436709066 24	Stock 2	0.976	8.500	-0.06 ± 0.03		$0.63^{+0.07}_{-0.06}$	$0.234^{+0.043}_{-0.031}$
5071192655233871 36	Stock 2	0.995	8.500	-0.06 ± 0.03		–	–
5075559047795760 64	Stock 2	0.977	8.500	-0.06 ± 0.03		$0.35^{+0.05}_{-0.05}$	$0.118^{+0.018}_{-0.016}$
5068620785837090 56	Stock 2	0.999	8.500	-0.06 ± 0.03		$0.86^{+0.07}_{-0.08}$	$0.041^{+0.017}_{-0.013}$
4587789275734471 68	Stock 2	0.997	8.500	-0.06 ± 0.03		$0.48^{+0.09}_{-0.09}$	$0.069^{+0.021}_{-0.018}$
5073620127754155 52	Stock 2	0.990	8.500	-0.06 ± 0.03		$0.5^{+0.07}_{-0.07}$	$0.153^{+0.027}_{-0.029}$
5074140677822888 96	Stock 2	0.984	8.500	-0.06 ± 0.03		$0.29^{+0.02}_{-0.02}$	$0.028^{+0.004}_{-0.005}$
4580664096831983 36	Stock 2	0.994	8.500	-0.06 ± 0.03		$0.41^{+0.07}_{-0.05}$	$0.098^{+0.022}_{-0.014}$
4639372820755476 48	Stock 2	0.994	8.500	-0.06 ± 0.03		$0.36^{+0.05}_{-0.04}$	$0.065^{+0.012}_{-0.01}$
5071283321970813 44	Stock 2	0.861	8.500	-0.06 ± 0.03		$0.36^{+0.06}_{-0.05}$	$0.278^{+0.036}_{-0.03}$
5072778700801866 24	Stock 2	0.899	8.500	-0.06 ± 0.03		–	–
5068647930089016 32	Stock 2	0.698	8.500	-0.06 ± 0.03		$0.3^{+0.12}_{-0.08}$	$0.284^{+0.052}_{-0.054}$
5072218637019892 48	Stock 2	0.887	8.500	-0.06 ± 0.03		–	–
1992469104239732096	Stock 12	0.999	8.450			$0.35^{+0.44}_{-0.15}$	$0.127^{+0.176}_{-0.096}$

Notes. $P_{\rm WD}$ is the probability of the object being a WD, adopted from Gentile Fusillo et al. (2019), $\log t_{\rm cl}$ is the cluster age, and [Fe/H]/[M/H] is the cluster metallicity. Assuming that all recovered WDs are of the DA type, $M_{\rm WD}$ and $t_{\rm cool}$ are WD mass and WD cooling age estimates, respectively. [a]Recovered in Holt et al. (2019) but not characterized. Missing values of $M_{\rm WD}$ and $t_{\rm cool}$ for some objects are due to GDR2 photometry problems for these objects.

References. OC metallicities: Bagdonas et al. (2018), Baratella et al. (2020), Carrera et al. (2019), Conrad et al. (2014), Fritzewski et al. (2019), Netopil et al. (2016), Netopil (2017), Reddy & Lambert (2019), Zhang et al. (2019).

$M_{\rm WD}$ and $t_{\rm cool}$ estimates and their errors for the novel or newly characterized WDs are listed in Table 2, where the listed values correspond to the median values obtained from the simulations and the quoted errors are derived from the 68% confidence intervals.

It is apparent that we recovered mostly intermediate- and low-mass WD members. This is understandable when the properties of massive ($\gtrsim 0.9\,M_\odot$) WDs and the magnitude limit of *Gaia* are considered. The highest-mass WDs are less luminous and cool more rapidly than their lower-mass counterparts. Thus, they remain bright enough for *Gaia* only in the closest and youngest OCs. Additionally, high-mass WDs can be ejected from their parent OC due to the potential velocity kicks imparted on them during their formation by asymmetric mass-loss or dynamical interactions with other OC stars (Fellhauer et al. 2003; Tremblay et al. 2012). Last, the number of young OCs potentially hosting sufficiently bright massive WDs in the solar neighborhood is low. Therefore, also taking the degradation of the astrometry and photometry quality of *Gaia* when approaching its magnitude limit into consideration, only very few massive WDs are recovered by our approach, as expected.

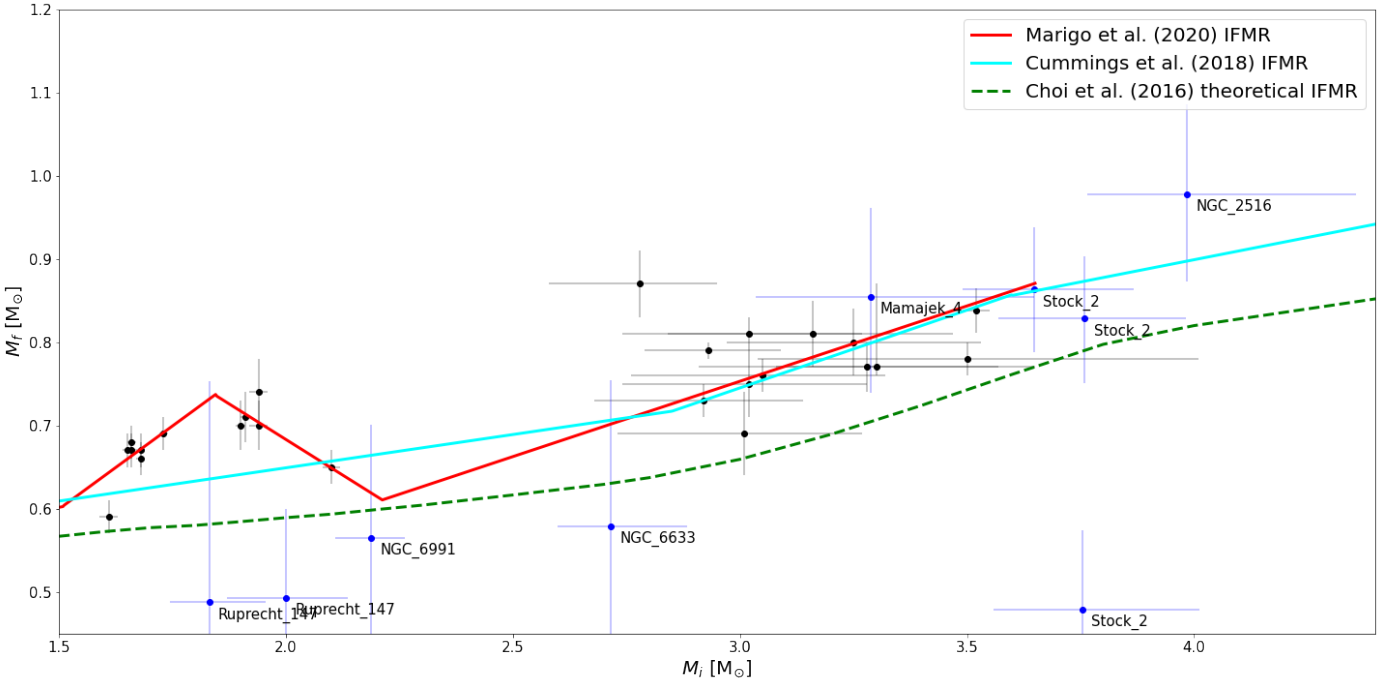

Fig. 6. Semi-empirical IFMRs in the range of M_i from 1.5 to 4.4 $M_\odot$. The data points include the newly recovered and characterized WD OC members (in blue, with parent OC labeled, Table 4) and the previously published OC WDs from Table 3 and Marigo et al. (2020) (in black). The four-piece IFMR fit (red) is adopted from Marigo et al. (2020). The cyan line represents the IFMR fit adopted from Cummings et al. (2018), and the dashed green line is the theoretical IFMR derived from Choi et al. (2016).

Table 3. Recovered WD-OC associations previously discussed in the literature.

GDR2 source id	Associated cluster	Refs.
66697547870378368	Melotte 22	Eggen & Greenstein (1965)
3029912407273360512	NGC 2422	Richer et al. (2019)
5289447182180342016	NGC 2516	Holt et al. (2019)
5294015515555860608	NGC 2516	Holt et al. (2019)
5290767695648992128	NGC 2516	Reimers & Koester (1982)
659494049367276544	NGC 2632	Salaris & Bedin (2019)
661841163095377024	NGC 2632	Salaris & Bedin (2019)
665139697978259200	NGC 2632	Salaris & Bedin (2019)
664325543977630464	NGC 2632	Salaris & Bedin (2019)
662798086105290112	NGC 2632	Salaris & Bedin (2019)
661297901272035456	NGC 2632	Salaris & Bedin (2019)
661353224747229184	NGC 2632	Salaris & Bedin (2019)
662998983199228032	NGC 2632	Salaris & Bedin (2019)
661270898815358720	NGC 2632	Salaris & Bedin (2019)
661010005319096192	NGC 2632	Salaris & Bedin (2019)
660178942032517760	NGC 2632	Salaris & Bedin (2019)
661311267210542080	NGC 2632	Salaris & Bedin (2019)
5338718261060841472	NGC 3532	Koester & Reimers (1993)
4477214475044842368	NGC 6633	Reimers & Koester (1994)
2170776080281869056	NGC 7092	Caiazzo et al. (2020)
4088108859141437056	Ruprecht 147	Marigo et al. (2020)
4087806832745520128	Ruprecht 147	Marigo et al. (2020)
4183919237232621056	Ruprecht 147	Marigo et al. (2020)
4184169822810795648	Ruprecht 147	Marigo et al. (2020)

6. IFMR

Using the previously obtained $M_{\rm WD}$ and $t_{\rm cool}$ values and supplementing them with the values obtained from the literature, we can investigate the IFMR. In the IFMR analysis, an accurate determination of the OC age is critical. This is particularly true for young OCs with young WDs, where the derived masses of the WD progenitors are very sensitive to the evolutionary time, which is derived from the OC age and WD cooling age.

We are interested in objects that have undergone single-star evolution, so we restricted the analysis to objects with $M_{\rm WD} > 0.45\,M_\odot$. Below this mass boundary, all objects are thought to be the product of close binary evolution (Tremblay et al. 2016).

If the cluster age $t_{\rm cl}$ and the WD cooling age $t_{\rm cool}$ are known, the lifetime of the progenitor can be given by $t_{\rm prog} = t_{\rm cl} - t_{\rm cool}$. To calculate the progenitor mass from $t_{\rm prog}$, an approximate mass-luminosity relation is commonly used for back-of-the-envelope calculations:

$$L/L_\odot \sim (M/M_\odot)^\alpha\,. \tag{5}$$

In order to obtain more credible results, we used PARSEC version 1.2S (Bressan et al. 2012) and COLIBRI S_35 (Pastorelli et al. 2019) isochrones[4] to determine the initial mass of the progenitor. For each WD, we performed 100 Monte Carlo simulations, each time drawing a value from the normal distribution of $t_{\rm cl}$, cluster metallicity, and $t_{\rm cool}$ distribution obtained in the previous section. All distributions were assumed to be independent. Since $t_{\rm cl}$ measurements generally lack uncertainties, the 1σ error for $t_{\rm cl}$ was assumed to be 10% of its measured value. The metallicity distribution was also centered on its measured value, with 1σ being its uncertainty as adopted from the literature. The initial progenitor masses M_i and their errors were obtained in the same way as $M_{\rm WD}$ and $t_{\rm cool}$ in the previous section. The resulting IFMR is plotted in Fig. 6.

It can be seen from Fig. 6 that the newly characterized WDs are consistent with the nonlinear IFMR from Marigo et al. (2020), with a kink located over $1.65\,M_\odot \lesssim M_i \lesssim 2.1\,M_\odot$, which

[4] http://stev.oapd.inaf.it/cgi-bin/cmd_3.3

Table 4. Initial progenitor masses M_i for the newly characterized WDs in Fig. 6.

GDR2 source id	Associated cluster	M_i ($M_\odot$)
6653447981289591808	Mamajek 4	$3.3^{+0.4}_{-0.3}$
5294015515555860608	NGC 2516	$4.0^{+0.4}_{-0.2}$
4476643725433841920	NGC 6633	$2.7^{+0.2}_{-0.1}$
2166915179559503232	NGC 6991	$2.2^{+0.1}_{-0.1}$
4183928888026931328	Ruprecht 147	$1.8^{+0.1}_{-0.1}$
4183926006112672768	Ruprecht 147	$2.0^{+0.1}_{-0.1}$
507054806657042944	Stock 2	$3.8^{+0.3}_{-0.2}$
506862078583709056	Stock 2	$3.6^{+0.2}_{-0.2}$
458778927573447168	Stock 2	$3.8^{+0.3}_{-0.2}$

they interpreted as a signature of the lowest-mass stars in the Galaxy that become carbon stars during the thermally pulsing asymptotic giant branch phase. Of particular interest are the WDs hosted by NGC 6991 and NGC 6633, which fall into the IFMR dip that, until then, had not been sufficiently characterized. There are also other WDs that fall into this gap (members of IC 4756, Alessi 62, and NGC 2527), which were either below the mass cutoff or had problems in their GDR2 parameters. The three-piece IFMR fit from Cummings et al. (2018) and the theoretical IFMR adopted from Choi et al. (2016) are also shown in Fig. 6. It can be seen that the IFMR fits of Marigo et al. (2020) and Cummings et al. (2018) are almost identical from $M_i \gtrsim 2.9\,M_\odot$.

Apart from the IFMR kink at $1.65\,M_\odot \lesssim M_i \lesssim 2.1\,M_\odot$, there is a visible offset between the theoretical and observed masses from approximately $M_i \gtrsim 3.0\,M_\odot$, where the observed WD masses are $\sim$0.1 $M_\odot$ more massive than predicted, as has been noted in Cummings et al. (2018). Cummings et al. (2019) have later attributed this offset mainly to the effects of convective-core overshoot and rotational mixing in the main-sequence progenitors, where the rotational effects are not taken into consideration in the theoretical IFMR models. The newly characterized OC WDs with $M_i \gtrsim 3.0\,M_\odot$ also continue to follow this trend, being $\sim$0.1 $M_\odot$ more massive than what the theoretical IFMRs (e.g., Choi et al. 2016) predict.

Other WDs below the IFMR fit are most likely binaries, or possibly foreground objects, that have been incorrectly assigned to the OC. Interestingly, Stock 2 seems to host a large number of WDs scattered in the IFMR; some of them follow the IFMR fit by Marigo et al. (2020), but others are clustered around $M_{\rm WD} = 0.4\,M_\odot$. Such WDs may be members of binary systems. Additional scatter can be attributed to the effects of strong and variable extinction, which has been noted for this cluster (Spagna et al. 2009).

White dwarfs are the final products of the evolution of stars with initial masses (assuming solar metallicity) less than 8–10 $M_\odot$ (Langer 2012; Smartt 2009); however, in binary systems, the initial mass for one of the components can be as high as 15 $M_\odot$ (Wellstein et al. 2001) or as low as 6 $M_\odot$ (Podsiadlowski et al. 2004). Finding a high-mass WD in a young OC can help identify initial masses for stars that undergo electron-capture SNe. We managed to identify one potential high-mass WD in NGC 2516. However, its cooling time only suggests a $\sim$4 $M_\odot$ progenitor. Due to the shortcomings of this analysis, as described above, we did not recover any other high-mass WDs and are therefore unable to put any new constraints on the boundary between neutron stars and WD formation.

7. Summary and conclusions

We searched for new potential WDs that are possible OC members using the WD catalog by Gentile Fusillo et al. (2019) and the OC catalog by Cantat-Gaudin et al. (2018a), both based on GDR2 data. Such associations are very valuable as ascertaining the membership of a WD to an OC allows us to adopt the OC distance to the WD. This distance is more precise than the distance determined from the WD parallax by itself as it is based on a large number of stars and because the WD parallaxes in the GDR2 exhibit high uncertainties due to their faintness and blue colors. This enables a more precise determination of the WD parameters. Furthermore, the nature of OCs as a coeval group of stars with a common origin allows us to study a number of topics, such as IFMR and metallicity effects.

Our study confirmed the cluster membership of several literature WD cluster members and uncovered a number of new associations. On the other hand, there are a lot of established literature OC WDs that do not seem to satisfy the astrometric and photometric criteria for cluster membership in the GDR2. Removing them from IFMR studies may alleviate the scatter that is present in the data.

The derived WD and progenitor masses of the novel WDs are broadly in line with the IFMR fit of Marigo et al. (2020), although a large number of binaries falling below the fit are also likely present. Some of the recovered WDs from NGC 6991 and NGC 6633 fall into the IFMR dip, which has been poorly characterized and deserves further study. There are several WDs lying in this gap that had to be discarded from the analysis due to their low derived masses (possibly due to binarity with a low-mass companion) or problems with the GDR2 photometry or astrometric solution (such as WDs hosted by IC 4756, Alessi 62, and NGC 2527). It could be worthwhile to observe these objects spectroscopically or revisit them in the next *Gaia* data release.

This work showcases the possibilities that precise astrometry can bring to WD studies. Naturally, spectroscopic observations of the WD cluster member candidates are still needed to confirm their WD status and type, as well as to provide more precise parameters and an additional check for cluster membership.

Acknowledgements. This work has made use of data from the European Space Agency (ESA) mission *Gaia* (https://www.cosmos.esa.int/gaia), processed by the *Gaia* Data Processing and Analysis Consortium (DPAC, https://www.cosmos.esa.int/web/gaia/dpac/consortium). Funding for the DPAC has been provided by national institutions, in particular the institutions participating in the *Gaia* Multilateral Agreement. This research has made use of the WEBDA database, operated at the Department of Theoretical Physics and Astrophysics of the Masaryk University.

References

Agertz, O., & Kravtsov, A. V. 2015, ApJ, 804, 18
Althaus, L. G., Córsico, A. H., Isern, J., & García-Berro, E. 2010, A&A Rev., 18, 471
Angelo, M. S., Santos, J. F. C., Corradi, W. J. B., & Maia, F. F. S. 2019, A&A, 624, A8
Anthony-Twarog, B. J. 1982, ApJ, 255, 245
Bagdonas, V., Drazdauskas, A., Tautvaišienė, G., Smiljanic, R., & Chorniy, Y. 2018, A&A, 615, A165
Baratella, M., D'Orazi, V., Carraro, G., et al. 2020, A&A, 634, A34
Bossini, D., Vallenari, A., Bragaglia, A., et al. 2019, A&A, 623, A108
Bressan, A., Marigo, P., Girardi, L., et al. 2012, MNRAS, 427, 127
Caiazzo, I., Heyl, J., Richer, H., et al. 2020, ApJ, 901, L14

Camisassa, M. E., Miller Bertolami, M. M., & Althaus, L. G. 2015, Boletin de la Asociacion Argentina de Astronomia La Plata Argentina, 57, 117
Camisassa, M. E., Althaus, L. G., Córsico, A. H., et al. 2019, A&A, 625, A87
Cantat-Gaudin, T., Jordi, C., Vallenari, A., et al. 2018a, A&A, 618, A93
Cantat-Gaudin, T., Vallenari, A., Sordo, R., et al. 2018b, A&A, 615, A49
Carrera, R., Bragaglia, A., Cantat-Gaudin, T., et al. 2019, A&A, 623, A80
Cheng, S. 2020, WD_models, https://github.com/SihaoCheng/WD_models
Choi, J., Dotter, A., Conroy, C., et al. 2016, ApJ, 823, 102
Claver, C. F., Liebert, J., Bergeron, P., & Koester, D. 2001, ApJ, 563, 987
Conrad, C., Scholz, R. D., Kharchenko, N. V., et al. 2014, A&A, 562, A54
Córsico, A. H., Althaus, L. G., Miller Bertolami, M. M., & Kepler, S. O. 2019, A&A Rev., 27, 7
Cummings, J. D. 2017, in Planetary Nebulae: Multi-Wavelength Probes of Stellar and Galactic Evolution, eds. X. Liu, L. Stanghellini, & A. Karakas, IAU Symp., 323, 157
Cummings, J. D., Kalirai, J. S., Tremblay, P. E., Ramirez-Ruiz, E., & Choi, J. 2018, ApJ, 866, 21
Cummings, J. D., Kalirai, J. S., Choi, J., et al. 2019, ApJ, 871, L18
Dias, W. S., Alessi, B. S., Moitinho, A., & Lépine, J. R. D. 2002, A&A, 389, 871
Dobbie, P. D., Napiwotzki, R., Burleigh, M. R., et al. 2009, MNRAS, 395, 2248
Dobbie, P. D., Day-Jones, A., Williams, K. A., et al. 2012, MNRAS, 423, 2815
Donor, J., Frinchaboy, P. M., Cunha, K., et al. 2018, AJ, 156, 142
Eggen, O. J., & Greenstein, J. L. 1965, ApJ, 141, 83
Evans, D. W., Riello, M., De Angeli, F., et al. 2018, A&A, 616, A4
Fellhauer, M., Lin, D. N. C., Bolte, M., Aarseth, S. J., & Williams, K. A. 2003, ApJ, 595, L53
Fontaine, G., Brassard, P., & Bergeron, P. 2001, PASP, 113, 409
Fritzewski, D. J., Barnes, S. A., James, D. J., et al. 2019, A&A, 622, A110
Gaia Collaboration (Prusti, T., et al.) 2016, A&A, 595, A1
Gaia Collaboration (van Leeuwen, F., et al.) 2017, A&A, 601, A19
Gaia Collaboration (Brown, A. G. A., et al.) 2018a, A&A, 616, A1
Gaia Collaboration (Babusiaux, C., et al.) 2018b, A&A, 616, A10
Gentile Fusillo, N. P., Tremblay, P.-E., Gänsicke, B. T., et al. 2019, MNRAS, 482, 4570
Greggio, L. 2010, MNRAS, 406, 22
Holt, W., Tucker, G., Buckner, A. J., & Sandquist, E. L. 2019, Res. Notes Am. Astron. Soc., 3, 49
Iben, I. Jr, & Tutukov, A. V. 1984, ApJ, 282, 615
Kalirai, J. S., Richer, H. B., Hansen, B. M. S., Reitzel, D., & Rich, R. M. 2005, ApJ, 618, L129
Kharchenko, N. V., Piskunov, A. E., Röser, S., Schilbach, E., & Scholz, R. D. 2005, A&A, 440, 403
Kharchenko, N. V., Piskunov, A. E., Schilbach, E., Röser, S., & Scholz, R. D. 2013, A&A, 558, A53
Koester, D., & Reimers, D. 1981, A&A, 99, L8
Koester, D., & Reimers, D. 1985, A&A, 153, 260
Koester, D., & Reimers, D. 1993, A&A, 275, 479
Koester, D., & Reimers, D. 1996, A&A, 313, 810
Langer, N. 2012, ARA&A, 50, 107
Liebert, J. 1980, ARA&A, 18, 363
Lindegren, L., Hernández, J., Bombrun, A., et al. 2018, A&A, 616, A2
Lodieu, N., Pérez-Garrido, A., Smart, R. L., & Silvotti, R. 2019, A&A, 628, A66
Marigo, P., Cummings, J. D., Curtis, J. L., et al. 2020, Nat. Astron., 4, 1102
Netopil, M. 2017, MNRAS, 469, 3042
Netopil, M., Paunzen, E., Heiter, U., & Soubiran, C. 2016, A&A, 585, A150
Olivares, J., Bouy, H., Sarro, L. M., et al. 2019, A&A, 625, A115
Pancino, E., Lardo, C., Altavilla, G., et al. 2017, A&A, 598, A5
Pasquini, L., Pala, A. F., Ludwig, H. G., et al. 2019, A&A, 627, L8
Pastorelli, G., Marigo, P., Girardi, L., et al. 2019, MNRAS, 485, 5666
Podsiadlowski, P., Langer, N., Poelarends, A. J. T., et al. 2004, ApJ, 612, 1044
Raddi, R., Catalán, S., Gänsicke, B. T., et al. 2016, MNRAS, 457, 1988
Reddy, A. B. S., & Lambert, D. L. 2019, MNRAS, 485, 3623
Reimers, D., & Koester, D. 1982, A&A, 116, 341
Reimers, D., & Koester, D. 1988, A&A, 202, 77
Reimers, D., & Koester, D. 1989, A&A, 218, 118
Reimers, D., & Koester, D. 1994, A&A, 285, 451
Renedo, I., Althaus, L. G., Miller Bertolami, M. M., et al. 2010, ApJ, 717, 183
Richer, H. B., Fahlman, G. G., Rosvick, J., & Ibata, R. 1998, ApJ, 504, L91
Richer, H. B., Kerr, R., Heyl, J., et al. 2019, ApJ, 880, 75
Romanishin, W., & Angel, J. R. P. 1980, ApJ, 235, 992
Röser, S., Schilbach, E., & Goldman, B. 2016, A&A, 595, A22
Salaris, M., & Bedin, L. R. 2018, MNRAS, 480, 3170
Salaris, M., & Bedin, L. R. 2019, MNRAS, 483, 3098
Smartt, S. J. 2009, ARA&A, 47, 63
Spagna, A., Cossu, F., Lattanzi, M. G., & Massone, G. 2009, Mem. Soc. Astron. It., 80, 129
Tinsley, B. M. 1974, PASP, 86, 554
Tremblay, P. E., Schilbach, E., Röser, S., et al. 2012, A&A, 547, A99
Tremblay, P. E., Cummings, J., Kalirai, J. S., et al. 2016, MNRAS, 461, 2100
Vagnozzi, S. 2019, Atoms, 7,
van den Heuvel, E. P. J. 1975, ApJ, 196, L121
Weidemann, V. 1977, A&A, 59, 411
Wellstein, S., Langer, N., & Braun, H. 2001, A&A, 369, 939
Williams, K. 2002, PhD thesis
Williams, K. A., & Bolte, M. 2007, AJ, 133, 1490
Zhang, J., Zhao, J., Oswalt, T. D., et al. 2019, ApJ, 887, 84

Appendix A: Proper motion diagrams, parallax distributions, and CMDs of the OC-WD associations

In this section, we provide the proper motion diagrams, parallax distributions, and CMDs for the rest of the cluster-WD pairs from Sect. 3. They are either novel candidates or were gathered from the literature.

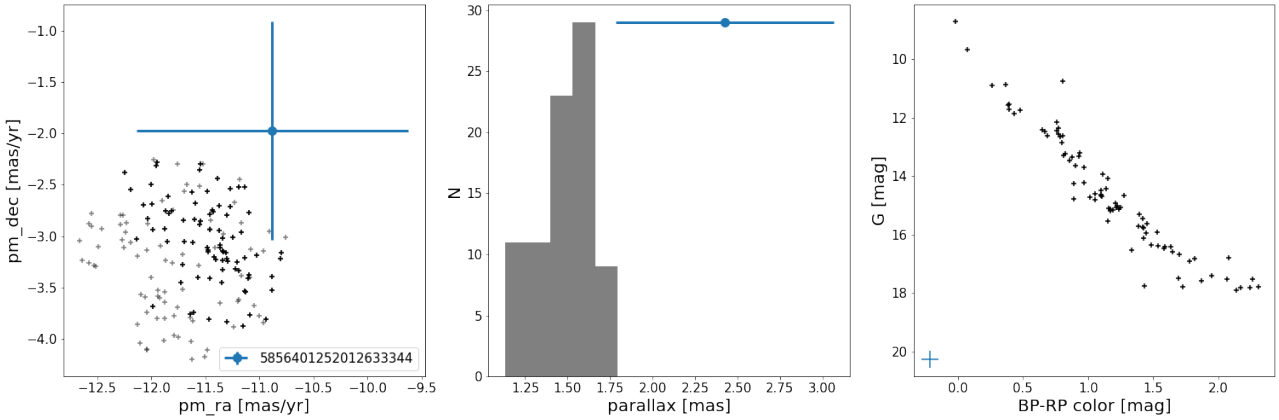

Fig. A.1. Same as in Fig. 5, but for ASCC 73.

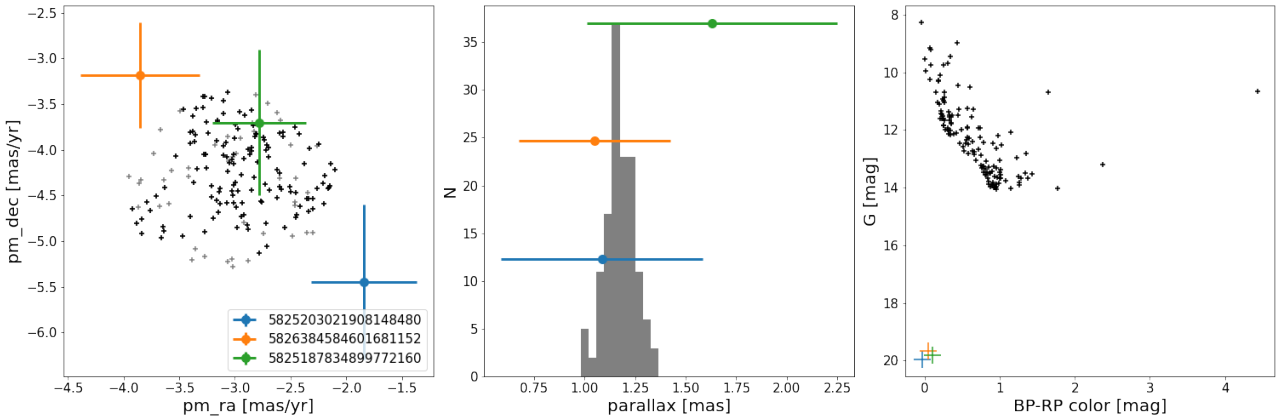

Fig. A.2. Same as in Fig. 5, but for ASCC 79.

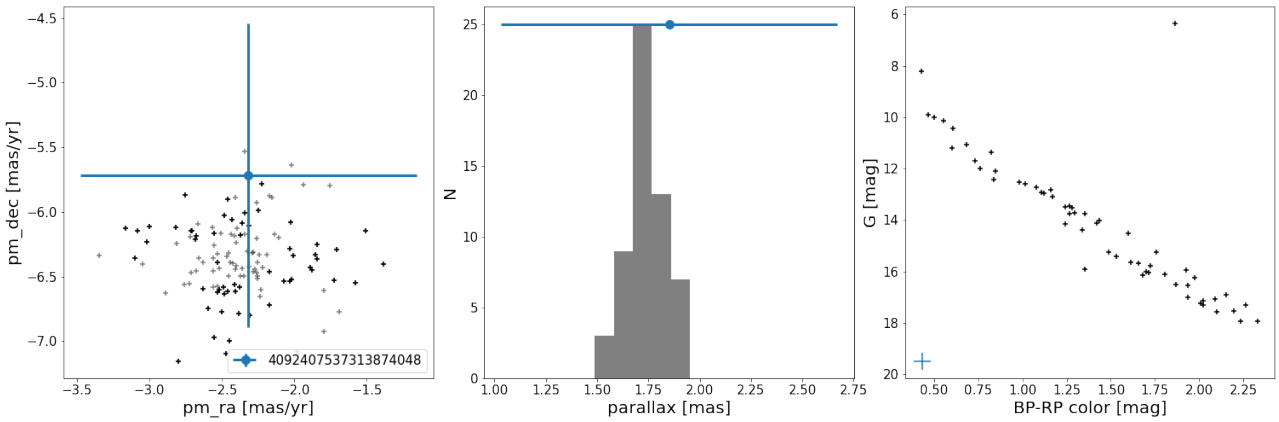

Fig. A.3. Same as in Fig. 5, but for ASCC 97.

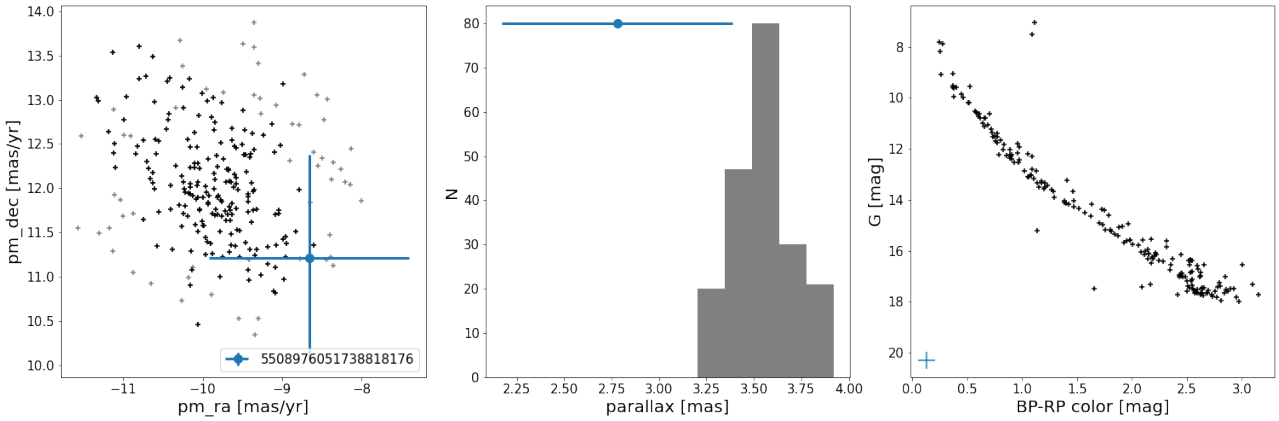

Fig. A.4. Same as in Fig. 5, but for Alessi 3.

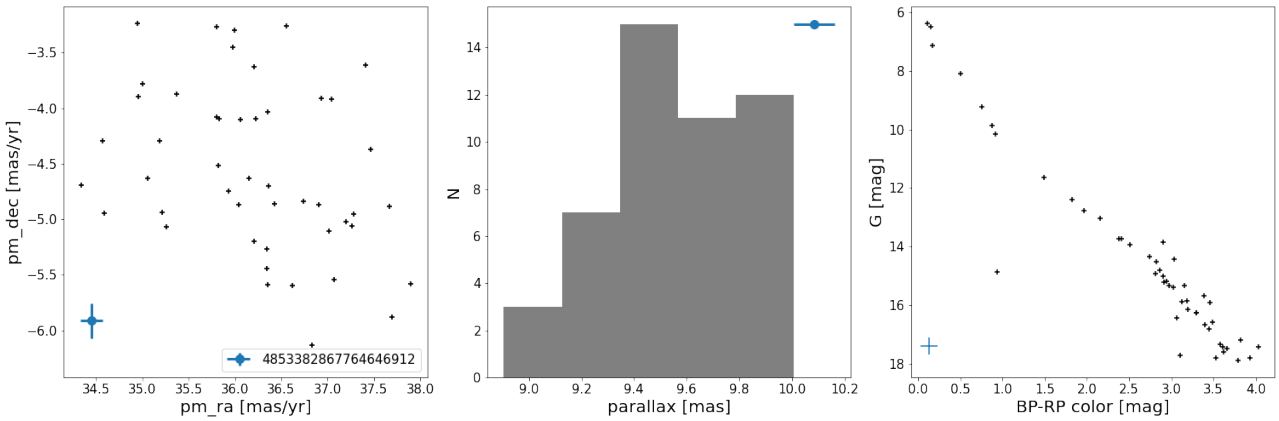

Fig. A.5. Same as in Fig. 5, but for Alessi 13.

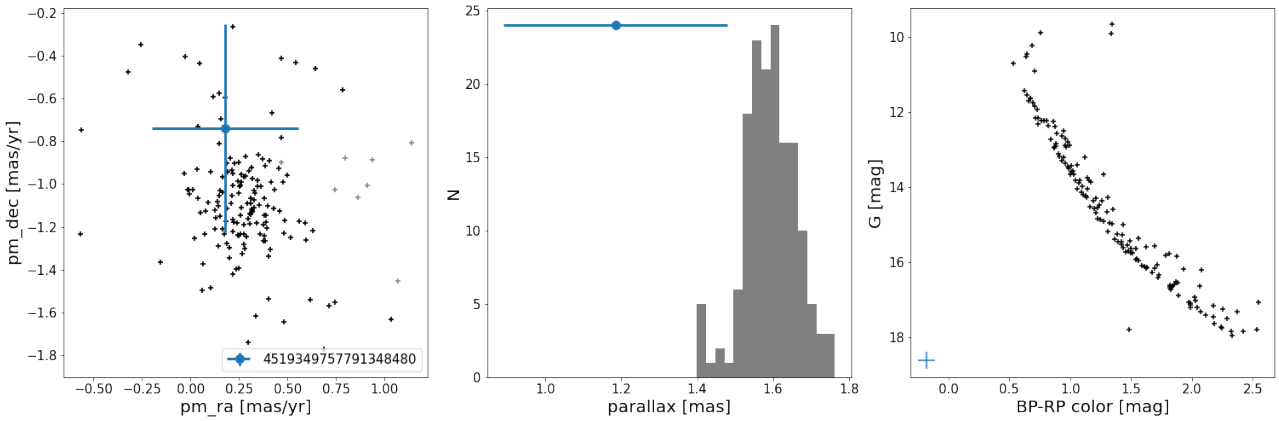

Fig. A.6. Same as in Fig. 5, but for Alessi 62.

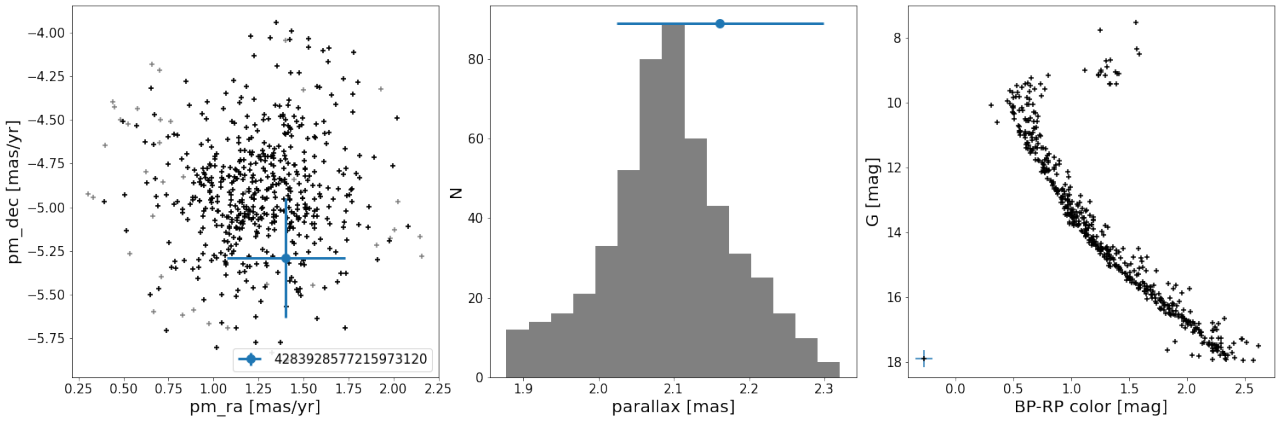

Fig. A.7. Same as in Fig. 5, but for IC 4756.

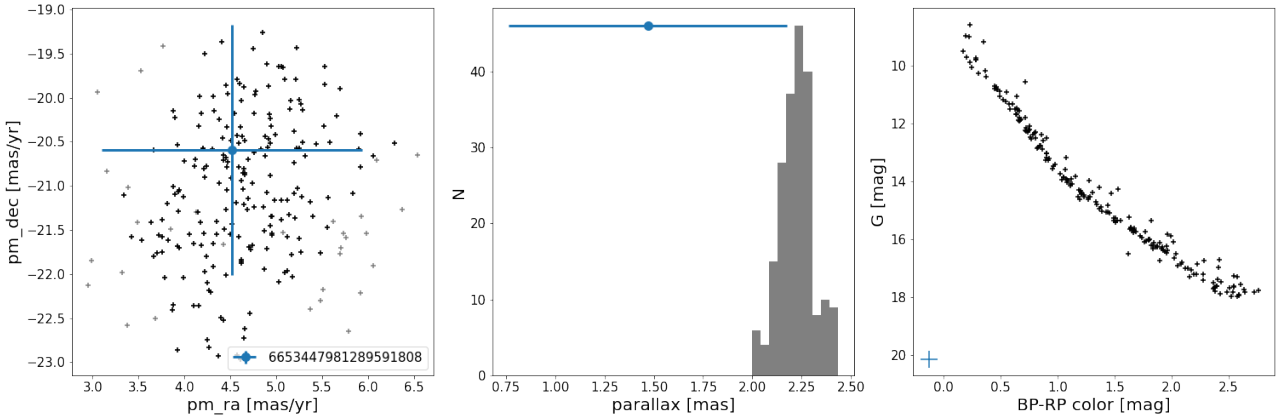

Fig. A.8. Same as in Fig. 5, but for Mamajek 4.

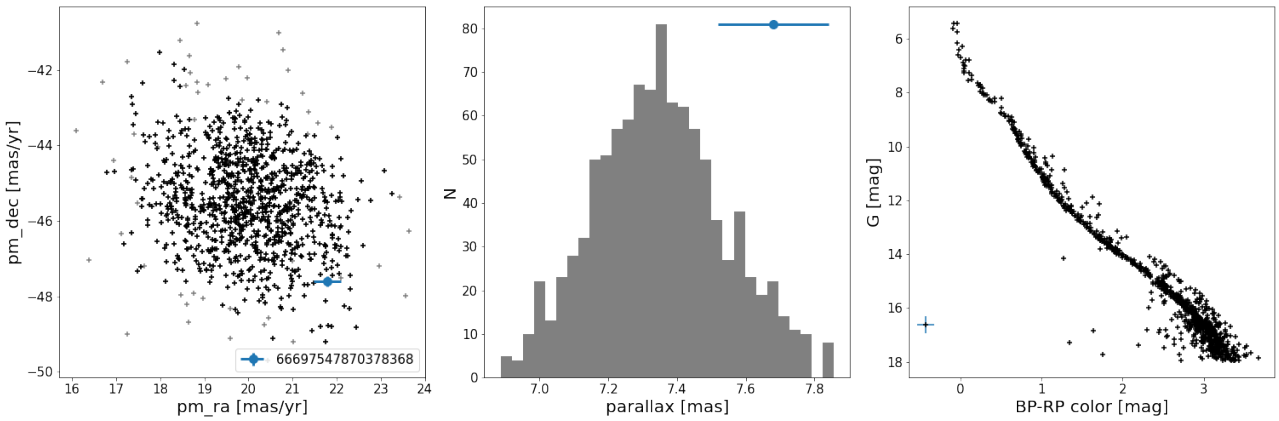

Fig. A.9. Same as in Fig. 5, but for Melotte 22.

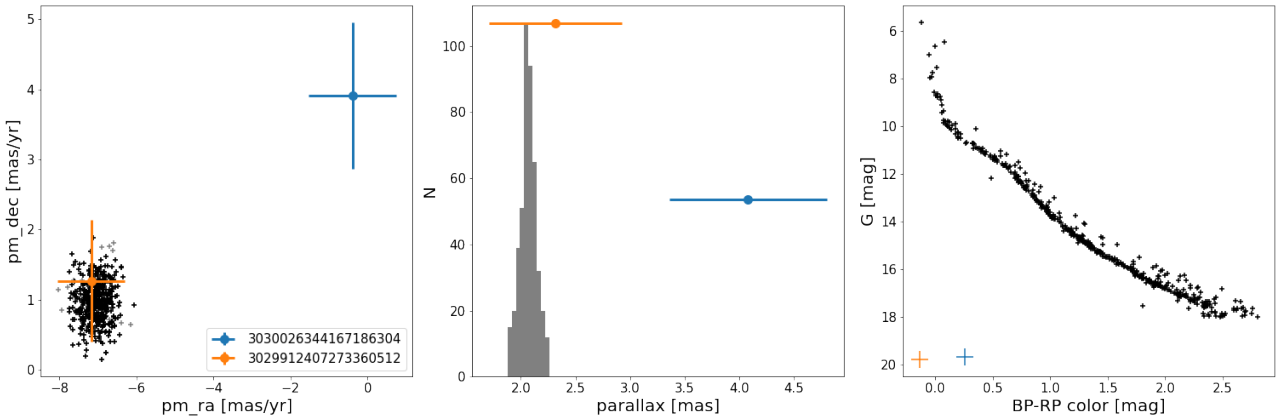

Fig. A.10. Same as in Fig. 5, but for NGC 2422.

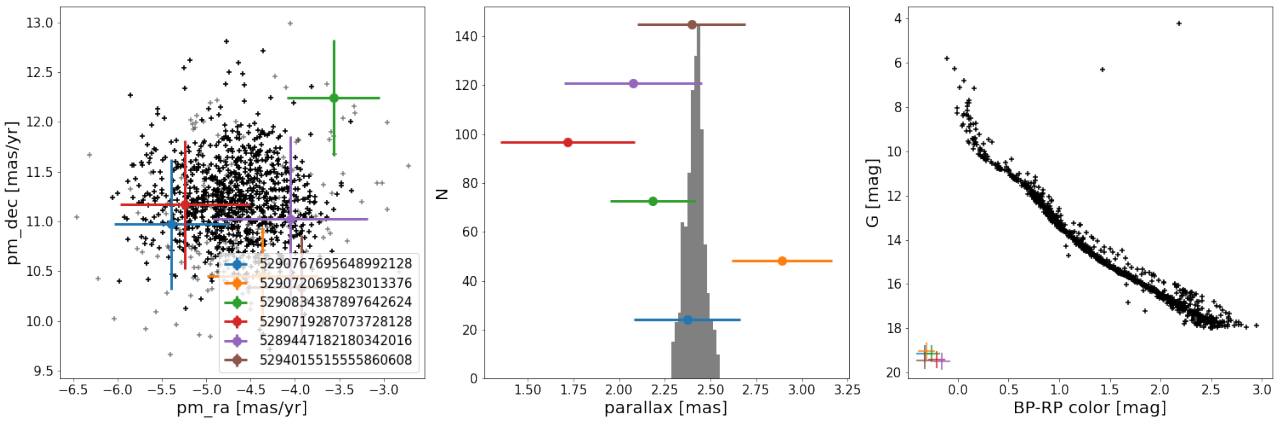

Fig. A.11. Same as in Fig. 5, but for NGC 2516.

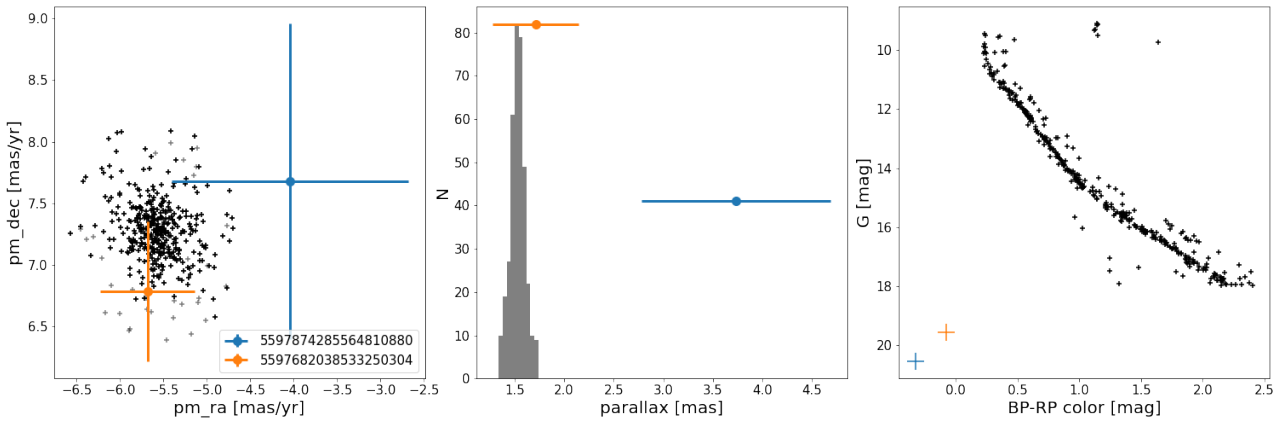

Fig. A.12. Same as in Fig. 5, but for NGC 2527.

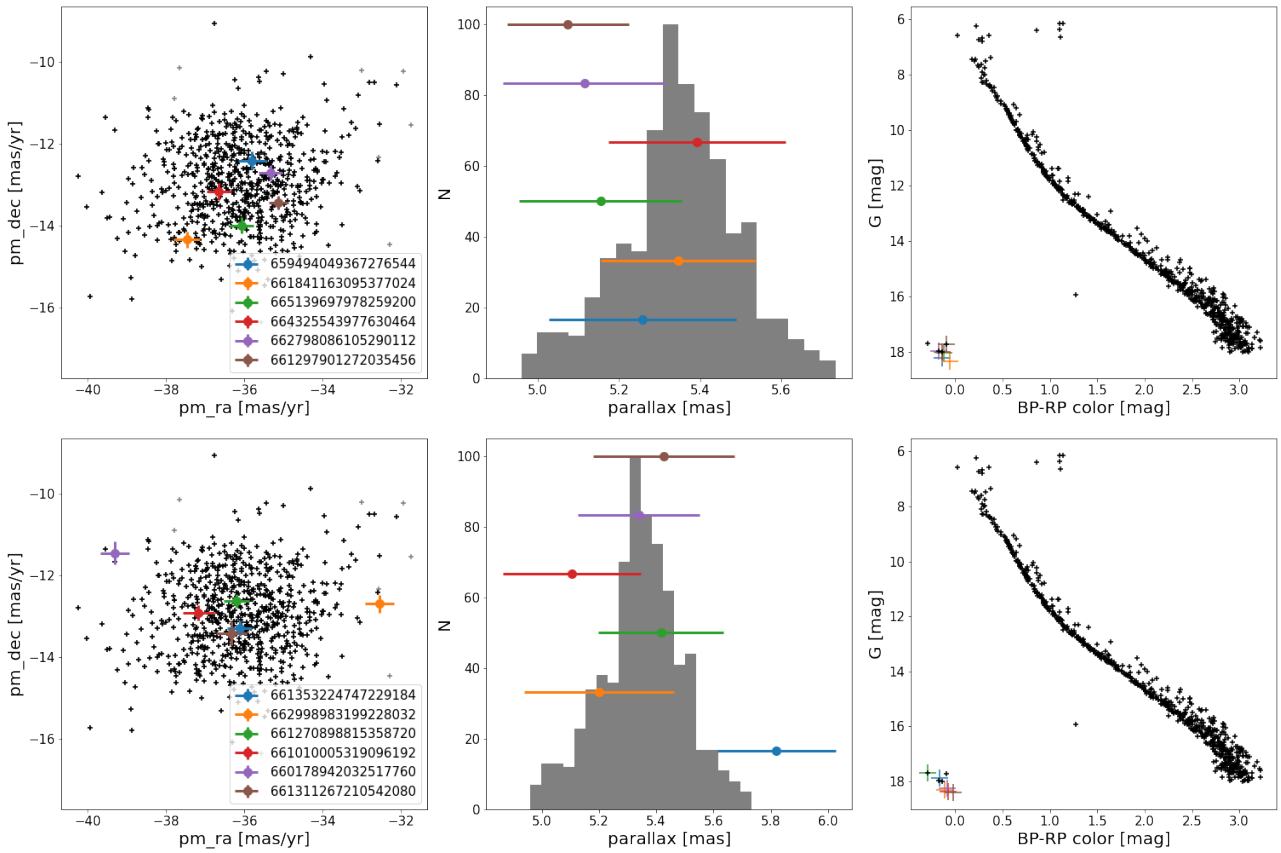

Fig. A.13. Same as in Fig. 5, but for NGC 2632.

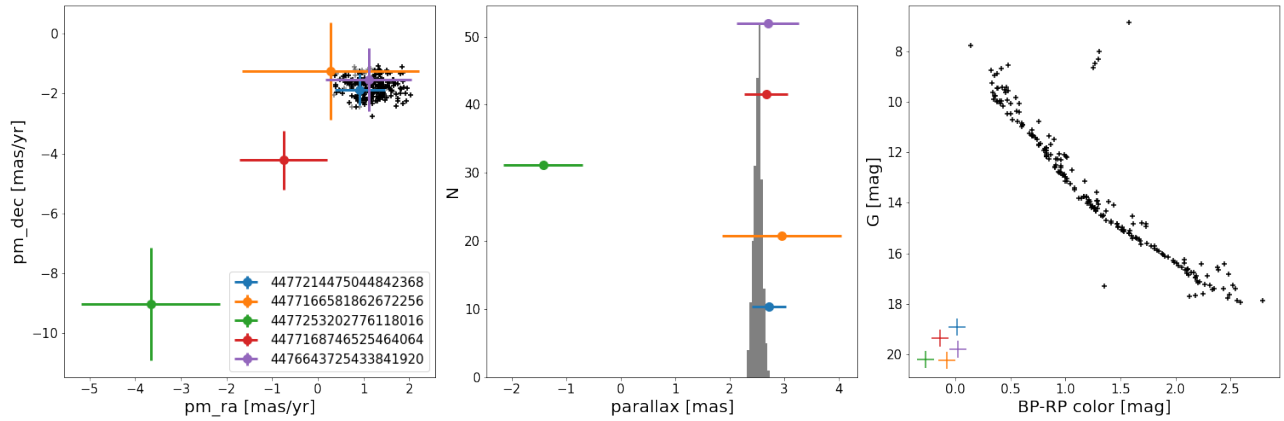

Fig. A.14. Same as in Fig. 5, but for NGC 6633.

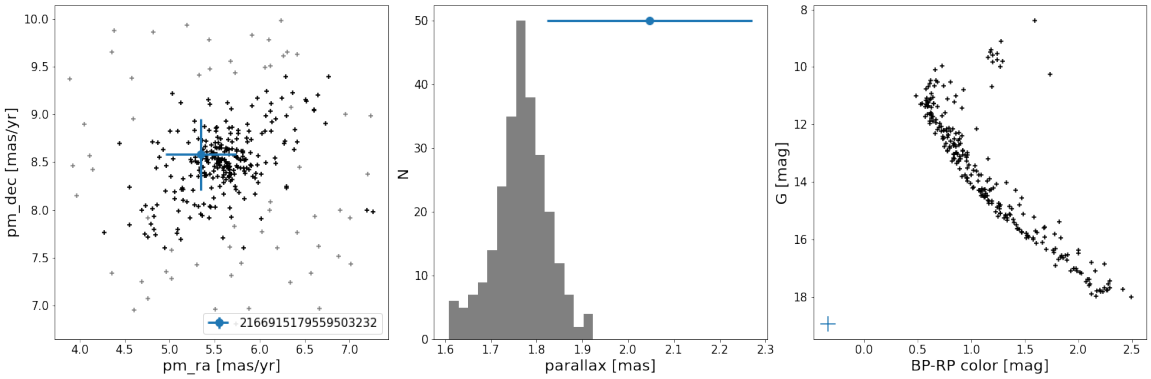

Fig. A.15. Same as in Fig. 5, but for NGC 6991.

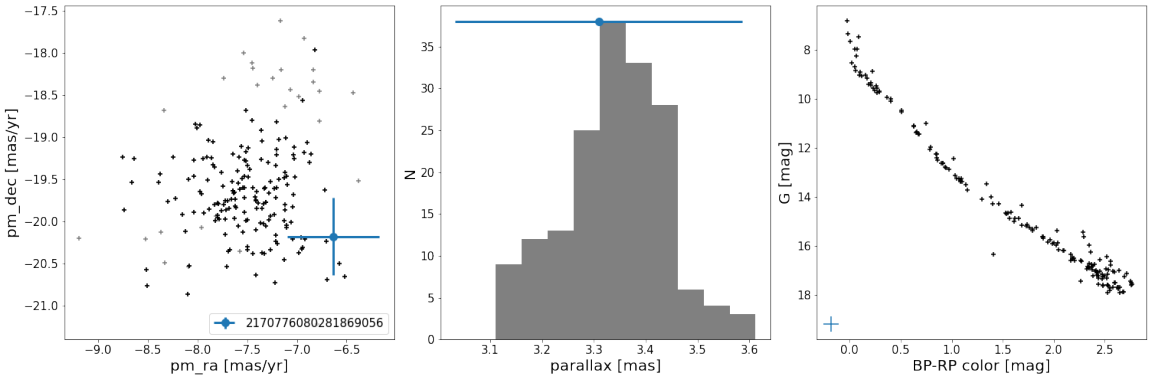

Fig. A.16. Same as in Fig. 5, but for NGC 7092.

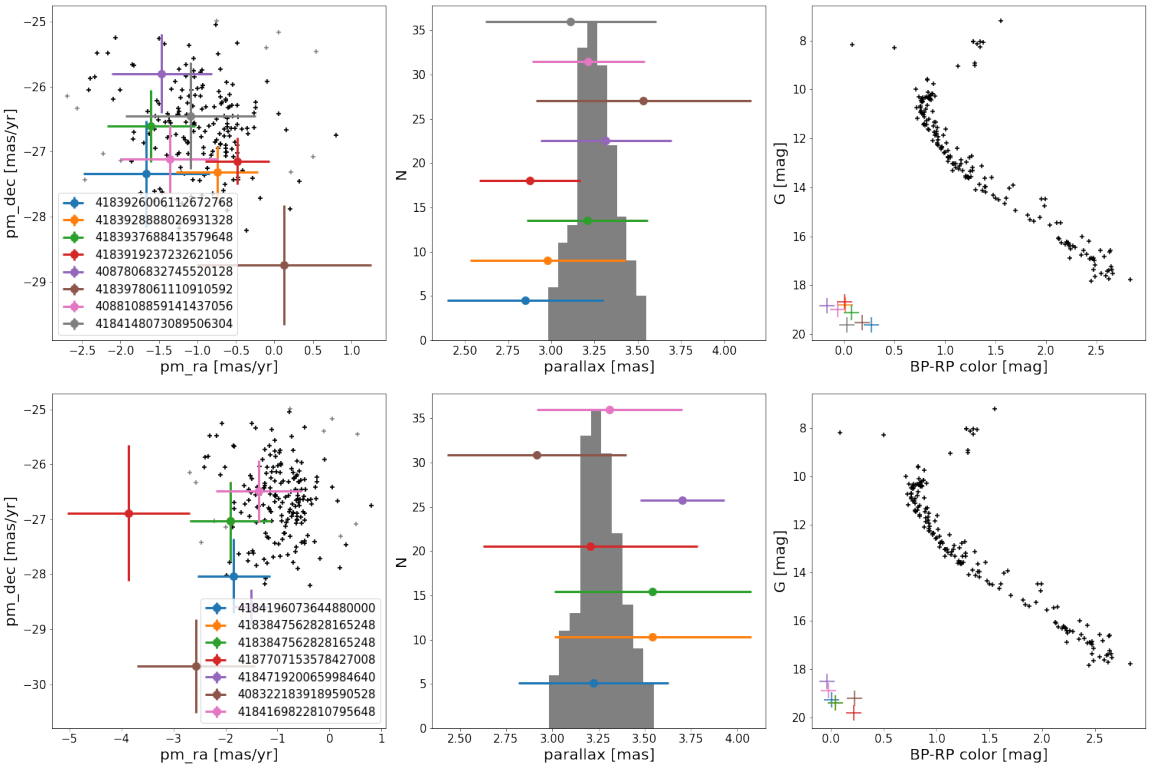

Fig. A.17. Same as in Fig. 5, but for Ruprecht 147.

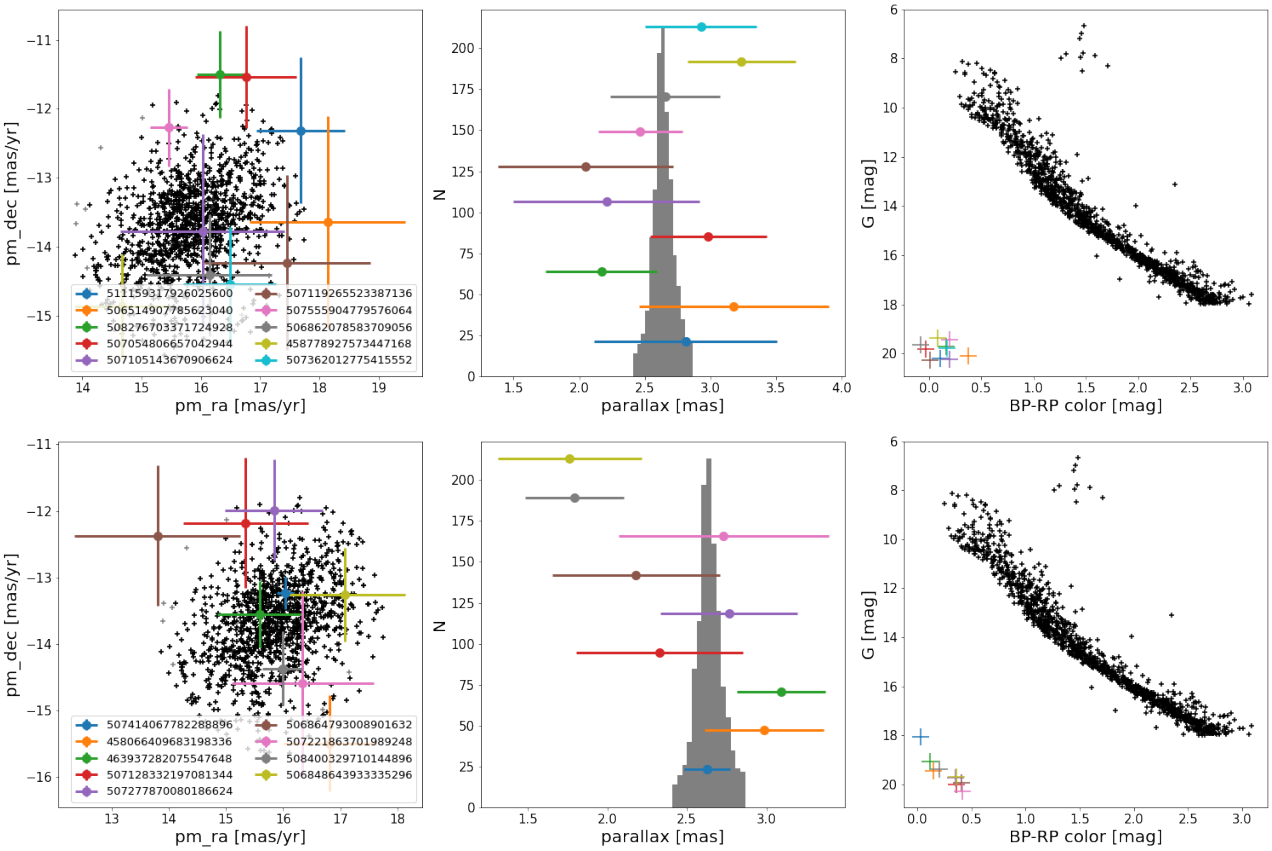

Fig. A.18. Same as in Fig. 5, but for Stock 2.

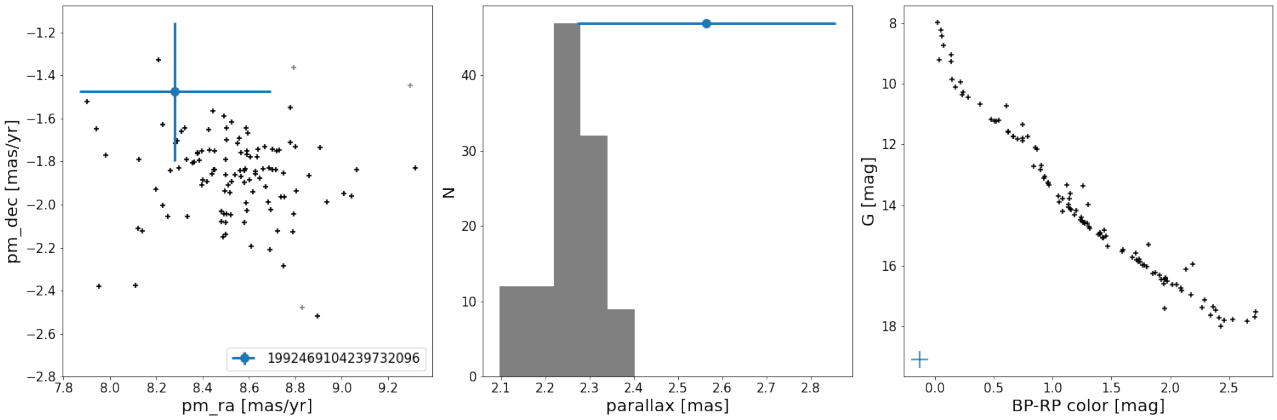

Fig. A.19. Same as in Fig. 5, but for Stock 12.

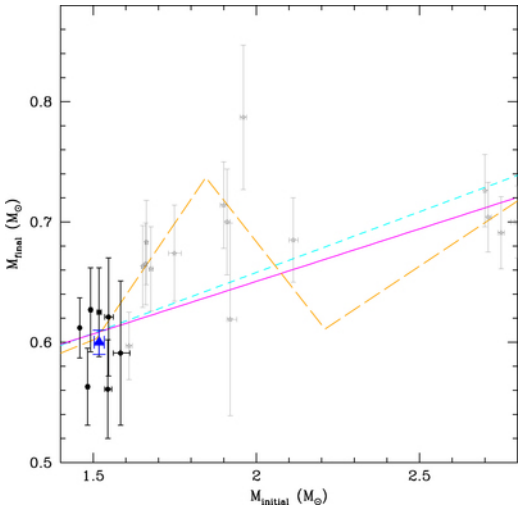

FIGURE 4.1: Low-mass end of the WD IFMR (Canton et al., 2021). Black circles represent individual M67 WDs and the associated errors. The large blue triangle is the mean value for these points, with the error bar indicating the error on the mean. The solid magenta line is the PARSEC IFMR from Cummings et al. (2018), the dashed cyan line is the IFMR fit from Canton (2018), the long-dashed orange line is the IFMR from Marigo et al. (2020), and the gray points with error bars are individual WDs from these works. Figure reproduced from Canton et al. (2021).

4.3 Further developments

Searching for massive WDs in OCs is particularly important, as these objects trace the high-mass end of the IFMR and can be used to establish the stellar mass boundary at which the SN explosion can occur. Shortly after the publication of our paper, Richer et al. (2021) presented their search for massive WDs in the direction of young OCs using the GDR2 data. Similarly to us, they identified new WD candidates as bona fide OC members, confirmed their nature as WDs, and also derived their parameters using spectroscopy. However, they failed to identify OC WDs with masses exceeding 1.1 $M_\odot$ or with progenitors over 6.0 $M_\odot$. This leaves a significant gap near the high-mass end of the IFMR.

Canton et al. (2021) investigated the WD content of M67. They determined the WD masses and derived their progenitor masses using high signal-to-noise spectroscopy. This work provides important constraints to the low mass IFMR because old OCs such as M67 are relatively rare due to their dissolution by Galactic tidal forces. The mean WD masses of $M_{\rm WD} = 0.60 \pm 0.01$ $M_\odot$ and the progenitor masses of $M_{\rm i} = 1.52 \pm 0.04$ $M_\odot$ are fully consistent with the recently published IFMR prescriptions. Nevertheless, this is a useful datum for the low-mass end of the IFMR, since the majority of field WDs used in studies of the Galactic thin disk, thick disk, and halo star populations originated from stars with initial masses $<2.0 M_\odot$ (e.g., Torres et al., 2021).

Recently, Heyl, Caiazzo, and Richer (2022) investigated the Pleiades OC for current and former OC members. They concluded that the OC has lost $\sim$20% of its mass over the last 100 Myr, including two massive WDs. Together with the known Pleiades WD EGGR 25, all three WDs have masses in the range 1.01–1.06 $M_\odot$ with the progenitor masses of about 6.0 $M_\odot$.

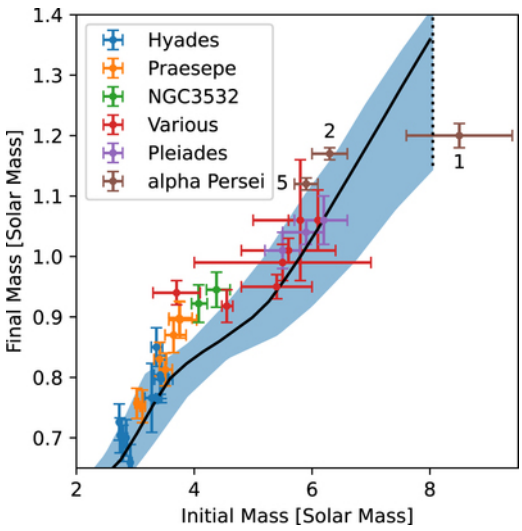

FIGURE 4.2: High-mass end of the WD IFMR (Miller et al., 2022). The Alpha Persei WDs based ONe models masses are from Miller et al. (2022). Pleiades are from Heyl, Caiazzo, and Richer (2022), WDs from "Various" clusters are from Richer et al. (2021), and the rest are from Cummings et al. (2018). The black line and blue region around it outline the empirical IFMR from El-Badry, Rix, and Weisz (2018) and its uncertainty bounds. Figure reproduced from Miller et al. (2022).

Realizing that the most massive WDs may no longer reside in their parent OCs, perhaps due to receiving a natal kick of a few $\mathrm{km\,s^{-1}}$, Miller et al. (2022) investigated the vicinity of the Alpha Persei OC for the potential escapees. They identified three WDs with the kinematic properties consistent with their origin in the OC. All of them are more massive than any previously identified OC WD. The most massive one among them, Gaia EDR3 4395978097863572, has a mass of $\sim$1.2 $M_\odot$ with the derived progenitor mass of $\sim$8.5 $M_\odot$. This has pushed our knowledge of the IFMR towards higher masses, but even these WD masses still leave a significant unexplored gap towards the Chandrasekhar limit. Miller et al. (2022) hypothesized that presence of this mass gap below the Chandrasekhar limit may suggest an increased stellar mass limit for the WD production (well above 8 $M_\odot$), which is more consistent with expectations from observed rates of type II SNe. Another possibility is that single-star evolution does not produce WDs with masses approaching the Chandrasekhar limit.

Chapter 5

Summary and future prospects

5.1 Summary and conclusions

The objects linked with the terminal stages of stellar evolution have proven to be priceless astrophysical laboratories that have been used to address some of the most fundamental questions about the physics of matter in extreme conditions, stellar evolution, galactic archeology, and many other topics. Still, many important questions, such as how these objects are formed and what are the conditions required for their formation remain an active field of research. The advent of modern all-sky surveys and space missions has been instrumental in advancing this field. Particularly, the availability of precise astrometry for an unprecedented number of objects after the GDR2 and the subsequent *Gaia* data releases has opened a completely new window of opportunities to study these objects. These data allowed us to derive precise model-free distances to a lot of these objects for the first time, refining our knowledge of their other fundamental properties which are often distance-dependent. Also, these distances can be used for calibrating other means of distance estimation, and also for gaining some insight into their kinematics, which encodes a lot of information about their formation. It is particularly interesting when these objects are investigated in the context of their formation sites – their parent star clusters.

Interestingly, there is a notable lack of bow shocks and other types of nebulae associated with HMXBs. Since past studies recovered two bow shocks associated with HMXBs in the sample of eleven sources, it was expected that expanding this sample more than ten times, and also making use of the modern mid-infrared data, would yield many new bow shocks associated with HMXBs. These would be very useful, as the bow shock morphology links together the kinematics of the system, stellar wind properties of the secondary, and the properties of the local ISM. Interestingly, this expanded systematic search has yielded only one new bow shock candidate. Therefore, the observed occurrence of HMXB bow shocks is ∼2%, significantly lower than the observed bow shock frequency around OB runaway stars (which ranges from around 40% to 6%, depending on the study; van Buren, Noriega-Crespo, and Dgani, 1995; Huthoff and Kaper, 2002; Peri et al., 2012; Peri, Benaglia, and Isequilla, 2015). This could be interpreted as HXMBs being generally kinematically younger than OB runaways. HMXBs probably attained their large peculiar velocities after one of the binary components exploded as a SN, while OB runaways have predominantly escaped their parent clusters early on through dynamical interactions with other cluster stars in dense environments. Since a large fraction of HMXBs is retained by their parent cluster or association until the SN explosion in their progenitor binaries, they can be directly traced back to their birthplace. This means that the two-step ejection process (Pflamm-Altenburg and Kroupa, 2010) – where the HMXB progenitor would get ejected from its parent cluster dynamically early in the cluster evolution, attaining additional velocity kick in a random direction after an SN explosion at a later time

– is not at work for a large portion of HMXBs. Tracing back an HMXB back to its birthplace and studying the stellar population of its parent cluster or association can yield the age of the HMXB compact object, the mass and metallicity of its progenitor, and the SN properties.

One of the HMXBs subclasses, known as BeXRBs, are particularly useful test sites for many astrophysical applications since they (almost exclusively) host an NS primary with a mass of $\sim$1.4 $M_\odot$ and a secondary star from a relatively narrow spectral distribution peaking at B0. It has been theorized for some time that BeXRBs may consist of several subpopulations with different characteristics, which are a consequence of different SN types forming NSs in their systems. Most notably, Knigge, Coe, and Podsiadlowski (2011) observed that there is a bimodality in the distribution of the orbital ($P_{\rm orb}$) and the spin periods ($P_{\rm s}$) of BeXRBs. The short-period subpopulation has a characteristic $P_{\rm orb} \approx 40$ d and $P_{\rm s} \approx 10$ s, and the long-period subpopulation has $P_{\rm orb} \approx 100$ d and $P_{\rm s} \approx 200$ s, with the division between them more pronounced in $P_{\rm s}$. Knigge, Coe, and Podsiadlowski (2011) proposed that these two subpopulations arise due to two different SNe types that occur in these binaries, where ECSNe reportedly produce the short-period subpopulation and CCSNe produce the long-period subpopulation. Therefore, since ECSNe are thought to impart smaller kicks to the nascent NSs and eject less material during the SN explosion, the short-period subpopulation should also have systematically lower peculiar (systemic) velocities. Using the *Gaia* astrometry, I calculated the peculiar tangential velocities for all BeXRBs with a secure optical counterpart and complete *Gaia* astrometric solution. With the division in the $P_{\rm s}$ used as the criterion to distinguish the two subpopulations, the peculiar velocity distribution yielded that the short-spin subpopulation possesses a mean tangential peculiar velocity of approximately 29 ± 11 km s^{-1}, while for the long-spin subpopulation it is about 16 ± 8 km s^{-1}. The same trend is recovered also in the SMC, where the projected distances of BeXRBs to the nearest young star cluster were used as a proxy for peculiar velocities. This trend is statistically robust and opposite to the one predicted in Knigge, Coe, and Podsiadlowski (2011). This discrepancy can be explained if the scenario proposed by Podsiadlowski et al. (2004) is adopted instead, where the systems with short $P_{\rm orb}$ (and therefore short $P_{\rm s}$, as these two quantities are correlated for BeXRBs) are expected to arise from CCSNe. Other interesting trends in the kinematics of BeXRBs are the absence of a correlation between $P_{\rm orb}$ and peculiar velocities, and a tentative anti-correlation between the orbital eccentricities and peculiar velocities.

Going towards the lower masses, the WDs associated with star clusters are also valuable. By identifying the WDs in star clusters, it is possible to calculate the initial masses of their progenitors and the total mass lost to the ISM during their evolution, using the total age of the cluster, the cooling age of the WD, its current mass, and stellar evolutionary models. To search for such WDs, we made use of the *Gaia* astrometry, and the catalogs of WDs and OCs by Gentile Fusillo et al. (2019) and Cantat-Gaudin et al. (2018). Around 20 new WD-OC pairings were identified. We also confirmed or disproved numerous WD-OC associations from the literature. This allowed us the refine the mapping between the initial stellar mass and the final WD mass for single star evolution, known as the IFMR. The current masses and the progenitor masses of the newly characterized WDs are consistent with the nonlinear IFMR of Marigo et al. (2020) with a kink located over $1.65\ M_\odot \lesssim M_i \lesssim 2.1\ M_\odot$, which can be interpreted as a signature of the lowest-mass stars that become carbon stars during the thermally-pulsing AGB phase. Also, it seems that the intermediate-mass WDs are systematically more massive than waht is predicted by the theoretical IFMR prescriptions, most likely due to the incompleteness of the relevant physics in these

models. One of the most interesting results is the absence of high-mass (> 1.0 $M_\odot$) WDs in OCs. The absence of these WDs can be explained if they were imparted a velocity kick at formation, which would be sufficient to eject them from the parent OCs. This explanation is supported by the recent discovery of massive WDs ejected from the Pleiades and Alpha Persei OC by Heyl, Caiazzo, and Richer (2022) and Miller et al. (2022).

5.2 Future outlook

In this last section, I will try to outline and envision some of the future prospects for finding the answers to the important questions about SN pathways and compact object formation.

Some of the work presented in this thesis relied on the sample of Galactic HMXBs. It has become clear that many science cases would benefit from expanding the number of known systems. The data archives of the modern X-ray missions such as *Chandra* and *XMM-Newton* still have a lot of potential to search for X-ray binary candidates. Especially potent for this are the catalogs of point sources, which can be used to update and expand the catalog of the Galactic HMXBs by Liu, van Paradijs, and van den Heuvel (2006), which is now almost two decades old. Also, the census of the Galactic HMXBs can be expanded through all-sky X-ray surveys, such as the eROSITA mission (Merloni et al., 2012) that was launched in 2019. The angular on-axis resolution of the telescope is comparable to that of *XMM-Newton*, and its wavelength range of 0.2–8 keV enables the first imaging X-ray survey to be conducted that also extends to hard X-rays. It will also be significantly deeper than the only existing all-sky survey with an X-ray imaging telescope, performed by ROSAT in 1990 at energies 0.1–2.4 keV. The German eROSITA consortium plans to release the first all-sky data of their part of the sky near the end of 2022.[1]

An expanded census would allow addressing numerous questions. To illustrate its importance, I briefly outline several possible avenues. For instance, a larger sample of HMXBs would make it possible to study their kinematics in more detail. In Chapter 3. I discussed the kinematic bimodality between the subpopulations of BeXRBs with the short and the long P_s. While there are more than a hundred HMXBs in the Galaxy, only a portion of them are BeXRBs. Out of this portion, only about a half are X-ray pulsars and have reliable optical counterparts. Further, splitting these objects into the long and short P_s subpopulations decreases the number of objects that can be studied as a group even more. For this reason, it is not surprising that the short P_s subpopulation ended up containing less than ten objects. Such a low number makes a reliable inference of any statistical properties tricky and prone to errors. Therefore, an expanded HMXB sample would greatly benefit this type of analysis.

Together with the expanded HMXB sample, the updated *Gaia* EDR3 astrometry, especially more precise parallaxes, can be very useful to study all types of X-ray binaries, as precise distances are crucial for calculating the size of an NS in an X-ray binary, component masses of the binary, the mass transfer rate between the components, and gaining insight into various accretion physics processes (e.g., Arnason et al., 2021, and the references therein). With these improved distances, it is also possible to revisit the uncertain correlation between the positions of the Galactic HMXBs and spiral arms, especially as the knowledge of spiral arms continues to improve as well (Castro-Ginard et al., 2021b).

[1] https://erosita.mpe.mpg.de/erass/

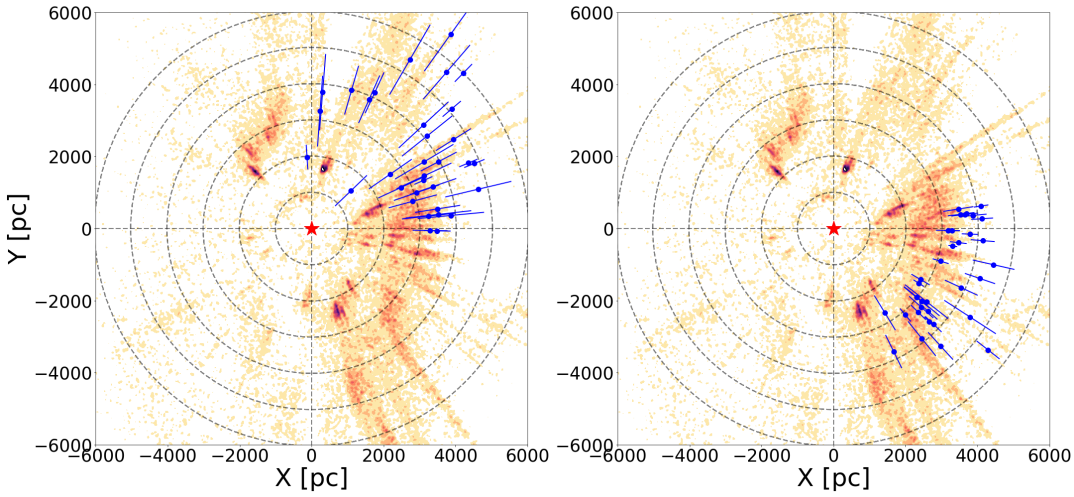

FIGURE 5.1: Surface densities of the stars brighter than M_{K_s} = -2 mag, (corresponding to approximately B1V-type stars) projected on the Galactic plane, adapted from Zari et al. (2021). The density is in arbitrary units. The Sun is located at the origin and the dashed circles have radii in steps of 1 kpc. Left: The locations of the SNRs towards the inner Galaxy, obtained using the UKIDSS data from Wang et al. (2020) shown in blue. Right: The locations of the SNRs obtained using the VVV data from Wang et al. (2020).

The recent progress in the applications of machine learning and neural networks to astronomical surveys and images offers opportunities to mine the infrared surveys for unusual nebulae and structures associated with various types of stars (not only the early-type stars). There has been a lot of effort to search for such sources by the visual examination of the fields of interest and the potential benefit of this kind of science has been demonstrated in this thesis and elsewhere in the literature (e.g., Beaumont et al., 2014; Lieu et al., 2019; Xu et al., 2020). One of the major advantages of machine learning and neural networks techniques is the elimination of the subjective factor of the visual examination for feature detection. The development of these techniques is a very active field of work and a large improvement in their applicability and performance can be expected in the near future.

In Chapter 1., I briefly mentioned the possible association of BDSB 141 with the SNR G049.2–00.7, which seem to be projected on top of each other in the sky and also seem to lie at the same distance. The OC is heavily reddened, making it a difficult target for optical observations. No studies of this OC were published since the work of Kharchenko et al. (2016). Another interesting possible association might be between NGC 6834 and SNR G065.7+01.2. However, the distance of the SNR is unknown. A dedicated study of these pairings might be very valuable. The recent study by Kochanek (2022) showed the potential of studying stellar populations in the vicinity of SNRs, even if no true OC can be identified near the SNR. I argue that a lot more SNRs can be studied in this way.

To demonstrate this, I collect the sample of SNRs with known distances from Wang et al. (2020) and overplot them onto the distribution of the early-type stars in the solar neighbourhood from Zari et al. (2021), which is constructed using the 2MASS and *Gaia* data (see Fig. 5.1). As can be seen in the figure, a lot of SNRs fall into the regions well-populated by early-type stars. These stars can be studied to see

if they form previously unidentified clusters or associations in the vicinity of SNRs. Alternatively, they could be employed to model the local stellar population similarly as in Kochanek (2022). It can also be expected that the SNR distances will be further refined in the near future, thanks to the improved data quality and calibrations (e.g., Wang and Chen, 2021). This would make it possible to get more estimates of SN progenitor masses, which are especially valuable for the Galactic objects.

It seems that a complex picture emerges here. The studies of SNRs by Díaz-Rodríguez et al. (2018) and Kochanek (2022) suggest that the minimum initial stellar mass for SN explosions and NS formation is around 8 $M_\odot$. Yet, it seems that there are high-mass WDs with the progenitors exceeding this mass. The minimum mass limit might be affected by metallicity and binarity. It has been suspected for some time that the mass limit for NS formation might be substantially lower in close binaries (e.g., Podsiadlowski et al., 2004). This is also supported by the presence of two kinematic subpopulations in BeXRBs, where the low-velocity subpopulation might be the result of ECSNe. It is possible that stars with the masses of about 8 $M_\odot$ may explode in an ECSN if they are in a close binary system, while single stars or stars in wide binaries will experience a second dredge-up phase and are more likely to end their evolution as heavy ONeMg WDs. A second dredge-up phase occurs after the stars up to $\sim$11 $M_\odot$ ascend the AGB and when the convective envelope penetrates deep into the stellar core and dredges up a large amount of material, which can significantly reduce the core's mass so it may not be massive enough for an SN explosion (Iben, 1974). The second dredge-up at the beginning of the AGB can be avoided for close binaries as it does not occur if the hydrogen envelope is already lost due to the binary interaction. A way to confirm this scenario would be the detection of both massive WDs and a binary system with an NS, associated with an OC with a turnoff mass of around 8 $M_\odot$. Since a lot of HMXBs should be trackable back to their parent OCs and associations and our census of OCs and WDs continues to improve, finding such pairing might be possible. It is certain that the future *Gaia* data releases will advance this field further.

Bibliography

Adams, S. M. et al. (July 2017). "The search for failed supernovae with the Large Binocular Telescope: confirmation of a disappearing star". In: *MNRAS* 468.4, pp. 4968–4981. DOI: 10.1093/mnras/stx816. arXiv: 1609.01283 [astro-ph.SR].

Agertz, Oscar and Andrey V. Kravtsov (May 2015). "On the Interplay between Star Formation and Feedback in Galaxy Formation Simulations". In: *ApJ* 804.1, 18, p. 18. DOI: 10.1088/0004-637X/804/1/18. arXiv: 1404.2613 [astro-ph.GA].

Althaus, Leandro G. et al. (Oct. 2010). "Evolutionary and pulsational properties of white dwarf stars". In: *A&A Rev.* 18.4, pp. 471–566. DOI: 10.1007/s00159-010-0033-1. arXiv: 1007.2659 [astro-ph.SR].

Anderson, J. P. and M. Soto (Feb. 2013). "On the multiplicity of supernovae within host galaxies". In: *A&A* 550, A69, A69. DOI: 10.1051/0004-6361/201220600. arXiv: 1212.4153 [astro-ph.CO].

Ankay, A. et al. (Apr. 2001). "The origin of the runaway high-mass X-ray binary HD 153919/4U1700-37". In: *A&A* 370, pp. 170–175. DOI: 10.1051/0004-6361:20010192. arXiv: astro-ph/0102118 [astro-ph].

Antoniadis, John (Dec. 2020). "Gaia Pulsars and Where to Find Them in EDR3". In: *Research Notes of the American Astronomical Society* 4.12, 223, p. 223. DOI: 10.3847/2515-5172/abd189. arXiv: 2012.06335 [astro-ph.HE].

— (Feb. 2021). "Gaia pulsars and where to find them". In: *MNRAS* 501.1, pp. 1116–1126. DOI: 10.1093/mnras/staa3595. arXiv: 2011.08075 [astro-ph.HE].

Antoniou, V. and A. Zezas (June 2016). "Star formation history and X-ray binary populations: the case of the Large Magellanic Cloud". In: *MNRAS* 459.1, pp. 528–553. DOI: 10.1093/mnras/stw167. arXiv: 1603.08011 [astro-ph.HE].

Antoniou, V. et al. (June 2010). "Star Formation History and X-ray Binary Populations: The Case of the Small Magellanic Cloud". In: *ApJ* 716.2, pp. L140–L145. DOI: 10.1088/2041-8205/716/2/L140. arXiv: 1006.2381 [astro-ph.HE].

Antoniou, Vallia et al. (Dec. 2019). "Deep Chandra Survey of the Small Magellanic Cloud. III. Formation Efficiency of High-mass X-Ray Binaries". In: *ApJ* 887.1, 20, p. 20. DOI: 10.3847/1538-4357/ab4a7a. arXiv: 1901.01237 [astro-ph.HE].

Arnason, R. M. et al. (Apr. 2021). "Distances to Galactic X-ray binaries with Gaia DR2". In: *MNRAS* 502.4, pp. 5455–5470. DOI: 10.1093/mnras/stab345. arXiv: 2102.02615 [astro-ph.HE].

Arzoumanian, Z., D. F. Chernoff, and J. M. Cordes (Mar. 2002). "The Velocity Distribution of Isolated Radio Pulsars". In: *ApJ* 568.1, pp. 289–301. DOI: 10.1086/338805. arXiv: astro-ph/0106159 [astro-ph].

Atri, P. et al. (Nov. 2019). "Potential kick velocity distribution of black hole X-ray binaries and implications for natal kicks". In: *MNRAS* 489.3, pp. 3116–3134. DOI: 10.1093/mnras/stz2335. arXiv: 1908.07199 [astro-ph.HE].

Auchettl, Katie et al. (Jan. 2019). "Measurement of the Core-collapse Progenitor Mass Distribution of the Small Magellanic Cloud". In: *ApJ* 871.1, 64, p. 64. DOI: 10.3847/1538-4357/aaf395. arXiv: 1804.10210 [astro-ph.SR].

Badenes, Carles et al. (July 2009). "The Stellar Ancestry of Supernovae in the Magellanic Clouds. I. The Most Recent Supernovae in the Large Magellanic Cloud". In:

ApJ 700.1, pp. 727–740. DOI: 10.1088/0004-637X/700/1/727. arXiv: 0902.2787 [astro-ph.SR].

Bailer-Jones, C. A. L. et al. (Aug. 2018). "Estimating Distance from Parallaxes. IV. Distances to 1.33 Billion Stars in Gaia Data Release 2". In: *AJ* 156.2, 58, p. 58. DOI: 10.3847/1538-3881/aacb21. arXiv: 1804.10121 [astro-ph.SR].

Barrado, D. (Nov. 2016). "Clusters: Age Scales for Stellar Physics". In: *EAS Publications Series*. Vol. 80-81. EAS Publications Series, pp. 115–175. DOI: 10.1051/eas/1680005. arXiv: 1606.09448 [astro-ph.SR].

Barrientos, Manuel and Julio Chanamé (Dec. 2021). "Improved Constraints on the Initial-to-final Mass Relation of White Dwarfs Using Wide Binaries". In: *ApJ* 923.2, 181, p. 181. DOI: 10.3847/1538-4357/ac2f49. arXiv: 2102.07790 [astro-ph.SR].

Barth, Aaron J. et al. (May 1996). "The Environments of Supernovae in Archival Hubble Space Telescope Images". In: *AJ* 111, p. 2047. DOI: 10.1086/117940.

Beaumont, Christopher N. et al. (Sept. 2014). "The Milky Way Project: Leveraging Citizen Science and Machine Learning to Detect Interstellar Bubbles". In: *ApJS* 214.1, 3, p. 3. DOI: 10.1088/0067-0049/214/1/3. arXiv: 1406.2692 [astro-ph.GA].

Bédard, A., P. Bergeron, and G. Fontaine (Oct. 2017). "Measurements of Physical Parameters of White Dwarfs: A Test of the Mass-Radius Relation". In: *ApJ* 848.1, 11, p. 11. DOI: 10.3847/1538-4357/aa8bb6. arXiv: 1709.02324 [astro-ph.SR].

Bédard, A. et al. (Oct. 2020). "On the Spectral Evolution of Hot White Dwarf Stars. I. A Detailed Model Atmosphere Analysis of Hot White Dwarfs from SDSS DR12". In: *ApJ* 901.2, 93, p. 93. DOI: 10.3847/1538-4357/abafbe. arXiv: 2008.07469 [astro-ph.SR].

Benaglia, P. et al. (July 2010). "Detection of nonthermal emission from the bow shock of a massive runaway star". In: *A&A* 517, L10, p. L10. DOI: 10.1051/0004-6361/201015232. arXiv: 1007.3279 [astro-ph.SR].

Benaglia, Paula et al. (May 2021). "High-sensitivity radio study of the non-thermal stellar bow shock EB27". In: *MNRAS* 503.2, pp. 2514–2522. DOI: 10.1093/mnras/stab662. arXiv: 2103.01317 [astro-ph.SR].

Beniamini, Paz and Tsvi Piran (Mar. 2016). "Formation of double neutron star systems as implied by observations". In: *MNRAS* 456.4, pp. 4089–4099. DOI: 10.1093/mnras/stv2903. arXiv: 1510.03111 [astro-ph.HE].

Bergeron, P. et al. (May 2019). "On the Measurement of Fundamental Parameters of White Dwarfs in the Gaia Era". In: *ApJ* 876.1, 67, p. 67. DOI: 10.3847/1538-4357/ab153a. arXiv: 1904.02022 [astro-ph.SR].

Beskin, V. S. et al. (Oct. 2015). "Radio Pulsars". In: *Space Sci. Rev.* 191.1-4, pp. 207–237. DOI: 10.1007/s11214-015-0173-8. arXiv: 1506.07881 [astro-ph.HE].

Bhattacharya, D. and E. P. J. van den Heuvel (Jan. 1991). "Formation and evolution of binary and millisecond radio pulsars". In: *Phys. Rep.* 203.1-2, pp. 1–124. DOI: 10.1016/0370-1573(91)90064-S.

Bica, E. et al. (Sept. 2008). "A general catalogue of extended objects in the Magellanic System". In: *MNRAS* 389.2, pp. 678–690. DOI: 10.1111/j.1365-2966.2008.13612.x. arXiv: 0806.3049 [astro-ph].

Bica, Eduardo et al. (Jan. 2019). "A Multi-band Catalog of 10978 Star Clusters, Associations, and Candidates in the Milky Way". In: *AJ* 157.1, 12, p. 12. DOI: 10.3847/1538-3881/aaef8d. arXiv: 1812.10292 [astro-ph.GA].

Blaauw, A. (May 1961). "On the origin of the O- and B-type stars with high velocities (the "run-away" stars), and some related problems". In: *Bull. Astron. Inst. Netherlands* 15, p. 265.

Bland-Hawthorn, Joss and Ortwin Gerhard (Sept. 2016). "The Galaxy in Context: Structural, Kinematic, and Integrated Properties". In: *ARA&A* 54, pp. 529–596. DOI: 10.1146/annurev-astro-081915-023441. arXiv: 1602.07702 [astro-ph.GA].

Bobylev, V. V. (Oct. 2008). "Open clusters IC 4665 and Cr 359 and a probable birthplace of the pulsar PSR B1929+10". In: *Astronomy Letters* 34.10, pp. 686–698. DOI: 10.1134/S1063773708100046. arXiv: 0810.0217 [astro-ph].

Bobylev, V. V. and A. T. Bajkova (June 2009). "Open cluster ASCC21 as a probable birthplace of the neutron star Geminga". In: *Astronomy Letters* 35.6, pp. 396–405. DOI: 10.1134/S106377370906005X. arXiv: 0904.3085 [astro-ph.GA].

Bodaghee, A. et al. (Jan. 2012). "Clustering between High-mass X-Ray Binaries and OB Associations in the Milky Way". In: *ApJ* 744.2, 108, p. 108. DOI: 10.1088/0004-637X/744/2/108. arXiv: 1109.3466 [astro-ph.HE].

Bodaghee, Arash et al. (Oct. 2021). "Evidence for Low Kick Velocities among High-mass X-Ray Binaries in the Small Magellanic Cloud from the Spatial Correlation Function". In: *ApJ* 919.2, 81, p. 81. DOI: 10.3847/1538-4357/ac11f4. arXiv: 2107.02802 [astro-ph.HE].

Bodensteiner, J. et al. (Oct. 2018). "Infrared nebulae around bright massive stars as indicators for binary interactions". In: *A&A* 618, A110, A110. DOI: 10.1051/0004-6361/201832722. arXiv: 1806.01294 [astro-ph.SR].

Boggs, S. E. et al. (May 2015). "^{44}Ti gamma-ray emission lines from SN1987A reveal an asymmetric explosion". In: *Science* 348.6235, pp. 670–671. DOI: 10.1126/science.aaa2259.

Bonatto, C., E. Bica, and J. F. C. Santos (May 2008). "Discovery of an open cluster with a possible physical association with a planetary nebula". In: *MNRAS* 386.1, pp. 324–336. DOI: 10.1111/j.1365-2966.2008.13042.x. arXiv: 0801.4539 [astro-ph].

Bond, Howard E., Andrea Bellini, and Kailash C. Sahu (June 2020). "Proper-motion Membership Tests for Four Planetary Nebulae in Galactic Globular Clusters". In: *AJ* 159.6, 276, p. 276. DOI: 10.3847/1538-3881/ab8f9e. arXiv: 2002.11653 [astro-ph.SR].

Bossini, D. et al. (Mar. 2019). "Age determination for 269 Gaia DR2 open clusters". In: *A&A* 623, A108, A108. DOI: 10.1051/0004-6361/201834693. arXiv: 1901.04733 [astro-ph.SR].

Boubert, D. et al. (Aug. 2017). "Hypervelocity runaways from the Large Magellanic Cloud". In: *MNRAS* 469.2, pp. 2151–2162. DOI: 10.1093/mnras/stx848. arXiv: 1704.01373 [astro-ph.GA].

Bramich, D. M. (Oct. 2018). "Predicted microlensing events from analysis of Gaia Data Release 2". In: *A&A* 618, A44, A44. DOI: 10.1051/0004-6361/201833505. arXiv: 1805.10630 [astro-ph.SR].

Brandt, Niel and Philipp Podsiadlowski (May 1995). "The effects of high-velocity supernova kicks on the orbital properties and sky distributions of neutron-star binaries". In: *MNRAS* 274.2, pp. 461–484. DOI: 10.1093/mnras/274.2.461.

Bressan, Alessandro et al. (Nov. 2012). "PARSEC: stellar tracks and isochrones with the PAdova and TRieste Stellar Evolution Code". In: *MNRAS* 427.1, pp. 127–145. DOI: 10.1111/j.1365-2966.2012.21948.x. arXiv: 1208.4498 [astro-ph.SR].

Brown, Anthony G. A. (Sept. 2021). "Microarcsecond Astrometry: Science Highlights from Gaia". In: *ARA&A* 59. DOI: 10.1146/annurev-astro-112320-035628. arXiv: 2102.11712 [astro-ph.IM].

Brown, D. and D. J. Bomans (Aug. 2005). "To see or not to see a bow shock. Identifying bow shocks with Hα allsky surveys". In: *A&A* 439.1, pp. 183–194. DOI: 10.1051/0004-6361:20041054. arXiv: astro-ph/0505098 [astro-ph].

Brown, Warren R. (Aug. 2015). "Hypervelocity Stars". In: *ARA&A* 53, pp. 15–49. DOI: 10.1146/annurev-astro-082214-122230.

Brown, Warren R. et al. (Mar. 2005). "Discovery of an Unbound Hypervelocity Star in the Milky Way Halo". In: *ApJ* 622.1, pp. L33–L36. DOI: 10.1086/429378. arXiv: astro-ph/0501177 [astro-ph].

Burrows, A. and D. Vartanyan (Jan. 2021). "Core-collapse supernova explosion theory". In: *Nature* 589.7840, pp. 29–39. DOI: 10.1038/s41586-020-03059-w. arXiv: 2009.14157 [astro-ph.SR].

Camargo, D., E. Bica, and C. Bonatto (Jan. 2016). "Characterizing star cluster formation with WISE: 652 newly found star clusters and candidates". In: *MNRAS* 455.3, pp. 3126–3135. DOI: 10.1093/mnras/stv2517. arXiv: 1511.01978 [astro-ph.GA].

Camisassa, María E. et al. (May 2019). "The evolution of ultra-massive white dwarfs". In: *A&A* 625, A87, A87. DOI: 10.1051/0004-6361/201833822. arXiv: 1807.03894 [astro-ph.SR].

Camps-Fariña, A. et al. (Sept. 2016). "Three supernova shells around a young M33 star cluster". In: *MNRAS* 461.1, pp. L87–L91. DOI: 10.1093/mnrasl/slw106. arXiv: 1605.06403 [astro-ph.GA].

Cantat-Gaudin, T. and F. Anders (Jan. 2020). "Clusters and mirages: cataloguing stellar aggregates in the Milky Way". In: *A&A* 633, A99, A99. DOI: 10.1051/0004-6361/201936691. arXiv: 1911.07075 [astro-ph.SR].

Cantat-Gaudin, T. et al. (Oct. 2018). "A Gaia DR2 view of the open cluster population in the Milky Way". In: *A&A* 618, A93, A93. DOI: 10.1051/0004-6361/201833476. arXiv: 1805.08726 [astro-ph.GA].

Cantat-Gaudin, T. et al. (June 2019). "Expanding associations in the Vela-Puppis region. 3D structure and kinematics of the young population". In: *A&A* 626, A17, A17. DOI: 10.1051/0004-6361/201834957. arXiv: 1812.08114 [astro-ph.GA].

Cantat-Gaudin, T. et al. (Aug. 2020). "Painting a portrait of the Galactic disc with its stellar clusters". In: *A&A* 640, A1, A1. DOI: 10.1051/0004-6361/202038192. arXiv: 2004.07274 [astro-ph.GA].

Cantat-Gaudin, Tristan (Feb. 2022). "Milky Way Star Clusters and Gaia: A Review of the Ongoing Revolution". In: *Universe* 8.2, p. 111. DOI: 10.3390/universe8020111.

Canton, Paul (Dec. 2018). "The Initial-Final Mass Relation Revisited: A Monte Carlo Approach with the Addition of the M67 White Dwarf Population". PhD thesis. University of Oklahoma.

Canton, Paul A. et al. (Apr. 2021). "The White Dwarfs of the Old, Solar-metallicity Open Star Cluster Messier 67: Properties and Progenitors". In: *AJ* 161.4, 169, p. 169. DOI: 10.3847/1538-3881/abe1ad. arXiv: 2103.01747 [astro-ph.SR].

Cappellaro, E., R. Evans, and M. Turatto (Nov. 1999). "A new determination of supernova rates and a comparison with indicators for galactic star formation". In: *A&A* 351, pp. 459–466. arXiv: astro-ph/9904225 [astro-ph].

Carrera, R. et al. (Mar. 2019). "Open clusters in APOGEE and GALAH. Combining Gaia and ground-based spectroscopic surveys". In: *A&A* 623, A80, A80. DOI: 10.1051/0004-6361/201834546. arXiv: 1901.09302 [astro-ph.GA].

Casares, J. et al. (Jan. 2014). "A Be-type star with a black-hole companion". In: *Nature* 505.7483, pp. 378–381. DOI: 10.1038/nature12916. arXiv: 1401.3711 [astro-ph.SR].

Casares, Jorge, Peter Gustaaf Jonker, and Garik Israelian (2017). "X-Ray Binaries". In: *Handbook of Supernovae*. Ed. by Athem W. Alsabti and Paul Murdin, p. 1499. DOI: 10.1007/978-3-319-21846-5_111.

Castro-Ginard, A. et al. (Oct. 2018). "A new method for unveiling open clusters in Gaia. New nearby open clusters confirmed by DR2". In: *A&A* 618, A59, A59. DOI: 10.1051/0004-6361/201833390. arXiv: 1805.03045 [astro-ph.GA].

Castro-Ginard, A. et al. (July 2019). "Hunting for open clusters in Gaia DR2: the Galactic anticentre". In: *A&A* 627, A35, A35. DOI: 10.1051/0004-6361/201935531. arXiv: 1905.06161 [astro-ph.GA].

Castro-Ginard, A. et al. (Mar. 2020). "Hunting for open clusters in Gaia DR2: 582 new open clusters in the Galactic disc". In: *A&A* 635, A45, A45. DOI: 10.1051/0004-6361/201937386. arXiv: 2001.07122 [astro-ph.GA].

Castro-Ginard, A. et al. (Nov. 2021a). "Hunting for open clusters in Gaia EDR3: 664 new open clusters found with OCfinder". In: *arXiv e-prints*, arXiv:2111.01819, arXiv:2111.01819. arXiv: 2111.01819 [astro-ph.GA].

Castro-Ginard, A. et al. (Aug. 2021b). "Milky Way spiral arms from open clusters in Gaia EDR3". In: *A&A* 652, A162, A162. DOI: 10.1051/0004-6361/202039751. arXiv: 2105.04590 [astro-ph.GA].

Cerda-Duran, Pablo and Nancy Elias-Rosa (Jan. 2018). "Neutron Stars Formation and Core Collapse Supernovae". In: *Astrophysics and Space Science Library*. Ed. by Luciano Rezzolla et al. Vol. 457. Astrophysics and Space Science Library, p. 1. DOI: 10.1007/978-3-319-97616-7_1. arXiv: 1806.07267 [astro-ph.HE].

Chakrabarty, Deepto et al. (Feb. 2001). "The Central X-Ray Point Source in Cassiopeia A". In: *ApJ* 548.2, pp. 800–810. DOI: 10.1086/318994. arXiv: astro-ph/0001026 [astro-ph].

Chandrasekhar, S. (July 1931). "The Maximum Mass of Ideal White Dwarfs". In: *ApJ* 74, p. 81. DOI: 10.1086/143324.

Chandrasekhar, Subrahmanyan (1939). *An introduction to the study of stellar structure*.

Chaty, Sylvain (Jan. 2018). "High mass X-ray binaries: Progenitors of double neutron star systems". In: *Fourteenth Marcel Grossmann Meeting - MG14*. Ed. by Massimo Bianchi, Robert T. Jansen, and Remo Ruffini, pp. 1883–1888. DOI: 10.1142/9789813226609_0198. arXiv: 1510.07681 [astro-ph.HE].

Chen, Xuepeng et al. (Dec. 2021). "Feedback from γ Cassiopeiae: Large Expanding Cavity, Accelerating Cometary Globules, and Peculiar X-Ray Emission". In: *ApJ* 922.2, 183, p. 183. DOI: 10.3847/1538-4357/ac2507. arXiv: 2111.00686 [astro-ph.SR].

Cheng, S. (2020). *WD_models*. https://github.com/SihaoCheng/WD_models.

Cheng, Z. Q., Y. Shao, and X. D. Li (May 2014). "On the Spin Period Distribution in Be/X-Ray Binaries". In: *ApJ* 786.2, 128, p. 128. DOI: 10.1088/0004-637X/786/2/128. arXiv: 1404.0219 [astro-ph.HE].

Chiosi, E. et al. (June 2006). "Age distribution of young clusters and field stars in the Small Magellanic Cloud". In: *A&A* 452.1, pp. 179–193. DOI: 10.1051/0004-6361:20054559. arXiv: astro-ph/0604166 [astro-ph].

Choi, Jieun et al. (June 2016). "Mesa Isochrones and Stellar Tracks (MIST). I. Solar-scaled Models". In: *ApJ* 823.2, 102, p. 102. DOI: 10.3847/0004-637X/823/2/102. arXiv: 1604.08592 [astro-ph.SR].

Chornay, N. and N. A. Walton (June 2020). "Searching for central stars of planetary nebulae in Gaia DR2". In: *A&A* 638, A103, A103. DOI: 10.1051/0004-6361/202037554. arXiv: 2001.08266 [astro-ph.SR].

— (Dec. 2021). "One star, two star, red star, blue star: an updated planetary nebula central star distance catalogue from Gaia EDR3". In: *A&A* 656, A110, A110. DOI: 10.1051/0004-6361/202142008. arXiv: 2102.13654 [astro-ph.SR].

Cigan, Phil et al. (Nov. 2019). "High Angular Resolution ALMA Images of Dust and Molecules in the SN 1987A Ejecta". In: *ApJ* 886.1, 51, p. 51. DOI: 10.3847/1538-4357/ab4b46. arXiv: 1910.02960 [astro-ph.HE].

Coe, M. J. (Apr. 2005). "An estimate of the supernova kick velocities for high-mass X-ray binaries in the Small Magellanic Cloud". In: *MNRAS* 358.4, pp. 1379–1382. DOI: 10.1111/j.1365-2966.2005.08857.x. arXiv: astro-ph/0501505 [astro-ph].

Comerón, F. and A. Pasquali (May 2007). "A very massive runaway star from Cygnus OB2". In: *A&A* 467.1, pp. L23–L27. DOI: 10.1051/0004-6361:20077304. arXiv: 0704.0676 [astro-ph].

Corbet, R. H. D. (Dec. 1984). "Be/neutron star binaries : a relationship between orbital period and neutron star spin period." In: *A&A* 141, pp. 91–93.

— (June 1986). "The three types of high-mass X-ray pulsator." In: *MNRAS* 220, pp. 1047–1056. DOI: 10.1093/mnras/220.4.1047.

Corral-Santana, J. M. et al. (Mar. 2016). "BlackCAT: A catalogue of stellar-mass black holes in X-ray transients". In: *A&A* 587, A61, A61. DOI: 10.1051/0004-6361/201527130. arXiv: 1510.08869 [astro-ph.HE].

Crockett, R. M. et al. (Nov. 2008). "The type IIb SN 2008ax: the nature of the progenitor". In: *MNRAS* 391.1, pp. L5–L9. DOI: 10.1111/j.1745-3933.2008.00540.x. arXiv: 0805.1913 [astro-ph].

Cromartie, H. T. et al. (Jan. 2020). "Relativistic Shapiro delay measurements of an extremely massive millisecond pulsar". In: *Nature Astronomy* 4, pp. 72–76. DOI: 10.1038/s41550-019-0880-2. arXiv: 1904.06759 [astro-ph.HE].

Cropper, M. et al. (Aug. 2018). "Gaia Data Release 2. Gaia Radial Velocity Spectrometer". In: *A&A* 616, A5, A5. DOI: 10.1051/0004-6361/201832763. arXiv: 1804.09369 [astro-ph.IM].

Cummings, Jeffrey D. et al. (Mar. 2016a). "An Ultramassive 1.28 $M_{\odot}$ White Dwarf in NGC 2099". In: *ApJ* 820.1, L18, p. L18. DOI: 10.3847/2041-8205/820/1/L18. arXiv: 1603.00471 [astro-ph.SR].

Cummings, Jeffrey D. et al. (Feb. 2016b). "Two Massive White Dwarfs from NGC 2323 and the Initial-Final Mass Relation for Progenitors of 4 to 6.5 M". In: *ApJ* 818.1, 84, p. 84. DOI: 10.3847/0004-637X/818/1/84. arXiv: 1601.03053 [astro-ph.SR].

Cummings, Jeffrey D. et al. (Oct. 2018). "The White Dwarf Initial-Final Mass Relation for Progenitor Stars from 0.85 to 7.5 M $_{\odot}$". In: *ApJ* 866.1, 21, p. 21. DOI: 10.3847/1538-4357/aadfd6. arXiv: 1809.01673 [astro-ph.SR].

Cummings, Jeffrey D. et al. (Jan. 2019). "A Novel Approach to Constrain Rotational Mixing and Convective-core Overshoot in Stars Using the Initial-Final Mass Relation". In: *ApJ* 871.1, L18, p. L18. DOI: 10.3847/2041-8213/aafc2d. arXiv: 1901.02904 [astro-ph.SR].

Davies, Melvyn B. and Brad M. S. Hansen (Nov. 1998). "Neutron star retention and millisecond pulsar production in globular clusters". In: *MNRAS* 301.1, pp. 15–24. DOI: 10.1046/j.1365-8711.1998.01923.x.

Davis, Brian D. et al. (Oct. 2019). "Hubble Space Telescope Spectroscopy of a Planetary Nebula in an M31 Open Cluster: Hot-bottom Burning at 3.4 M $_{\odot}$". In: *ApJ* 884.2, 115, p. 115. DOI: 10.3847/1538-4357/ab44d4. arXiv: 1909.08007 [astro-ph.SR].

Deller, A. T. et al. (Apr. 2019). "Microarcsecond VLBI Pulsar Astrometry with PSRπ II. Parallax Distances for 57 Pulsars". In: *ApJ* 875.2, 100, p. 100. DOI: 10.3847/1538-4357/ab11c7. arXiv: 1808.09046 [astro-ph.IM].

Dias, W. S. et al. (July 2002). "New catalogue of optically visible open clusters and candidates". In: *A&A* 389, pp. 871–873. DOI: 10.1051/0004-6361:20020668. arXiv: astro-ph/0203351 [astro-ph].

Dias, W. S. et al. (June 2021). "Updated parameters of 1743 open clusters based on Gaia DR2". In: *MNRAS* 504.1, pp. 356–371. DOI: 10.1093/mnras/stab770. arXiv: 2103.12829 [astro-ph.SR].

Díaz-Rodríguez, Mariangelly et al. (July 2018). "Progenitor Mass Distribution for Core-collapse Supernova Remnants in M31 and M33". In: *ApJ* 861.2, 92, p. 92. DOI: 10.3847/1538-4357/aac6e1. arXiv: 1802.07870 [astro-ph.SR].

Díaz-Rodríguez, Mariangelly et al. (Sept. 2021). "Progenitor mass distribution for 22 historic core-collapse supernovae". In: *MNRAS* 506.1, pp. 781–790. DOI: 10.1093/mnras/stab1800. arXiv: 2101.11012 [astro-ph.HE].

Dickey, John M. and Felix J. Lockman (Jan. 1990). "H I in the galaxy." In: *ARA&A* 28, pp. 215–261. DOI: 10.1146/annurev.aa.28.090190.001243.

Donor, John et al. (May 2020). "The Open Cluster Chemical Abundances and Mapping Survey. IV. Abundances for 128 Open Clusters Using SDSS/APOGEE DR16". In: *AJ* 159.5, 199, p. 199. DOI: 10.3847/1538-3881/ab77bc. arXiv: 2002.08980 [astro-ph.GA].

Efremov, Y. N. (May 1991). "The Large Magellanic Cloud Star Cluster Containing Supernova 1987A". In: *Soviet Astronomy Letters* 17, p. 173.

El-Badry, Kareem, Hans-Walter Rix, and Daniel R. Weisz (June 2018). "An Empirical Measurement of the Initial-Final Mass Relation with Gaia White Dwarfs". In: *ApJ* 860.2, L17, p. L17. DOI: 10.3847/2041-8213/aaca9c. arXiv: 1805.05849 [astro-ph.SR].

El-Badry, Kareem et al. (Mar. 2022). "Unicorns and Giraffes in the binary zoo: stripped giants with subgiant companions". In: *arXiv e-prints*, arXiv:2203.06348, arXiv:2203.06348. arXiv: 2203.06348 [astro-ph.SR].

Erkal, Denis et al. (Feb. 2019). "A hypervelocity star with a Magellanic origin". In: *MNRAS* 483.2, pp. 2007–2013. DOI: 10.1093/mnras/sty2674. arXiv: 1804.10197 [astro-ph.GA].

Fazio, G. G. et al. (Sept. 2004). "The Infrared Array Camera (IRAC) for the Spitzer Space Telescope". In: *ApJS* 154.1, pp. 10–17. DOI: 10.1086/422843. arXiv: astro-ph/0405616 [astro-ph].

Fellhauer, M. et al. (Sept. 2003). "The White Dwarf Deficit in Open Clusters: Dynamical Processes". In: *ApJ* 595.1, pp. L53–L56. DOI: 10.1086/379005. arXiv: astro-ph/0308261 [astro-ph].

Ferreira, F. A. et al. (Mar. 2021). "New star clusters discovered towards the Galactic bulge direction using Gaia DR2". In: *MNRAS* 502.1, pp. L90–L94. DOI: 10.1093/mnrasl/slab011. arXiv: 2101.10982 [astro-ph.GA].

Ferreira, Filipe A. et al. (Mar. 2019). "Three new Galactic star clusters discovered in the field of the open cluster NGC 5999 with Gaia DR2". In: *MNRAS* 483.4, pp. 5508–5517. DOI: 10.1093/mnras/sty3511. arXiv: 1812.10795 [astro-ph.GA].

Fontaine, G., P. Brassard, and P. Bergeron (Apr. 2001). "The Potential of White Dwarf Cosmochronology". In: *PASP* 113.782, pp. 409–435. DOI: 10.1086/319535.

Fragkou, V. et al. (June 2019a). "A high-mass planetary nebula in a Galactic open cluster". In: *Nature Astronomy* 3, pp. 851–857. DOI: 10.1038/s41550-019-0796-x. arXiv: 1906.10556 [astro-ph.SR].

Fragkou, V. et al. (Apr. 2019b). "The central star of planetary nebula PHR 1315 - 6555 and its host Galactic open cluster AL 1". In: *MNRAS* 484.3, pp. 3078–3092. DOI: 10.1093/mnras/stz108. arXiv: 1901.04174 [astro-ph.SR].

Fragos, T. et al. (Oct. 2013a). "Energy Feedback from X-Ray Binaries in the Early Universe". In: *ApJ* 776.2, L31, p. L31. DOI: 10.1088/2041-8205/776/2/L31. arXiv: 1306.1405 [astro-ph.CO].

Fragos, T. et al. (Feb. 2013b). "X-Ray Binary Evolution Across Cosmic Time". In: *ApJ* 764.1, 41, p. 41. DOI: 10.1088/0004-637X/764/1/41. arXiv: 1206.2395 [astro-ph.HE].

Gaia Collaboration et al. (Nov. 2016a). "Gaia Data Release 1. Summary of the astrometric, photometric, and survey properties". In: *A&A* 595, A2, A2. DOI: 10.1051/0004-6361/201629512. arXiv: 1609.04172 [astro-ph.IM].

Gaia Collaboration et al. (Nov. 2016b). "The Gaia mission". In: *A&A* 595, A1, A1. DOI: 10.1051/0004-6361/201629272. arXiv: 1609.04153 [astro-ph.IM].

Gaia Collaboration et al. (Aug. 2018). "Gaia Data Release 2. Summary of the contents and survey properties". In: *A&A* 616, A1, A1. DOI: 10.1051/0004-6361/201833051. arXiv: 1804.09365 [astro-ph.GA].

Gaia Collaboration et al. (May 2021). "Gaia Early Data Release 3. Summary of the contents and survey properties". In: *A&A* 649, A1, A1. DOI: 10.1051/0004-6361/202039657. arXiv: 2012.01533 [astro-ph.GA].

Gandhi, Poshak et al. (May 2019). "Gaia Data Release 2 distances and peculiar velocities for Galactic black hole transients". In: *MNRAS* 485.2, pp. 2642–2655. DOI: 10.1093/mnras/stz438. arXiv: 1804.11349 [astro-ph.HE].

Gatto, A. et al. (May 2015). "Modelling the supernova-driven ISM in different environments". In: *MNRAS* 449.1, pp. 1057–1075. DOI: 10.1093/mnras/stv324. arXiv: 1411.0009 [astro-ph.GA].

Geldzahler, B. J., T. Pauls, and C. J. Salter (Apr. 1980). "Continuum observations of the SNR W50 and G 74.9+1.2 at 2695 MHz." In: *A&A* 84, pp. 237–244.

Gentile Fusillo, N. P. et al. (Dec. 2021). "A catalogue of white dwarfs in Gaia EDR3". In: *MNRAS* 508.3, pp. 3877–3896. DOI: 10.1093/mnras/stab2672. arXiv: 2106.07669 [astro-ph.SR].

Gentile Fusillo, Nicola Pietro et al. (Feb. 2019). "A Gaia Data Release 2 catalogue of white dwarfs and a comparison with SDSS". In: *MNRAS* 482.4, pp. 4570–4591. DOI: 10.1093/mnras/sty3016. arXiv: 1807.03315 [astro-ph.SR].

Gerke, J. R., C. S. Kochanek, and K. Z. Stanek (July 2015). "The search for failed supernovae with the Large Binocular Telescope: first candidates". In: *MNRAS* 450.3, pp. 3289–3305. DOI: 10.1093/mnras/stv776. arXiv: 1411.1761 [astro-ph.SR].

Gieles, Mark et al. (July 2021). "A supra-massive population of stellar-mass black holes in the globular cluster Palomar 5". In: *Nature Astronomy* 5, pp. 957–966. DOI: 10.1038/s41550-021-01392-2. arXiv: 2102.11348 [astro-ph.GA].

Gillett, F. C. et al. (Mar. 1989). "The Optical/Infrared Counterpart(s) of IRAS 18333-2357". In: *ApJ* 338, p. 862. DOI: 10.1086/167241.

Gilmozzi, R. et al. (July 1987). "The progenitor of SN1987A". In: *Nature* 328.6128, pp. 318–320. DOI: 10.1038/328318a0.

Glatt, K., E. K. Grebel, and A. Koch (July 2010). "Ages and luminosities of young SMC/LMC star clusters and the recent star formation history of the Clouds". In: *A&A* 517, A50, A50. DOI: 10.1051/0004-6361/201014187. arXiv: 1004.1247 [astro-ph.GA].

Gogarten, Stephanie M. et al. (Sept. 2009). "The NGC 300 Transient: An Alternative Method for Measuring Progenitor Masses". In: *ApJ* 703.1, pp. 300–310. DOI: 10.1088/0004-637X/703/1/300. arXiv: 0907.0710 [astro-ph.SR].

González-Díaz, D. et al. (June 2019). "Solving the distance discrepancy for the open cluster NGC 2453. The planetary nebula NGC 2452 is not a cluster member". In:

A&A 626, A10, A10. DOI: 10.1051/0004-6361/201935243. arXiv: 1906.09500 [astro-ph.GA].

González-Santamaría, I. et al. (Oct. 2019). "Properties of central stars of planetary nebulae with distances in Gaia DR2". In: *A&A* 630, A150, A150. DOI: 10.1051/0004-6361/201936162. arXiv: 1909.04601 [astro-ph.SR].

González-Santamaría, I. et al. (Dec. 2021). "Planetary nebulae in Gaia EDR3: Central star identification, properties, and binarity". In: *A&A* 656, A51, A51. DOI: 10.1051/0004-6361/202141916. arXiv: 2109.12114 [astro-ph.GA].

Göttgens, Fabian et al. (Nov. 2019). "A stellar census in globular clusters with MUSE: A spectral catalogue of emission-line sources". In: *A&A* 631, A118, A118. DOI: 10.1051/0004-6361/201936485. arXiv: 1909.05872 [astro-ph.SR].

Graczyk, Dariusz et al. (Nov. 2020). "A Distance Determination to the Small Magellanic Cloud with an Accuracy of Better than Two Percent Based on Late-type Eclipsing Binary Stars". In: *ApJ* 904.1, 13, p. 13. DOI: 10.3847/1538-4357/abbb2b. arXiv: 2010.08754 [astro-ph.GA].

Gratton, Raffaele et al. (Nov. 2019). "What is a globular cluster? An observational perspective". In: *A&A Rev.* 27.1, 8, p. 8. DOI: 10.1007/s00159-019-0119-3. arXiv: 1911.02835 [astro-ph.SR].

Greco, Emanuele et al. (Feb. 2021). "Indication of a Pulsar Wind Nebula in the Hard X-Ray Emission from SN 1987A". In: *ApJ* 908.2, L45, p. L45. DOI: 10.3847/2041-8213/abdf5a. arXiv: 2101.09029 [astro-ph.HE].

Green, D. A. (Aug. 2019). "A revised catalogue of 294 Galactic supernova remnants". In: *Journal of Astrophysics and Astronomy* 40.4, 36, p. 36. DOI: 10.1007/s12036-019-9601-6. arXiv: 1907.02638 [astro-ph.GA].

Greggio, Laura (July 2010). "The rates of type Ia supernovae - II. Diversity of events at low and high redshifts". In: *MNRAS* 406.1, pp. 22–42. DOI: 10.1111/j.1365-2966.2010.16371.x. arXiv: 1001.3033 [astro-ph.CO].

Guillochon, James et al. (Jan. 2017). "An Open Catalog for Supernova Data". In: *ApJ* 835.1, 64, p. 64. DOI: 10.3847/1538-4357/835/1/64. arXiv: 1605.01054 [astro-ph.SR].

Gull, T. R. and S. Sofia (June 1979). "Discovery of two distorted interstellar bubbles." In: *ApJ* 230, pp. 782–785. DOI: 10.1086/157137.

Gvaramadze, V. V. (Nov. 2018). "MN44: A Luminous Blue Variable Running Away from Westerlund 1". In: *Research Notes of the American Astronomical Society* 2.4, 214, p. 214. DOI: 10.3847/2515-5172/aaf23d. arXiv: 1811.07899 [astro-ph.SR].

Gvaramadze, V. V., A. Y. Kniazev, and L. N. Berdnikov (Dec. 2015). "Discovery of a new bona fide luminous blue variable in Norma". In: *MNRAS* 454.4, pp. 3710–3721. DOI: 10.1093/mnras/stv2278. arXiv: 1509.08931 [astro-ph.SR].

Gvaramadze, V. V., A. Y. Kniazev, and S. Fabrika (June 2010). "Revealing evolved massive stars with Spitzer". In: *MNRAS* 405.2, pp. 1047–1060. DOI: 10.1111/j.1365-2966.2010.16496.x. arXiv: 0909.0458 [astro-ph.SR].

Gvaramadze, V. V., A. Y. Kniazev, and L. M. Oskinova (May 2019). "Discovery of a putative supernova remnant around the long-period X-ray pulsar SXP 1323 in the Small Magellanic Cloud". In: *MNRAS* 485.1, pp. L6–L10. DOI: 10.1093/mnrasl/slz018. arXiv: 1902.02351 [astro-ph.SR].

Gvaramadze, V. V., P. Kroupa, and J. Pflamm-Altenburg (Sept. 2010). "Massive runaway stars in the Large Magellanic Cloud". In: *A&A* 519, A33, A33. DOI: 10.1051/0004-6361/201014871. arXiv: 1006.0225 [astro-ph.GA].

Gvaramadze, V. V., J. Pflamm-Altenburg, and P. Kroupa (Jan. 2011). "Massive runaway stars in the Small Magellanic Cloud". In: *A&A* 525, A17, A17. DOI: 10.1051/0004-6361/201015656. arXiv: 1010.2490 [astro-ph.GA].

Gvaramadze, V. V. et al. (May 2011). "4U 1907+09: an HMXB running away from the Galactic plane". In: *A&A* 529, A14, A14. DOI: 10.1051/0004-6361/201016256. arXiv: 1102.2437 [astro-ph.SR].

Gvaramadze, V. V. et al. (Mar. 2018). "Modelling interstellar structures around Vela X-1". In: *MNRAS* 474.4, pp. 4421–4431. DOI: 10.1093/mnras/stx3089. arXiv: 1711.09910 [astro-ph.SR].

Gvaramadze, V. V. et al. (Feb. 2019). "CPD-64°2731: a massive spun-up and rejuvenated high-velocity runaway star". In: *MNRAS* 482.4, pp. 4408–4421. DOI: 10.1093/mnras/sty2987. arXiv: 1810.12916 [astro-ph.SR].

Gvaramadze, Vasilii V. (Dec. 2019). "Circumstellar structures around high-mass X-ray binaries". In: *IAU Symposium* 346, pp. 67–73. DOI: 10.1017/S1743921318008013. arXiv: 1811.01953 [astro-ph.SR].

Haberl, F. and R. Sturm (Feb. 2016). "High-mass X-ray binaries in the Small Magellanic Cloud". In: *A&A* 586, A81, A81. DOI: 10.1051/0004-6361/201527326. arXiv: 1511.00445 [astro-ph.GA].

Haberl, F. et al. (Dec. 2021). "eRASSU J050810.4-660653 in the LMC: Discovery of X-ray pulsations with XMM-Newton and NuSTAR". In: *The Astronomer's Telegram* 15133, p. 1.

Haberl, F. et al. (Mar. 2022). "Three new high-mass X-ray binaries in the Large Magellanic Cloud". In: *arXiv e-prints*, arXiv:2203.00625, arXiv:2203.00625. arXiv: 2203.00625 [astro-ph.SR].

Haberl, Frank (Apr. 2007). "The magnificent seven: magnetic fields and surface temperature distributions". In: *Ap&SS* 308.1-4, pp. 181–190. DOI: 10.1007/s10509-007-9342-x. arXiv: astro-ph/0609066 [astro-ph].

Hambaryan, V. et al. (Apr. 2022). "The origin of the high-mass X-ray binary 4U 2206+54/BD+532790". In: *MNRAS* 511.3, pp. 4123–4133. DOI: 10.1093/mnras/stac184. arXiv: 2201.07770 [astro-ph.SR].

Harrus, Ilana M., John P. Hughes, and Patrick O. Slane (May 1998). "Study of the Composite Supernova Remnant MSH 11-62". In: *ApJ* 499.1, pp. 273–281. DOI: 10.1086/305634. arXiv: astro-ph/9801204 [astro-ph].

He, Zhihong et al. (Mar. 2022). "New Open Cluster candidates Found in Galactic Disk Using Gaia DR2/EDR3 Data". In: *arXiv e-prints*, arXiv:2203.05177, arXiv:2203.05177. arXiv: 2203.05177 [astro-ph.GA].

Heger, A. et al. (July 2003). "How Massive Single Stars End Their Life". In: *ApJ* 591.1, pp. 288–300. DOI: 10.1086/375341. arXiv: astro-ph/0212469 [astro-ph].

Heinz, S. et al. (Dec. 2013). "The Youngest Known X-Ray Binary: Circinus X-1 and Its Natal Supernova Remnant". In: *ApJ* 779.2, 171, p. 171. DOI: 10.1088/0004-637X/779/2/171. arXiv: 1312.0632 [astro-ph.HE].

Hénault-Brunet, V. et al. (Feb. 2012). "Discovery of a Be/X-ray pulsar binary and associated supernova remnant in the Wing of the Small Magellanic Cloud". In: *MNRAS* 420.1, pp. L13–L17. DOI: 10.1111/j.1745-3933.2011.01183.x. arXiv: 1110.6404 [astro-ph.SR].

Hénault-Brunet, V. et al. (Jan. 2020). "On the black hole content and initial mass function of 47 Tuc". In: *MNRAS* 491.1, pp. 113–128. DOI: 10.1093/mnras/stz2995. arXiv: 1908.08538 [astro-ph.GA].

Heyl, Jeremy, Ilaria Caiazzo, and Harvey B. Richer (Feb. 2022). "Reconstructing the Pleiades with Gaia EDR3". In: *ApJ* 926.2, 132, p. 132. DOI: 10.3847/1538-4357/ac45fc. arXiv: 2110.03837 [astro-ph.SR].

Hills, J. G. (Feb. 1988). "Hyper-velocity and tidal stars from binaries disrupted by a massive Galactic black hole". In: *Nature* 331.6158, pp. 687–689. DOI: 10.1038/331687a0.

Hiramatsu, Daichi et al. (June 2021). "The electron-capture origin of supernova 2018zd". In: *Nature Astronomy* 5, pp. 903–910. DOI: 10.1038/s41550-021-01384-2. arXiv: 2011.02176 [astro-ph.HE].

Hirsch, H. A. et al. (Dec. 2005). "US 708 - an unbound hyper-velocity subluminous O star". In: *A&A* 444.3, pp. L61–L64. DOI: 10.1051/0004-6361:200500212. arXiv: astro-ph/0511323 [astro-ph].

Høg, E. et al. (Mar. 2000). "The Tycho-2 catalogue of the 2.5 million brightest stars". In: *A&A* 355, pp. L27–L30.

Hoogerwerf, R., J. H. J. de Bruijne, and P. T. de Zeeuw (Jan. 2001). "On the origin of the O and B-type stars with high velocities. II. Runaway stars and pulsars ejected from the nearby young stellar groups". In: *A&A* 365, pp. 49–77. DOI: 10.1051/0004-6361:20000014. arXiv: astro-ph/0010057 [astro-ph].

Hunt, Emily L. and Sabine Reffert (Feb. 2021). "Improving the open cluster census. I. Comparison of clustering algorithms applied to Gaia DR2 data". In: *A&A* 646, A104, A104. DOI: 10.1051/0004-6361/202039341. arXiv: 2012.04267 [astro-ph.GA].

Huthoff, F. and L. Kaper (Mar. 2002). "On the absence of wind bow-shocks around OB-runaway stars: Probing the physical conditions of the interstellar medium". In: *A&A* 383, pp. 999–1010. DOI: 10.1051/0004-6361:20011793. arXiv: astro-ph/0112428 [astro-ph].

Hyde, E. A. et al. (Sept. 2017). "LMC X-1: A New Spectral Analysis of the O-star in the Binary and Surrounding Nebula". In: *PASP* 129.979, p. 094201. DOI: 10.1088/1538-3873/aa7407. arXiv: 1706.01203 [astro-ph.HE].

Iben I., Jr. (Jan. 1974). "Post main sequence evolution of single stars." In: *ARA&A* 12, pp. 215–256. DOI: 10.1146/annurev.aa.12.090174.001243.

Iben Icko, Jr. and Alexander V. Tutukov (Dec. 1997). "On Space Velocities of Binary Stars in Which One Component Has Experienced a Supernova Explosion". In: *ApJ* 491.1, pp. 303–311. DOI: 10.1086/304922.

Igoshev, Andrei P. et al. (Dec. 2021). "Combined analysis of neutron star natal kicks using proper motions and parallax measurements for radio pulsars and Be X-ray binaries". In: *MNRAS* 508.3, pp. 3345–3364. DOI: 10.1093/mnras/stab2734. arXiv: 2109.10362 [astro-ph.HE].

Irrgang, Andreas et al. (Feb. 2021). "Blue extreme disk-runaway stars with Gaia EDR3". In: *A&A* 646, L4, p. L4. DOI: 10.1051/0004-6361/202040178. arXiv: 2101.10878 [astro-ph.GA].

Ivanov, Valentin D. et al. (Apr. 2017). "Candidate star clusters toward the inner Milky Way discovered on deep-stacked K_S-band images from the VVV Survey". In: *A&A* 600, A112, A112. DOI: 10.1051/0004-6361/201630179. arXiv: 1702.02394 [astro-ph.GA].

Jacoby, George H. et al. (Dec. 1997). "Planetary Nebulae in the Globular Cluster PAL 6 and NGC 6441". In: *AJ* 114, p. 2611. DOI: 10.1086/118671.

Jacoby, George H. et al. (May 2013). "A Survey for Planetary Nebulae in M31 Globular Clusters". In: *ApJ* 769.1, 10, p. 10. DOI: 10.1088/0004-637X/769/1/10. arXiv: 1303.3867 [astro-ph.CO].

Jacoby, George H. et al. (Feb. 2017). "Masses of the Planetary Nebula Central Stars in the Galactic Globular Cluster System from HST Imaging and Spectroscopy". In: *ApJ* 836.1, 93, p. 93. DOI: 10.3847/1538-4357/836/1/93. arXiv: 1701.03516 [astro-ph.SR].

Janka, Hans-Thomas (2017). "Neutrino-Driven Explosions". In: *Handbook of Supernovae*. Ed. by Athem W. Alsabti and Paul Murdin, p. 1095. DOI: 10.1007/978-3-319-21846-5_109.

Jayasinghe, Tharindu et al. (Sept. 2019). "The Milky Way Project second data release: bubbles and bow shocks". In: *MNRAS* 488.1, pp. 1141–1165. DOI: 10.1093/mnras/stz1738. arXiv: 1905.12625 [astro-ph.GA].

Jennings, Ross J. et al. (Sept. 2018). "Binary Pulsar Distances and Velocities from Gaia Data Release 2". In: *ApJ* 864.1, 26, p. 26. DOI: 10.3847/1538-4357/aad084. arXiv: 1806.06076 [astro-ph.SR].

Jennings, Zachary G. et al. (Dec. 2012). "Supernova Remnant Progenitor Masses in M31". In: *ApJ* 761.1, 26, p. 26. DOI: 10.1088/0004-637X/761/1/26. arXiv: 1210.6353 [astro-ph.GA].

Jennings, Zachary G. et al. (Nov. 2014). "The Supernova Progenitor Mass Distributions of M31 and M33: Further Evidence for an Upper Mass Limit". In: *ApJ* 795.2, 170, p. 170. DOI: 10.1088/0004-637X/795/2/170. arXiv: 1410.0018 [astro-ph.GA].

Johnson, Dean R. H. and David R. Soderblom (Apr. 1987). "Calculating Galactic Space Velocities and Their Uncertainties, with an Application to the Ursa Major Group". In: *AJ* 93, p. 864. DOI: 10.1086/114370.

Jonker, P. G. and G. Nelemans (Oct. 2004). "The distances to Galactic low-mass X-ray binaries: consequences for black hole luminosities and kicks". In: *MNRAS* 354.2, pp. 355–366. DOI: 10.1111/j.1365-2966.2004.08193.x. arXiv: astro-ph/0407168 [astro-ph].

Joyce, S. R. G. et al. (Sept. 2018). "Testing the white dwarf mass-radius relation and comparing optical and far-UV spectroscopic results with Gaia DR2, HST, and FUSE". In: *MNRAS* 479.2, pp. 1612–1626. DOI: 10.1093/mnras/sty1425. arXiv: 1806.00061 [astro-ph.SR].

Kalirai, Jason S. et al. (Nov. 2009). "The Masses of Population II White Dwarfs". In: *ApJ* 705.1, pp. 408–425. DOI: 10.1088/0004-637X/705/1/408. arXiv: 0909.2253 [astro-ph.SR].

Kalirai, Jasonjot Singh et al. (Jan. 2005). "The Dearth of Massive, Helium-rich White Dwarfs in Young Open Star Clusters". In: *ApJ* 618.2, pp. L129–L132. DOI: 10.1086/427551.

Kaper, L. et al. (Jan. 1997). "Discovery of a Bow Shock around VELA X-1". In: *ApJ* 475.1, pp. L37–L40. DOI: 10.1086/310454. arXiv: astro-ph/9611017 [astro-ph].

Katsuda, Satoru et al. (Aug. 2018). "Progenitor Mass Distribution of Core-collapse Supernova Remnants in Our Galaxy and Magellanic Clouds Based on Elemental Abundances". In: *ApJ* 863.2, 127, p. 127. DOI: 10.3847/1538-4357/aad2d8. arXiv: 1807.03426 [astro-ph.HE].

Kepler, S. O. et al. (Feb. 2016). "New white dwarf and subdwarf stars in the Sloan Digital Sky Survey Data Release 12". In: *MNRAS* 455.4, pp. 3413–3423. DOI: 10.1093/mnras/stv2526. arXiv: 1510.08409 [astro-ph.SR].

Kepler, S. O. et al. (Nov. 2021). "White dwarf and subdwarf stars in the Sloan Digital Sky Survey Data Release 16". In: *MNRAS* 507.3, pp. 4646–4660. DOI: 10.1093/mnras/stab2411. arXiv: 2108.10915 [astro-ph.SR].

Kharchenko, N. V. et al. (Oct. 2013). "Global survey of star clusters in the Milky Way. II. The catalogue of basic parameters". In: *A&A* 558, A53, A53. DOI: 10.1051/0004-6361/201322302. arXiv: 1308.5822 [astro-ph.GA].

— (Jan. 2016). "Global survey of star clusters in the Milky Way. V. Integrated JHK$_S$ magnitudes and luminosity functions". In: *A&A* 585, A101, A101. DOI: 10.1051/0004-6361/201527292.

Khokhriakova, A. D. and S. B. Popov (Apr. 2022). "Origin of young accreting neutron stars in high-mass X-ray binaries in supernova remnants". In: *MNRAS* 511.3, pp. 4447–4453. DOI: 10.1093/mnras/stac332. arXiv: 2201.03602 [astro-ph.HE].

Kilic, Mukremin, K. Z. Stanek, and M. H. Pinsonneault (Dec. 2007). "The Future Is Now: The Formation of Single Low-Mass White Dwarfs in the Solar Neighborhood". In: *ApJ* 671.1, pp. 761–766. DOI: 10.1086/522228. arXiv: 0706.3045 [astro-ph].

Kilpatrick, Charles D. et al. (June 2021). "A cool and inflated progenitor candidate for the Type Ib supernova 2019yvr at 2.6 yr before explosion". In: *MNRAS* 504.2, pp. 2073–2093. DOI: 10.1093/mnras/stab838. arXiv: 2101.03206 [astro-ph.HE].

Kimeswenger, S. and D. Barría (Aug. 2018). "Planetary nebula distances in Gaia DR2". In: *A&A* 616, L2, p. L2. DOI: 10.1051/0004-6361/201833647. arXiv: 1807.06368 [astro-ph.SR].

Kimm, Taysun and Renyue Cen (June 2014). "Escape Fraction of Ionizing Photons during Reionization: Effects due to Supernova Feedback and Runaway OB Stars". In: *ApJ* 788.2, 121, p. 121. DOI: 10.1088/0004-637X/788/2/121. arXiv: 1405.0552 [astro-ph.GA].

Knigge, Christian, Malcolm J. Coe, and Philipp Podsiadlowski (Nov. 2011). "Two populations of X-ray pulsars produced by two types of supernova". In: *Nature* 479.7373, pp. 372–375. DOI: 10.1038/nature10529. arXiv: 1111.2051 [astro-ph.SR].

Kobulnicky, Henry A., William T. Chick, and Matthew S. Povich (Aug. 2019). "Mass-loss Rates for O and Early B Stars Powering Bow Shock Nebulae: Evidence for Bistability Behavior". In: *AJ* 158.2, 73, p. 73. DOI: 10.3847/1538-3881/ab2716.

Kobulnicky, Henry A., Ian J. Gilbert, and Daniel C. Kiminki (Feb. 2010). "OB Stars and Stellar Bow shocks in Cygnus-X: A Novel Laboratory Estimating Stellar Mass Loss Rates". In: *ApJ* 710.1, pp. 549–566. DOI: 10.1088/0004-637X/710/1/549. arXiv: 0912.1314 [astro-ph.GA].

Kobulnicky, Henry A. et al. (Dec. 2016). "A Comprehensive Search for Stellar Bow-shock Nebulae in the Milky Way: A Catalog of 709 Mid-infrared Selected Candidates". In: *ApJS* 227.2, 18, p. 18. DOI: 10.3847/0067-0049/227/2/18. arXiv: 1609.02204 [astro-ph.SR].

Kochanek, C. S. (Apr. 2022). "The progenitor of the Vela pulsar". In: *MNRAS* 511.3, pp. 3428–3439. DOI: 10.1093/mnras/stac098. arXiv: 2110.11369 [astro-ph.GA].

Koester, D. and D. Reimers (Oct. 1989). "Discovery of a planetary nebula in the field of the open cluster NGC 6087." In: *A&A* 223, pp. 326–328.

Koplitz, Brad et al. (July 2021). "The Masses of Supernova Remnant Progenitors in NGC 6946". In: *ApJ* 916.1, 58, p. 58. DOI: 10.3847/1538-4357/abfb7b. arXiv: 2104.11118 [astro-ph.HE].

Koposov, Sergey E. et al. (Jan. 2020). "Discovery of a nearby 1700 km s^{-1} star ejected from the Milky Way by Sgr A*". In: *MNRAS* 491.2, pp. 2465–2480. DOI: 10.1093/mnras/stz3081. arXiv: 1907.11725 [astro-ph.GA].

Köppen, J. and A. Acker (Jan. 2000). "Planetary Nebulae in Clusters". In: *Massive Stellar Clusters*. Ed. by Ariane Lançon and Christian M. Boily. Vol. 211. Astronomical Society of the Pacific Conference Series, p. 151.

Kretschmar, P. et al. (Aug. 2021). "Revisiting the archetypical wind accretor Vela X-1 in depth. Case study of a well-known X-ray binary and the limits of our knowledge". In: *A&A* 652, A95, A95. DOI: 10.1051/0004-6361/202040272. arXiv: 2104.13148 [astro-ph.HE].

Krumholz, Mark R., Christopher F. McKee, and Joss Bland-Hawthorn (Aug. 2019). "Star Clusters Across Cosmic Time". In: *ARA&A* 57, pp. 227–303. DOI: 10.1146/annurev-astro-091918-104430. arXiv: 1812.01615 [astro-ph.GA].

Kulkarni, S. R., Piet Hut, and Steve McMillan (July 1993). "Stellar black holes in globular clusters". In: *Nature* 364.6436, pp. 421–423. DOI: 10.1038/364421a0.

Kumar, C. K. (Jan. 1978). "Supernova remnants in open clusters". In: *ApJ* 219, pp. L13–L15. DOI: 10.1086/182597.

Kwitter, Karen B. and R. B. C. Henry (Feb. 2022). "Planetary Nebulae: Sources of Enlightenment". In: *PASP* 134.1032, 022001, p. 022001. DOI: 10.1088/1538-3873/ac32b1. arXiv: 2110.13993 [astro-ph.SR].

Lada, Charles J. and Elizabeth A. Lada (Jan. 2003). "Embedded Clusters in Molecular Clouds". In: *ARA&A* 41, pp. 57–115. DOI: 10.1146/annurev.astro.41.011802.094844. arXiv: astro-ph/0301540 [astro-ph].

Lam, Casey Y. et al. (Feb. 2022). "An isolated mass gap black hole or neutron star detected with astrometric microlensing". In: *arXiv e-prints*, arXiv:2202.01903, arXiv:2202.01903. arXiv: 2202.01903 [astro-ph.GA].

Langer, N. et al. (Jan. 2020). "γ Cas stars: Normal Be stars with discs impacted by the wind of a helium-star companion?" In: *A&A* 633, A40, A40. DOI: 10.1051/0004-6361/201936736. arXiv: 1911.06508 [astro-ph.SR].

Larsen, S. S. (Jan. 2008). "A peculiar planetary nebula candidate in a globular cluster in the Fornax dwarf spheroidal galaxy". In: *A&A* 477.2, pp. L17–L20. DOI: 10.1051/0004-6361:20078950. arXiv: 0711.2249 [astro-ph].

Larsen, S. S. and T. Richtler (Nov. 2006). "Planetary nebula candidates in extragalactic young star clusters". In: *A&A* 459.1, pp. 103–111. DOI: 10.1051/0004-6361:20065816. arXiv: astro-ph/0608459 [astro-ph].

Lattimer, J. M. and M. Prakash (Apr. 2004). "The Physics of Neutron Stars". In: *Science* 304.5670, pp. 536–542. DOI: 10.1126/science.1090720. arXiv: astro-ph/0405262 [astro-ph].

Leahy, D. and W. Tian (May 2006). "Radio observations and spectrum of the SNR G127.1+0.5 and its central source 0125+628". In: *A&A* 451.1, pp. 251–257. DOI: 10.1051/0004-6361:20054661. arXiv: astro-ph/0601487 [astro-ph].

Lewin, Walter H. G. and Michiel van der Klis (2006). *Compact Stellar X-ray Sources*. Vol. 39.

Li, Zhongmu et al. (Mar. 2022). "LISC Catalog of Star Clusters. I. Galactic Disk Clusters in Gaia EDR3". In: *ApJS* 259.1, 19, p. 19. DOI: 10.3847/1538-4365/ac3c49.

Lieu, Maggie et al. (Oct. 2019). "Deep Learning of Astronomical Features with Big Data". In: *Astronomical Data Analysis Software and Systems XXVII*. Ed. by Peter J. Teuben et al. Vol. 523. Astronomical Society of the Pacific Conference Series, p. 49.

Lindegren, L. et al. (Aug. 2018). "Gaia Data Release 2. The astrometric solution". In: *A&A* 616, A2, A2. DOI: 10.1051/0004-6361/201832727. arXiv: 1804.09366 [astro-ph.IM].

Lindegren, L. et al. (May 2021a). "Gaia Early Data Release 3. Parallax bias versus magnitude, colour, and position". In: *A&A* 649, A4, A4. DOI: 10.1051/0004-6361/202039653. arXiv: 2012.01742 [astro-ph.IM].

Lindegren, L. et al. (May 2021b). "Gaia Early Data Release 3. The astrometric solution". In: *A&A* 649, A2, A2. DOI: 10.1051/0004-6361/202039709. arXiv: 2012.03380 [astro-ph.IM].

Liu, Lei and Xiaoying Pang (Dec. 2019). "A Catalog of Newly Identified Star Clusters in Gaia DR2". In: *ApJS* 245.2, 32, p. 32. DOI: 10.3847/1538-4365/ab530a. arXiv: 1910.12600 [astro-ph.GA].

Liu, Q. Z., J. van Paradijs, and E. P. J. van den Heuvel (Sept. 2006). "Catalogue of high-mass X-ray binaries in the Galaxy (4th edition)". In: *A&A* 455.3, pp. 1165–1168. DOI: 10.1051/0004-6361:20064987. arXiv: 0707.0549 [astro-ph].

— (July 2007). "A catalogue of low-mass X-ray binaries in the Galaxy, LMC, and SMC (Fourth edition)". In: *A&A* 469.2, pp. 807–810. DOI: 10.1051/0004-6361:20077303. arXiv: 0707.0544 [astro-ph].

Luri, X. et al. (Aug. 2018). "Gaia Data Release 2. Using Gaia parallaxes". In: *A&A* 616, A9, A9. DOI: 10.1051/0004-6361/201832964. arXiv: 1804.09376 [astro-ph.IM].

Ma, Xiangcheng et al. (July 2016). "Binary stars can provide the 'missing photons' needed for reionization". In: *MNRAS* 459.4, pp. 3614–3619. DOI: 10.1093/mnras/stw941. arXiv: 1601.07559 [astro-ph.GA].

Maccarone, Thomas J. et al. (Jan. 2007). "A black hole in a globular cluster". In: *Nature* 445.7124, pp. 183–185. DOI: 10.1038/nature05434. arXiv: astro-ph/0701310 [astro-ph].

Maggi, P. et al. (Jan. 2016). "The population of X-ray supernova remnants in the Large Magellanic Cloud". In: *A&A* 585, A162, A162. DOI: 10.1051/0004-6361/201526932. arXiv: 1509.09223 [astro-ph.HE].

Maggi, Pierre et al. (Nov. 2019). "The supernova remnant population of the Small Magellanic Cloud". In: *A&A* 631, A127, A127. DOI: 10.1051/0004-6361/201936583. arXiv: 1908.11234 [astro-ph.HE].

Maitra, C. et al. (Dec. 2019). "Discovery of a very young high-mass X-ray binary associated with the supernova remnant MCSNR J0513-6724 in the LMC". In: *MNRAS* 490.4, pp. 5494–5502. DOI: 10.1093/mnras/stz2831. arXiv: 1910.02792 [astro-ph.HE].

Maitra, C. et al. (June 2021). "XMMU J050722.1-684758: discovery of a new Be X-ray binary pulsar likely associated with the supernova remnant MCSNR J0507-6847". In: *MNRAS* 504.1, pp. 326–337. DOI: 10.1093/mnras/stab716. arXiv: 2103.03657 [astro-ph.HE].

Maíz-Apellániz, J. et al. (Nov. 2004). "The Progenitor of the Type II-P SN 2004dj in NGC 2403". In: *ApJ* 615.2, pp. L113–L116. DOI: 10.1086/426120. arXiv: astro-ph/0408265 [astro-ph].

Majaess, D. et al. (July 2014). "On the crucial cluster Andrews-Lindsay 1 and a 4% distance solution for its planetary nebula". In: *A&A* 567, A1, A1. DOI: 10.1051/0004-6361/201423673. arXiv: 1404.5949 [astro-ph.SR].

Majaess, Daniel J., David G. Turner, and David J. Lane (Dec. 2007). "In Search of Possible Associations between Planetary Nebulae and Open Clusters". In: *PASP* 119.862, pp. 1349–1360. DOI: 10.1086/524414. arXiv: 0710.2900 [astro-ph].

Makovoz, D. and I. Khan (Dec. 2005). "Mosaicking with MOPEX". In: *Astronomical Data Analysis Software and Systems XIV*. Ed. by P. Shopbell, M. Britton, and R. Ebert. Vol. 347. Astronomical Society of the Pacific Conference Series, p. 81.

Manchester, R. N. (Mar. 2015). "Pulsars and gravity". In: *International Journal of Modern Physics D* 24.6, 1530018, p. 1530018. DOI: 10.1142/S0218271815300189. arXiv: 1502.05474 [gr-qc].

Manchester, R. N. et al. (Apr. 2005). "The Australia Telescope National Facility Pulsar Catalogue". In: *AJ* 129.4, pp. 1993–2006. DOI: 10.1086/428488. arXiv: astro-ph/0412641 [astro-ph].

Marigo, P. and L. Girardi (July 2007). "Evolution of asymptotic giant branch stars. I. Updated synthetic TP-AGB models and their basic calibration". In: *A&A* 469.1, pp. 239–263. DOI: 10.1051/0004-6361:20066772. arXiv: astro-ph/0703139 [astro-ph].

Marigo, Paola et al. (July 2020). "Carbon star formation as seen through the non-monotonic initial-final mass relation". In: *Nature Astronomy* 4, pp. 1102–1110. DOI: 10.1038/s41550-020-1132-1. arXiv: 2007.04163 [astro-ph.SR].

Masetti, N. et al. (Sept. 2010). "Unveiling the nature of INTEGRAL objects through optical spectroscopy. VIII. Identification of 44 newly detected hard X-ray sources". In: *A&A* 519, A96, A96. DOI: 10.1051/0004-6361/201014852. arXiv: 1006.4513 [astro-ph.HE].

Matz, S. M. et al. (Feb. 1988). "Gamma-ray line emission from SN1987A". In: *Nature* 331.6155, pp. 416–418. DOI: 10.1038/331416a0.

McCray, Richard and Claes Fransson (Sept. 2016). "The Remnant of Supernova 1987A". In: *ARA&A* 54, pp. 19–52. DOI: 10.1146/annurev-astro-082615-105405.

Mdzinarishvili, T. G. and K. B. Chargeishvili (Feb. 2005). "New runaway OB stars with HIPPARCOS". In: *A&A* 431, pp. L1–L4. DOI: 10.1051/0004-6361:200400134.

Merloni, A. et al. (Sept. 2012). "eROSITA Science Book: Mapping the Structure of the Energetic Universe". In: *arXiv e-prints*, arXiv:1209.3114, arXiv:1209.3114. arXiv: 1209.3114 [astro-ph.HE].

Messineo, Maria et al. (Aug. 2020). "Massive Stars in Molecular Clouds Rich in High-energy Sources: The Bridge of G332.809-0.132 and CS 78 in NGC 6334". In: *AJ* 160.2, 65, p. 65. DOI: 10.3847/1538-3881/ab9950. arXiv: 2007.11074 [astro-ph.GA].

Meynet, Georges and André Maeder (2017). "Supernovae from Rotating Stars". In: *Handbook of Supernovae*. Ed. by Athem W. Alsabti and Paul Murdin, p. 601. DOI: 10.1007/978-3-319-21846-5_122.

Miller, David R. et al. (Feb. 2022). "The Ultramassive White Dwarfs of the Alpha Persei Cluster". In: *ApJ* 926.2, L24, p. L24. DOI: 10.3847/2041-8213/ac50a5. arXiv: 2110.09668 [astro-ph.SR].

Miller Bertolami, Marcelo Miguel (Apr. 2016). "New models for the evolution of post-asymptotic giant branch stars and central stars of planetary nebulae". In: *A&A* 588, A25, A25. DOI: 10.1051/0004-6361/201526577. arXiv: 1512.04129 [astro-ph.SR].

Miller-Jones, James C. A. et al. (Mar. 2021). "Cygnus X-1 contains a 21-solar mass black hole—Implications for massive star winds". In: *Science* 371.6533, pp. 1046–1049. DOI: 10.1126/science.abb3363. arXiv: 2102.09091 [astro-ph.HE].

Minkowski, R. (Aug. 1941). "Spectra of Supernovae". In: *PASP* 53.314, p. 224. DOI: 10.1086/125315.

Minniti, Dante and Marina Rejkuba (Aug. 2002). "Extragalactic Globular Cluster Planetary Nebulae: Discovery of a Planetary Nebula in the NGC 5128 Globular Cluster G169 Using the Magellan I Baade Telescope". In: *ApJ* 575.2, pp. L59–L62. DOI: 10.1086/342827.

Minniti, Dante et al. (Oct. 2019). "New Candidate Planetary Nebulae in Galactic Globular Clusters from the VVV Survey". In: *ApJ* 884.1, L15, p. L15. DOI: 10.3847/2041-8213/ab4424. arXiv: 1909.09109 [astro-ph.SR].

Mirabel, Félix (Aug. 2017). "The formation of stellar black holes". In: *New A Rev.* 78, pp. 1–15. DOI: 10.1016/j.newar.2017.04.002.

Mirabel, I. Félix and Irapuan Rodrigues (May 2003). "Formation of a Black Hole in the Dark". In: *Science* 300.5622, pp. 1119–1121. DOI: 10.1126/science.1083451. arXiv: astro-ph/0305205 [astro-ph].

Mokiem, M. R. et al. (Oct. 2007). "The empirical metallicity dependence of the mass-loss rate of O- and early B-type stars". In: *A&A* 473.2, pp. 603–614. DOI: 10.1051/0004-6361:20077545. arXiv: 0708.2042 [astro-ph].

Moni Bidin, C. et al. (Jan. 2014). "Investigating potential planetary nebula/cluster pairs". In: *A&A* 561, A119, A119. DOI: 10.1051/0004-6361/201220802. arXiv: 1311.0760 [astro-ph.GA].

Monteiro, Hektor et al. (May 2021). "The distribution of open clusters in the Galaxy". In: *Frontiers in Astronomy and Space Sciences* 8, 62, p. 62. DOI: 10.3389/fspas.2021.656474. arXiv: 2104.00134 [astro-ph.GA].

Moraux, E. (Nov. 2016). "Open clusters and associations in the Gaia era". In: *EAS Publications Series*. Vol. 80-81. EAS Publications Series, pp. 73–114. DOI: 10.1051/eas/1680004. arXiv: 1607.00027 [astro-ph.SR].

Moss, Adam et al. (Mar. 2022). "Improving white dwarfs as chronometers with Gaia parallaxes and spectroscopic metallicities". In: *arXiv e-prints*, arXiv:2203.08971, arXiv:2203.08971. arXiv: 2203.08971 [astro-ph.SR].

Murphy, Jeremiah W. et al. (Nov. 2011). "The Progenitor Mass of SN 2011dh from Stellar Population Analysis". In: *ApJ* 742.1, L4, p. L4. DOI: 10.1088/2041-8205/742/1/L4. arXiv: 1107.6046 [astro-ph.SR].

Murphy, Jeremiah W. et al. (June 2018). "The Progenitor Age and Mass of the Black Hole Formation Candidate N6946-BH1". In: *ApJ* 860.2, 117, p. 117. DOI: 10.3847/1538-4357/aac2be. arXiv: 1803.00024 [astro-ph.SR].

Nayak, P. K. et al. (Sept. 2018). "Star clusters in the Magellanic Clouds. II. Age-dating, classification, and spatio-temporal distribution of the SMC clusters". In: *A&A* 616, A187, A187. DOI: 10.1051/0004-6361/201732227. arXiv: 1804.00635 [astro-ph.GA].

Netopil, M. et al. (Jan. 2016). "On the metallicity of open clusters. III. Homogenised sample". In: *A&A* 585, A150, A150. DOI: 10.1051/0004-6361/201526370. arXiv: 1511.08884 [astro-ph.SR].

Netopil, Martin et al. (Jan. 2022). "The Galactic metallicity gradient shown by open clusters in the light of radial migration". In: *MNRAS* 509.1, pp. 421–439. DOI: 10.1093/mnras/stab2961. arXiv: 2110.11893 [astro-ph.GA].

Neuhäuser, R., F. Gießler, and V. V. Hambaryan (Oct. 2020). "A nearby recent supernova that ejected the runaway star ζ Oph, the pulsar PSR B1706-16, and ^{60}Fe found on Earth". In: *MNRAS* 498.1, pp. 899–917. DOI: 10.1093/mnras/stz2629. arXiv: 1909.06850 [astro-ph.HE].

Neustadt, J. M. M. et al. (Nov. 2021). "The search for failed supernovae with the Large Binocular Telescope: a new candidate and the failed SN fraction with 11 yr of data". In: *MNRAS* 508.1, pp. 516–528. DOI: 10.1093/mnras/stab2605. arXiv: 2104.03318 [astro-ph.SR].

Nomoto, K. (Feb. 1984). "Evolution of 8-10 solar mass stars toward electron capture supernovae. I - Formation of electron-degenerate O + NE + MG cores." In: *ApJ* 277, pp. 791–805. DOI: 10.1086/161749.

Nomoto, Ken'ichi (Nov. 1987). "Evolution of 8–10 M_{sun} Stars toward Electron Capture Supernovae. II. Collapse of an O + NE + MG Core". In: *ApJ* 322, p. 206. DOI: 10.1086/165716.

Packet, W. (Sept. 1981). "On the spin-up of the mass accreting component in a close binary system". In: *A&A* 102.1, pp. 17–19.

Paczynski, Bohdan (Jan. 1996). "Gravitational Microlensing in the Local Group". In: *ARA&A* 34, pp. 419–460. DOI: 10.1146/annurev.astro.34.1.419. arXiv: astro-ph/9604011 [astro-ph].

Page, Dany et al. (Dec. 2004). "Minimal Cooling of Neutron Stars: A New Paradigm". In: *ApJS* 155.2, pp. 623–650. DOI: 10.1086/424844. arXiv: astro-ph/0403657 [astro-ph].

Page, Dany et al. (July 2020). "Ns 1987A in SN 1987A". In: *ApJ* 898.2, 125, p. 125. DOI: 10.3847/1538-4357/ab93c2. arXiv: 2004.06078 [astro-ph.HE].

Panagia, Nino et al. (Aug. 2000). "Young Stellar Populations around SN 1987A". In: *ApJ* 539.1, pp. 197–208. DOI: 10.1086/309212. arXiv: astro-ph/0001476 [astro-ph].

Parker, Quentin A. et al. (Sept. 2005). "The AAO/UKST SuperCOSMOS Hα survey". In: *MNRAS* 362.2, pp. 689–710. DOI: 10.1111/j.1365-2966.2005.09350.x. arXiv: astro-ph/0506599 [astro-ph].

Pastorelli, Giada et al. (June 2019). "Constraining the thermally pulsing asymptotic giant branch phase with resolved stellar populations in the Small Magellanic Cloud". In: *MNRAS* 485.4, pp. 5666–5692. DOI: 10.1093/mnras/stz725. arXiv: 1903.04499 [astro-ph.SR].

Pauls, T. (July 1977). "A possible supernova remnant in an open cluster." In: *A&A* 59, pp. L13–L14.

Pease, F. G. (Oct. 1928). "A Planetary Nebula in the Globular Cluster Messier 15". In: *PASP* 40.237, pp. 342–342. DOI: 10.1086/123857.

Pejcha, Ondřej and Todd A. Thompson (Mar. 2015). "The Landscape of the Neutrino Mechanism of Core-collapse Supernovae: Neutron Star and Black Hole Mass Functions, Explosion Energies, and Nickel Yields". In: *ApJ* 801.2, 90, p. 90. DOI: 10.1088/0004-637X/801/2/90. arXiv: 1409.0540 [astro-ph.HE].

Peri, C. S., P. Benaglia, and N. L. Isequilla (June 2015). "E-BOSS: An Extensive stellar BOw Shock Survey. II. Catalogue second release". In: *A&A* 578, A45, A45. DOI: 10.1051/0004-6361/201424676. arXiv: 1504.04264 [astro-ph.SR].

Peri, C. S. et al. (Feb. 2012). "E-BOSS: an Extensive stellar BOw Shock Survey. I. Methods and first catalogue". In: *A&A* 538, A108, A108. DOI: 10.1051/0004-6361/201118116. arXiv: 1109.3689 [astro-ph.SR].

Perryman, M. A. C. et al. (July 1997). "The HIPPARCOS Catalogue". In: *A&A* 323, pp. L49–L52.

Perryman, Michael (2009). *Astronomical Applications of Astrometry: Ten Years of Exploitation of the Hipparcos Satellite Data*.

Peterson, Charles J. and M. P. Fitzgerald (Dec. 1988). "UBV photometry in four southern open clusters with suspected supernova remnants." In: *MNRAS* 235, pp. 1439–1450. DOI: 10.1093/mnras/235.4.1439.

Petre, R., C. M. Becker, and P. F. Winkler (July 1996). "A Central Stellar Remnant in Puppis A". In: *ApJ* 465, p. L43. DOI: 10.1086/310141.

Peuten, M. et al. (Nov. 2016). "A stellar-mass black hole population in the globular cluster NGC 6101?" In: *MNRAS* 462.3, pp. 2333–2342. DOI: 10.1093/mnras/stw1726. arXiv: 1609.01720 [astro-ph.GA].

Pfahl, Eric et al. (July 2002). "A New Class of High-Mass X-Ray Binaries: Implications for Core Collapse and Neutron Star Recoil". In: *ApJ* 574.1, pp. 364–376. DOI: 10.1086/340794. arXiv: astro-ph/0109521 [astro-ph].

Pflamm-Altenburg, Jan and Pavel Kroupa (May 2010). "The two-step ejection of massive stars and the issue of their formation in isolation". In: *MNRAS* 404.3, pp. 1564–1568. DOI: 10.1111/j.1365-2966.2010.16376.x. arXiv: 1001.3671 [astro-ph.GA].

Piatti, A. E. (July 2018). "Towards a comprehensive knowledge of the star cluster population in the Small Magellanic Cloud". In: *MNRAS* 478.1, pp. 784–790. DOI: 10.1093/mnras/sty1249. arXiv: 1805.04017 [astro-ph.GA].

Pilbratt, G. L. et al. (July 2010). "Herschel Space Observatory. An ESA facility for far-infrared and submillimetre astronomy". In: *A&A* 518, L1, p. L1. DOI: 10.1051/0004-6361/201014759. arXiv: 1005.5331 [astro-ph.IM].

Pittard, J. M. and B. Dawson (July 2018). "Colliding stellar winds structure and X-ray emission". In: *MNRAS* 477.4, pp. 5640–5645. DOI: 10.1093/mnras/sty1025. arXiv: 1804.05672 [astro-ph.SR].

Podsiadlowski, Ph. et al. (Sept. 2004). "The Effects of Binary Evolution on the Dynamics of Core Collapse and Neutron Star Kicks". In: *ApJ* 612.2, pp. 1044–1051. DOI: 10.1086/421713. arXiv: astro-ph/0309588 [astro-ph].

Poglitsch, A. et al. (July 2010). "The Photodetector Array Camera and Spectrometer (PACS) on the Herschel Space Observatory". In: *A&A* 518, L2, p. L2. DOI: 10.1051/0004-6361/201014535. arXiv: 1005.1487 [astro-ph.IM].

Portegies Zwart, Simon F., Stephen L. W. McMillan, and Mark Gieles (Sept. 2010). "Young Massive Star Clusters". In: *ARA&A* 48, pp. 431–493. DOI: 10.1146/annurev-astro-081309-130834. arXiv: 1002.1961 [astro-ph.GA].

Poveda, A., J. Ruiz, and C. Allen (Apr. 1967). "Run-away Stars as the Result of the Gravitational Collapse of Proto-stellar Clusters". In: *Boletin de los Observatorios Tonantzintla y Tacubaya* 4, pp. 86–90.

Povich, Matthew S. et al. (Dec. 2008). "Interstellar Weather Vanes: GLIMPSE Mid-Infrared Stellar Wind Bow Shocks in M17 and RCW 49". In: *ApJ* 689.1, pp. 242–248. DOI: 10.1086/592565. arXiv: 0808.2168 [astro-ph].

Raddi, R. et al. (Sept. 2018). "Anatomy of the hyper-runaway star LP 40-365 with Gaia". In: *MNRAS* 479.1, pp. L96–L101. DOI: 10.1093/mnrasl/sly103. arXiv: 1804.09677 [astro-ph.SR].

Raddi, R. et al. (Oct. 2019). "Partly burnt runaway stellar remnants from peculiar thermonuclear supernovae". In: *MNRAS* 489.2, pp. 1489–1508. DOI: 10.1093/mnras/stz1618. arXiv: 1902.05061 [astro-ph.SR].

Rafelski, Marc and Dennis Zaritsky (June 2005). "The Star Clusters of the Small Magellanic Cloud: Age Distribution". In: *AJ* 129.6, pp. 2701–2713. DOI: 10.1086/424938. arXiv: astro-ph/0408186 [astro-ph].

Raguzova, N. V. and S. B. Popov (June 2005). "Be X-ray binaries and candidates". In: *Astronomical and Astrophysical Transactions* 24.3, pp. 151–185. DOI: 10.1080/10556790500497311. arXiv: astro-ph/0505275 [astro-ph].

Ransom, Scott M. (May 2008). "Pulsars in Globular Clusters". In: *Dynamical Evolution of Dense Stellar Systems*. Ed. by Enrico Vesperini, Mirek Giersz, and Alison Sills. Vol. 246, pp. 291–300. DOI: 10.1017/S1743921308015810.

Rao, Anjali et al. (June 2020). "Kinematic study of the association Cyg OB3 with Gaia DR2". In: *MNRAS* 495.1, pp. 1491–1500. DOI: 10.1093/mnras/staa1217. arXiv: 1908.00810 [astro-ph.SR].

Rauw, Gregor and Yaël Nazé (Sept. 2016). "X-ray emission from interacting wind massive binaries: A review of 15 years of progress". In: *Advances in Space Research* 58.5, pp. 761–781. DOI: 10.1016/j.asr.2015.09.026. arXiv: 1509.06480 [astro-ph.SR].

Reig, Pablo (Mar. 2011). "Be/X-ray binaries". In: *Ap&SS* 332.1, pp. 1–29. DOI: 10.1007/s10509-010-0575-8. arXiv: 1101.5036 [astro-ph.HE].

Renedo, I. et al. (July 2010). "New Cooling Sequences for Old White Dwarfs". In: *ApJ* 717.1, pp. 183–195. DOI: 10.1088/0004-637X/717/1/183. arXiv: 1005.2170 [astro-ph.SR].

Renzo, M. et al. (Apr. 2019). "Massive runaway and walkaway stars. A study of the kinematical imprints of the physical processes governing the evolution and explosion of their binary progenitors". In: *A&A* 624, A66, A66. DOI: 10.1051/0004-6361/201833297. arXiv: 1804.09164 [astro-ph.SR].

Repetto, Serena, Andrei P. Igoshev, and Gijs Nelemans (May 2017). "The Galactic distribution of X-ray binaries and its implications for compact object formation

and natal kicks". In: *MNRAS* 467.1, pp. 298–310. DOI: 10.1093/mnras/stx027. arXiv: 1701.01347 [astro-ph.HE].

Rezzolla, Luciano, Elias R. Most, and Lukas R. Weih (Jan. 2018). "Using Gravitational-wave Observations and Quasi-universal Relations to Constrain the Maximum Mass of Neutron Stars". In: *ApJ* 852.2, L25, p. L25. DOI: 10.3847/2041-8213/aaa401. arXiv: 1711.00314 [astro-ph.HE].

Richer, Harvey B. et al. (Aug. 2019). "A Massive Magnetic Helium Atmosphere White Dwarf Binary in a Young Star Cluster". In: *ApJ* 880.2, 75, p. 75. DOI: 10.3847/1538-4357/ab2874. arXiv: 1906.04727 [astro-ph.SR].

Richer, Harvey B. et al. (May 2021). "Massive White Dwarfs in Young Star Clusters". In: *ApJ* 912.2, 165, p. 165. DOI: 10.3847/1538-4357/abdeb7. arXiv: 2101.08300 [astro-ph.SR].

Rieke, G. H. et al. (Sept. 2004). "The Multiband Imaging Photometer for Spitzer (MIPS)". In: *ApJS* 154.1, pp. 25–29. DOI: 10.1086/422717.

Rivinius, Thomas, Alex C. Carciofi, and Christophe Martayan (Oct. 2013). "Classical Be stars. Rapidly rotating B stars with viscous Keplerian decretion disks". In: *A&A Rev.* 21, 69, p. 69. DOI: 10.1007/s00159-013-0069-0. arXiv: 1310.3962 [astro-ph.SR].

Röser, Siegfried, Elena Schilbach, and Bertrand Goldman (Oct. 2016). "Nine new open clusters within 500 pc from the Sun". In: *A&A* 595, A22, A22. DOI: 10.1051/0004-6361/201629158.

Sahu, Kailash C. et al. (Jan. 2022). "An Isolated Stellar-Mass Black Hole Detected Through Astrometric Microlensing". In: *arXiv e-prints*, arXiv:2201.13296, arXiv:2201.13296. arXiv: 2201.13296 [astro-ph.SR].

Salaris, M. and L. R. Bedin (Mar. 2019). "Praesepe white dwarfs in Gaia DR2". In: *MNRAS* 483.3, pp. 3098–3107. DOI: 10.1093/mnras/sty3316. arXiv: 1811.12825 [astro-ph.GA].

Sana, H. et al. (July 2012). "Binary Interaction Dominates the Evolution of Massive Stars". In: *Science* 337.6093, p. 444. DOI: 10.1126/science.1223344. arXiv: 1207.6397 [astro-ph.SR].

Sasaki, Manami (Feb. 2020). "Supernova remnants in nearby galaxies". In: *Astronomische Nachrichten* 341.2, pp. 156–162. DOI: 10.1002/asna.202023772.

Schoenberner, D. (Sept. 1983). "Late stages of stellar evolution. II. Mass loss and the transition ofasymptotic giant branch stars into hot remnants." In: *ApJ* 272, pp. 708–714. DOI: 10.1086/161333.

Scholz, F.-W. and Michael A. Stephens (1987). "K-Sample Anderson–Darling Tests". In: *Journal of the American Statistical Association* 82, pp. 918–924.

Schönberner, D. and T. Blöcker (Sept. 1996). "Structure and Evolution of Central Stars of Planetary Nebulae". In: *Ap&SS* 245.2, pp. 201–217. DOI: 10.1007/BF00642226.

Seward, F. D. et al. (Nov. 2012). "DEM L241, a Supernova Remnant Containing a High-mass X-Ray Binary". In: *ApJ* 759.2, 123, p. 123. DOI: 10.1088/0004-637X/759/2/123. arXiv: 1208.1453 [astro-ph.HE].

Shapiro, Stuart L. and Saul A. Teukolsky (1983). *Black holes, white dwarfs, and neutron stars : the physics of compact objects.*

Shen, Ken J. et al. (Sept. 2018). "Three Hypervelocity White Dwarfs in Gaia DR2: Evidence for Dynamically Driven Double-degenerate Double-detonation Type Ia Supernovae". In: *ApJ* 865.1, 15, p. 15. DOI: 10.3847/1538-4357/aad55b. arXiv: 1804.11163 [astro-ph.SR].

Shu, F. H. and S. H. Lubow (Jan. 1981). "Mass, angular momentum, and energy transfer in close binary stars". In: *ARA&A* 19, pp. 277–293. DOI: 10.1146/annurev.aa.19.090181.001425.

Sim, Gyuheon et al. (Oct. 2019). "207 New Open Star Clusters within 1 kpc from Gaia Data Release 2". In: *Journal of Korean Astronomical Society* 52, pp. 145–158. DOI: 10.5303/JKAS.2019.52.5.145. arXiv: 1907.06872 [astro-ph.SR].

Smartt, S. J. (Apr. 2015). "Observational Constraints on the Progenitors of Core-Collapse Supernovae: The Case for Missing High-Mass Stars". In: *PASA* 32, e016, e016. DOI: 10.1017/pasa.2015.17. arXiv: 1504.02635 [astro-ph.SR].

Smartt, S. J. et al. (May 2009). "The death of massive stars - I. Observational constraints on the progenitors of Type II-P supernovae". In: *MNRAS* 395.3, pp. 1409–1437. DOI: 10.1111/j.1365-2966.2009.14506.x. arXiv: 0809.0403 [astro-ph].

Smith, Myron A., R. Lopes de Oliveira, and C. Motch (Sept. 2016). "The X-ray emission of the γ Cassiopeiae stars". In: *Advances in Space Research* 58.5, pp. 782–808. DOI: 10.1016/j.asr.2015.12.032. arXiv: 1512.06446 [astro-ph.SR].

Spina, L. et al. (May 2021). "The GALAH survey: tracing the Galactic disc with open clusters". In: *MNRAS* 503.3, pp. 3279–3296. DOI: 10.1093/mnras/stab471. arXiv: 2011.02533 [astro-ph.GA].

Stanghellini, Letizia et al. (Jan. 2020). "The Population of Galactic Planetary Nebulae: a Study of Distance Scales and Central Stars Based on the Second Gaia Release". In: *ApJ* 889.1, 21, p. 21. DOI: 10.3847/1538-4357/ab59e4. arXiv: 1910.09680 [astro-ph.SR].

Stevance, H. F., S. G. Parsons, and J. J. Eldridge (Mar. 2022). "To be or not to be a black hole: detailed binary population models as a sanity check". In: *MNRAS* 511.1, pp. L77–L81. DOI: 10.1093/mnrasl/slac001. arXiv: 2112.00015 [astro-ph.SR].

Stone, R. C. (Sept. 1979). "Kinematics, close binary evolution, and ages of the O stars." In: *ApJ* 232, pp. 520–530. DOI: 10.1086/157311.

Strader, Jay et al. (Oct. 2012). "Two stellar-mass black holes in the globular cluster M22". In: *Nature* 490.7418, pp. 71–73. DOI: 10.1038/nature11490. arXiv: 1210.0901 [astro-ph.HE].

Sukhbold, Tuguldur and S. E. Woosley (Mar. 2014). "The Compactness of Presupernova Stellar Cores". In: *ApJ* 783.1, 10, p. 10. DOI: 10.1088/0004-637X/783/1/10. arXiv: 1311.6546 [astro-ph.SR].

Sukhbold, Tuguldur et al. (Apr. 2016). "Core-collapse Supernovae from 9 to 120 Solar Masses Based on Neutrino-powered Explosions". In: *ApJ* 821.1, 38, p. 38. DOI: 10.3847/0004-637X/821/1/38. arXiv: 1510.04643 [astro-ph.HE].

Sun, Weijia et al. (Nov. 2019). "The Next Generation Virgo Cluster Survey. XVII. A Search for Planetary Nebulae in Virgo Cluster Globular Clusters". In: *ApJ* 885.2, 145, p. 145. DOI: 10.3847/1538-4357/ab49fb. arXiv: 1910.00169 [astro-ph.GA].

Takahashi, Koh, Takashi Yoshida, and Hideyuki Umeda (July 2013). "Evolution of Progenitors for Electron Capture Supernovae". In: *ApJ* 771.1, 28, p. 28. DOI: 10.1088/0004-637X/771/1/28. arXiv: 1302.6402 [astro-ph.SR].

Tatton, B. L. et al. (June 2021). "The VMC Survey - XL. Three-dimensional structure of the Small Magellanic Cloud as derived from red clump stars". In: *MNRAS* 504.2, pp. 2983–2997. DOI: 10.1093/mnras/staa3857. arXiv: 2012.12288 [astro-ph.GA].

Tauris, T. M. and E. P. J. van den Heuvel (2006). "Formation and evolution of compact stellar X-ray sources". In: *Compact stellar X-ray sources*. Vol. 39, pp. 623–665.

Tetarenko, B. E. et al. (Feb. 2016). "WATCHDOG: A Comprehensive All-sky Database of Galactic Black Hole X-ray Binaries". In: *ApJS* 222.2, 15, p. 15. DOI: 10.3847/0067-0049/222/2/15. arXiv: 1512.00778 [astro-ph.HE].

Tetzlaff, N., R. Neuhäuser, and M. M. Hohle (Nov. 2009). "The origin of the Guitar pulsar". In: *MNRAS* 400.1, pp. L99–L102. DOI: 10.1111/j.1745-3933.2009.00774.x. arXiv: 0910.4453 [astro-ph.GA].

Tetzlaff, N. et al. (Mar. 2010). "Identifying birth places of young isolated neutron stars". In: *MNRAS* 402.4, pp. 2369–2387. DOI: 10.1111/j.1365-2966.2009.16093.x. arXiv: 0911.4441 [astro-ph.GA].

Tetzlaff, N. et al. (Oct. 2011). "The origin of RX J1856.5-3754 and RX J0720.4-3125 - updated using new parallax measurements". In: *MNRAS* 417.1, pp. 617–626. DOI: 10.1111/j.1365-2966.2011.19302.x. arXiv: 1107.1673 [astro-ph.GA].

Tetzlaff, N. et al. (Mar. 2012). "Neutron Stars From Young Nearby Associations: The Origin of RX J1605.3+3249". In: *PASA* 29.2, pp. 98–108. DOI: 10.1071/AS11057. arXiv: 1202.1388 [astro-ph.GA].

Tetzlaff, N. et al. (Oct. 2013). "The neutron star born in the Antlia supernova remnant". In: *MNRAS* 435.1, pp. 879–884. DOI: 10.1093/mnras/stt1358. arXiv: 1307.5616 [astro-ph.GA].

Tetzlaff, N. et al. (Mar. 2014). "The origin of the young pulsar PSR J0826+2637 and its possible former companion HIP 13962". In: *MNRAS* 438.4, pp. 3587–3593. DOI: 10.1093/mnras/stt2478. arXiv: 1401.4678 [astro-ph.GA].

Torres, Santiago et al. (Apr. 2021). "The Gaia DR2 halo white dwarf population: the luminosity function, mass distribution, and its star formation history". In: *MNRAS* 502.2, pp. 1753–1767. DOI: 10.1093/mnras/stab079. arXiv: 2101.03341 [astro-ph.GA].

Tremblay, P. E. et al. (Nov. 2012). "Spectroscopic and photometric studies of white dwarfs in the Hyades". In: *A&A* 547, A99, A99. DOI: 10.1051/0004-6361/201220057. arXiv: 1209.4309 [astro-ph.GA].

Tremblay, P. E. et al. (Feb. 2019). "Fundamental parameter accuracy of DA and DB white dwarfs in Gaia Data Release 2". In: *MNRAS* 482.4, pp. 5222–5232. DOI: 10.1093/mnras/sty3067. arXiv: 1811.03084 [astro-ph.SR].

Tremblay, P. E. et al. (Sept. 2020). "Gaia white dwarfs within 40 pc - I. Spectroscopic observations of new candidates". In: *MNRAS* 497.1, pp. 130–145. DOI: 10.1093/mnras/staa1892. arXiv: 2006.00965 [astro-ph.SR].

Turner, D. G. et al. (Nov. 2011). "New Results for the Open Cluster Bica 6 and Its Associated Planetary Nebula Abell 8". In: *PASP* 123.909, p. 1249. DOI: 10.1086/662663. arXiv: 1109.6006 [astro-ph.SR].

van Altena, W. F., J. T. Lee, and E. D. Hoffleit (1995). *The general catalogue of trigonometric [stellar] parallaxes.*

van Altena, William F. (2012). *Astrometry for Astrophysics.*

van Buren, Dave and Richard McCray (June 1988). "Bow Shocks and Bubbles Are Seen around Hot Stars by IRAS". In: *ApJ* 329, p. L93. DOI: 10.1086/185184.

van Buren, Dave, Alberto Noriega-Crespo, and Ruth Dgani (Dec. 1995). "An IRAS/ISSA Survey of Bow Shocks Around Runaway Stars". In: *AJ* 110, p. 2914. DOI: 10.1086/117739.

van den Eijnden, J. et al. (Feb. 2022). "MeerKAT discovery of radio emission from the Vela X-1 bow shock". In: *MNRAS* 510.1, pp. 515–530. DOI: 10.1093/mnras/stab3395. arXiv: 2111.10159 [astro-ph.HE].

van den Heuvel, E. P. J. (Mar. 1975). "The upper mass limit for white dwarf formation as derived from the stellar content of the Hyades cluster." In: *ApJ* 196, pp. L121–L123. DOI: 10.1086/181759.

— (Oct. 2004). "X-Ray Binaries and Their Descendants: Binary Radio Pulsars; Evidence for Three Classes of Neutron Stars?" In: *5th INTEGRAL Workshop on the*

INTEGRAL Universe. Ed. by V. Schoenfelder, G. Lichti, and C. Winkler. Vol. 552. ESA Special Publication, p. 185. arXiv: astro-ph/0407451 [astro-ph].

van den Heuvel, E. P. J. et al. (Dec. 2000). "On the origin of the difference between the runaway velocities of the OB-supergiant X-ray binaries and the Be/X-ray binaries". In: *A&A* 364, pp. 563–572. arXiv: astro-ph/0005245 [astro-ph].

van der Meij, Vincent et al. (Nov. 2021). "Confirming NGC 6231 as the parent cluster of the runaway high-mass X-ray binary HD 153919/4U 1700-37 with Gaia DR2". In: *A&A* 655, A31, A31. DOI: 10.1051/0004-6361/202040114. arXiv: 2108.12918 [astro-ph.HE].

Van Dyk, Schuyler D. (Sept. 2017). "The direct identification of core-collapse supernova progenitors". In: *Philosophical Transactions of the Royal Society of London Series A* 375.2105, 20160277, p. 20160277. DOI: 10.1098/rsta.2016.0277.

Van Dyk, Schuyler D. et al. (Nov. 1999). "The Environments of Supernovae in Post-Refurbishment Hubble Space Telescope Images". In: *AJ* 118.5, pp. 2331–2349. DOI: 10.1086/301068. arXiv: astro-ph/9907252 [astro-ph].

van Leeuwen, Floor (2007). *Hipparcos, the New Reduction of the Raw Data*. Vol. 350. DOI: 10.1007/978-1-4020-6342-8.

van Oijen, J. G. J. (June 1989). "Are massive X-ray binaries runaway stars ?" In: *A&A* 217, pp. 115–126.

van Rensbergen, W., D. Vanbeveren, and C. De Loore (Jan. 1996). "OB-runaways as a result of massive star evolution." In: *A&A* 305, p. 825.

Vasilopoulos, G. et al. (Mar. 2018). "Identification of two new HMXBs in the LMC: an ∼2013 s pulsar and a probable SFXT". In: *MNRAS* 475.1, pp. 220–231. DOI: 10.1093/mnras/stx3139. arXiv: 1712.00096 [astro-ph.HE].

Vennes, S. et al. (Aug. 2017). "An unusual white dwarf star may be a surviving remnant of a subluminous Type Ia supernova". In: *Science* 357.6352, pp. 680–683. DOI: 10.1126/science.aam8378. arXiv: 1708.05568 [astro-ph.SR].

Verbunt, Frank, Andrei Igoshev, and Eric Cator (Dec. 2017). "The observed velocity distribution of young pulsars". In: *A&A* 608, A57, A57. DOI: 10.1051/0004-6361/201731518. arXiv: 1708.08281 [astro-ph.HE].

Vigna-Gómez, Alejandro and Enrico Ramirez-Ruiz (Mar. 2022). "A binary origin for the first isolated stellar-mass black hole detected with astrometric microlensing". In: *arXiv e-prints*, arXiv:2203.08478, arXiv:2203.08478. arXiv: 2203.08478 [astro-ph.GA].

Vink, Jacco (Dec. 2012). "Supernova remnants: the X-ray perspective". In: *A&A Rev.* 20, 49, p. 49. DOI: 10.1007/s00159-011-0049-1. arXiv: 1112.0576 [astro-ph.HE].

Vink, Jorick S. and Andreas A. C. Sander (June 2021). "Metallicity-dependent wind parameter predictions for OB stars". In: *MNRAS* 504.2, pp. 2051–2061. DOI: 10.1093/mnras/stab902. arXiv: 2103.12736 [astro-ph.SR].

Vinkó, J. et al. (Apr. 2009). "The Young, Massive, Star Cluster Sandage-96 After the Explosion of Supernova 2004dj in NGC 2403". In: *ApJ* 695.1, pp. 619–635. DOI: 10.1088/0004-637X/695/1/619. arXiv: 0812.1589 [astro-ph].

Walsh, J. R., M. Rejkuba, and N. A. Walton (Feb. 2015). "An imaging and spectroscopic study of the planetary nebulae in NGC 5128 (Centaurus A). Planetary nebulae catalogues". In: *A&A* 574, A109, A109. DOI: 10.1051/0004-6361/201424316. arXiv: 1501.01853 [astro-ph.GA].

Walter, Roland et al. (Aug. 2015). "High-mass X-ray binaries in the Milky Way. A closer look with INTEGRAL". In: *A&A Rev.* 23, 2, p. 2. DOI: 10.1007/s00159-015-0082-6. arXiv: 1505.03651 [astro-ph.HE].

Wang, Shu and Xiaodian Chen (Dec. 2021). "3D Parameter Maps of Red Clump Stars in the Milky Way: Absolute Magnitudes and Intrinsic Colors". In: *ApJ* 923.2, 145, p. 145. DOI: 10.3847/1538-4357/ac22a7. arXiv: 2108.13605 [astro-ph.GA].

Wang, Shu et al. (July 2020). "Distances to the supernova remnants in the inner disk". In: *A&A* 639, A72, A72. DOI: 10.1051/0004-6361/201936868. arXiv: 2005.08270 [astro-ph.GA].

Wang, Xiaofeng et al. (June 2005). "The Progenitor of SN 2004dj in a Star Cluster". In: *ApJ* 626.2, pp. L89–L92. DOI: 10.1086/431903. arXiv: astro-ph/0505305 [astro-ph].

Waters, L. B. F. M. and M. H. van Kerkwijk (Oct. 1989). "The relation between orbital and spin periods in massive X-ray binaries." In: *A&A* 223, pp. 196–206.

Weatherford, Newlin C. et al. (Aug. 2020). "A Dynamical Survey of Stellar-mass Black Holes in 50 Milky Way Globular Clusters". In: *ApJ* 898.2, 162, p. 162. DOI: 10.3847/1538-4357/ab9f98. arXiv: 1911.09125 [astro-ph.SR].

Wellstein, S., N. Langer, and H. Braun (Apr. 2001). "Formation of contact in massive close binaries". In: *A&A* 369, pp. 939–959. DOI: 10.1051/0004-6361:20010151. arXiv: astro-ph/0102244 [astro-ph].

Werner, M. W. et al. (Sept. 2004). "The Spitzer Space Telescope Mission". In: *ApJS* 154.1, pp. 1–9. DOI: 10.1086/422992. arXiv: astro-ph/0406223 [astro-ph].

Wilkin, Francis P. (Mar. 1996). "Exact Analytic Solutions for Stellar Wind Bow Shocks". In: *ApJ* 459, p. L31. DOI: 10.1086/309939.

Williams, Benjamin F. et al. (June 2018). "Constraints for the Progenitor Masses of Historic Core-collapse Supernovae". In: *ApJ* 860.1, 39, p. 39. DOI: 10.3847/1538-4357/aaba7d. arXiv: 1803.08112 [astro-ph.GA].

Wright, Edward L. et al. (Dec. 2010). "The Wide-field Infrared Survey Explorer (WISE): Mission Description and Initial On-orbit Performance". In: *AJ* 140.6, pp. 1868–1881. DOI: 10.1088/0004-6256/140/6/1868. arXiv: 1008.0031 [astro-ph.IM].

Wright, Nicholas J. (Nov. 2020). "OB Associations and their origins". In: *New A Rev.* 90, 101549, p. 101549. DOI: 10.1016/j.newar.2020.101549. arXiv: 2011.09483 [astro-ph.SR].

Wright, Nicholas J. et al. (Mar. 2022). "OB Associations". In: *arXiv e-prints*, arXiv:2203.10007, arXiv:2203.10007. arXiv: 2203.10007 [astro-ph.SR].

Xu, Duo et al. (Feb. 2020). "Application of Convolutional Neural Networks to Identify Stellar Feedback Bubbles in CO Emission". In: *ApJ* 890.1, 64, p. 64. DOI: 10.3847/1538-4357/ab6607. arXiv: 2001.04506 [astro-ph.GA].

York, Donald G. et al. (Sept. 2000). "The Sloan Digital Sky Survey: Technical Summary". In: *AJ* 120.3, pp. 1579–1587. DOI: 10.1086/301513. arXiv: astro-ph/0006396 [astro-ph].

Zari, E. et al. (June 2021). "Mapping luminous hot stars in the Galaxy". In: *A&A* 650, A112, A112. DOI: 10.1051/0004-6361/202039726. arXiv: 2102.08684 [astro-ph.GA].

Zaritsky, Dennis et al. (Feb. 2002). "The Magellanic Clouds Photometric Survey: The Small Magellanic Cloud Stellar Catalog and Extinction Map". In: *AJ* 123.2, pp. 855–872. DOI: 10.1086/338437. arXiv: astro-ph/0110665 [astro-ph].

Zhang, C. Y. (June 1995). "A Statistical Distance Scale for Galactic Planetary Nebulae". In: *ApJS* 98, p. 659. DOI: 10.1086/192173.

Zhao, He et al. (Mar. 2020). "A Systematic Study of the Dust of Galactic Supernova Remnants. I. The Distance and the Extinction". In: *ApJ* 891.2, 137, p. 137. DOI: 10.3847/1538-4357/ab75ef. arXiv: 2002.04748 [astro-ph.SR].